

Application of machine learning in the structural design process of bascule bridges

Using an artificial neural network to generate structural bascule bridge designs in Grasshopper

G.W. Vos

Application of machine learning in the structural design process of bascule bridges

Using an artificial neural network to generate structural bascule bridge designs in Grasshopper

by

G.W. Vos

in partial fulfilment of the requirements to obtain the degree of

Master of Science
in Civil Engineering

Track
Building Engineering – Structural Design

at the Delft University of Technology,
to be defended publicly on May 24th 2024, at 11:30.

Student number:	4709233	
Project duration:	July 10, 2023 – May 24, 2024	
Thesis committee:	Prof. dr. ir. P.C. Louter,	TU Delft, Chair
	Dr. ir. G.A. van Nederveen,	TU Delft
	Ir. P. Eigenraam,	TU Delft
	Ir. S. van Rossum,	Ingenieursbureau Gemeente Amsterdam

Cover: Kadoelenbrug Amsterdam by ipv Delft (Top) and Hogesluis by
Ons Amsterdam (Bottom)

An electronic version of this thesis is available at <http://repository.tudelft.nl/>.

Preface

This report presents my thesis titled 'Application of machine learning in the structural design process of bascule bridges', to complete the degree of Building Engineering. In this thesis, I have aimed to implement the ongoing developments in the world of artificial intelligence in a practical application, namely the structural design of bascule bridges.

This thesis marks the end of my journey at TU Delft. I look back at a seven year study period in which I have been inspired by professors, lecturers and fellow students, and in which my aspiration to become a structural engineer has become clear. Throughout my studies I have developed many interests and skills that I am grateful for, some of which I have been able to apply within this project. In the future, I hope that I will be able to continue combining the fields of structural and parametric design, with the possibilities that artificial intelligence will provide.

I would first like to thank my committee members for their advice and time throughout the project. Their feedback during meetings and on the report was most valuable. Next I would like to thank Peter Schoonderbeek, for allowing me to investigate this, still uncertain and new, development within the civil engineering field, within IB Amsterdam. Also for his assistance in getting acquainted within the company, helping me in finding information and for always showing interest in what I was doing during the project. I would like to thank Sebastiaan van Rossum, who was excited to take over the supporting role from Peter halfway during the project, and who has helped a great deal in the final part of this project, namely with configuring the structural modelling. Thanks to both for your guidance during the project. Lastly, I would like to thank my colleagues within the structural design teams, for always showing great interest in my project and for having helped me with what I needed.

G.W. Vos
Delft, May 2024

Summary

This research aims to investigate the possibility of applying a neural network algorithm into the structural design process of bascule bridge leaves, by creating a workflow in Grasshopper. The demand for this tool, originates from the fact that the current design process is experienced as linear and slow, and does not fit the dynamic design environment within Amsterdam. Because of this slow design process, too much time is available in which extra boundary conditions can be added to the project. Hence, there is a demand to create viable, realistic structural designs for bascule bridge leaves, already in the conceptual and preliminary phases of a design project.

The development method, with which the Grasshopper workflow was constructed, is schematized with the figure below.

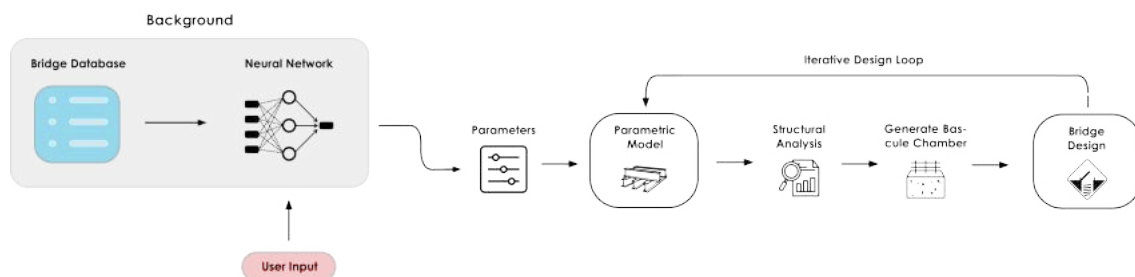


Figure 1: Steps of the workflow.

The foundation for the generative design workflow, is a parametric model for an orthotropic bridge deck made out of steel. The model is made out of main beams, which are modeled as tubular profiles, cross beams and rib elements, which are modeled as line elements, and a bridge deck plate on top, to which all elements are welded. The parametric model is controlled by a total of 24 parameters which describe its dimensions, profiles and spacing of elements. Based on the user input for three parameters, namely the bridge deck length, bridge deck width and distance to the rotational axis, the neural network algorithm does a suggestion for the remaining parameters, based on information in the bridge database. The bridge database consists of 35 bascule bridges. A design for a steel bridge leaf is then generated. In the next step, the generated structure is forwarded into SCIA Engineer via a .xml file, for structural analysis. Within SCIA Engineer, the structural performance is assessed based on occurring Von Mises stresses under defined load combinations.

In the validation stage of the research, three steps were undertaken. In the first validation step, the predicting behavior of the neural network was optimized based on the mean squared error. This led to a neural network with one hidden layer containing four nodes, using a sigmoid activation function, a learning rate of 0.2 and a momentum of zero. The learning algorithm for the neural network that was chosen is backpropagation. The predicting behavior of the workflow was assessed using 5-fold cross validation. It appeared that the neural network had a prediction accuracy of 25.91%. Therefore, in the second validation step, the neural network's complexity was reduced. In the improved model, the neural network predicts fourteen parameters, of which all but two, are predicted with an inaccuracy of 15 to 45 percent. The two remaining parameters have a higher inaccuracy of around seventy percent. The total predicting accuracy of the improved model is equal to 61.07%.

In the last validation step, five random cases were generated, of which their SCIA model output was compared to simplified models and the predicting behavior of the neural network was assessed. In two out of five cases, the neural network immediately suggests a good structure, while in two others, only one parameter had to be altered to create a viable structure. From validation of the SCIA models,

it appeared that the moment, shear force and stress distribution for both the main beam and cross beam showed consistent behavior through all five models. The magnitude of occurring moments, shear force and stress was checked in two cross sections for both the main beam and cross beam. For the main beams, a simple MatrixFrame model was constructed for comparison. There were significant differences in the magnitude of occurring moments and shear forces between the MatrixFrame model and SCIA model. The magnitudes of moments, shear forces and stresses in the cross beams were compared to a hand calculation of a clamped beam. The difference between the majority of these values was between ten to thirty percent. It was concluded that the SCIA models generated in the validation stage of the research, behaved correctly.

In the results section, the output of the workflow was compared to two reference cases, the Berlagebrug and Elizabeth Admiraalbrug. For the Berlagebrug, the SCIA model had such a significant error that no useful results could be extracted from this case study. The comparison in structural performance for the Elizabeth Admiraalbrug can be seen in the next table.

Table 1: Structural performance comparison Elizabeth Admiraalbrug

Generated design by neural network			
Mass [kg]	97603 kg		
Load combination	Norm. element	$\sigma_{E,max}$	U.C.
LC4	Main beam	245.4	0.69
LC5	Cross beam	24.8	0.07
LC6	Rib	67.8	0.19
Elizabeth Admiraalbrug			
Mass [kg]	46325 kg		
Load combination	Norm. element	$\sigma_{E,max}$	U.C.
LC4	Main beam	150.1	0.42
LC5	Cross beam	248	0.7
LC6	Rib	137	0.39

It can be seen that the neural network suggests a structure which is approximately 2 times larger in mass. This translates into the unity checks which were obtained by evaluating the structural performance under three normative load combinations for the Elizabeth Admiraalbrug. The main beams in both designs are of similar dimensions, yet the cross beams and ribs are over-designed in the design alternative generated by the neural network. A qualitative comparison between the current design process and when the created workflow would be implemented, was also done. The main advantages are that time could be saved in future projects, in the renovation task of existing bridge leaves and that structural engineers can become more time efficient. Main disadvantages are that it is difficult to get insight into the working of the neural network, that there is no knowledge yet in the firm about the use of Grasshopper, and that a general model strategy must first be constructed in order for the workflow to save time in future projects, which takes time.

Based on the quantitative results obtained in the research, it was concluded that the neural network algorithm in the application developed in its current form, will not significantly improve the structural design process, due to a lack of consistency in generated results. There is a lack of consistency in the predicting behavior of the neural network, in most cases the neural network does not directly predict a viable structure. There are also still errors in the SCIA models generated by the workflow, meaning that the benefit of the coupled structural analysis, does not reach its full potential. Taking into account the scope of this assignment, which was focused on the conceptual and preliminary design phase of bascule bridge projects, it can be said that the developed workflow, can improve the design process in general. For most user inputs, the neural network does a representative suggestion, except for few parameters. These parameters can easily be altered by the user to create a design alternative, which can function as starting point in the design process. The combination of the neural network and parametric model which can be controlled by the user, can help speed up the design process by being able to quickly generate design alternatives.

Contents

Preface	i
Summary	ii
List of Abbreviations	vii
List of Figures	viii
List of Tables	xii
1 Introduction	1
1.1 Problem statement	1
1.2 Vision	2
1.3 Research goals	3
1.4 Research question	4
1.5 Research method.	4
1.6 Development method.	6
1.7 Scope	6
2 Theoretical Background	8
2.1 Architectural Bridge Design	8
2.1.1 Bridge typology	8
2.1.2 Bridge Components	9
2.2 Structural Bridge Design	14
2.2.1 Structural system.	15
2.2.2 Loading	16
2.2.3 Pedestrian and cycle paths	19
2.2.4 Structural Verification.	19
2.3 Machine Learning	24
2.3.1 Theory.	24
2.3.2 Model Training & Accuracy.	28
2.3.3 Data Processing	31
2.4 Software & Digital Tools	32
2.4.1 Rhinoceros	32
2.4.2 Grasshopper3D.	33
2.4.3 Grasshopper3D Plug-ins	33
2.4.4 SCIA Engineer	34
2.5 Interview & Discussions	34
3 Development of workflow	37
3.1 Parametric model.	37
3.1.1 Parameters	38
3.1.2 Bascule chamber	42
3.2 Bridge Database	42
3.2.1 Bridge information	43
3.2.2 Sources	44
3.3 Configuration of neural network	45
3.3.1 Post-processing data.	47
3.4 Structural Analysis	47
3.4.1 Load cases	47
3.4.2 Load Combinations.	52

4	Validation	54
4.1	Neural network validation	54
4.1.1	Neural Network Configuration	54
4.1.2	5-Fold Cross Validation	57
4.1.3	Prediction behavior	58
4.2	Re-configuring the model	60
4.2.1	Training behaviour	61
4.2.2	Prediction performance	62
4.3	Validation of workflow	64
4.3.1	Calculation procedure	64
4.3.2	Application	66
5	Results	92
5.1	Design Comparison	92
5.1.1	Renovation Berlagebrug	93
5.1.2	Elizabeth Admiraalbrug	96
5.2	Integration in design process	100
5.3	Evaluation	102
6	Discussion	104
6.1	Discussion	104
6.1.1	Application of neural network	104
6.1.2	Shortcomings of parametric model	105
6.1.3	Error in SCIA model	106
6.1.4	Obtained results	106
6.2	Lessons learned	108
7	Conclusion & Recommendations	110
7.1	Conclusion	110
7.2	Recommendations	111
	References	114
A	Bridge overview	115
B	SBS Bascule bridge	117
C	Calculation procedure loading on bridge deck	118
C.1	Wind loading	118
C.2	Traffic loading	120
C.3	Fatigue	124
C.4	Friction and roll resistance	124
C.5	Thermal loading	125
C.6	Accidental loading	126
C.7	Pedestrian and cycle paths	126
C.7.1	Traffic loading	126
C.7.2	Accidental loading	127
C.7.3	Dynamic loading	128
D	Interview Documentation	129
E	Bridge Database	130
E.1	Data set	130
E.2	Cross section properties	134
F	Validation	137
F.1	Cross-Validation Test sets	137
F.2	Cross-Validation Results	137
F.2.1	Fold 1	137
F.2.2	Fold 2	141
F.2.3	Fold 3	145

F.2.4	Fold 4149
F.2.5	Fold 5153
F.3	Cross-Validation results of re-configured model158
F.3.1	Mean-squared error158
F.3.2	Prediction inaccuracy.169
F.4	SCIA Model validation184
F.4.1	MatrixFrame models of main beams184
F.4.2	Hand calculation for loading on cross beam186
F.4.3	Excel sheets hand calculations188
F.4.4	Forces in the main beam flanges193
F.4.5	Stress distribution bridge leaf194
G	Results	198
G.1	Case Study 1: Renovation Berlagebrug.198
G.2	Case Study 2: Elizabeth Admiraalbrug201
G.3	Results for design alternative Berlagebrug205
G.4	Results for design alternative Elizabeth Admiraalbrug206

List of Abbreviations

Rhino	Rhinoceros
GH	Grasshopper3D
BRU0026	Bridge 0026
ANN	Artificial Neural Network
SBS	System Breakdown Structure

List of Figures

1	Steps of the workflow.	ii
1.1	Difficulties in the design process for bascule bridges.	1
1.2	Vision for this research.	2
1.3	Strengths of the neural network algorithm within bascule bridge design.	3
1.4	Strengths of the total workflow.	3
1.5	Steps of the research.	4
1.6	Steps of the workflow.	6
1.7	New bascule bridge in Elzenhagen-Zuid.	7
1.8	Kinkerbrug.(Bruggen & Overwegen Europa)	7
2.1	Types of bascule bridges. (Parke & Hewson, 2008)	8
2.2	Components of a bascule bridge.	9
2.3	Trunnion bascule bridge and its components. (WisDOT, 2017)	9
2.4	Bridge leaf structure.	10
2.5	Cross-section of an orthotropic bridge deck.(CivilEngineeringX,2023)	10
2.6	Ribs used in an orthotropic bridge deck.(Natsheh & Menzemer,2022)	10
2.7	Bridge leaf of Amaliabrug. (Nationale Staal Prijs,2022)	11
2.8	Bridge leaf of Haringvlietbrug. (Hollandia Infra,2023)	11
2.9	Reinforced connection element. (University of South Florida,2003)	11
2.10	Trunnion support. (University of South Florida,2001)	11
2.11	Typical operating mechanisms of a bascule bridge. (Parke & Hewson, 2008)	11
2.12	Mechanism of a bascule bridge. (Van Zantvliet, 2015)	12
2.13	Isometric view on operating system. (Movares,2016)	12
2.14	Hinged connection between push-pull rod and main beam. (ipv Delft,2023)	12
2.15	Operating system of Ketelbrug. (Nationale Staal Prijs, 2022)	12
2.16	Bascule chamber Amaliabrug. (EPC-Groep,n.d.)	14
2.17	Bascule chamber Ouderkerk.(Van Hattum en Blankevoort,n.d.)	14
2.18	Conceptual design of bascule chamber Elizabeth Admiraalbrug. (IB Amsterdam,2023)	14
2.19	Conceptual design of bascule chamber Elizabeth Admiraalbrug. (IB Amsterdam,2023)	14
2.20	Components of an orthotropic bridge deck.(Connor et al.,2012)	15
2.21	Connection between troughs and cross beams.(Connor et al.,2012)	15
2.22	Membrane action of the bridge deck and troughs (top) and bending of the deck plate (bottom).(Pavlovic, 2022)	16
2.23	Local bending of the bridge deck due to high point load. (Pavlovic,2022)	16
2.24	Components of a generic machine learning model. (Alzubi et al.,2018)	25
2.25	Supervised machine learning model.(Dhage & Raina,2016)	25
2.26	Linear regression model.(Sharma, 2022)	26
2.27	Simple neural network.(Pannell et al., 2022)	26
2.28	Mathematical operation between two nodes. (Prasad, 2021)	26
2.29	Sigmoid activation function.	27
2.30	Bipolar sigmoid activation function.	27
2.31	Linear activation function.	28
2.32	Rectified linear activation function.	28
2.33	Threshold activation function.(Van der Zwaag & Spaanenburg,2004)	28
2.34	Model with a good fit.(DigitalSreeni,2020)	29
2.35	Two example learning curves of an underfit model. (DigitalSreeni,2020)	29
2.36	Learning curves of an overfit model.(Brownlee,2019)	30
2.37	Two example learning curves of an unrepresentative model. (DigitalSreeni,2020)	30

2.38 5-Fold Cross-validation.(scikit-learn,2024)	30
2.39 Normal distribution.	32
2.40 Rhino interface.(McNeel & Associates,2023)	32
2.41 Grasshopper interface.(Rutten,2011)	32
2.42 Neural network training component.	33
2.43 Neural network tester component.	33
3.1 Generated bridge design in Rhino.	37
3.2 Generated bridge design in SCIA Engineer.	37
3.3 Dimensions of main beams.	38
3.4 Division of main beam.	39
3.5 Cross section definition.	39
3.6 Parameters describing the structure.	41
3.7 Parameters describing the bascule chamber.	42
3.8 Bridge leaves per construction year.	43
3.9 Properties of bridges in data set.	44
3.10 Traffic profiles of bascule bridges in data set.	44
3.11 Schematic representation of neural network.	45
3.12 Load case two.	48
3.13 Load case three.	48
3.14 Load case four.	49
3.15 Load case five.	49
3.16 Load case six.	49
3.17 Load case seven.	49
3.18 Load case eight.	50
3.19 Load case nine.	50
3.20 Load case ten.	50
3.21 Load case eleven.	51
3.22 Load case twelve.	51
3.23 Load case thirteen.	52
3.24 Load case fourteen.	52
4.1 Loss curves of neural network.	54
4.2 Loss curves of neural network.	55
4.3 Loss curves for different learning rates and momentum.	56
4.4 Training loss for momentum equal to zero.	56
4.5 Loss curve of neural network in improved model.	61
4.6 Schematization of main beam.	65
4.7 Moment diagram (top) and shear force diagram (bottom) of main beam.	65
4.8 Schematization of crossbeam.	66
4.9 Moment diagram (left) and shear force diagram (right) of cross beam.	66
4.10 Suggested structure by workflow.	67
4.11 Top view of suggested structure by workflow.	67
4.12 Top main beam in the design.	68
4.13 Improved structure by user.	68
4.14 Main beam case one (top), moment diagram (middle) and shear force diagram (bottom).	68
4.15 Stresses in the main beam.	69
4.16 Moment (top), shear force (middle) and stress distribution over the cross beam.	70
4.17 Suggested structure by workflow.	72
4.18 Top view of suggested structure by workflow.	72
4.19 Main beam case two (top), moment diagram (middle) and shear force diagram (bottom).	73
4.20 Stresses in the main beam.	74
4.21 Moment (top), shear force (middle) and stress distribution over the cross beam.	75
4.22 Suggested structure by workflow.	77
4.23 Top view of suggested structure by workflow.	77
4.24 Main beam case three (top), moment diagram (middle) and shear force diagram (bottom).	78

4.25 Stresses in the main beam.	79
4.26 Moment (top), shear force (middle) and stress distribution over the cross beam.	80
4.27 Suggested structure by workflow.	82
4.28 Top view of altered structure.	82
4.29 Main beam case four (top), moment diagram (middle) and shear force diagram (bottom).	83
4.30 Stresses in the main beam.	84
4.31 Moment (top), shear force (middle) and stress distribution over the cross beam.	85
4.32 Suggested structure by workflow.	87
4.33 Top view of suggested structure by workflow.	87
4.34 Main beam case five (top), moment diagram (middle) and shear force diagram (bottom).	87
4.35 Stresses in the main beam.	88
4.36 Moment (top), shear force (middle) and stress distribution over the cross beam.	89
4.37 Locations of stress concentrations in the SCIA model.	91
5.1 Normative cross section for stresses in the main beam near the bridge deck.	93
5.2 Suggestion by the neural network for the Berlagebrug.	94
5.3 Top view of suggestion by the neural network for the Berlagebrug.	94
5.4 Von Mises stress in plate element S87.	95
5.5 Von Mises stress in the governing cross beam.	95
5.6 Von Mises stress in the governing cross beam.	95
5.7 Suggestion by the neural network for the Elizabeth Admiraalbrug.	97
5.8 3D view of the generated design alternative.	97
5.9 Top view of the design alternative.	97
5.10 Von Mises stresses in governing plate element S26.	98
5.11 Von Mises stresses in foremost crossbeam.	99
5.12 Stress distribution in rib elements under axle loads.	99
5.13 Normative rib element in load combination six.	99
B.1 System Breakdown Structure of Bascule bridge.	117
C.1 Local axis system for wind loading on a bridge deck.(NEN-EN1991-1-4:2005+C2:2011+NB:2019)118	
C.2 Wind form factor(NEN 6786-1:2017+C1:2021).	120
C.3 Examples of carriageway widths and restraint systems.(Pavlovic, 2022)	121
C.4 Division of notional lanes.(NEN-EN1991-2:2003+C1:2015+NB:2019)	121
C.5 Load model 1.(NEN-EN1991-2:2003+C1:2015+NB:2019)	122
C.6 Parallel vehicles in load model 1.(NEN-EN1991-2:2003+C1:2015+NB:2019)	122
C.7 Load model 2.(NEN-EN1991-2:2003+C1:2015+NB:2019)	122
C.8 Example of axle loads of special vehicle.(Pavlovic,2022)	123
C.9 Deck loading around special vehicle.(NEN-EN1991-2:2003+C1:2015+NB:2019)	123
C.10 Fatigue load model 3.(NEN-EN1991-2:2003+C1:2015+NB:2019)	124
C.11 Uniformly distributed load on sidewalk.(NEN-EN1991-2:2003+C1:2015+NB:2019)	127
C.12 Accidental vehicle on a pedestrianbridge.(NEN-EN1991-2:2003+C1:2015+NB:2019)	127
E.1 Dataset in Excel.	131
E.2 Dataset in Excel.	132
E.3 Dataset in Excel.	133
F.1 Test sets.	137
F.2 2D model of loaded main beam in validation case one.	184
F.3 2D model of loaded main beam in validation case two.	184
F.4 2D model of loaded main beam in validation case three.	185
F.5 2D model of loaded main beam in validation case four.	185
F.6 2D model of loaded main beam in validation case five.	186
F.7 Hand calculation validation case one.	188
F.8 Hand calculation validation case two.	189
F.9 Hand calculation validation case three.	190
F.10 Hand calculation validation case four.	191

F.11 Hand calculation validation case five.	192
F.12 Zoom on force n_y in the bottom flange of the main beam in case one.	193
F.13 Force n_y in the bottom flange of the main beam in case one.	193
F.14 Zoom on force n_y in the bottom flange of the main beam in case two.	193
F.15 Force n_y in the bottom flange of the main beam in case two.	193
F.16 Zoom on force n_y in the bottom flange of the main beam in case three.	193
F.17 Force n_y in the bottom flange of the main beam in case three.	193
F.18 Zoom on force n_y in the bottom flange of the main beam in case four.	194
F.19 Force n_y in the bottom flange of the main beam in case four.	194
F.20 Zoom on force n_y in the bottom flange of the main beam in case five.	194
F.21 Force n_y in the bottom flange of the main beam in case five.	194
F.22 Stresses $\sigma_y +$ in the top flange of the main beam and deck plate.	194
F.23 Stresses $\sigma_y +$ in the top flange of the main beam and deck plate.	195
F.24 Stresses $\sigma_y +$ in the top flange of the main beam and deck plate.	195
F.25 Stresses $\sigma_y +$ in the top flange of the main beam and deck plate.	196
F.26 Stresses $\sigma_y +$ in the top flange of the main beam and deck plate.	197
G.1 A bridge leaf part being hoisted into place.	198
G.2 Overview of new bridge leaf.	198
G.3 Cross section of bridge deck.	199
G.4 Side view on the bridge leaf.	199
G.5 Governing Von Mises stresses in main beams for ULS envelope.	200
G.6 Governing Von Mises stresses in cross beam G for ULS envelope.	200
G.7 Governing Von Mises stresses in cross beam B for ULS envelope.	201
G.8 3D render of bridge 0925.	201
G.9 Top view of bridge 0925.	201
G.10 Cross section of bridge deck.	202
G.11 Side view on the bridge leaf.	202
G.12 Rib element in the bridge deck.	203
G.13 View on the bridge deck from underneath.	203
G.14 Governing Von Mises stresses in main beam of Elizabeth Admiraalbrug.	203
G.15 Governing Von Mises stresses in "voorhar" of Elizabeth Admiraalbrug.	204
G.16 Governing Von Mises stresses in rib of Elizabeth Admiraalbrug.	204
G.17 Von Mises stresses under load combination one.	205
G.18 Von Mises stresses under load combination two.	205
G.19 Von Mises stress in governing element B199.	206
G.20 Von Mises stresses under load combination three.	206
G.21 Von Mises stresses under load combination three.	206
G.22 Von Mises stresses under load combination four.	207
G.23 Von Mises stresses in governing plate element S26.	207
G.24 Von Mises stresses under load combination five.	208
G.25 Von Mises stresses in governing cross beam elements.	208
G.26 Von Mises stresses under load combination six.	209
G.27 Maximum stresses in governing rib elements.	209

List of Tables

1	Structural performance comparison Elizabeth Admiraalbrug	iii
2.1	Definition of groups of traffic loads.(NEN-EN1991-2:2003+C1:2015+NB:2019)	18
2.2	Bridge properties.	31
4.1	Model Loss	55
4.2	Model Loss	56
4.3	Training loss for momentum equal to zero.	56
4.4	Results from cross-validation.	57
4.5	Average MSE value per step.	57
4.6	Prediction inaccuracy per bridge.	58
4.7	Prediction inaccuracy per parameter.	58
4.8	Relative prediction inaccuracy per parameter.	60
4.9	Test fold error and prediction difference.	60
4.10	Cross-validation of improved model.	62
4.11	Average MSE value per step.	62
4.12	Absolute prediction inaccuracy per bridge in improved model.	63
4.13	Absolute prediction inaccuracy per parameter in improved model.	63
4.14	Relative prediction inaccuracy per parameter in improved model.	64
4.15	Parameters for validation case one.	67
4.16	Comparison between MatrixFrame model, hand calculation and SCIA model for validation case one.	71
4.17	Parameters for validation case two.	72
4.18	Comparison between MatrixFrame model, hand calculation and SCIA model for validation case two.	76
4.19	Parameters for validation case three.	77
4.20	Comparison between MatrixFrame model, hand calculation and SCIA model for validation case three.	81
4.21	Parameters for validation case four.	81
4.22	Comparison between MatrixFrame model, hand calculation and SCIA model for validation case four.	86
4.23	Parameters for validation case five.	86
4.24	Comparison between MatrixFrame model, hand calculation and SCIA model for validation case five.	90
5.1	Parameters for alternative design Berlagebrug.	93
5.2	Structural performance comparison Berlagebrug.	96
5.3	Parameters for alternative design Elizabeth Admiraalbrug.	97
5.4	Structural performance comparison Elizabeth Admiraalbrug	99
6.1	Prediction inaccuracy for validation case three.	107
6.2	Prediction inaccuracy per relevant parameter.	107
A.1	Bascule bridges in Amsterdam.	116
C.1	Windspeeds per area.(NEN-EN1991-1-4:2005)	118
C.2	Maximum hours non-operational due to high wind loads(NEN 6786-1:2017+C1:2021).	119
C.3	Division of notional lanes.(NEN-EN1991-2:2003+C1:2015+NB:2019)	121
C.4	Definition of traffic categories.(NEN-EN1991-2:2003+C1:2015+NB:2019)	123
C.5	Table NB.I.1(NEN-EN 1991-2:2003+C1:2015+NB:2019)	128

Introduction

The municipality of Amsterdam has a total of more than 1420 bridges in their inventory, of which 41 are bascule bridges. Movable bridges play a crucial role in important traffic routes through the city, for car, slow and nautical traffic. Their correct functioning is important, hence a lot of effort is put into their design. Within projects in Amsterdam, many stakeholders are involved, which results in a complex design puzzle in the urban landscape. Additionally, bridges are always one-off and unique projects, which further increases the time and effort needed for the design. This thesis has aimed to improve the structural design process of steel bridge leaves for bascule bridges.

1.1. Problem statement

The demand for this research ensues from existing difficulties that are encountered in the design process of bascule bridges. These are summarized with the following four points.

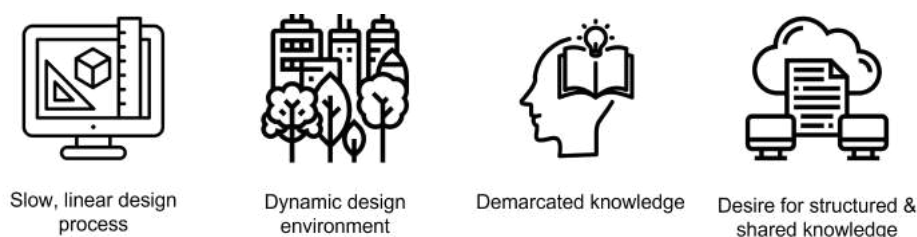


Figure 1.1: Difficulties in the design process for bascule bridges.

Traditional bridge design process & design environment

Bridge design projects are unique of nature, since their architectural and structural design highly depend on the environment. The traditional design process is experienced to be linear and time-consuming. A design project consecutively flows through the conceptual, preliminary and definitive design phases. This traditional, linear design process within bridge projects, is being overtaken by the continuously changing design requirements and boundary conditions of the busy urban environment in Amsterdam. Many stakeholders can have influence on their surroundings. Because there are many exterior parties, but also engineering disciplines and contractors involved, a lot of time is spent on mapping boundary conditions and rules. The main problem statement originates from this fact. There is a desire to be able to generate and evaluate realistic design alternatives already in an early phase of a project, so a project can continue into the definitive design phase sooner, which limits the time spent on processing boundary conditions and limits the possibility of new boundary conditions coming in.

Demarcated knowledge

In a bascule bridge project, the disciplines of civil engineering, mechanical engineering, electrical engineering and architecture come together. Civil engineers are responsible for the overall structural integrity and stability of the bridge, while mechanical engineers design and oversee the functionality of the

basculer mechanism. Electrical engineers ensure that the bridge's lighting, signaling, and control systems operate flawlessly, and architects harmonize the bridge's aesthetic appeal with its surroundings. This convergence of expertise, however, presents a unique challenge: the demarcation of knowledge between these disciplines. While each group possesses an understanding of their respective domains, bridging the gaps between their areas of expertise can be time-consuming and complex. Decisions made in the design, influence every discipline's working domain. What is currently experienced, is that engineers have limited knowledge about the other domains involved. Meaning that more time is spent in meetings and discussions during the design phases, to evaluate design choices and possibilities.

Structured & shared knowledge

On a larger scale, the municipality and its engineering department are responsible for a large array of assets. Currently, thorough reassessment of the structural capacity of bridges in the city needs to be done, since most of them have been built in the previous century. At the moment, information about existing assets is stored in various places, namely in city archives, local data management systems in the cloud, and on hard drives. Up until this point in time, re-evaluation of assets was done on individual basis. Where information about the relevant asset, was gathered by the engineer himself, tailored to his assignment. The municipality wants to shift to a more structured approach, in which more assets can be recalculated in a more effective way. There is thus a desire for a more structured and comprehensive database on the properties of bascule bridges in the city, which different departments can use and exchange information about.

1.2. Vision

The results of this research mitigate the difficulties named, by adhering to the following vision points:



Figure 1.2: Vision for this research.

Innovate design process

The workflow developed in this thesis contributes significantly to the dynamics of the conceptual and preliminary design phases. Users are namely directly able to generate designs for bridge leaves, and get insight into their structural performance. This can either be done by making use of the capacities of the parametric model, in which the user generates his or her own design. Or with assistance of the neural network, in which knowledge about constructability, maintenance accessibility, costs and functionality, that has been applied in the design of existing bridges, is indirectly used again in new designs. Design teams do not have to start from scratch, in new bridge projects. Secondly, design choices can be made on more substantiated grounds, namely the expected structural performance, already in the early design phases. Because decisions on design alternatives can be made faster and conclusions can be reached sooner, the project will flow towards the definitive design phase sooner.

Structure bridge data

To create the data set for the neural network algorithm used in the workflow, the parameters that are used to describe the model, were collected for the 35 bascule bridges in the city that have a similar typology. This dataset is now stored in one file, and can be used for further analysis to find possible relations between parameters, in the future. It can also contribute to the asset-wide approach of re-assessing the structural capacity that is left in existing bridges. The method in which the parametric model of the bridge leaf has been set up, helps the system engineering department, to better map the assets that are present in the city. From this point onward, more data about bascule bridges could be added into the data set, which further increases its accuracy.

Increased collaboration

Because of the tool, realistic and viable design alternatives can be drawn up in the early design phases of the project. This enables specialists and engineering departments to collaborate and engage in discussion way earlier, since it takes less time to draw up a 3D-model. The design team can make live alterations to the structural design. The coupled structural verification can lead to more informed decisions, from which engineers in different disciplines can get a better grasp on how design choices influence the domain they are responsible for. Once the tool and neural network has been established, the workflow can easily be expanded to other types of geometry and structures, possibly increasing the collaboration between design teams and between the asset management and engineering departments within the municipality.

Summarizing, the strengths of the neural network developed in this thesis are:

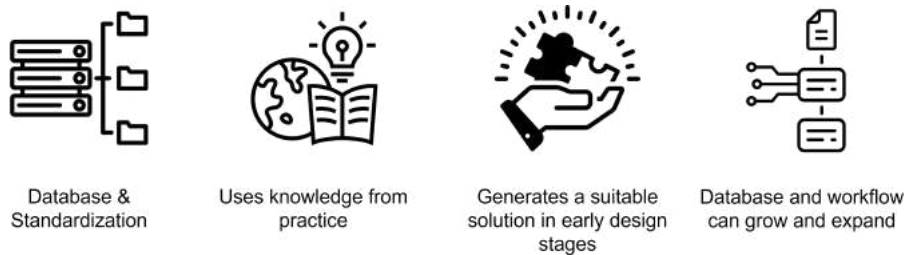


Figure 1.3: Strengths of the neural network algorithm within bascule bridge design.

And the strengths of the workflow are:

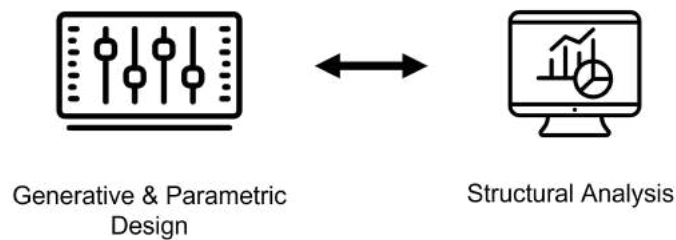


Figure 1.4: Strengths of the total workflow.

1.3. Research goals

The aim of this research is to investigate whether machine learning can be usefully applied within the conceptual and preliminary design phases of bascule bridge projects, and whether it can improve the design process. This is translated into a development goal. The development goal consists of creating a workflow in Grasshopper, which builds a link between parametric modeling and the structural analysis software SCIA Engineer. The results of this workflow are used to determine whether the neural network algorithm can assist the engineer in quickly generating viable design alternatives.

A secondary research goal is to investigate whether data about bridge design is suitable to implement in a neural network application, and whether the neural network can find relations between the variables in the data set.

With an answer to the above research goals, an evaluation can be made about whether the machine learning algorithm proves useful and adds value within the Grasshopper workflow, or whether it is only the generative and parametric design aspect of the workflow, that is useful for engineers in practice. To ultimately formulate an answer to the question of whether a machine learning algorithm can be used to automate structural design tasks in bascule bridge projects. In a broader scope, the

outcomes of this research could prove as a stepping stone towards applying machine learning onto larger data sets and in different fields of civil engineering.

1.4. Research question

The main research question that will be answered in this thesis is:

How can machine learning be used to improve the structural design process of bascule bridges?

Sub-questions that were formed are:

1. What loading effects and which verification checks should be considered in the structural design procedure of the bridge leaf?
2. What is a neural network algorithm and how does it work?
3. How does the bridge design process work in practice?
4. What does the parametric and digital modeling environment within IB Amsterdam currently look like and how can the generative design tool improve the design process, according to engineers in the firm?
5. How can the structural design of a bascule bridge leaf be described and standardized?
6. How can a neural network algorithm be applied onto a data set and to which criteria must data adhere to?
7. How is the performance of the neural network described and assessed?
8. How is the performance of the structural analysis models verified?

1.5. Research method

This section explains the methodology that is followed in this research. Firstly, the research method is presented. Afterwards, the development method to create the digital workflow, is presented in section 1.6.

The research method is shown in the figure below.

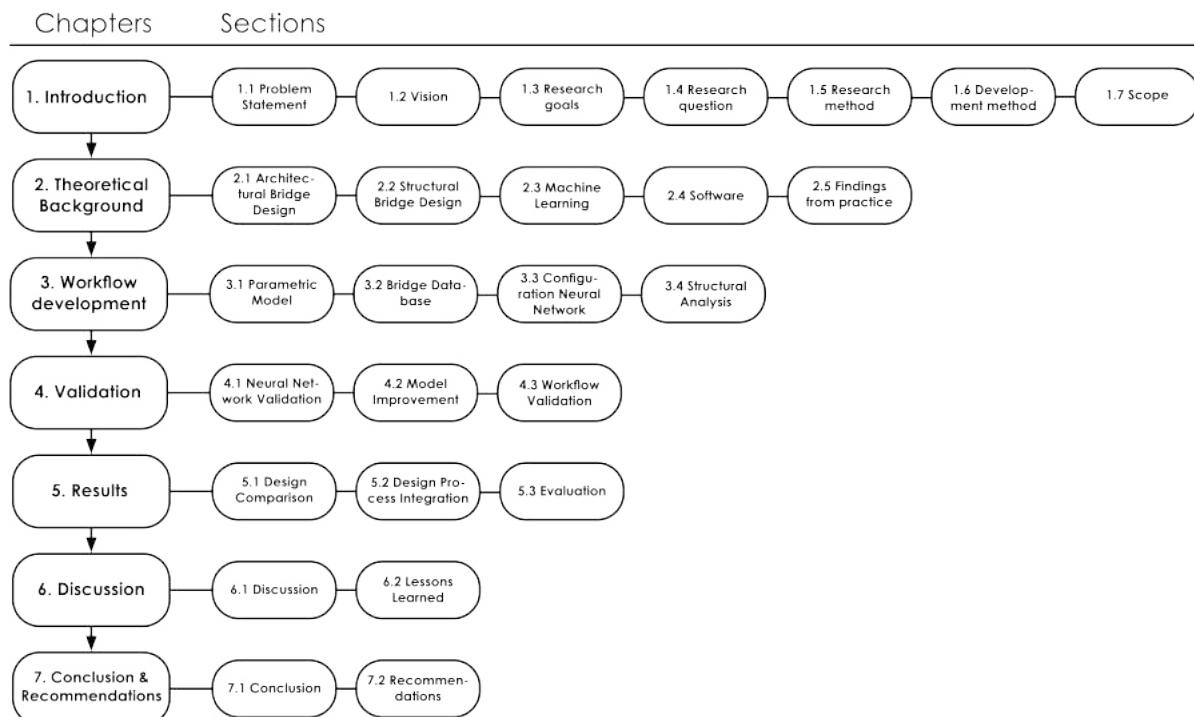


Figure 1.5: Steps of the research.

2. Theoretical Background

The theoretical part consists of a literature study, covering the required knowledge of the different topics that are relevant. Background information is presented on four topics, which are the architectural and structural design of bascule bridge (leaves), machine learning and about the software that has been used in this thesis. These topics can be found in sections 2.1 to 2.4, respectively.

The second item within the theoretical part of the research, consists of findings that result from an interview and talks with people in the engineering firm. Talks were held with structural engineers with ranging experience and disciplines, at multiple moments during the research. Their input was used for the development of the Grasshopper workflow and their advice was consulted regarding the structural design of bridge leaves. In the beginning, an interview was held with a structural engineer, that covered the procedure of bascule bridge design, knowledge on parametric and generative design, knowledge about machine learning and about the digital modeling environment that is currently used within the firm. The findings from these talks and the interview are described in section 2.5.

Chapter two answers sub-questions one to four.

3. Development of the workflow

Chapter 3 describes the development of the workflow in the visual programming environment of Grasshopper. An explanation is given on how the parametric model is constructed, about the bridge data that was gathered and about the properties of the neural network. Paragraph 3.4 presents the load cases and combinations that are used to assess the structural performance of design alternatives generated in the results.

This chapter answers sub-questions five and six.

4. Validation

An explanation about the validation of the neural network and SCIA Engineer models, is given in chapter 4. In the first paragraph, the most optimal configuration for the neural network is described, based on a trained model with the complete data set of 35 bridges. It's prediction performance is measured and described. In paragraph 4.2, an improved model is presented, since the prediction performance of the original model appeared to be very poor. In paragraph 4.3, the generation of designs with the whole workflow is evaluated with five example cases. For these cases with randomized inputs, an assessment is made whether the neural network does correct predictions, and whether the SCIA Engineer models behave correctly.

This chapter answers sub-questions seven and eight.

5. Results

The results of the research are presented in chapter 5. Two types of results are obtained from this research. The first part of the results consists of a quantitative comparison between design alternatives generated by the workflow, and two reference cases, the Berlagebrug and Elizabeth Admiraalbrug. For these input parameters, a design alternative was generated with the created workflow. The architectural design and structural performance is compared. Based on the comparison of structural performance, an assessment is made whether the workflow generates structurally sound bridge designs, and whether they are under- or overdimensioned. Secondly, a comparison is done between the current design process and a new one in which the developed tool would be implemented. Advantages and disadvantages of implementing the created workflow into the bridge design process, are named.

Paragraph 5.3 also presents an evaluation of the obtained results, in which the accuracy and usefulness of the obtained results is evaluated.

6. Discussion

This chapter describes the discussion of the results, which describes possible inaccuracies and shortcomings of the research. Paragraph 6.2 describes the lessons that were learned from this project.

7. Conclusion & Recommendations

In chapter 7, the conclusion to the main research question is given. Additionally, paragraph 7.2 describes the recommendations for future research that are done based on the outcomes of this thesis.

1.6. Development method

This section describes the methodology that was followed to construct the Grasshopper workflow, and how its use can be described.

How the script is built up and operates, is elaborated with the next figure. Here, the bridge database and machine learning algorithm, a supervised neural network, operate in the background.

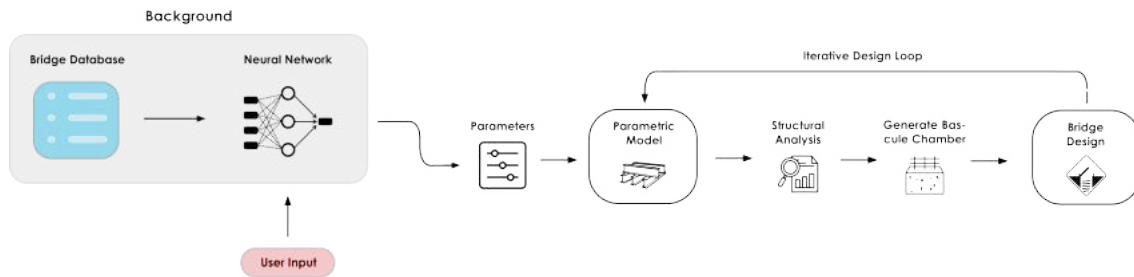


Figure 1.6: Steps of the workflow.

The foundation for the generative design workflow, is a parametric model for an orthotropic bridge deck made out of steel. This is visible in the center of the graph. Such an orthotropic bridge deck is used in all bascule bridges in Amsterdam. More information about this steel structure is given in section 2.2. The parametric model is controlled by parameters which describe its dimensions, material, profiles and spacing of elements. Based on the user input for three parameters, the machine learning algorithm fills in the remaining parameters, based on information in the bridge database. A design for a steel bridge leaf is then generated. In the parameter overview, an overrule component is present, so users can manually change the input for a parameter, if a suggestion done by the algorithm, is not appropriate. Meaning that the parametric model is also operable without the neural network algorithm attached.

In the next step, the generated structure is forwarded into SCIA Engineer via a ".xml" file, for structural analysis. Within SCIA Engineer, a finite element analysis for stresses is done. The bridge deck is validated for the load combinations that are defined in this research. Additionally, the user has the option to view the structure in SCIA Engineer, and to obtain visual representations of the occurring loads, stresses and forces in the bridge leaf. An overview of the generated design is also always visible in the Rhinoceros viewport.

1.7. Scope

Bridge typology

This thesis is aimed at simple (trunnion) bascule bridges, in which the counterweight lowers into a bascule chamber and where the bridge leaf rotates around an axis. More specifically, this thesis focuses on an orthotropic bridge deck made out of steel. The majority of bascule bridges follow this typology. The steel superstructure considered, consists of main beams that rotate around the rotational axis, which form the connection between the bridge deck and the counterweight. The structure of the bridge deck consists of main beams, cross beams, beams in longitudinal direction, called ribs, and a steel plate on top. All joints in the bridge leaf are welded connections. Local adaptations to the bridge deck structure are present in some bridges which have a tram rails running across, like shown in figure 1.8

The bascule chamber is usually of rectangular or square layout and its structure is made out of concrete. Older bridges have brickwork cladding on the exterior parts that are above water level. Most of the engine rooms are built on top of an underwater concrete slab, which in turn forms a connection

to the foundation piles. The size of the structure depends on the span, loading conditions and type of operating system. Only minor attention is paid to the bascule chamber in this thesis. Within Rhino, a bascule chamber can be generated around the created bridge leaf, so the user can obtain a sense of its size and physical appearance when generating design alternatives.



Figure 1.7: New bascule bridge in Elzenhagen-Zuid.



Figure 1.8: Kinkerbrug.(Bruggen & Overwegen Europa)

Bridge Database

There are a total of 41 bridges within the municipality of Amsterdam, that are classified as bascule bridge. These are shown in appendix A. The bridges indicated in red, are disregarded in this thesis. The Schinkelmetrobridge is disregarded, since there is not enough information available about this bridge. Additionally, its traffic function does not fit the rest of the dataset. The Han Lammersbridge and Uiverbridge are also disregarded, since the bridge decks of these bridges are made out of aluminium. The Schellingwouderbridge is also disregarded, since this bridge is managed by Rijkswaterstaat. Lastly, the Bongerdbrug is disregarded in this thesis, because there was no time left to find its technical details. This bridge could still be added to the data set in the future. The Berlagebrug is also not included in the data set, since this design is used as case study in the results phase of the research. The machine learning algorithm will be trained with structural data of the remaining 35 bascule bridges that are present within the municipality of Amsterdam. All information is manually collected in an Excel file, which functions as database for the digital workflow.

Theoretical Background

2.1. Architectural Bridge Design

This section discusses important aspects that are relevant for the architectural design of a bascule bridge. An explanation of the bascule bridge typology is given and all of the different bridge components are identified.

2.1.1. Bridge typology

According to Parke & Hewson (2008), a distinction can be made between four main types of bascule bridges, which are shown in figure 2.1. In the Netherlands, the latest is often referred to as a drawbridge or "ophaalbrug", even though its rotation around the horizontal axis characterizes it as a type of bascule bridge. Bascule bridges can be single leaf or double leaf, depending on the required span and design wishes. This thesis is focused on simply supported trunnion bascule bridges, in which the bridge deck rotates around a fixed horizontal axis. A schematic representation of this bridge typology is shown in the top left of figure 2.1. These are from now on referenced simply as bascule bridges.

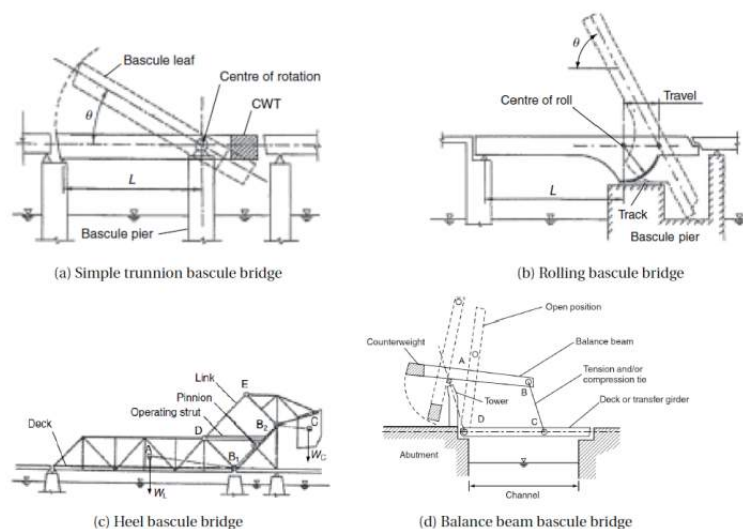


Figure 2.1: Types of bascule bridges. (Parke & Hewson, 2008)

The working mechanism of a bascule bridge is based on the balance between the bridge deck and counterweight. The counterweight makes it easier for the operating system to rotate the bridge leaf in the vertical plane. It usually moves within a closed environment, called the bascule chamber or engine room. The center of gravity of the bridge deck is located outward of the rotational axis, meaning that a

moment of inertia is always present. The bridge leaf and operating system are connected with a push-pull rod. This element must be able to withstand the large forces that can occur during both movement of the bridge deck, and loading in opened position.

2.1.2. Bridge Components

The components of which a bascule bridge, spanning over a waterway, is comprised of, are summarized in the system breakdown structure in appendix B. Its components can be divided under five main categories. Which are the civil structure, system rooms, systems, road infrastructure and fairway infrastructure. In this section, further attention is only given to the civil structure components of a bascule bridge, since these are the most relevant for this thesis. The macro scale components of the civil structure of a bascule bridge are shown in the next figure. One can identify:

- On- and offramps ("Aanbrug")
- Bascule chamber ("Bascule kelder")
- Bridge leaf ("Val")
- Abutments ("Landhoofden")
- Intermediate supports ("Opleggingen")

A schematic cross-section of the movable part of a bascule bridge is shown in figure 2.3.

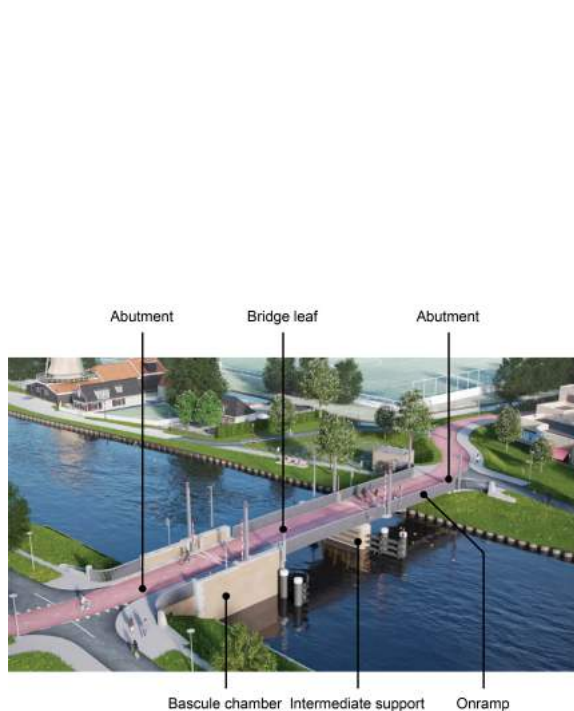


Figure 2.2: Components of a bascule bridge.

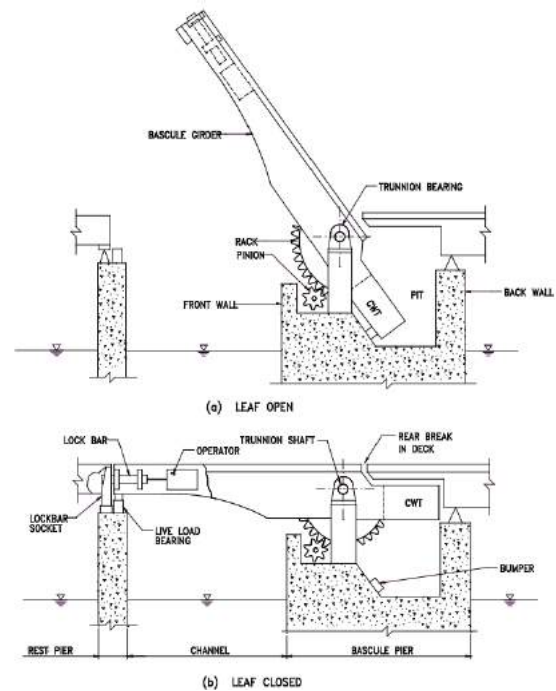


Figure 2.3: Trunnion bascule bridge and its components. (WisDOT, 2017)

Bridge leaf

As mentioned, this thesis focuses on the structural design of the bridge leaf of a bascule bridge. The bridge leaf is the component of a bascule bridge that rotates when opening. The leaf of a bascule bridge consists of a composite structure, made up out of different steel elements. A visual representation of such an orthotropic bridge deck, is shown in figure 2.4. The bridge leaf superstructure consists of main beams, cross beams and rib profiles. The main beams are either I-sections or rectangular box sections, made up of welded steel plates. The cross beams are spaced evenly in transverse direction, and are usually of smaller dimensions. They are welded in between the main beams, with the top flanges aligned to the same height.

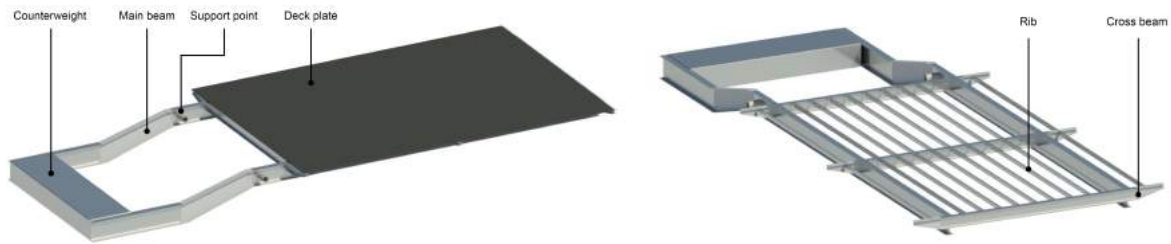


Figure 2.4: Bridge leaf structure.

Ribs are the smaller elements that are placed in parallel direction at constant spacing intervals. These are firstly welded onto the bridge deck plate, after which the deck plate and rib component, are welded onto the structure of main and cross beams. Different types of rib profiles can be used. In older bridges within Amsterdam, custom bulb profiles like shown in the left of figure 2.6, were used. In newer bridges, square or V-shaped box profiles are commonly used.

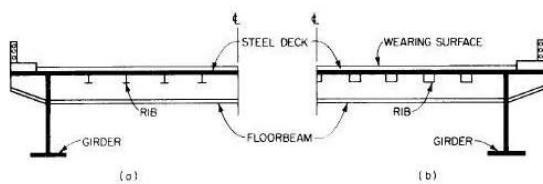


Figure 2.5: Cross-section of an orthotropic bridge deck. (CivilEngineeringX, 2023)

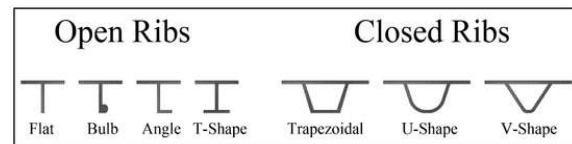


Figure 2.6: Ribs used in an orthotropic bridge deck. (Natsheh & Menzemer, 2022)

Counterweight

The counterweight is rigidly connected onto the opposite side of the main girders. Its goal is to balance the weight of the bridge leaf, so that the gravitational center of the bridge leaf moves towards the rotational axis. Because of this, less energy is required to rotate the bridge deck. The counterweight must be less heavier than the bridge leaf, so that a downward force is always present on the opposite support. This is specified in both Eurocode and VOB. The counterweight is comprised of a steel casing, that is usually filled with steel plates, which are called "broodjes" in Dutch, to reach the required weight. According to Moen (2014), room for supplementary plates is also factored in, with which the counterweight can be adjusted slightly over the bridge's lifetime, when re-calibration is needed. This is relevant when maintenance of for example the deck finishing is done. When an asphalt layer or objects on the bridge deck are adapted, the weight distribution over the bridge changes, and a small change in the counterweight might be needed (Van Zantvliet, 2015). Adequate attention needs to be spent towards the design of a counterweight, since its size and distance to the rotational axis, greatly influence the required dimensions of the bascule chamber.

Support axis

The leaf of bascule bridges, is supported on its rotational axis. The bridge leaf rotates around a trunnion, which is a solid steel alloy shaft. Two configurations for this trunnion are possible. It can run across the width of both main beams, like shown in figure 2.7, or it can consist of two smaller pieces, which connect each main beam to its own support point, like shown in figure 2.8. Because the trunnion has to pass on all loading, via the bearings towards the supports, it is firmly fitted into the bridge leaf by force- or shrink fitting it into a hole with smaller diameter. Such a reinforced connection is shown in figure 2.9. As can be seen in figure 2.10, the trunnion shaft rotates inside the support point. The rotation is facilitated by the bearings in between the trunnion and steel casing of the support point. The steel casing of the support point is mounted mechanically onto a concrete block with a transfer structure, so the loads get forwarded to the concrete structure of the bascule chamber.

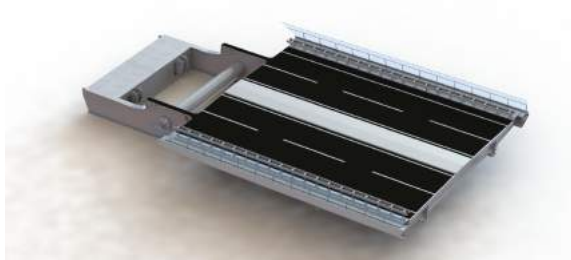


Figure 2.7: Bridge leaf of Amaliabrug. (Nationale Staal Prijs,2022)



Figure 2.8: Bridge leaf of Haringvlietbrug. (Hollandia Infra,2023)



Figure 2.9: Reinforced connection element. (University of South Florida,2003)



Figure 2.10: Trunnion support. (University of South Florida,2001)

Operating system

Controlling the movement of the bridge deck is done by its operating system. This system is either a completely hydraulic or mechanical operating mechanism, because a mix of the two requires more difficult maintenance tasks, which can lead to unnecessary costs (Van Zantvliet, 2015). There are two separate systems present in a bascule bridge. Firstly, the main engine and pinion or piston system in the engine room, which moves the bridge deck. Secondly, a locking mechanism, often called the stabilising machinery, to lock the bridge deck in place, when closed. Standard engine configurations can be seen in figure 2.11.

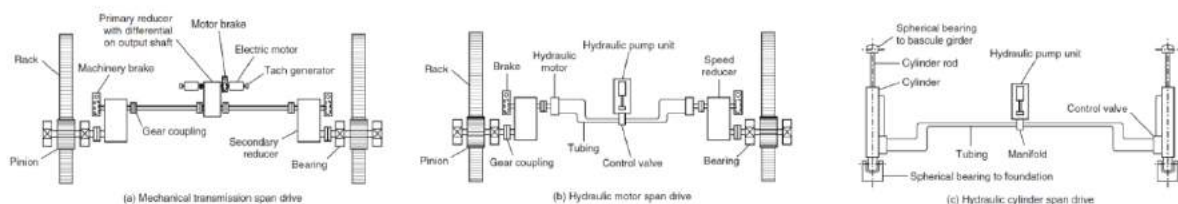


Figure 2.11: Typical operating mechanisms of a bascule bridge. (Parke & Hewson, 2008)

The majority of bridges in Amsterdam are equipped with an electro-mechanical operating system, of which an impression is given in figure 2.13. The main components of a mechanical operating system

that can be distinguished are the panamawheel, push-pull rod, pinion, engine, gearbox, brakes, gear coupling units, axles and bearings. For a hydraulic system, one can identify a hydraulic pump unit, motor, tubing, a speed reducer and bearings.

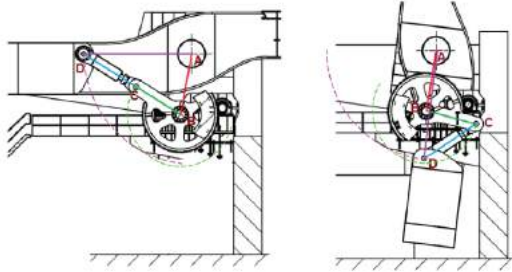


Figure 2.12: Mechanism of a bascule bridge. (Van Zantvliet, 2015)

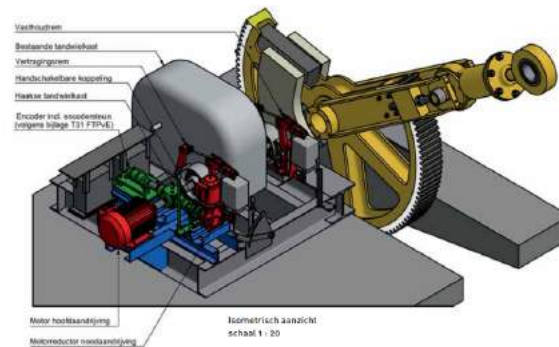


Figure 2.13: Isometric view on operating system. (Movares, 2016)

The engine system activates a smaller pinion by a series of shafts and a gearbox, which in turn, drives the panamawheel. The push-pull rod accounts for small deflections and movements in longitudinal direction of the bridge. It contains a spring, which takes up the extra forces acting on the mechanism due to the leaf moving. The rod connects the leaf with the large wheel, and is connected by hinges on both ends. A view of a closed and open situation of a generic bascule bridge, is shown in figure 2.12. The push and pull rod is usually connected with the leaf, either directly to the main beam, or onto the counterweight, with an additional steel fin. Examples of these connections are shown in figures 2.14 and 2.15 respectively.



Figure 2.14: Hinged connection between push-pull rod and main beam. (ipv Delft, 2023)

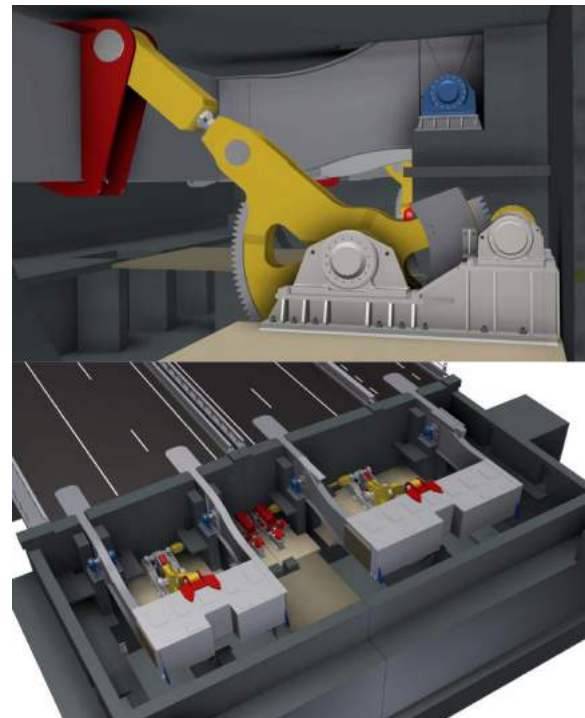


Figure 2.15: Operating system of Ketelbrug. (Nationale Staal Prijs, 2022)

The size and configuration of the operating system depends largely on the design space and requirements, and is highly variable. The types of engine and driving mechanism, and sizes of panamawheels,

gear racks, couplings, shafts and pinion wheels are all variable. As can be seen in the bottom of figure 2.15, the engine and drive components are located in the center of the bascule chamber. The drive connects to both pinions with a long intermediate axle, to reduce the forces on the engine system. Configuring the operating system is up to the responsible engineer, unlimited possibilities are possible to configure such a system.

Stabilizing system

At the toe of the leaf, a stabilizing operating system makes sure that the bridge deck is fully closed and locked in place. According to Moen (2014), the stabilizing system is comprised of five main elements. Firstly, the live load shoe, which takes up the live traffic loads acting on the bridge. Steel notches are made in the main steel girders of the bridge deck, which make contact with a steel plate on top of the supporting pier. Secondly, the lock and anchor system. This is schematized in the bottom of figure 2.3. The lock makes sure that there is good contact between the live load shoe and its support plate. Part of the stabilizing system are the engine brakes, which makes sure that the leaf closes and opens within a certain time frame, and which lock the bridge in place, either in closed or open position. This means that the brakes need to be able to withstand a large wind load, when the bridge is in open position (Moen, 2014). Part of the stabilizing system are also buffering cylinders. In case of operating system failure, which could be engine, brake or electrical failure, the bridge leaf can impact the rest piers with large force. Buffering cylinders are meant to take up as much of the energy in case of an emergency impact. Lastly, placement of bumper blocks inside of the engine room, is also part of the stabilizing mechanism. These are simple devices which prevent the bascule leaf from opening too far, to mitigate the risk of damage.

In case of a double leaf bascule bridge, the toe ends of the leafs meet each other in the middle of the span. The toes interlock with each other, with a locking and anchor system that is built onto the main girders of both bridge leafs.

Bearings

Bearings are important components within the operational system of a bascule bridge, and guarantee that the moving parts of a bascule bridge can operate safely and smoothly. Bearings are mainly found inside the support points of the rotational axis, shown in figure 2.10, and in between axles and components of the engine and driving mechanism. Within the supports, the type of bearing applied is usually a spherical roller bearing, which requires less maintenance and has a higher life span, compared to bronze sleeve bearings, which have been applied in most older bascule bridges (Detweiler, 2008) (Moen, 2014).

Basculer chamber

The basculer chamber houses the operating system of the bridge, and provides a protected environment for the counterweight. A basculer chamber is a concrete structure, built on a (underwater) concrete floor slab, which is connected to the foundation piles. Its dimensions are highly dependent on the size of the bridge leaf and counterweight, and thus also on the dimensions of the operating system that is required. Typical basculer chambers are shown in figures 2.16 and 2.17. The left figure shows a basculer chamber for a large basculer bridge, which has multiple floors and a walkway around the counterweight pit. The figure on the right shows a basculer chamber for a smaller basculer bridge, in which the operating system is also located in between the two main girders of the bridge leaf.



Figure 2.16: Bascule chamber Amaliabrug. (EPC-Groep,n.d.)



Figure 2.17: Bascule chamber Ouderkerk.(Van Hattum en Blankevoort,n.d.)

Adequate attention must be spent on the layout of a bascule chamber. The operating system and electrical systems must be reachable for inspection and maintenance. The counterweight must not interfere with any objects or people. As shown in figure 2.17, which shows a bascule bridge under construction, the bridge leaf and counterweight precisely fit into the bascule chamber. A transfer structure of steel and concrete is placed, to transfer the forces of the trunnion support to the concrete structure of the bascule chamber. Such a transfer is also shown in the next two figures, which show the conceptual design of a generic bascule chamber for a smaller size bascule bridge. Bridges of similar dimensions are found in Amsterdam. To create a small bascule chamber as possible, the electro-mechanical drive system is placed in between the main beams. just below the steel structure. A walkway is present around the pit, to be able to access the platform that hosts the machinery. A staircase is present to access the bottom level and its installations.



Figure 2.18: Conceptual design of bascule chamber Elizabeth Admiraalbrug. (IB Amsterdam,2023)



Figure 2.19: Conceptual design of bascule chamber Elizabeth Admiraalbrug. (IB Amsterdam,2023)

Substructure

For the substructure, one can also identify the foundation, abutments and intermediate support piers. The focus of this thesis is on the steel bridge leaf, therefore these components were not considered in the literature study.

2.2. Structural Bridge Design

This paragraph will zoom into the structural design of the bridge leaf. The following sub-question is answered in this paragraph:

1. What loading effects and which verification checks should be considered in the structural design procedure of the bridge leaf?

Firstly, a description of its structural system and load transfer will be given. Afterwards, an overview of loading acting on the bridge leaf of a bascule bridge, is given. Concluding is a summary of the structural verification procedure, both for the cross section of the bridge deck, as well for the individual

members and cross-sections of the orthotropic bridge deck. For the exact procedure, the Eurocode can be consulted, this chapter is intended to give an overview of what should be taken into account specifically for the bridge leaf, so that generated bridge designs within the workflow, can be verified adequately.

2.2.1. Structural system

A detailed view of an orthotropic bridge deck is given in the figure below. The troughs/ribs of the bridge deck are welded onto the steel deck plate. They increase the torsional stiffness of the deck plate. Structurally, the ribs and deck plate work as one element. The aim is to design the troughs continuously, as can be seen in figure 2.21. Troughs have a limited length, they are connected to each other with stiffeners or mechanical connections. Stiffeners are usually placed at points where the bending moment acting on the bridge in longitudinal direction, is low. In case for a bascule bridge, this is less relevant, since the movable part is only one span, so troughs usually span the whole required distance.

The cross beams have openings for the troughs to go through. The troughs are then welded to the cross beams. However, not along the complete opening. To reduce peak stresses occurring at the bottom of the ribs, as result of cyclic loading, cope holes are created. Lastly, the cross beams are firmly welded to the main girders, with the top of the flanges aligning. In some cases, extra web stiffeners underneath the cross beams are placed, for better load transfer towards the main girders.

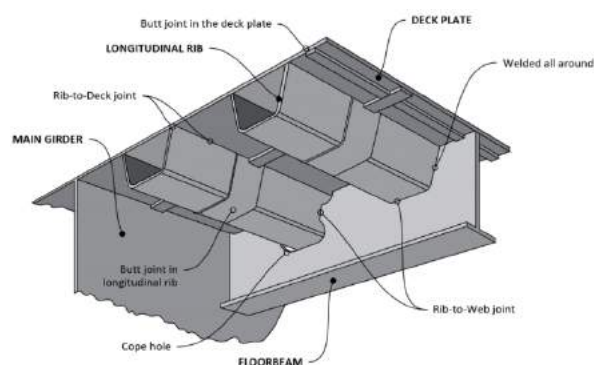


Figure 2.20: Components of an orthotropic bridge deck.(Connor et al.,2012)



Figure 2.21: Connection between troughs and cross beams.(Connor et al.,2012)

Often, standard profiles are chosen for the ribs and cross beams. I-shaped profiles for the cross beams like IPE and HEA are often applied. For the open and closed rib profiles shown in figure 2.6, also standard profiles are chosen. The main beams of a bascule bridge deck, are usually custom, and consist of box girders or I-shaped sections which consist of steel plates that are welded together. From the counterweight up until the bridge deck, the width of the main beams is constant. The profile inside the bridge deck is usually slightly wider or slimmer.

Load transfer

The steel plate and its troughs act as one stiff element. They transfer the load towards the system of main and cross beams. Eventually, all loading gets transferred to the main beams. This is done on global and local scale. On global scale, the bridge deck plate and the troughs act as the top flange of the bridge cross section. The membrane stresses get forwarded from the plate to the cross beams through the ribs, as can be seen in the top of figure 2.22. Locally, loads are transferred through bending of the deck in both longitudinal and transverse direction. In transverse direction, the cross beams directly transfer the loads to the main beams, while in longitudinal direction, the stiffeners together with the corresponding width of the deck plate, transfer the load to the main girders. Lastly, loads are transferred due to local bending of the deck plate between the stiffeners, in case of high point loads, which is shown in figure 2.23.

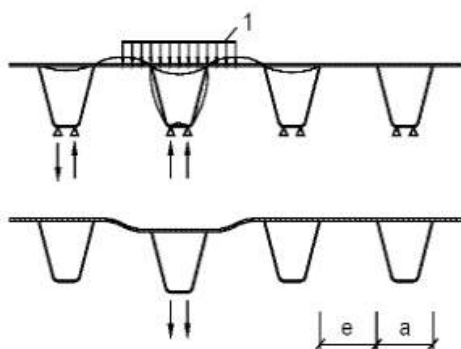


Figure 2.22: Membrane action of the bridge deck and troughs (top) and bending of the deck plate (bottom). (Pavlovic, 2022)

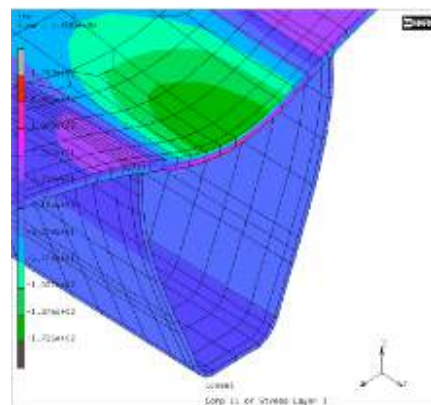


Figure 2.23: Local bending of the bridge deck due to high point load. (Pavlovic, 2022)

This complex system of load transfer, leads to an extensive structural analysis, where peak stresses throughout the whole structure should be checked. Also because of the large amount of load cases and combinations which a bridge deck needs to withhold, bridge decks are usually calculated with software, where the engineers' expertise judges the outcomes.

Eventually, the main beams transfer the loads to the support points of the bridge leaf. In closed position, the main girders can be schematized as beams that are supported on four hinges. The four support points are at the toe of the leaf, at the abutment before the bridge span, at the rotational axis and if applicable, the push-pull rod attached to the counterweight. In opened position or during opening, the system can be schematized as a simply support beam on two support points. In this situation the bridge leaf is supported at the rotational axis and by the push-pull rod of the operating system.

2.2.2. Loading

The structural design procedure of the components of a bascule bridge, follows the standard procedure with loading combinations, as specified in NEN-EN 1990 and NEN-EN1991-1. Additionally, for movable bridges, NEN6786 should be consulted, which is the VOBB ("Voorschriften Ontwerp Beweegbare Bruggen"). This code describes additional load cases that a movable bridge must be able to resist, which are mostly related to extra wind loads, traffic and dynamic loading from the movable parts. Summarizing, the following norms are used in the structural design procedure for a bascule bridge:

- NEN-EN 1990
- NEN-EN 1991
- NEN-EN 1992
- NEN-EN 1993
- NEN 6786-1:2017+C1:2021 Beweegbare bruggen (VOBB)

The forces acting on the components of a bascule bridge can be divided under two categories, permanent loading and variable loading. For an orthotropic bridge deck in a movable bridge, fatigue is also of great importance. In the following two sections, a concise overview is given on the loading and condition classes that apply to bascule bridges. Eurocode specifies four types of loading, these are:

- Permanent loading G
- Variable loading Q
- Accidental loading A
- Fatigue

The following types of permanent and variable loading are applicable for the bridge deck of a bascule bridge. For a bascule bridge, loading on the bridge must be considered in closed state (static), during opening of the bridge and in opened stance (NEN 6786-1:2017).

- Self-weight
- Snow loading
- Wind loading
- Traffic loading
- Fatigue
- Creep
- Friction and roll resistance
- Thermal loading
- Accidental loading
- Loading due to operation of the bridge.

Which types of loading and to what extent they should be taken into account, is also dependent on the traffic profile of the bridge. Three cases can be distinguished, namely a regular traffic bridge, a cycle- and pedestrian bridge with an incidental vehicle and without an incidental vehicle. Extra structural verification checks should be performed if there are also tram tracks on a bridge. Creep and loading of the operating mechanism onto the bridge leaf, are not considered in this thesis, since their description in the Eurocode is already limited.

Self-weight

The self weight of the structure is the only permanent load acting on the structure. The nominal masses and densities of materials of the structure are used, which are named in the Eurocode. In addition to the self-weight of the main girders, cross beams, troughs and deck plate, also the self-weight of attributes on the bridge deck such as parapets, the deck finishing and road dividers must be taken into account(NEN 6786-1:2017).

Snow loading

Snow loading should be taken into account as variable load in the load combinations, as defined in NEN-EN1991-1-3. It should only be considered in load combinations for the closed position of the bridge(NEN6786-1:2017).

Wind loading

Wind loading plays an important role in the calculation procedure for a bridge leaf. Especially for large, single span bridge leafs, wind loading is significant during the operational cycle and in opened stance. Wind loading must be taken into account both during and outside of the movement cycle of the bridge. Therefore, four different scenario's can be distinguished, namely the closed position, opened position, during opening of the leaf and during closing of the leaf(NEN-EN 6786-1:2017).

The procedure for calculating wind loading on a bridge deck is explained in more detail in section C.1 of appendix C.

Traffic loading

Traffic is a form of variable loading on the bridge deck. Four load models are used in the Eurocode, to simulate vertical traffic loads. These are:

- LM1: Concentrated and uniformly distributed loads
- LM2: A single axis load
- LM3: Special vehicles
- LM4: Crowd loading

In addition, traffic can also cause horizontal loading on the bridge deck, due to accelerating and braking. Rail traffic can also cause horizontal loading.

An explanation of the different traffic load models and their calculation procedure, is given in section C.2 of appendix C.

The simultaneous occurrence of the previously mentioned load models, is accounted for in traffic load groups. The load groups that have to be checked, that are built up of the characteristic values for load models, are mentioned in the next table.

Table 2.1: Definition of groups of traffic loads.(NEN-EN1991-2:2003+C1:2015+NB:2019)

Belastings-type	Rijweg						Voet- en fietspaden
	Verticale krachten				Horizontale krachten		Alleen verticale krachten
Verwijzing	4.3.2	4.3.3	4.3.4	4.3.5	4.4.1	4.4.2	5.3.2.1
Belastings-systeem	BM1 (TS en UDL)	BM2 (enkele as)	BM3 (bijzondere voertuigen)	BM4 (mensenmenigte)	Rem- en versnellingskrachten	Centrifugaalkrachten en krachten in dwarsrichting	Gelijkmatig verdeelde belastingen
Groepen van belastingen	gr1a	Karakteristieke waarde			$0,8 \times$ karakteristieke waarde	$0,8 \times$ karakteristieke waarde	$0,4 \times$ karakteristieke waarde
	gr1b		Karakteristieke waarde				
	gr2	$0,8 \times$ karakteristieke waarde			Karakteristieke waarde	Karakteristieke waarde	$0,4 \times$ karakteristieke waarde
	gr3						Karakteristieke waarde ^a
	gr4			Karakteristieke waarde ^b			
	gr5	$0,8 \times$ karakteristieke waarde ^c	Karakteristieke waarde		$0,8 \times$ karakteristieke waarde ^c	$0,8 \times$ karakteristieke waarde ^c	
De gearceerde vakken zijn de overheersende belastingscomponent (aangeduid als component behorend bij de groep)							
^a Zie 5.3.2.1. Er behoort slechts één voetpad als belast te zijn beschouwd, indien het effect hiervan ongunstiger is dan bij belasting op twee voetpaden.							
^b Inclusief de belasting op voet- en fietspaden.							
^c Vast te stellen voor afzonderlijke projecten.							

Fatigue

Given reoccurring traffic loads onto the bridge deck, and the bridge deck opening and closing, fatigue is an important aspect to consider when designing a bascule bridge. Eurocode mentions five fatigue models to check for fatigue loading. Fatigue load model 1,2 and 3 are meant to determine the maximum and minimum stresses that can occur due to the load groups mentioned in the previous section. Fatigue load model 4 and 5 are meant to illustrate the stress range that can occur due to heavy traffic traveling over the bridge. Additionally, model 1 and 2 are meant to determine whether the fatigue life time of a structure can be assumed to be infinite, under a given value for the constant stress amplitude. Model 1 is more conservative regarding this aspect. Model 3,4 and 5 are meant to assess the fatigue life time of the steel structure, of which model 5 is the most generic model.

Friction and roll resistance

The bridge deck can be susceptible to loading because of the friction resistance between the trunnion and bearings at the rotational axis. A brief description of this loading type is given in section C.4. This is disregarded in this thesis.

Thermal loading

Temperature differences can cause elongation or shrinkage of steel elements, if this movement is obstructed, extra stresses will occur in the bridge leaf structure. This movement should ideally be taken up by the bearings and dilatation joints that are present in a bascule bridge. The VOB states that thermal loading should be calculated according to chapter 6 of NEN-EN 1991-1-5:2003+C1:2009+NB:2019, which is the code for thermal loading.

An explanation of how thermal loading should be calculated is given in section C.5 of appendix C.

Accidental loading

Eurocode makes a distinction between accidental loading due to accidents with vehicles on the bridge deck, or by collision between a vessel and the substructure of the bridge. The procedure for determining these loads is explained in section C.6.

The design goals for a structure include measures to prevent collisions from happening, or to minimize damage if a collision does occur. In Amsterdam, most bascule bridges are located in the city center, where traffic speeds are low. Meaning that, the chances of significant collisions with vehicles and bridge components is minimal. Nonetheless, it is useful to protect important structural elements from collision. An example are timber fender structures in the fairway, which prevent vessels from colliding with the bridge's substructure, raised sidewalks and cycle paths and raised road dividers or kerbs.

Loading due to operating mechanism

Opening and closing the bridge leaf leads to an interaction of dynamic forces between the operating mechanism and the steel structure. The VOBG gives a detailed description of the loading onto the mechanical driving system of a bascule bridge, but not about the occurring forces within the steel bridge leaf due to operation. Closing and opening of the bridge leaf leads to radical stress changes in the steel structure, increasing the possibilities of fatigue (Moen, 2014).

2.2.3. Pedestrian and cycle paths

For dedicated pedestrian- and cyclebridges, and pedestrian and cycle paths on traffic bridges, separate traffic loading rules, additional accidental loading and additional dynamic loading rules apply. These are explained in section C.7.

Traffic loading

Similarly to what is applicable for heavy traffic bridges, traffic loading on pedestrian and cyclebridges should be applied in load groups. These load groups are defined in table NB.10 in section 5.5 of NEN-EN 1991-2:2003+C1:2015+NB:2019.

Accidental loading

For pedestrian- and cycle bridges, a different loading situation should be regarded for accidental loading, which is when a vehicle accidentally ends up on the bridge. In this case, a vehicle with two different axle loads should be applied on the bridge deck. This also holds for pedestrian and cycle paths on bridges designated for regular traffic, in which a clear curb is present between the road and cycle path.

Dynamic loading

Pedestrian bridges are susceptible to dynamic loading due to for example pedestrian traffic and wind. When pedestrians travel over the bridge in a certain rhythm, the structure can start to resonate, when one of its eigenfrequencies is reached. According to NEN-EN 1991-2, the relevant eigenfrequencies of the structure, should be determined for vertical, horizontal and torsional vibrations. Dynamic load models for both regular pedestrian traffic and joggers are named in annex NB.I of NEN-EN 1991-2:2003+C1:2015+NB:2019.

Pedestrian bridges are assigned a traffic class, ranging from TC1 to TC5, and a joggersclass, ranging from JC1 to JC3. For regular use, dynamic loading should be based on classes TC3 and JC2, unless specified differently in the project requirements. The procedure to determine the dynamic loading is explained in section C.7.3.

2.2.4. Structural Verification

To ensure a sufficient design for the bridge leaf, it must be able to withstand the loading to which it is subjected, during its design life time. According to EN 1990, a structure must be designed so that it can resist all of the loading that is applied onto the structure, and that it complies to all of the usability criteria for both individual components and the whole structure. To guarantee this, the structure must provide enough strength, stiffness and stability, which is assessed using two limit states. These are

the ultimate limit state and serviceability limit state. These will be explained below. NEN-EN1990 first defines how the design values for loading, material properties, geometrical properties and resistance come about, following from their respective characteristic values.

Design values

Design values of material properties are given by:

$$X_d = \eta \frac{X_k}{\gamma_m} \quad (2.1)$$

where:

X_k is the characteristic value of the material property.

γ_m is the material factor, which takes into account uncertainties in properties.

η is the average value of the conversion factor. Which is a factor that takes into account volume scaling, time and moisture effects.

η is often substituted by a factor combined with the partial factor γ_m , which is named as γ_M .

The design values of loading F_d are given by the following set of equations.

$$F_d = \gamma_f \cdot F_{rep} \quad (2.2)$$

and

$$F_{rep} = \psi \cdot F_k \quad (2.3)$$

where:

F_k is the characteristic value of the load.

F_{rep} is the representative value of the load.

γ_f is the partial load factor, which takes into account the possibility of unfavorable deviations in the loading.

ψ is the load combination factor, which takes into account the simultaneous occurrence of different loading types. This value is used in load combinations, which are described at a later point in this paragraph. ψ is equal to 1.0, ψ_0, ψ_1 or ψ_2 .

The design value of the eventual resistance of a structure or element, is dependent on the material factor named above, and geometrical deviations within the model. These geometrical inaccuracies are defined per construction type and building material, in EN 1991 to EN 1999. Hence, on global scale, it can be said that the resistance of a component is given by equation 2.4, which is of similar nature as equation 2.1.

$$R_d = \frac{R_k}{\gamma_M} \quad (2.4)$$

Ultimate Limit State

The ultimate limit state governs the safety of the structure in terms of strength and stability, both for the whole structure and for individual structural elements. The structure must be able to resist excessive loading without members failing or loss of equilibrium of the whole structure. Additionally, this load situation is used to investigate whether a structure is prone to fail due to fatigue.

Stability

This limit state considers the loss of equilibrium of (parts of) the structure. To guarantee the stability of the structure, the following must hold:

$$E_{d,dst} \leq E_{d,stb} \quad (2.5)$$

where:

$E_{d,dst}$ is the design value for the destabilising load effect.

$E_{d,stab}$ is the design value for the stabilising load effect.

The structure and its individual structural components must be checked for (NEN-EN 1990:2002+A1:2019 +NB:2019) (Moen, 2014):

- Buckling
- Lateral-Torsional Buckling
- Flexural-Torsional Buckling
- Local Instability
- Rigid body movement

Strength

When a limit state of failure or excessive deformation of a structural element or connection is considered, the strength of the cross section of the individual members is verified. The following must hold:

$$E_d \leq R_d \quad (2.6)$$

where:

E_d is the design value of the loading effect.

R_d is the design value of the respective resistance.

The cross-sections of all members need to be able to withstand (NEN-EN 1993-2):

- Axial tensile and compressive forces ('N')
- Bending moments over both axes ('M')
- Shear ('V')
- Torsion
- Combinations of the above mentioned forces

Serviceability Limit State

The serviceability limit state describes limits regarding the functionality, comfort and aesthetics of a structure. For steel bascule bridges, stress limitations, displacements and vibrations are relevant to consider with the SLS loading combinations. For the serviceability limit state, it must be made sure that:

$$E_d \leq C_d \quad (2.7)$$

where:

C_d is the upper boundary of the design value of the design criterion.

E_d is the design value of the loads that result from the loading combination.

Chapter seven of NEN-EN1993-2 names six usability criteria for steel bridges. These are:

- Limitation of the elastic behaviour
- Limitation of displacements and curvatures
- Limitation of the eigenfrequencies
- Limitation of the plate slenderness, mainly to prevent web breathing
- Improved durability by appropriate detailing to reduce corrosion and unnecessary wear
- Guarantee comfortable maintenance and repair works

In this thesis, the scope for serviceability limit state checks, is limited to stress checks, displacements and vibrations.

Stress limitations

It must be made sure, that during serviceability limit state conditions, where the partial factors in the loading combinations are equal to one, the plastic behaviour of components is not reached. Even though the structure suffices the ULS strength criteria, it could still occur that the plastic strain region of components is reached under SLS loading situations. Meaning that additional deformations can still occur over time. Therefore, checks are in place for SLS situations, to make sure that the yield strength of the components is not surpassed. Two checks need to be done, for the characteristic and frequent load combination.

For the characteristic load combination, three requirements must hold, when taking into account the shear lag effect of the bridge cross section. These are:

$$\sigma_{Ed,ser} \leq \frac{f_y}{\gamma_{M,ser}} \quad (2.8)$$

$$\tau_{Ed,ser} \leq \frac{f_y}{\sqrt{3}\gamma_{M,ser}} \quad (2.9)$$

$$\sqrt{\sigma_{Ed,ser}^2 + 3\tau_{Ed,ser}^2} \leq \frac{f_y}{\gamma_{M,ser}} \quad (2.10)$$

where:

$\gamma_{M,ser}$ is equal to one according to the national annex.

For the frequent loading combination, one criteria must be met:

$$\Delta\sigma_{fre} \leq 1.5 \frac{f_y}{\gamma_{M,ser}} \quad (2.11)$$

where:

$\Delta\sigma_{fre}$ is the nominal stress range due to the frequent loading combination.

Fatigue

Cyclic loading can result in loss of strength and stiffness of the structural elements of the bridge. Therefore, the elements must be able to withstand a number of repeated loading cycles, before replacement is needed. Fatigue loading for steel structures is described in NEN-EN 1993-1-9:2006+C2:2009+NB:2011 and its application onto steel bridges in chapter 9 of NEN-EN 1993-2:2007+C1:2009+NB:2011. The resistance to fatigue loading is calculated separate from the load combinations with permanent, variable and accidental loading.

According to NEN-EN 1993-2, it is allowed to only take into account fatigue load model 3 for steel bridges. Based on this traffic model, the amount of stress changes during the lifetime of the structure, and the maximum stress interval over which the stresses change, is determined. The damage effects of fatigue should be calculated with the equivalent stress interval for $2 \cdot 10^6$ cycles. This is given by:

$$\Delta\sigma_{E,2} = \lambda\phi_2\Delta\sigma_p \quad (2.12)$$

where:

λ is the equivalent damage factor, which is calculated according to section 9.5 of NEN-EN 1993-2:2007+C1:2009+NB:2011.

ϕ_2 is the damage equivalent impact factor, which is 1.0 for traffic bridges, since this factor is already incorporated in the fatigue load model.

Δ_p is the fatigue stress interval, obtained from applying fatigue load model 3 onto the bridge.

To satisfy the fatigue requirements in ultimate limit state conditions, the following equations must hold:

$$\gamma_{Ff}\Delta\sigma_{E2} \leq \frac{\Delta\sigma_c}{\gamma_{Mf}} \quad (2.13)$$

and

$$\gamma_{Ff} \Delta \tau_{E2} \leq \frac{\Delta \tau_c}{\gamma_{Mf}} \quad (2.14)$$

where:

γ_{Ff} is the partial factor for the fatigue load, which has a value of 1.0.

γ_{Mf} is the partial factor for the fatigue resistance, which should be obtained from table NB.1 in the national annex to NEN-EN 1993-1-9.

$\Delta \sigma_c$ and $\Delta \tau_c$ represent the resistance to fatigue for normal and torsional stress variations, which are obtained with the procedure described in chapter seven of NEN-EN 1993-1-9:2006+C2:2009+NB:2011.

Displacements

No requirements regarding the displacement of the steel bridge leaf, are stated in the Eurocode. Normally, serviceability requirements for bascule bridges are not normative, and a design based on strength and stability suffices. Limitations for the displacements can be put in place when there are requirements for aesthetic reasons. Eurocode states that the bridge leaf structure should be designed in such a way that the displacement in the longitudinal direction is evenly distributed and that there are no abrupt changes in the cross-section which could lead to sudden forces. It also mentions that abrupt changes in slope near translation joints need to be prevented. For bascule bridges, this is less important, given that the bridge leaf has more space to elongate than a continuous bridge deck of a fixed bridge with translation joints. In practice, bridge decks are designed with an upwards camber, and a design rule is that the bridge deck should not deflect past the horizontal line between the supports.

Load combinations

Design values of the loading effect, are calculated with fundamental load combinations. These are given by equations 6.10a and 6.10b in NEN-EN 1990:2002+A1:2019+NB:2019¹:

$$\sum_{j \geq 1} \gamma_{G,j} G_{k,j} + \gamma_{Q,1} \psi_{0,1} Q_{k,1} + \sum_{i > 1} \gamma_{Q,i} \psi_{0,i} Q_{k,i} \quad (2.15)$$

$$\sum_{j \geq 1} \epsilon_j \gamma_{G,j} G_{k,j} + \gamma_{Q,1} Q_{k,1} + \sum_{i > 1} \gamma_{Q,i} \psi_{0,i} Q_{k,i} \quad (2.16)$$

Load combinations for extraordinary and earthquake loading situations are not considered in this thesis.

For serviceability limit state conditions, load combinations for characteristic and frequent loading are considered. The characteristic load combination in SLS is given by:

$$\sum_{j \geq 1} G_{k,j} + Q_{k,1} + \sum_{i > 1} \psi_{0,i} Q_{k,i} \quad (2.17)$$

and the frequent loading combination is given by:

$$\sum_{j \geq 1} G_{k,j} + \psi_{1,1} Q_{k,1} + \sum_{i > 1} \psi_{2,i} Q_{k,i} \quad (2.18)$$

The material factors, partial factors and psi-factors used to calculate the loading on the structure and the resistance of components, can be deducted from the Eurocodes and annexes named in this paragraph. It is still noted that for steel bridges, extended rule sets apply for the combination factors ψ_i , which are presented in annex A2.2 of NEN-EN 1990. Tables can be found for traffic bridges, pedestrian bridges and rail bridges. Some important rules to consider are:

- Wind and snow loads should not be combined with traffic load groups 2,3 and 4.
- Snow loads should not be combined with traffic load group 1.
- Wind and thermal loading should not be combined.
- Combination value of wind load resulting in loading equivalent to $v_{b,0} > 23 \text{ m/s}$ should not be combined with traffic load group 1a.

¹The pre-stress force P is left out of the equations.

Vibration

In addition to the SLS, ULS and fatigue checks on the structure, attention should be paid towards vibrations. The amount of vibration within a structure must mainly be limited for the comfort of the user. A vibrating bridge is unpleasant to travel over, and significant vibrations due to resonance can lead to other defects. The response of a bridge to dynamic loading must be addressed and analyzed adequately. The behaviour of cyclic loads on the structure must be known, as well as the eigenfrequencies of the structure. It must be made sure that the eigenfrequencies of the structure do not coincide with those of any of the load cases on the bridge. Wind and traffic loading are the main loads that need to be analyzed. As mentioned in NEN-EN 1991-2, pedestrians can exert a periodic force in both vertical and horizontal direction, within a frequency range of 1 to 3 Hertz, and 0.5 to 1.5 Hertz, in respective directions. Groups of joggers can exert a force with a frequency of up to 3 Hertz in horizontal direction.

Performance requirements for vibrations are named in NEN-EN1990, for traffic bridges and pedestrian bridges separately. For traffic bridges, no strict requirements are named. Vibrations due to traffic and wind should be assessed using their respective Eurocodes, and requirements for vibrations should be declared in a project's requirements. Eurocode does specify that this should be dependent on the uplifting force at support points, and the potential damage on support points.

For pedestrian bridges, requirements are named for the maximum acceleration due to wind and traffic. The maximum acceptable acceleration for a random part of the bridge deck is:

- 0.7 m/s^2 for vertical vibrations due to normal traffic use and wind.
- 0.2 m/s^2 for horizontal vibrations due to normal traffic use and wind.

Assessment to this criteria should only be done in case the eigenfrequency of the bridge leaf is lower than 5 hertz for vertical vibrations and 2.5 Hertz for horizontal and torsional vibrations. Additional requirements for vertical vibrations can be taken up in a project's program of requirements if necessary.

The structural verification procedure of the bridge design alternatives generated in chapter 5, is done for only three normative load combinations in ULS conditions, where the bridge leaf is in closed position.

2.3. Machine Learning

This section describes theoretical background about machine learning and the neural network algorithm. The following sub-question is answered:

2. *What is a neural network algorithm and how does it work?*

2.3.1. Theory

A universal definition of machine learning does not exist. Generally speaking, it could be said that machine learning deals with algorithms that learn from large data sets. A formal definition is given by Mitchell (1997): "A computer program is said to learn from experience E with respect to some task T and some performance measure P, if its performance on T, as measured by P, improves with experience E". This translates into a more subtle definition described by Nasteski, who says that machine learning is about algorithms that learn by finding patterns and statistical regularities in data, and whom can predict expected performance based on new input data (2017). Machine learning algorithms should represent the human approach to learning some task, thus by gaining experience from data sets.

Machine learning algorithms are applied in different work fields such as computer science, social media and the medical field. It has yet to see its introduction into practice within the civil engineering world. There have been some experiments, such as structural health monitoring of assets (Vilhjálmsón, 2023). However, the topic of analyzing bridge data with a machine learning algorithm, is yet to be done.

According to Alzubi et al. (2018), machine learning algorithms are applied to reach two goals. Firstly, to

automate tasks performed by human beings. Generally speaking, humans perform countless of repetitive tasks each day. Machine learning can be applied to assist or take over some of these repetitive tasks, saving time, as well as perform them with a consistent accuracy. Which in people, could be influenced by factors such as fatigue. Secondly, machine learning algorithms can be used to perform tasks that are beyond human capabilities.

Machine learning model

A machine learning model has three features, that need to be defined (Alzubi et al., 2018). These are the task to be learned, the performance measure to be improved, and the definition of the learning process. The components of a generic machine learning model are shown in figure 2.24.

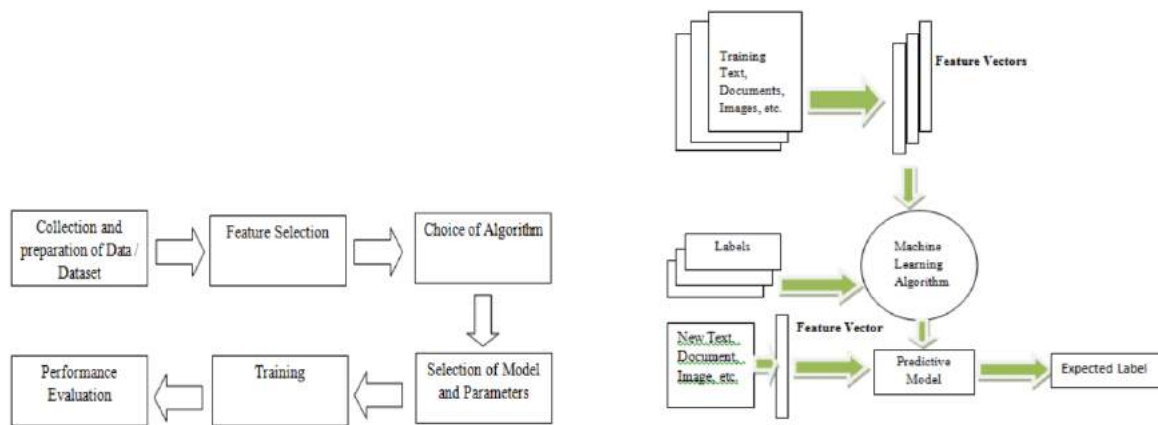


Figure 2.24: Components of a generic machine learning model. (Alzubi et al., 2018)

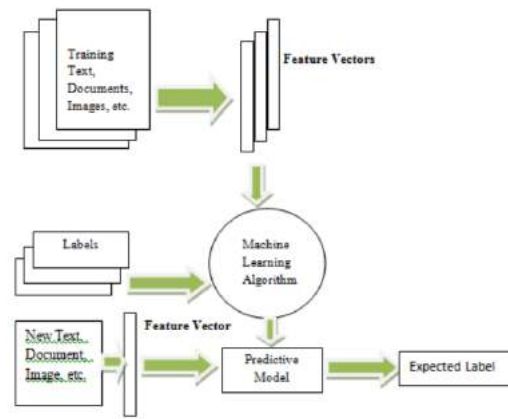


Figure 2.25: Supervised machine learning model. (Dhage & Raina, 2016)

Firstly, it must be decided what data will be used, and this data must be collected in a structured database. Next, a selection of features must be made, which are deemed to be useful for the machine learning procedure. With these features and the goal of the machine learning model in mind, a choice for a machine learning algorithm can be made. After the configuration of the machine learning environment has been set, the model can be trained with a training data set. Its performance can then be evaluated using a testing data set.

The following sections give a concise description of the supervised neural network algorithm that has been used in the Grasshopper workflow. The algorithm predicts values for the output parameters. Hence, it solves a regression task.

Supervised Learning

A supervised learning model uses labeled input and output data. It learns from examples and knows to generate an output with the same labels or attributes. Based on its knowledge, it can give a prediction of the performance P of the generated solution. The advantage of using a supervised learning model, is that it is highly accurate, and that there is more transparency into how a predicted solution comes about (Keen, 2022). A disadvantage is that it requires an organized data set, where the data is structured according to labels or attributes. This is often not the case in practice (Keen, 2022). In figure 2.25, a schematization of a supervised learning model is given.

Supervised learning models can be categorized further into classification or regression problems. In a classification problem, a generated solution or new piece of data, is classified under a label, based on linear decision boundaries. The goal is to group items that have similar properties (Osisanwo, 2017). Understanding the working of such a method, can best be compared to answering a closed question with either yes or no. For example, whether an e-mail is spam or not. The e-mail is then classified under the label spam, or not, after which it gets forwarded to the inbox. The outcome of a regression problem is a continuous value, which describes a relationship between two attributes within the data set. An example is shown in figure 2.26. The linear regression line, shows the relationship between the

two attributes, often calculated based on the minimal mean square error(Wang,2003). One attribute might thus be dependent on the other.

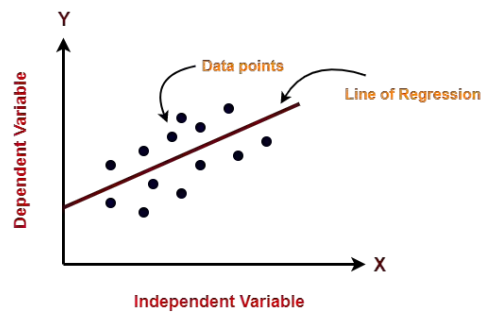


Figure 2.26: Linear regression model.(Sharma, 2022)

Artificial Neural Networks

A neural network is a series of algorithms that try to find relations between labels in a data set. Operation of these algorithms is inspired by biological neural networks(Mahesh,2018)(Gupta,2013). According to Gupta, ANNs are massive parallel computing systems, which consist of large amount of processors connected with many connections, which mimic the human brain with all of its neurons and neural wiring(2013). An artificial neural network consists of an input layer, one or multiple hidden layers and the output layer, as schematized in figure 2.27. The figure shows a simple neural network, with two input attributes, one hidden layer with three neurons, and one output attribute. The hidden layers of neurons perform the calculations and data transformations required to learn the task.

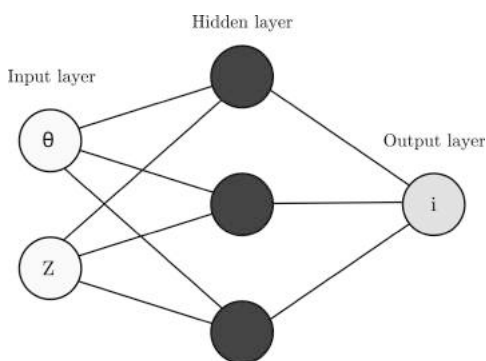


Figure 2.27: Simple neural network.(Pannell et al., 2022)

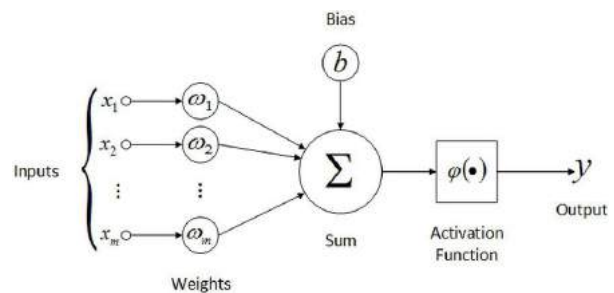


Figure 2.28: Mathematical operation between two nodes. (Prasad, 2021)

A neural network algorithm, learns a task and gives a prediction, by forwarding data through a series of operations, processed in hidden layers. Every connection between two nodes can be seen as a mathematical operation, with a weight attached to it, as illustrated by figure 2.28. The nodes act as activation function, and also add a bias value to the received data. This bias value is added on or subtracted from the data value, before it reaches the activation function inside the node. The node itself functions as an activation function, which helps the algorithm steer the data in the correct direction. Different types of activation functions exist, which are explained in the next paragraph. After the data is processed by the activation function inside the node, its output gets forwarded to the next node. The data finally gets forwarded to the nodes in the output layer. The predictions that roll out of the output layer, can thus be seen as the result of different calculations and data transformations that occur within the neural network. Neural networks usually have a complex dimension space. In practice, multiple input and output variables are determined, which require a neural network with a more complex architecture, in order to reach accurate results.

Similar to a human brain, the neural network has to learn what task it has to perform, which means that values have to be determined for the weight of every connection and bias of every node. The

algorithm learns based on a learning algorithm, which is applied onto a training data set. Neural network algorithms often make use of a learning algorithm called back propagation(LeCun et al.,2002). Initially, values for the weights and biases are assigned randomly by the neural network. In the first iteration with the training data set, the algorithm calculates its first output, which is likely to be far off the real answer. When the output is wrong, the data gets transformed in reverse order through the neural network, to re-establish the weights. The weights get altered to an extent that is related to the magnitude. A neural network needs iteration rounds, to alter the weights and biases, so an accurate solution is reached. The speed of learning is dependent on the complexity of the neural network and its properties. By adjusting the weights and bias values of the connections, the total error of the generated output, described by the mean squared error of equation 2.23, gets reduced over every iteration. At a certain point, the neural network has reached a point where its accuracy does not improve anymore. It could then be said that the algorithm has learned its intended task. The process of finding a correct algorithm configuration and accuracy, is a trial and error process. Building a neural network with more layers and neurons, and training it with more data over more iterations, all improve the accuracy, but also increase the required computing power and time. The application of an algorithm is usually a trade-off between an acceptable level of accuracy and computing time.

Activation functions

Every node within the neural network functions as activation function. In addition to the weight and bias, these also function to redistribute data over the different nodes, and to find relations between the input and output variables. Relevant activation functions are the sigmoid, bipolar sigmoid, linear, rectified linear and threshold functions.

A sigmoid activation function is described by the following equation. Its important properties are that it is a continuous function at any point, and that it outputs a value between zero and one.

$$\sigma(x) = \frac{1}{1 + e^{-x}} \quad (2.19)$$

The bipolar sigmoid function is similar to the sigmoid function, albeit that it ranges from -1 to 1 instead of 0 to 1. It is described by the following equation.

$$\sigma(x) = \frac{1 - e^{-x}}{1 + e^{-x}} \quad (2.20)$$

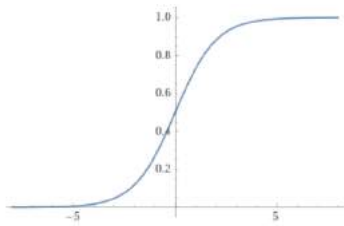


Figure 2.29: Sigmoid activation function.

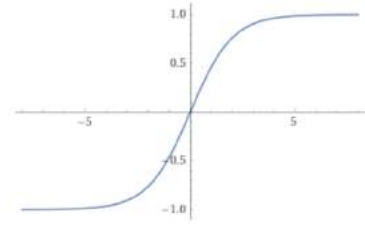


Figure 2.30: Bipolar sigmoid activation function.

The linear activation function is a simple function where $y(x) = x$. Whereas the rectified linear activation function has no negative y values. These activation functions are described by equations 2.21 and 2.22 respectively, and are shown in figure 2.31 and 2.32. Lastly, the threshold or binary step activation function, which has a value of 1, after a certain value of x. This function is shown in figure 2.33, where $y=1$ for x is greater than or equal to zero.

$$y(x) = x \quad (2.21)$$

$$y(x) = \max(0, x) \quad (2.22)$$

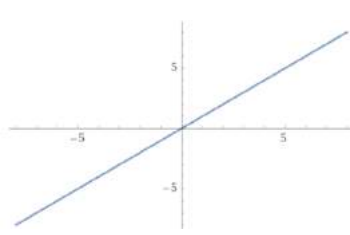


Figure 2.31: Linear activation function.

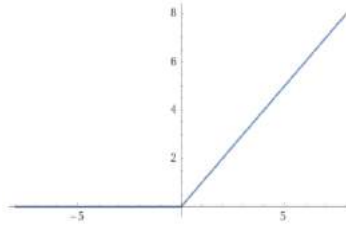


Figure 2.32: Rectified linear activation function.

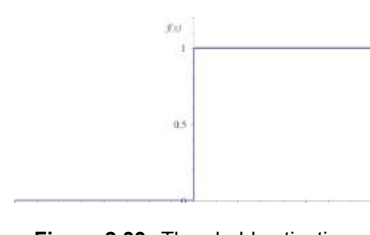


Figure 2.33: Threshold activation function.(Van der Zwaag & Spaanenburg,2004)

The choice for a specific activation function depends on the type of input data and problem to be solved. For a classification problem, threshold functions are suitable for example. When investigating possible relationships between attributes, usually a sigmoid function is applied. Since this activation function can investigate non-linear relationships between variables, while the linear activation functions cannot do so. Other frequently applied activation functions are the arc tangent, and hyperbolic tangent functions. These are derived from the sigmoid function and are similar in mathematical description, therefore are not considered separately.

In application, it must be taken into account that the values of input variables must be normalized to the range of the activation function. After computation, the data can be transformed back to its original format. The choice for an activation function also comes down to trial and error, namely to see which one yields the most accurate results.

Learning rate & momentum

Two additional neural network properties that influence the learning behaviour of a neural network are the learning rate and momentum. The learning rate is a value between zero and one, and regulates the degree to which weights are altered every iteration step(Mitchell,1997). The weights are updated every iteration step, with regards to the extent of the estimated error of the prediction. The learning rate is an extra factor with which the most optimum weight alteration is multiplied. The learning rate essentially describes how much information of the previous iteration step, is considered when updating the weights in the current iteration step. Choosing a low learning rate will result in a neural network that needs many iterations to come to its ultimate loss. Choosing a high learning rate will result in a fast-learning model, but may result in poor prediction performance(Brownlee,2020).

Momentum in a neural network can be best described by relating it to its physical meaning, in which an object continues in a set direction, even though it passes a local force of resistance, which is not big enough to stop it. The same applies to neural networks. Momentum is another factor that influences the weight updates, similarly to the learning rate. Instead of adding a factor to the magnitude of the weight update, like the learning rate does, the momentum adds a factor to the gradient of the loss function(Sutskever et al.,2013). Momentum helps the neural network ignore local extremities, and rather helps the neural network converge to the global optimum solution, instead of getting stuck at a local one. Momentum can help speed up the training process, since it also carries over information of previous iterations. However, momentum can also be used too aggressively, which can lead to oscillations and overfitting.

2.3.2. Model Training & Accuracy

Overfitting & Underfitting

To what extent the algorithm can approximate the training data set with a mathematical model, is described by the loss of the model. Over a series of iterations, the loss of the neural network, described by the mean squared error, should decrease. The mean squared error is given by equation 2.23. Before application of the neural network, a judgement should be made about whether the obtained loss is acceptable. This judgement is based on analyzing whether the neural network is under- or overfit to the training data set.

$$MSE = \frac{1}{n} \sum (y_i - \hat{y}_i)^2 \quad (2.23)$$

Common occurring problems within supervised machine learning models are that of overfitting(Dieterich,1995) and underfitting(Brownlee,2018).

The problem of underfitting can occur when the model has an inadequate or too small training data set, to learn the intended task. The result is that the neural network has a low accuracy after training, which can result in inaccurate predictions. The properties of an underfit model, are that the model has a high bias and low variance. The problem of underfitting can be solved by increasing the capacity of the model. This can be done by increasing the amount of data, and by changing the structure of the algorithm, by adding more nodes and hidden layers.

According to Brownlee, an underfit model is easily addressed and solved. Hence, an overfit model is usually more common(2018). The problem of overfitting can occur when the model has been trained with a training data set that is too large. The model has then found a hypothesis function that describes the training data set, including its peculiarities and outliers, too accurately. The result is that when it encounters new data points, it cannot give an accurate prediction(Brownlee,2018).The properties of an overfit model, is that it has a low bias, but high variance. According to Brownlee, there are two options to approach an overfit model. These are to change the structure of the network by reducing the amount of nodes, or by constraining the weights of the connections, to ensure that they remain small(2018).

Training and validation data set

Assessing whether the neural network fits the data set well, is done by studying the loss values and curves for the training and validation data set. The validation set is a distinctive part of the original training data set, with which the loss of the model is analyzed. This is thus new data that the neural network has not seen yet. Usually, the original training data set is split into the training and validation set in a 2/3 to 1/3 proportion(Olson et al.,2008), but this also depends on the size of the dataset. Firstly, the neural network is trained with the training data set. It is then retrained with the remaining validation data set. There are certain rules of thumb to judge the working of the neural network(Brownlee, 2019).

The neural network is a good fit to the training data set if:

- The values for the training set loss and validation set loss are low and both of equal magnitude.
- The loss curves of both the training and validation data set follow a typical exponential decrease curve, and are closely together, like shown in figure 2.34.

Judging whether a neural network model is underfit can simply by done by observing the learning curve of the training data set(Brownlee,2019). When the neural network cannot learn the training data set, the loss curve is either flat, or very noisy with a high loss value. This indicates that the model needs more complexity or epochs to learn the training data. Examples of an underfit model can be seen in figure 2.35.

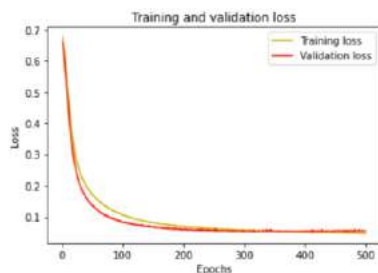


Figure 2.34: Model with a good fit.(DigitalSreeni,2020)

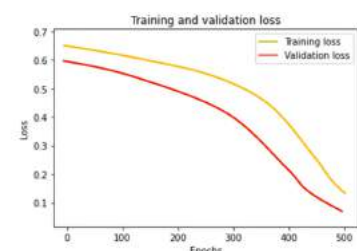
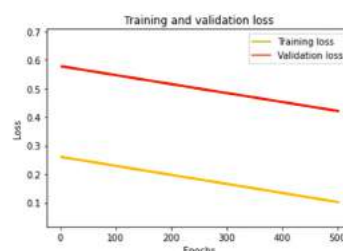


Figure 2.35: Two example learning curves of an underfit model. (DigitalSreeni,2020)

The neural network is overfit if the model has learned the training data set too specifically. When a model is overfit, a gap starts forming between the training and validation loss curves, like shown in figure 2.36. This means that the model has been trained for too long, or that the neural network's architecture is too complex. Lastly, the loss curves can also give an indication of whether the neural

network is a poor fit to the training or validation data set in general, if either or both of the loss values are large, or whether the functions are noisy, like shown in figure 2.37.

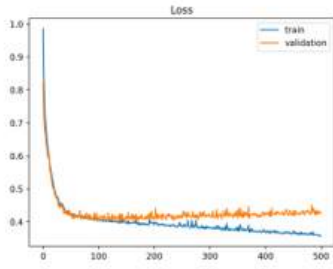


Figure 2.36: Learning curves of an overfit model.(Brownlee,2019)

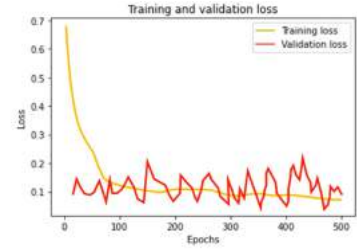
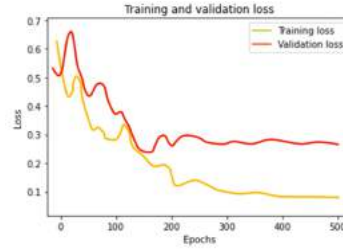


Figure 2.37: Two example learning curves of an unrepresentative model. (DigitalSreeni,2020)

Ultimately, configuring a neural network comes down to reaching an optimum in which the lowest loss value is reached, and in which the validation and training set can be approximated well. In this optimal situation, both the bias and variance of the model are low.

K-fold cross validation

To assess the prediction quality of the neural network even more adequately, the method of k-fold validation can be applied(Olson et al.,2008). This method is displayed with the scheme in figure 2.38. The training data set is divided into k folds, with each an equal amount of data points. Within each iteration, one fold functions as testing (validation) data, and the remaining k-1 folds function as training data. The neural network is thus trained k times with different configurations of training and validation data. Following such a procedure, are k approximations of the model loss, from which an average value can be determined. This method usually leads to more accurate loss descriptions compared to a simple train-test split(Kohavi,1995). The amount of data and in which order the neural network consumes it, can namely influence its convergence to an optimal solution. For the value of k, five or ten is often chosen(Kuhn & Johnson,2018, p.70).

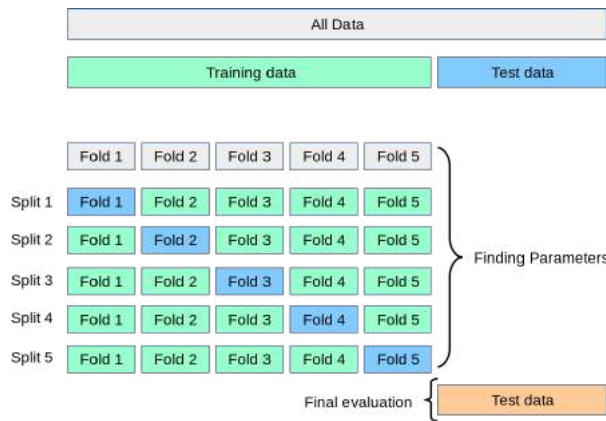


Figure 2.38: 5-Fold Cross-validation.(scikit-learn,2024)

Accuracy

Finally, the performance of the configured neural network can be described by its accuracy. The accuracy of a neural network is derived from its performance on new, unseen data, namely the testing set, indicated on the right side in figure 2.38. The accuracy is simply defined as the relative percentual difference between the predicted and real value, as shown in 2.24.

$$Accuracy = (1 - \frac{y_i - \hat{y}_i}{y_i}) \cdot 100\% \quad (2.24)$$

This metric can give a final insight into the network's prediction performance. Combining the findings about accuracy and model error, can help the user improve the neural network. There is no specific requirement to which the accuracy of a neural network must adhere to, it is up to the user to decide whether the neural network's performance is good enough.

2.3.3. Data Processing

Attributes

A supervised learning model finds relationships between the input parameters, to predict a value for the desired output parameters. Within machine learning, these parameters are called the attributes of the data set. In the example table below, the span, width and amount of main beams, are the attributes of the bridges in the data set. It is of importance that every value belongs to an attribute of an entry in the data set.

Table 2.2: Bridge properties.

Bridge	Span [m]	Width [m]	Amount of main beams
BRU0050	12.0	26.0	5
BRU0101	15.0	7.0	2
BRU0151	15.0	10.0	2
BRU0349	18.0	10.0	2
BRU0356	26.0	11.0	3

For the neural network to perform well, it must be made sure that the data set is structured and complete. The data must contain all of the information that the neural network needs to learn from. Missing values and outliers, can significantly impact the performance of the model (Goodfellow et al., 2016). Additionally, it must be made sure that the data is representative for real-world data and that it covers the range of values that are expected to be used as input. Testing the algorithm with data that reached beyond the range of data that it is trained with, could lead to inaccurate predictions (Goodfellow et al., 2016).

Standardization & Normalization

Pre-processing of the values in the data set is necessary, before the data can be used to train the machine learning algorithm. As mentioned before, the activation functions, process values that are in the domain of zero to one, or minus one to one. The ranges of values of every attribute in the data base is of different scale. It is therefore needed to scale down all input values, to increase the stability and accuracy of the neural network (LeCun et al., 2002). This is called normalization.

Normalization involves the procedure of remapping data between the interval of zero to one. There are two ways to do this. Firstly, the min-max normalization procedure, in which the values in the data set are simply scaled linearly, based on equation 2.25.

$$x_{normalized} = \frac{x - x_{min}}{x_{max} - x_{min}} \quad (2.25)$$

Secondly, standardization of the data set. This is often done to increase the performance and accuracy of a machine learning algorithm. Standardizing a data set involves shifting the values, so that the data set obtains a mean of zero and standard deviation of one. This is achieved with the following set of equations.

$$x_{normalized} = \frac{x - \mu}{\sigma} \quad (2.26)$$

$$\mu = \frac{\sum x_i}{N} \quad (2.27)$$

$$\sigma = \sqrt{\frac{1}{N} \sum (x_i - \mu)^2} \quad (2.28)$$

By doing this, the format of the data set coincides with the derivative of the sigmoid activation figure, meaning that accurate results are reached. Doing this however, only makes sense, if it is known that the training data has a somewhat normal distribution, as shown in figure 2.39.

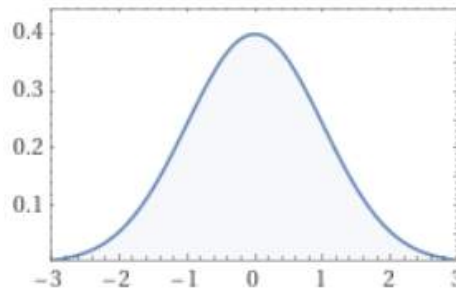


Figure 2.39: Normal distribution.

As mentioned by LeCun et al.(2002), choosing neural network activation functions and properties, is often a trial and error process. But some choices can be made based on the data available. In this thesis, bridge properties are used as input for the machine learning algorithm, which are not expected to have any particular statistical distribution or correlation with each other. Hence, in this application of a neural network, the values of the different attributes are simply scaled linearly to fit into the interval of zero to one, using equation 2.25.

2.4. Software & Digital Tools

This section gives an explanation of the different software, plug-ins and tools that were used, to create the workflow. The workflow was constructed within the visual programming environment Grasshopper3D. Grasshopper3D is part of Rhinoceros 7.

2.4.1. Rhinoceros

Rhinoceros, abbreviated as Rhino, is a 3D modelling software built by McNeel & Associates, that is mostly used by architects. According to McNeel & Associates (2023): "Rhino can create, edit, analyze, document, render, animate, and translate NURBS curves, surfaces and solids, subdivision geometry (SubD), point clouds, and polygon meshes. There are no limits on complexity, degree, or size beyond those of your hardware."

Many tools are available within the software, to model any desirable shape, including automatic generation of organic shapes. The software works by clicking on different tools, or typing in their commands in the command bar. Rhino also has a wide array of rendering options, to visualize the model that has been made. Unlike Revit, where the user models according to configured building schemes and floor plans, the user has complete freedom in Rhino. Different object layers, possible floor plans and views, have to be defined manually. Modeled objects also do not have a default material, appearance or thickness. Concisely speaking, all of the models attributes need to be modeled by the user. The interface of Rhino is shown in figure 2.40.

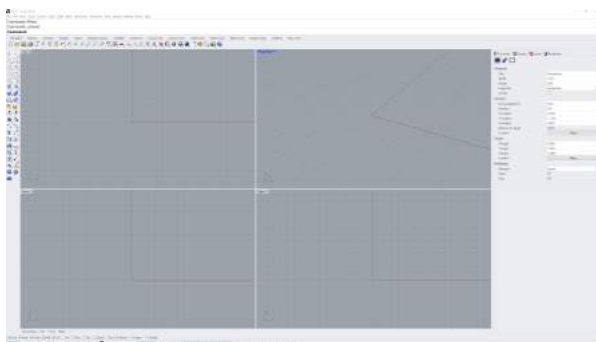


Figure 2.40: Rhino interface.(McNeel & Associates,2023)

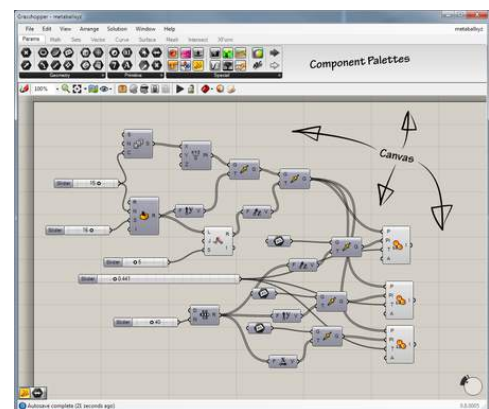


Figure 2.41: Grasshopper interface.(Rutten,2011)

2.4.2. Grasshopper3D

Grasshopper3D, often named Grasshopper, is a visual programming software within Rhino, that makes parametric design possible. It was designed by David Rutten, as part of McNeel & Associates, and first released in 2007. Grasshopper is a tool that is mainly used to create generative design workflows with algorithms and for parametric design and analysis. As can be seen in figure 2.41, workflows can be created by connecting different components on the canvas. The usable tools include all of the operations that are possible within Rhino, with options for parametrization. According to Scott Davidson, use of Grasshopper requires knowledge of the possibilities within Grasshopper, but does not require any programming experience(2023).

The environment handles different types of data such as text, numeric, audio-visual and haptic applications(Payne,2009). It can also import and export to different file types such as Excel and text, and can also directly be linked to objects modeled in the accompanying Rhino environment.

2.4.3. Grasshopper3D Plug-ins

There is a large community for developer tools within Grasshopper, to further extend its possibilities. Mainly, to fit different modeling and analysis needs related to structural design, building physics aspects, but also to simplify its interface to users. These plug-ins are available for everyone. The Grasshopper plug-ins that have been used in this thesis, are described below.

LunchboxML

The application of machine learning within Grasshopper, is facilitated with the LunchboxML plug-in. This plug-in is an addition to the Lunchbox suite. The original Lunchbox facilitated possibilities to explore more mathematical shapes, paneling and workflow options. The extra machine learning tab, provides pre-programmed modules for the application of most of the generic machine learning algorithms, such as (non-)linear regression algorithms, classifiers and neural networks. Its intention is to make machine learning more accessible within the building industry, by making easy to use components(Miller,2017). Application of a neural network is done with two components, which are shown in figures 2.42 and 2.43.

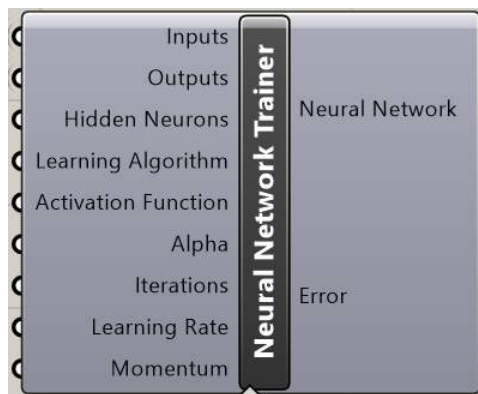


Figure 2.42: Neural network training component.

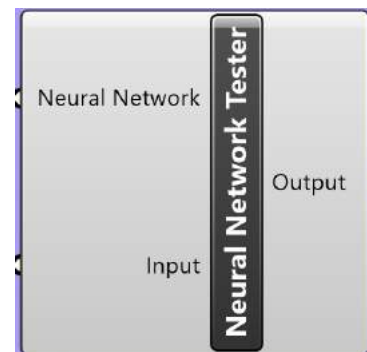


Figure 2.43: Neural network tester component.

The neural network trainer component, first takes the input and output data of the training data set. It then provides an option to select the amount of neurons in the hidden layer, the type of learning algorithm and activation function. The alpha value is an integer value which randomizes the output of the neural network, it does not resemble a model property. It is a trial and error process which alpha value yields the most accurate results. However, it is important to keep it constant during backtesting of the neural network, to be able to compare results. Mostly, alpha values between one and five are chosen, values beyond that only increase the loss of the model. Lastly, the amount of iterations, learning rate and momentum need to be specified. Resulting is a neural network, which can be connected directly into the neural network tester component. The remaining input in the component shown in figure 2.43, is the input data, with which the neural network will be tested. In the created workflow, this is the user input to create the model. A downside of the plug-in is that the neural network architecture

itself, is not configurable by the user. The neural network component creates a neural network with one input layer, one hidden layer and one output layer.

TT Toolbox

TT Toolbox is a simple plug-in which makes it possible to load, and read data from an Excel file. It also facilitates writing data to an Excel file, and reading data from other database file types such as "json" and "csv". This plug-in is used to load the data set in the beginning of the script.

Koala

Koala is a plug-in that is developed by the team behind SCIA Engineer. It connects Grasshopper with SCIA Engineer. Similar to other interfaces between Grasshopper and finite element analysis software, all relevant model properties such as the geometry, structural profiles, loading situations and structural analysis filters can be configured within the Grasshopper environment. Creating a workflow with Koala and SCIA Engineer is roughly defined by two steps. In the first step, all model information is entered in to the Koala ".xml" component, which stores all model data locally in a ".xml" file on the computer. The user can then load this file into SCIA Engineer manually, to perform structural analysis. The structural analysis procedure itself, can also be integrated into the Grasshopper script, which is usually done in the second step of configuration. The Koala plug-in contains a structural analysis component, which performs a finite element analysis within Grasshopper. To be able to do this, one must first manually configure a template engineering report in SCIA Engineer, in which a definition is given of the structural verification that has to be performed, and about what information should be returned in the engineering report. The input for the analysis component is the .xml file of the model, the engineering template, the location of SCIA Engineer on the operating machine, and the file output for the engineering report, which is usually an Excel document. This option facilitates rapid generative design workflows in which immediate insight is gained into for example unity checks for certain elements under defined loading combinations. The Koala plug-in is continuously under development by the Nemetschek group, hence it still contains minor errors in functionality.

2.4.4. SCIA Engineer

SCIA Engineer is a type of structural analysis software, which is based on finite element analysis. It was developed by SCIA nv, which is currently part of Nemetschek group (Nemetschek, 2024). SCIA Engineer is widely used in practice, it contains an intuitive user interface and supports a wide range of structure types. It is mostly known for its easy modeling environment, calculation methods, possibilities to create composite cross-sections, and automated documentation and design feedback. In addition to visual representations of occurring forces, stresses, moments and displacements on a 3D-model, it also provides the option to generate engineering reports, specifically tailored to configured Eurocode checks. It also features integrated solutions for BIM environments, such as live tracking of building changes, and multi-disciplinary interaction inside the model. Up until this point in civil engineering practice, the software has mainly been used to manually model structures. The connection to Grasshopper, to incorporate the software into generative and parametric design, has only been established recently.

2.5. Interview & Discussions

The following sub-questions are answered in this section:

3. How does the bridge design process work in practice?

4. What does the parametric and digital modeling environment within IB Amsterdam currently look like and how can the generative design tool improve the design process, according to engineers in the firm?

This section summarizes the most important findings from the interview and discussions held with engineers and employees within the team. Engineers with bridge design experience, were questioned about the following topics:

- Knowledge on parametric design & machine learning

- Thoughts about the application of machine learning and automation of tasks within the bridge design process and general civil engineering practice
- The current bridge design process including used software and digital environment
- Desired in- and output for the tool created in this thesis
- Technical questions about structural design

The questions that were discussed with employees are named in appendix D.

Design process

Following the interview with the concrete structural engineer, it appeared that the bridge design process is quite linear, and that **design freedom is limited** for the structural engineers. Three main phases for a bridge design project can be distinguished. These are the conceptual design ("schetsontwerp"), preliminary design ("voor ontwerp") and final design ("definitief ontwerp") phase.

Following the demand for a bridge project, architects come up with a conceptual design, which then gets forwarded to the structural engineers. Based on this concept, the structural engineers draw up a conceptual structural design, which is similar to reference projects. The structural engineer manually consults reference projects of similar size, to get an idea of all needed dimensions, or relies on his or her own knowledge to draft up a structure. A parametric model focusing on purely the structural design of the bridge leaf could be useful, since it is the structural engineers' task to design this within the architectural framework. Room for **automation** and thus a faster design process is available here. Instead of engineers having to manually look up reference projects during every bridge project, the machine learning algorithm can do this automatically with its own database. According to engineers, it is beneficiary to continue towards the preliminary and definitive design phases as soon as possible, to prevent extra requirements and boundary conditions from being added to the project. A generative and parametric workflow could assist in this because choices and decisions can be made earlier in the design process.

Structural Bridge Design

Most calculations within the conceptual and preliminary design phase, are performed with design rules and SCIA models. Some people in the firm argue that it is not beneficial to make a SCIA model in early design phases, while according to other people, it can be really useful, when kept simple. To perform calculations in early design phases, the structural system for both the bridge leaf and concrete bascule chamber, is simplified to simple static systems as much as possible. When beams or walls are simplified to a simply supported or clamped line element, the structural engineer obtains a sense of the range of forces and stresses occurring in the element. Detailing of elements, such as the placement of rebars, is initially also determined by copying details from reference projects. Detailed calculations are namely only done in the definitive design phase of a project. It is deemed useful if the tool can provide an extensive structural analysis right away, and if it can generate it quickly for every generated design. This will speed up the design process, given that currently SCIA models are drawn up manually.

Parametric Design

Engineers are familiar with the term parametric design, and a few are busy with creating parametric models for specific design problems within the city. Two important ones are the automatic calculation and modeling of foundation piles, and the parametric modeling of new quay structures. These are available to engineers via an online environment called Viktor.ai, which is managed by a firm that converts the parametric models created, into programmed language. What the engineers within "IB Amsterdam" encountered in its first application to create solutions for the quay wall issue, is that there were already three exceptions in practice, in which the parametric model did not hold up. What was advised from the engineers, is that the parametric model must be relatively basic, so adaptations can still be made manually after the design has been generated. On the other hand, it would be desirable for the engineers, to be able to change a lot of parameters of the model, after the neural network has generated a suggestion. There is thus a desire for both **adaptability** and **simplicity** in the model, for which a middle ground had to be found in this thesis.

According to the engineer, when done right, a parametric model can definitely save time in the

design process, since it currently takes time to recalculate every change in the design. Meaning that changes are mostly avoided. The engineers aim to make as less changes as possible during and after the preliminary design phase. This means that more optimal solutions to a problem might be disregarded unintentionally. A parametric model can assist in discovering the design space more quickly, and could also ease collaboration between the engineers and architects, since it gives quick insight into what results a design adjustment has.

Regarding the output of the digital workflow, it would be beneficial for engineers, to also have a qualitative substantiation of how the generated design has come about. Namely on what reference projects it is based for example, and what the advantages and disadvantages of that project were, or where problems occurred. And a qualitative assessment of whether the generated design is prone to significant problems that occur in similar bridges. Next to that, a clear overview of its structural performance would be desirable.

Machine Learning

Most people within the firm have a vague idea of artificial intelligence, and are familiar with ongoing developments around public tools such as ChatGPT. However, there is no significant knowledge on how such an algorithm would operate, or what it can be used for. There is no practical application of machine learning within the firm yet. As mentioned by an earlier report, the biggest hurdle in creating a digital workflow involving machine learning algorithms, is overcoming the black box effect(Viik,2019). Users must know how designs come about, and what parameters or options they are controlling.

Software & Digital Environment

The software used by the structural engineers in the bridge design process primarily consists of:

- SCIA Engineer
- Navisworks
- IDEA Statica
- Sketchup
- Autodesk products such as Navisworks and Design Viewer

Most people know about the existence of Rhinoceros and Grasshopper, but have not used it themselves. Meaning that after development of the tool described in this thesis, an extra piece of software is introduced to the structural engineers, of which it must be assumed that they have no knowledge about.

Conclusion

Many findings from talks with people in practice, connect to the conclusions drawn in similar research into the automation of tasks, such as a recent research by Willemsen(2020). On the one hand, a generative design tool based on a parametric model must not be too complex to avoid possible exceptions, which makes the tool less useful. On the other hand, engineers would like to have an adaptable model, and want to be able to change every aspect of the design easily. This is specifically a problem for bascule bridge design, since there are many variables that influence each other. A middle ground must be found between simplicity and adaptability.

Whether machine learning could be useful within the bascule bridge design process was difficult to answer by engineers, given the large amount of variables that govern bascule bridge design and the limited data set. What can be concluded is that it must be made clear to the user how designs come about, how they perform, and how their properties can be controlled within the user interface.

Development of workflow

This chapter describes the steps that were undertaken to develop the tool in Grasshopper, according to the workflow scheme presented in paragraph 1.6. It also describes the bridge data that was collected during this research and the configuration settings of the neural network. The following sub-questions are answered in this chapter:

5. *How can the structural design of a bascule bridge leaf be described and standardized?*
6. *How can a neural network algorithm be applied onto a data set and to which criteria must data adhere to?*

3.1. Parametric model

This section describes the parametric model of the bridge leaf, which stands central in the workflow.

An impression of a generated bridge leaf by the workflow is given in figures 3.1 and 3.2. The parametric model of the bridge leaf consists of the following components:

- Main beams
- Cross beams
- Rib profiles
- Deck plate
- Counterweight

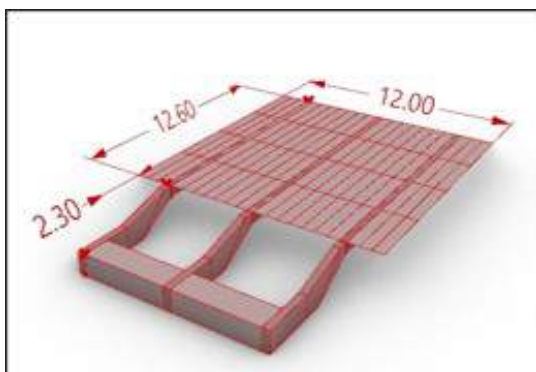


Figure 3.1: Generated bridge design in Rhino.

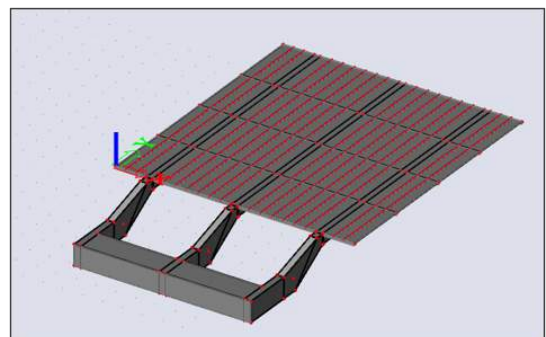


Figure 3.2: Generated bridge design in SCIA Engineer.

3.1.1. Parameters

The parametric model of the bridge leaf is controlled by 24 parameters in total. In the first step of the workflow, the user controls the following input parameters:

- Length bridge deck L_1
- Width bridge deck W_1
- Horizontal distance to rotational axis L_6

Based on the user input, values for the remaining 21 parameters, are predicted by the neural network. These are:

- Distance to end flange L_2
- Distance to start top flange bottom beam L_3
- Distance to start bottom flange bottom beam L_4
- Length bottom beam L_5
- Distance intermediate part L_7
- Depth bottom beam L_8
- Spacing main beams b_{main}
- Amount of main beams n_{main}
- Amount of cross beams n_{cross}
- Amount of ribs n_{rib}
- Thickness walls side t_{w1}
- Thickness wall back t_{w2}
- Thickness wall front t_{w3}
- Thickness roof t_{roof}
- Moment of inertia top beam $I_{zz,top}$
- Moment of inertia cross beam $I_{zz,cross}$
- Moment of inertia ribs $I_{zz,rib}$
- Height of bottom beam H_{bottom}
- Width of bottom beam W_{bottom}
- Web thickness of bottom beam $t_{w,bottom}$
- Flange thickness of bottom beam $t_{f,bottom}$

Main beams

The main beams of the bridge leaf are built up using 2D plate elements, and their shape is controlled by dimensions L_1 to L_8 . Figure 3.3 shows a cross-section of a typical main beam, along with the defined dimensions.

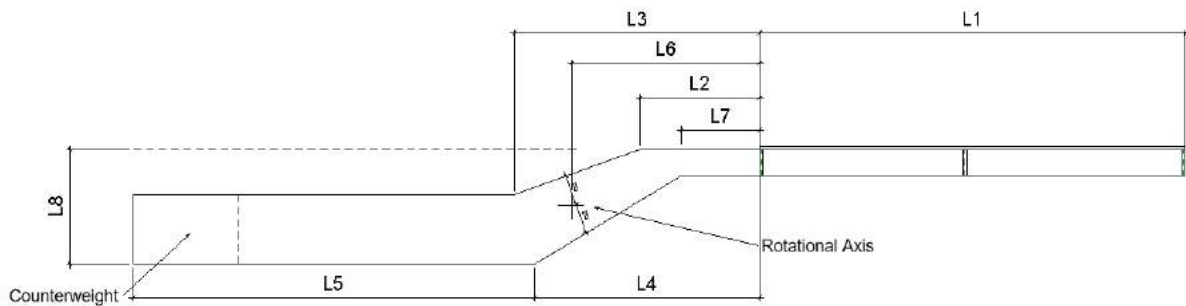


Figure 3.3: Dimensions of main beams.

Parameter L_1 describes the total length of the bridge deck.

Parameter L_2 describes the distance between the start of the bridge deck and the end of the upper part

flange of the top part of the main beam.

Parameter L_3 describes the distance between the start of the bridge deck and the start of the top flange of the bottom part of the main beam.

Parameter L_4 describes the distance between the start of the bridge deck and the start of the bottom flange of the bottom part of the main beam.

Parameter L_5 describes the total length of the bottom part of the main beam, measured along the bottom flange.

Parameter L_6 describes the distance between the start of the bridge deck and the rotational axis. The rotational axis is always placed exactly in the middle of the intermediate part. Parameter L_7 describes the distance between the start of the bridge deck and the end of the bottom flange of the top part of the main beam.

Parameter L_8 describes the vertical distance between the bridge deck and bottom of the main beam.

To further define the structure of the main beam, it can be roughly divided into three parts, for which different cross sections are defined. The main beams are modeled as box profiles. The cross section of the bottom and top main beam are described by four different parameters each, as can be seen in figure 3.5.

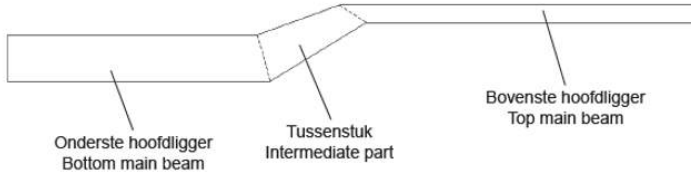


Figure 3.4: Division of main beam.

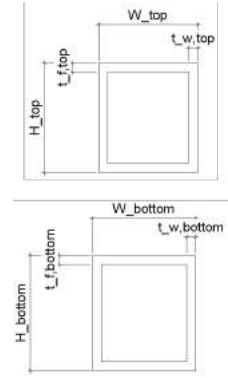


Figure 3.5: Cross section definition.

The parameters that describe the bottom main beam, are directly suggested by the neural network. The parameters that define the cross section of the top main beam, are derived from the required moment of inertia which is suggested by the neural network, namely $I_{zz,top}$. The moment of inertia of the steel box profile is described by:

$$I_{zz,top} = \frac{1}{12} \cdot W_{top} \cdot H_{top}^3 - \frac{1}{12} \cdot (W_{top} - 2t_{w,top}) \cdot (H_{top} - 2t_{f,top})^3 \quad (3.1)$$

The profiles of the main beams in the existing bridges were analyzed and the following ratio's were found:

$$W_{top} = 0.41366H \quad (3.2)$$

$$t_{w,top} = 0.01837H \quad (3.3)$$

$$t_{f,top} = 0.03605H \quad (3.4)$$

Substituting equations 3.2, 3.3 and 3.4 into equation 3.1, yields:

$$H_{top} = 3.21349 \sqrt[4]{I_{zz,top}} \quad (3.5)$$

With this equation, all properties of the top main beam are calculated inside the Grasshopper script. The values obtained for H_{top} and W_{top} , are rounded to the nearest tenfold. The values obtained for $t_{w,top}$ and $t_{f,top}$ are rounded to the nearest even integer.

The intermediate part of the main beams, connects both profiles with each other. Its cross-section is modeled with the same width, flange thickness and web thickness as the bottom main beam, which are W_{bottom} , $t_{f,bottom}$ and $t_{w,bottom}$ respectively. Its height alters, as it simply connects both profiles in a straight line.

Cross beams

The cross beams are modeled as line elements in between the main beams. The choice for a cross beam profile is in practice up to the structural engineer, the neural network does a prediction of the moment of inertia that is needed in the structural design of the bridge deck. The Grasshopper application searches through a profile database of HEA profiles. The first profile in the list that has a higher moment of inertia value than what the neural network suggests, is picked.

Ribs

The same holds for the ribs, which are also modeled as line elements. Based on the suggested $I_{zz,rib}$ value by the neural network, the script chooses the first Rectangular Hollow Section profile that suffices.

Deck plate

The bridge deck plate is modeled as a 2D-surface element, on top of the main beams, cross beams and rib profiles. The deck plate is modeled as steel plate with a thickness that can be specified by the user. For traffic bridges, this is usually twenty millimeters and for pedestrian and cycle bridges usually ten or twelve. The deck plate is rigidly connected to the underlying system of main beams, cross beams and ribs. All connections between the components in an orthotropic bridge deck are namely welded.

Bridge deck structure

The macro structure of the bridge deck, is controlled by the parameters $L_1, W_1, n_{main}, b_{main}, n_{cross}$ and n_{rib} . These parameters can be seen in figure 3.6.

L_1 and W_1 describe the total length and width of the bridge deck respectively.

The parameters n_{main} , n_{cross} and n_{rib} describe how many main beams, cross beams and ribs, the structural design is built up of. A property of the orthotropic bridge deck is, is that it is always symmetrical with respect to its central axis. Therefore, the main beams are always placed equidistant from the centroidal axis, with a distance b_{main} in between. b_{main} is the distance between the main beams, measured between the center axes of the cross sections.

The amount of cross beams is equally divided over the bridge deck's length L_1 . There is always a front and end beam needed. Hence, the minimal value for n_{cross} is two. The ribs are divided according to the ratio of surface area between the main beams, and outside the main beams, on the sides of the bridge deck.

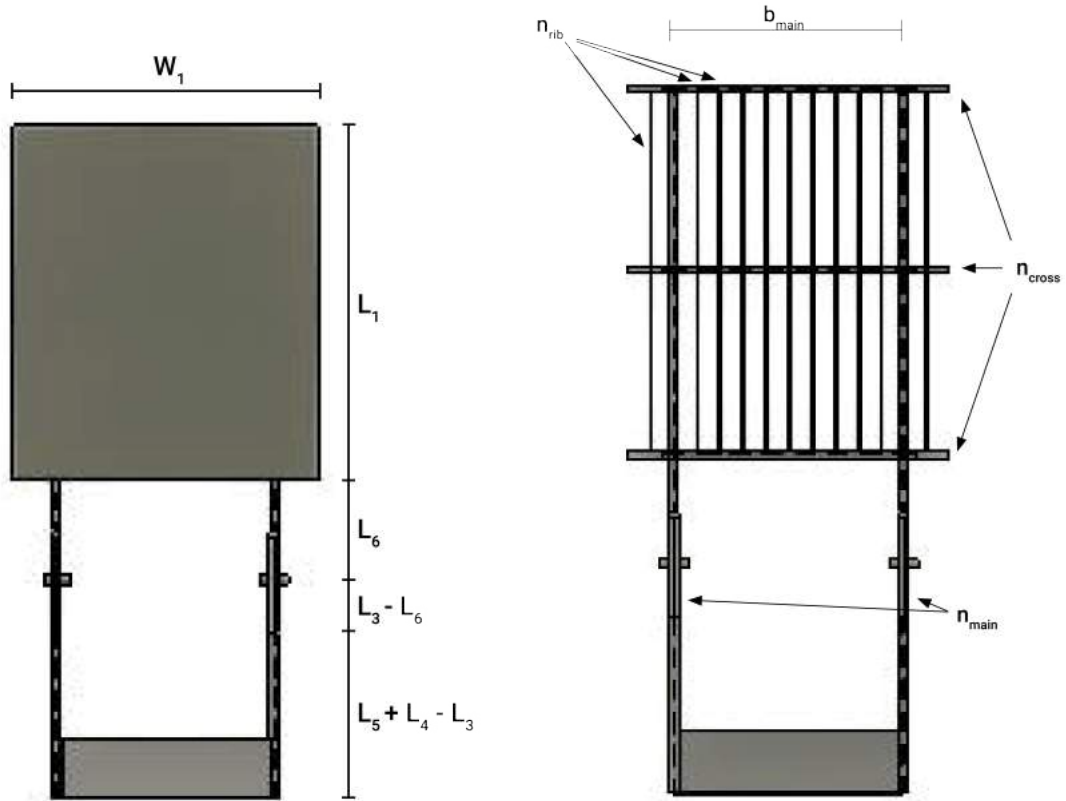


Figure 3.6: Parameters describing the structure.

Counterweight

The counterweight consists of a steel casing, in which steel plates can be placed to reach an almost equilibrium with the static moment caused by the bridge deck. The outer steel casing of the counterweight is modeled with steel plates of ten millimeters thickness, which are welded to the main beams. The mass of the counterweight itself is not modeled, but is rather modeled as loading on the main beams. It is assumed that the counterweight spans over the entire profile height of the bottom main beam. The required depth of the counterweight is automatically calculated based on the equilibrium of static moments around the rotational axis of the bridge. The static moment of the components of the bridge deck, should be in equilibrium with the static moment of the counterweight. At the bridge leaf toe, there should be a downward force of 10 kN, to prevent the bridge deck from moving under an uplifting wind force. This equilibrium can schematically be described by:

$$S_{cwt} + S_{rear} = S_{front} + S_{bridgedeck} - S_{force} [m^4] \quad (3.6)$$

In which:

S_{cwt} is the static moment of the counterweight.

S_{rear} is the static moment of the parts of the main beam that are on the rear side of the bridge leaf.

S_{front} is the static moment of the parts of the main beam that are on the front side of the bridge leaf.

$S_{bridgedeck}$ is the static moment of the components in the bridge deck.

S_{force} is the static moment of the required downward force at the leaf toe.

The required downward force of 10 kN, is translated into a static moment as follows.

$$\rho_{steel} = 7850 [kg/m^3]$$

$$m_{force} = 10kN \cdot 101.97 = 1019.7 [kg]$$

$$V_{force} = 1019.7/7850 = 0.129898 [m^3]$$

$$S_{force} = 0.129898 \cdot (L_1 + L_6) [m^4]$$

Within the Grasshopper model, the static moments of the individual steel components are obtained by multiplying their volume with the distance to the rotational axis. Equation 3.6 is then solved for S_{cwt} , which results in a minimum depth of the counterweight b_{cwt} , assuming it is built as a solid steel block. Because the neural network simply gives predictions based on the data set, it can occur that it suggests a too heavy bridge deck in combination with a too small value for the dimension L_5 . The distance between the centroid of the counterweight and the rotational axis is then too short. In this case, the counterweight is not modeled, and the model gives an error. Such a situation is regarded as a wrong prediction by the workflow. More on this is elaborated in section 4.3.

3.1.2. Bascule chamber

Accompanying with the generated structural design for the bridge leaf, the user can generate a bascule chamber, for illustrative purposes. The model of the bascule chamber around the bridge leaf, is steered by the following parameters:

- Thickness walls side t_{w1}
- Thickness wall back t_{w2}
- Thickness wall front t_{w3}
- Thickness roof t_{roof}
- Distance between counterweight and inside of back wall $d_{backwall}$
- Distance between main beams and inside of side walls $d_{sidewall}$
- Distance between bridge leaf and roof d_{roof}
- Distance between bridge leaf and floor in opened position d_{bottom}
- Thickness t_{floor}

As mentioned in section 3.1.1, thicknesses of the walls and roof of the bascule chamber are predicted by the neural network algorithm. The remaining parameters describe distances between the bridge leaf and the inner side of the walls, roof and floor. The user can input values for $d_{backwall}$, $d_{sidewall}$, d_{roof} , d_{bottom} and t_{floor} in the starting step of the Grasshopper script. The parameters that describe the bascule chamber are shown in figure 3.7.

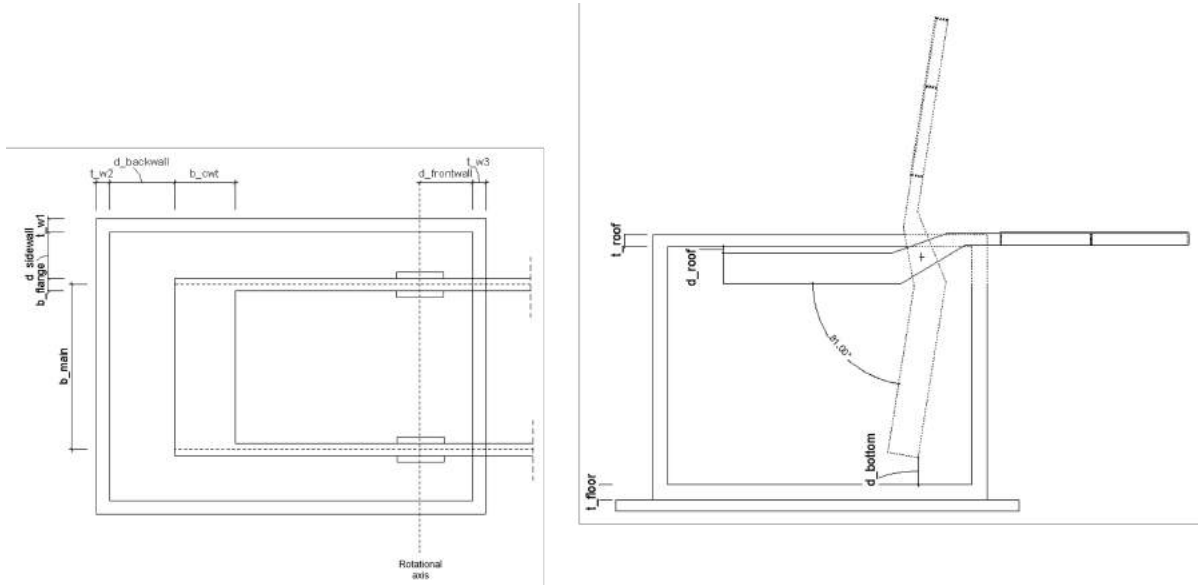


Figure 3.7: Parameters describing the bascule chamber.

3.2. Bridge Database

The bridge database forms the backbone of the tool that has been created, it contains all relevant information about bridge projects from which the machine learning algorithm learns. This section will

elaborate on what bridge information is collected, and which bridges are taken up in the database. Then a short description is given on how the data is loaded into Grasshopper.

3.2.1. Bridge information

An overview of the bascule bridges in Amsterdam is given in table A.1. 35 bascule bridges are taken up in the data set for the workflow. The Berlagebrug has the newest bridge leaf, its renovation is expected to finish in 2024. This bridge is used as case study for the results of this thesis, and is therefore not part of the data set for the neural network. The characteristics of the bascule bridges that are incorporated in the data set, are displayed with the following figures. Figure 3.8 displays the construction year of the steel bridge leaves that are currently in use. It can be seen that old bridges from 1928 onwards, are still in use, while some have also been reconstructed/revised in the meantime. Two time periods can be distinguished in which many bascule bridges were built, namely the 1960s and the early 2000s. This can also be seen in the bridge designs. A handful of bridges that were designed by the same engineer, or cover the same waterway, are identical or very similar.

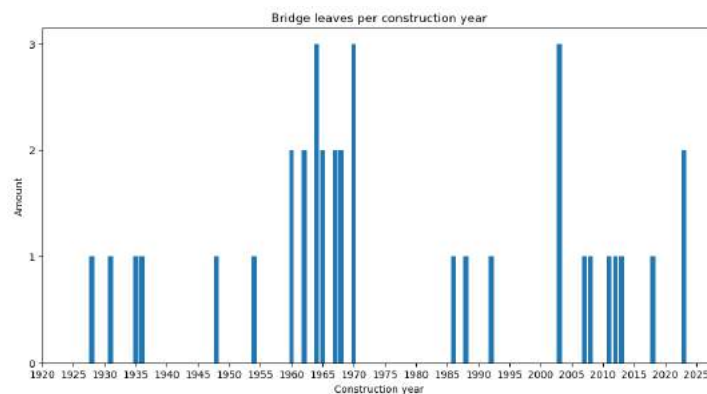


Figure 3.8: Bridge leaves per construction year.

The majority of bascule bridges is single span, only four are double span. Of the bridges that are double span, both leaves meet in exactly the middle of the waterway, and are identical. For these bridges, parameters of one of the bridge leaves were taken up in the data set. In the top left of figure 3.9, the construction materials per bridge can be seen, indicated as "bridge leaf/basculer chamber". The majority of bridges have been constructed with a steel bridge leaf and a concrete basculer chamber. The bridge leaf and upper structure of the Kadoelenbrug, which was built in 2010, is built using a hybrid structure of steel and fiber-reinforced epoxy resin, leading to a more slim structure than what could have been achieved with only a steel structure. The Solitudobrug, which is a newly built pedestrian- and cyclebridge in the Amstel district, was built using cortensteel.

The majority of the bridges have been built using electro-mechanical operating systems, which leads to significantly sized basculer chambers to house the equipment. A trend can be seen in recent decades, that movable bridges are built with hydraulic operating systems more often. Hydraulic operating systems can be built in possibly way smaller concrete environments, and thus lead to more compact designs.

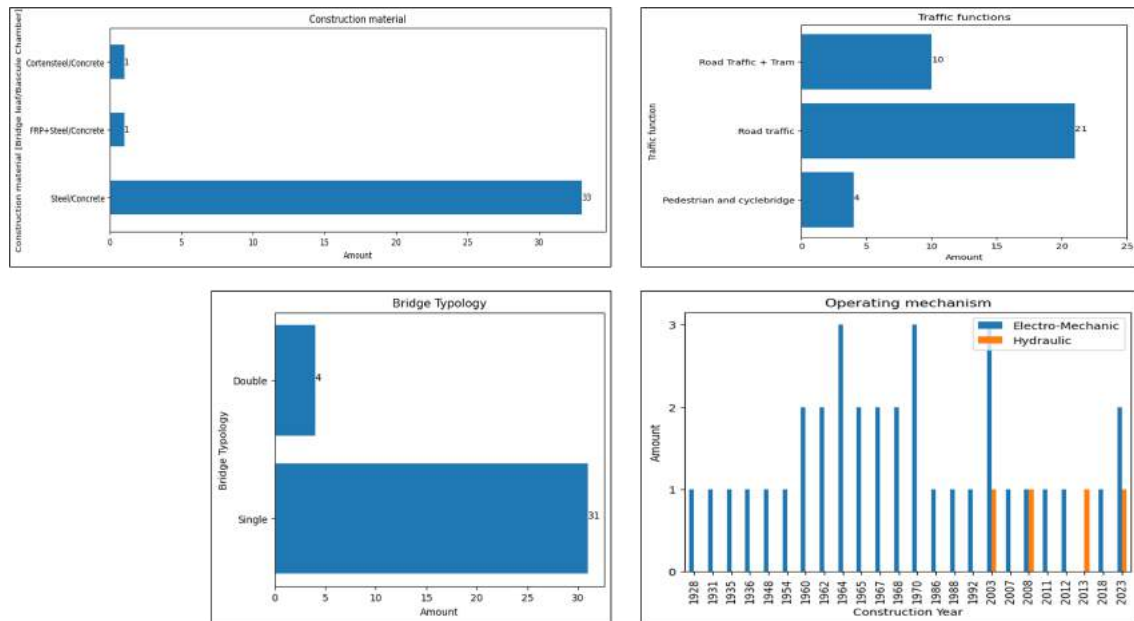


Figure 3.9: Properties of bridges in data set.

Lastly, bridges can be classified based on their traffic profiles. Pedestrian- and cycle bridges can be designed with a more slender structure, compared to traffic bridges with a tram for example. Within the data set, four bridges are pedestrian- and cycle bridges, and ten bridges have two tram tracks running across. In all cases, the tram tracks are placed near the center of the bridge. The traffic profiles of bridges within Amsterdam is fairly constant. Most traffic bridges are open for heavy traffic, and consist of multiple lanes of vehicle traffic, and have pedestrian and cycle paths on both sides. Figure 3.10 schematically shows the traffic profiles and their road layout.

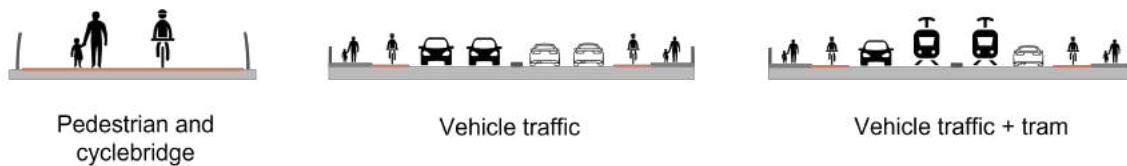


Figure 3.10: Traffic profiles of bascule bridges in data set.

Values for the 24 parameters that describe the parametric model, have been collected for every bridge, and were gathered in an Excel file. The geometrical properties that were collected, are shown in table E.1 and E.2 in appendix E. The structural properties of existing bridges that were collected, are shown in table E.3 and section E.2. All cross sections of components in the bridge decks of existing bridges, were modeled in SCIA Engineer, from which their moment of inertia was derived. Not every value could be found for every bridge. Gaps in the data set are indicated with "n.a" or left blank. In case of a blank space, the value could not be found. In case of a "n.a", the dimension or parameter was not applicable in the bridge deck for that bridge, or no representative value could be found.

3.2.2. Sources

The required information about existing bridges has been collected from three sources. These are the city archives, calculation and evaluation reports and project data on the hard drive.

Archives

The city of Amsterdam has digitized its archives, from which original drawings and project documents could be consulted. For many of the older bridges, the parameters that steer the parametric model had to be derived from their original technical drawings. Not all parameters that are defined in the

parametric model, were directly indicated in the drawings. Measurements had to be done on screen with a digital ruler, to find most dimensions of the main beams. There could thus be small measurement errors in the data due to incorrect readings from the ruler, or from an incorrect scan of the document, possibly leading to irregularly scaled images.

Engineering reports

Information about the structure of existing bridges was also collected from calculation reports done by either engineers within the firm or by other firms. For some older bridges in the data set, a recalculation has been done in the last two decades, to reassess the structural capacity of the bridge deck. In these calculation reports, the bridge decks were reevaluated with the current Eurocode standards. In all cases, a SCIA Engineer model had been constructed of the old bridge deck, from which also values and simplifications could be deduced to use in the data set of this assignment.

Project documents

For newer bridges in the data set, approximately from the year 2000 onwards, information is not stored in the archives yet. For these bridges, project documents were made available to consult. These documents consist of environmental plans, CAD drawings and calculation reports done by the project team.

3.3. Configuration of neural network

The supervised neural network, which is a standard component in LunchboxML, is trained with the data set in the beginning of the Grasshopper script. The neural network consists of a single input layer, one hidden layer, and a single output layer. The input layer of the neural network, consists of three nodes, which are the user input parameters L_1 , W_1 and L_6 . The hidden layer has an amount of nodes that can be specified by the user. The output layer consists of 21 nodes, which cover the remaining parameters for which the neural network does a prediction. The neural network is schematically displayed in figure 3.11.

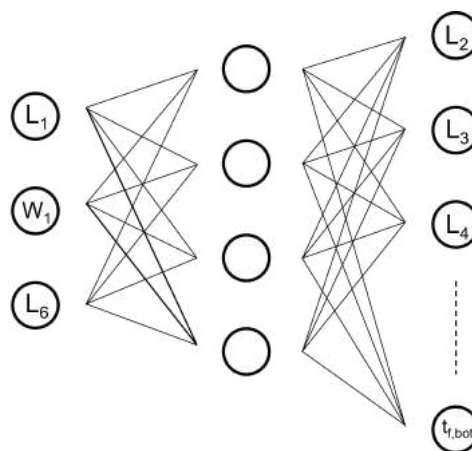


Figure 3.11: Schematic representation of neural network.

The following properties of the neural network had to be configured:

- Hidden neurons
- Learning algorithm
- Activation function
- Alpha
- Iterations
- Learning rate
- Momentum

Hidden neurons

According to Heaton(2008,p.158), choosing the amount of hidden neurons in the middle layer, is a trial-and error process. He suggests three rules of principle, as starting point, which are:

- The number of hidden neurons should be between the size of the input layer and the size of the output layer.
- The number of hidden neurons should be 2/3 the size of the input layer, plus the size of the output layer.
- The number of hidden neurons should be less than twice the size of the input layer.

The neural network has three input nodes, namely L_1 , W_1 and L_6 . The size of the output layer is equal to 21 nodes. Following the above principles, the choice for hidden neurons should be between one and 23. The complexity of the network will determine how well the neural network can learn the data set. A conclusion about what the right amount of hidden neurons in the middle layer is, is drawn in section 4.1.

Learning algorithm

For the learning algorithm, a choice can be made between the following four options in the Grasshopper component:

- Backpropagation
- Resilient backpropagation
- Evolutionary
- Levenberg Marquardt

A form of backpropagation will be used to train the neural network, since this is most often used (LeCun et al.,2002) and because the latter two are only applicable in specific cases. The component also has an option for resilient backpropagation. Instead of estimating the significance of each weight and how significant they should be changed, a resilient backpropagation algorithm only describes the direction in which the weight should be adapted. It thus only states whether the value should increase or decrease. This leads to possibly large increments or decrements, which can be detrimental for small data sets(Igel & Hüsken,2003). Resilient backpropagation could be more effective, since it reaches a solution faster. However, due to its quick convergence, it could also optimize for a sub-optimal solution.

During testing of the neural network within Grasshopper, it became apparent that the neural network did not work correctly with a resilient backpropagation algorithm, as it predicted mainly zero values for the output parameters. Meaning that it could not find relationships between the variables in the data set. With a regular backpropagation algorithm, the network does predict realistic values. Hence, the neural network is trained with a regular backpropagation algorithm.

Activation function

The collected data of existing bridges, only contains positive values. The choice of learning algorithm therefore comes down to two options, namely a sigmoid activation function, or a (rectified) linear activation function. A sigmoid activation function is more capable of capturing non-linear behaviour in a data set. Therefore, the choice was made to use a sigmoid function. During backtesting it was also concluded that the neural network gave more consistent predictions with a sigmoid activation function, compared to a (rectified) linear activation function.

Alpha

The alpha value describes the regularization rate, which is used to combat under- and overfitting(Oppermann,2020). The default value of one was used in this project.

Iterations, learning rate and momentum

The optimal values for the amount of iterations, learning rate and momentum were found during the validation phase of the project. This is described in section 4.1.

3.3.1. Post-processing data

The neural network solves a regression task, hence it predicts continuous values for the 21 parameters that were described earlier. For the predicted values to be used in the structural model, they first need to be rounded to valid values. This is done according to the following specifications:

- Dimensions L_2 to L_8 are rounded to three decimals.
- Main beam spacing b_{main} is rounded to two decimals.
- Amounts n_{main} , n_{cross} and n_{rib} are rounded to the nearest integer.
- Dimensions for the bascule chamber are rounded to two decimals.
- Bottom main beam dimensions H_{bottom} and W_{bottom} are rounded to the nearest tenfold.
- Web and flange dimensions $t_{w,bottom}$ and $t_{f,bottom}$ are rounded to the nearest even integer.

Lastly, before the model is final, there is an overrule step in the Grasshopper script. In this step, the user is presented with the values that the neural network has predicted. After which the user can manually change the value of every parameter, if an undesirable prediction was made by the neural network.

3.4. Structural Analysis

In the next step of the Grasshopper workflow, the generated design is forwarded into the structural analysis component of SCIA Engineer. In this phase, the structural design of the bridge leaf is verified with three normative load situations. These load situations have been constructed based on normative load combinations for the two reference cases, namely the renovated Berlagebrug and the pedestrian and cyclebridge in Elzenhagen-Zuid, of which a case description is given in appendix G. Meaning that for both a traffic bridge and pedestrian- and cyclebridge, three normative load combinations are defined.

Bascule bridges are designed with a design life time of 100 years, in consequence class 2. Given that the tool is meant for the conceptual and preliminary design phase of a project, the generated bridge designs are tested with simplified loading combinations. It has also not been possible to investigate all possible load combinations within the time frame of this project, since in practice, hundreds of load cases and load combinations need to be verified. The bridge is only considered in closed position.

The structural analysis procedure follows the following key points:

- Steel class S355
- Consequence class 2
- Design lifetime of 100 years.
- Verification for strength in Ultimate Limit State conditions
- Linear calculation in SCIA Engineer

The following types of loading are taken into account in the load situations:

- Permanent loading
 - Self weight of the steel structure
 - Self weight of the parapet
 - Self weight of the bridge deck finishing
- Variable loading
 - Traffic loading
 - Wind loading

3.4.1. Load cases

This section describes the different load cases and what their characteristic values are.

LC1: Self weight of steel structure

The characteristic value of the self weight of the steel structure, is automatically determined by SCIA Engineer.

LC2: Self weight of the parapet + counterweight

The self weight of the parapet on the bridge is equal to $q_{k,parapet} = 1.0 \text{ kN/m}$ (NEN-EN 1991-2+C1:2011, sec. 4.8 (1)). This line load is applied in longitudinal direction, on both sides of the bridge deck. It is located 0.2 meters inwards and acts on the bridge deck plate. This load case can be seen in figure 3.12. This load case also includes the self weight of the counterweight that acts as distributed load on the main beams.

LC3: Self weight of bridge deck finishing of traffic bridge

The deck finishing layer of a traffic bridge consists of a thicker wear layer compared to a pedestrian and cycle bridge. The characteristic load of the bridge deck finishing is $q_{k,sl} = 0.2 \text{ kN/m}^2$. This should be applied over the complete surface area of the bridge deck. Additional line loads can be placed along the trajectories of the tram rails, to model the self-weight of the steel rails. This leads to four line loads of $q_{k,tram} = 0.59 \text{ kN/m}$. This is however not considered in this thesis. Hence, load case three is only made up of the bridge deck finishing layer.

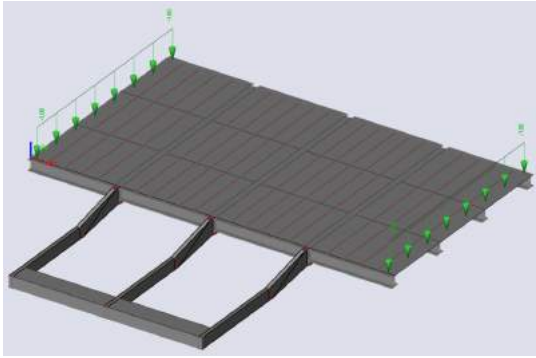


Figure 3.12: Load case two.

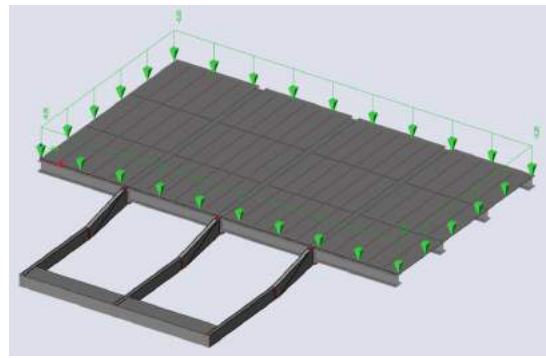


Figure 3.13: Load case three.

LC4: Self weight of bridge deck finishing of pedestrian and cycle bridge

The deck finishing layer of a modern, cycle and pedestrian bascule bridge consists of a thin epoxy or polyurethane layer. In this case, a layer of six millimeters is used. This leads to a characteristic load of:

$$q_{k,sl} = 0.15 \text{ kN/m}^2$$

LC5: Traffic load model 1 tandem systems in middle of bridge deck

This load model describes the tandem loads of traffic model one, which are applied in a maximum of three adjacent notional lanes. In this load case, the tandem loads are applied at mid-span on the bridge deck. The tandem loads are of descending magnitude inwards, the highest tandem load is placed outwards. The characteristic value of these tandem loads are:

$$Q_{k2,1} = 600 \text{ kN}$$

$$Q_{k2,1} = 400 \text{ kN}$$

$$Q_{k2,1} = 200 \text{ kN}$$

These values have to be multiplied with the factor α_{Qi} . This value is dependent on the amount of heavy traffic per lane. The value for α_{Qi} can be deducted from table NB1 in section 4.3 of NEN-EN1991-1-2. For simplicity, it is assumed that α_{Qi} is equal to one. The characteristic force per wheel is exerted on a contact area of 0.4 x 0.4 meters. It gets spread through the deck plate and wear layer. For the wear layer, a thickness of eight millimeters is assumed. The wheel load gets spread over an area:

$$A_{spr} = (0.4\text{m} + 2 \cdot (t_{sl} + 0.5 \cdot t_{dp}))^2 = 0.183 \text{ m}^2 \quad (3.7)$$

The wheel loads acting on the bridge deck can then be calculated with:

$$Q_{w,prent} = \frac{Q_{i,k}}{4 \cdot A_{spr}} \quad (3.8)$$

For the wheel loads, assuming a deck plate thickness of twelve millimeters, as is present in most bridges, one then obtains:

$$Q_{1k} = 819.67 \text{ kN/m}^2$$

$$Q_{2k} = 546.45 \text{ kN/m}^2$$

$$Q_{3k} = 273.22 \text{ kN/m}^2$$

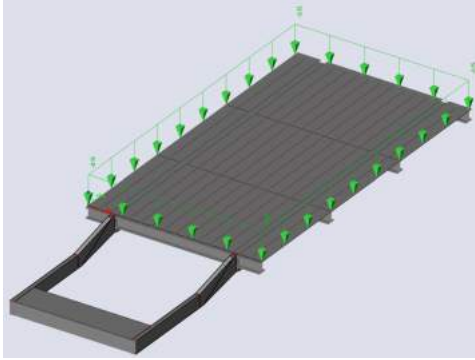


Figure 3.14: Load case four.

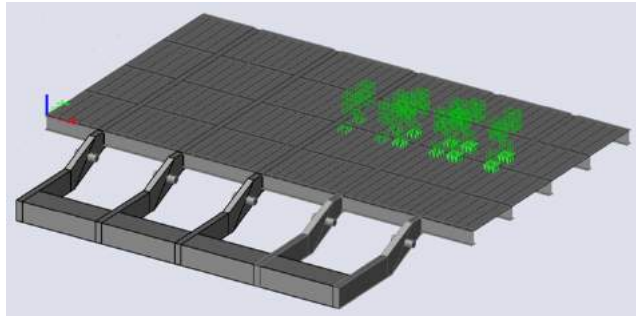


Figure 3.15: Load case five.

LC6: Traffic load model 1 uniformly distributed load

LC6 describes the uniformly distributed load accompanying the tandem loads of load case 5. It is assumed that α_{qi} is also equal to one, and that α_{Qr} is equal to 0.9. The first notional lane has a uniformly distributed load of $q_{1,k} = 9.0 \text{ kN/m}^2$. The second to fourth notional lane has a uniformly distributed load of $q_{2,k} = 2.5 \text{ kN/m}^2$ and the fifth notional lane and onwards have a uniformly distributed load of $q_{3,k} = 0.9 \cdot 2.5 = 2.25 \text{ kN/m}^2$.

LC7: Traffic load model 1 tandem systems on foremost crossbeam, middle

This load case describes the tandem loads of load model 1, in which the magnitude of loads decreases towards the edge of the bridge deck, as can be seen in figure 3.17. The values for the loads are equal to those described in load case five.

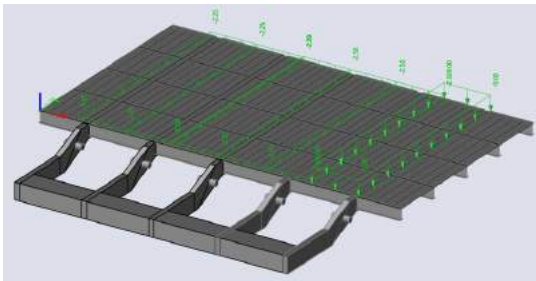


Figure 3.16: Load case six.

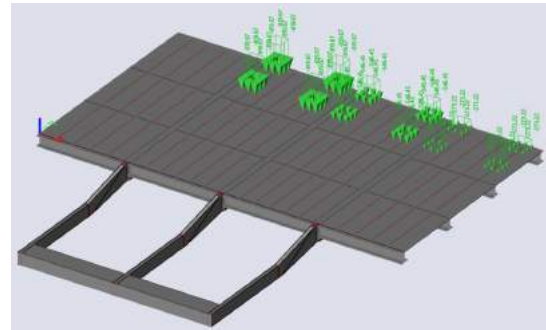


Figure 3.17: Load case seven.

LC8: Traffic load model 1 uniformly distributed load, middle

This load case describes the accompanying UDLs to load case seven. The highest UDL of 9.0 kN/m^2 , is placed in the middle of the bridge deck. The remaining notional lanes are loaded with a UDL of 2.5 kN/m^2 and the load of 2.25 kN/m^2 is applied furthest away from the middle.

LC9: Traffic load model 1 tandem loads on rearmost crossbeam

This load case describes the tandem loads of model 1, placed on the rearmost part of the bridge deck. The highest tandem load is placed in the center-most position of the bridge deck. The second highest at the side of the bridge deck, and the lowest tandem load on notional lane that is positioned in between. The values are equal to those described in load case five.

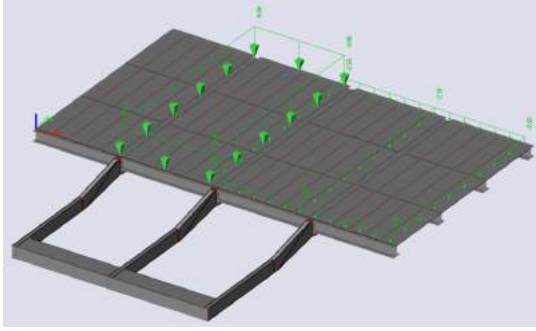


Figure 3.18: Load case eight.

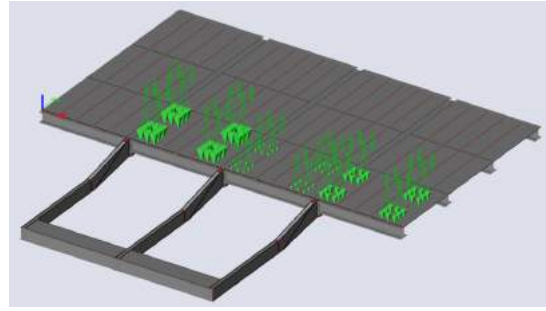


Figure 3.19: Load case nine.

LC10: Traffic load model 1 uniformly distributed load, rear

In this load case, the UDLs accompanying load case nine are described. The values are equal to those described in load case six.

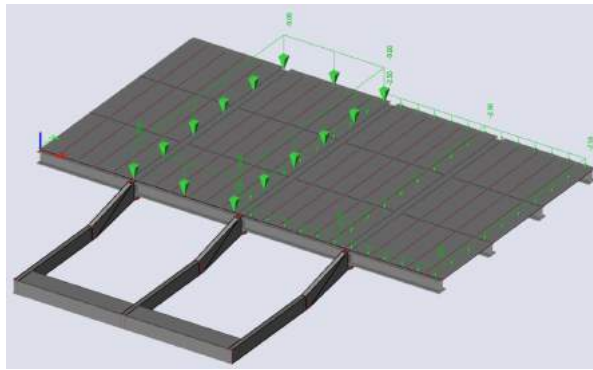


Figure 3.20: Load case ten.

LC11: Vertical wind loading on closed bridge

This load case describes the downward force of wind on top of the bridge deck, in closed position. The characteristic value of the vertical wind load is calculated with:

$$q_{w,z} = \frac{1}{2} \cdot \rho \cdot C_z \cdot v_{b,s}^2 \quad (3.9)$$

The value for C_z is calculated with:

$$C_z = c_e \cdot c_{f,z} \quad (3.10)$$

In which:

$c_{f,z}$ is chosen as 0.9, according to NEN-EN1991-1-4.

c_e is the exposure factor, which is calculated with:

$$c_e(z) = \frac{q_p(z)}{q_b} \quad (3.11)$$

The value q_b is calculated with:

$$q_b = \frac{1}{2} \cdot \rho \cdot v_b^2 = \frac{1}{2} \cdot 1.25 \cdot 27^2 = 455.63 \text{ [N/m}^2\text{]} \quad (3.12)$$

Substituting the factor $c_{f,z}$ and equation 3.12 into equation 3.10, yields for C_z :

$$C_z = 1.9753 \cdot 10^{-3} \cdot q_p(z) \quad (3.13)$$

In which $q_p(z)$ is calculated with equation 3.14.

$$q_{p,z} = \left(1 + 7 \cdot \frac{1.0}{\ln\left(\frac{L_1 + L_6 + 4}{0.5}\right)}\right) \cdot \frac{1}{2} \cdot \rho \cdot v_{m,z}^2 [N/m^2] \quad (3.14)$$

The value $v_{b,s}$ is calculated with:

$$v_{b,s} = c_d \cdot c_s \cdot v_{b,0,s} \quad (3.15)$$

The value $v_{b,0,s}$ represents a reduced wind speed which may be used in loading combinations that have traffic load models. From section 8.1 in NEN-EN 1991-1-4, it can be concluded that a base value of $v_{b,0,s} = 23 \text{ m/s}$ should be used. This means that $v_{b,s}$ is also equal to 23 m/s.

The vertical wind loading $q_{w,z}$ can then be expressed as:

$$q_{w,z} = \frac{1}{2} \cdot 1.25 \cdot 1.9753 \cdot 10^{-3} \cdot q_p(z) \cdot 23^2 = 0.6531 \cdot q_p(z) [N/m^2] \quad (3.16)$$

In which $q_p(z)$ is calculated with equations 3.14 and 3.17.

$$v_{m,z} = (0.223 \cdot \ln(L_1 + L_6 + 4) + 0.1546) \cdot 27.0 [m/s] \quad (3.17)$$

LC12: Tandem load front of bridge deck, pedestrian and cyclebridge

The axle loads that belong to an emergency vehicle on a pedestrian and cyclebridge, are explained by the figure in section C.6. The characteristic axle loads are described by:

$$Q_{serv1} = 80 \text{ kN}$$

$$Q_{serv2} = 40 \text{ kN}$$

These loads are applied on a surface area of 0.2 x 0.2 meters. Meaning that the axle loads are modeled as distributed loads on the surface area.

$$q_{k,serv1} = \frac{40}{0.2 \cdot 0.2} = 1000 \text{ kN/m}^2 \quad (3.18)$$

$$q_{k,serv2} = \frac{20}{0.2 \cdot 0.2} = 500 \text{ kN/m}^2 \quad (3.19)$$

The axles are spaced 3.0 meters apart, and the wheel loads 1.3 meters. In this load case, the vehicle is placed in the middle of the bridge leaf, at the end, as indicated in figure 3.22.

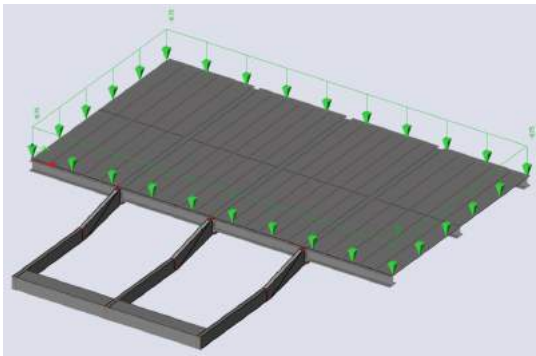


Figure 3.21: Load case eleven.

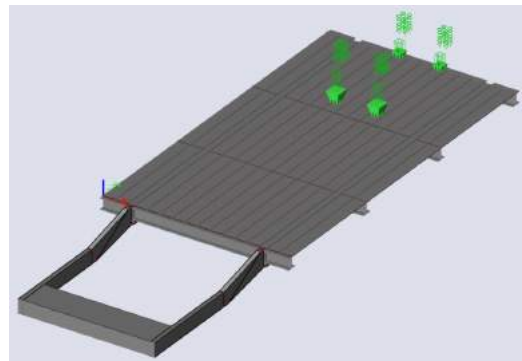


Figure 3.22: Load case twelve.

LC13: Rear of tandem load, pedestrian and cyclebridge

This load case corresponds to the situation where the vehicle has partly driven off the bridge leaf, when only its rear axle is still on the bridge deck. This load case can be seen in figure 3.23. The rear axle is located 2.0 meters inwards from the end of the bridge deck. The loads are also placed along the centroidal axis of the bridge deck.

LC14: Horizontal traffic load, pedestrian and cyclebridge

This load case describes the horizontal traffic load, that should be taken into account in combination with the vertical load from the service vehicle. It accounts for the loading due to braking of the vehicle.

$$Q_{k,fl} = 0.6 \cdot (Q_{k,serv1} + Q_{k,serv2}) = 72kN \quad (3.20)$$

This force should be divided by the total length of the bridge deck, namely L_1 . Hence, the characteristic value of load case 15 is described by:

$$q_{k,traffichorizontal} = \frac{72}{L_1} [kN/m] \quad (3.21)$$

This force acts directly underneath one of the wheel axes. A schematisation of this load case is given in figure 3.24.

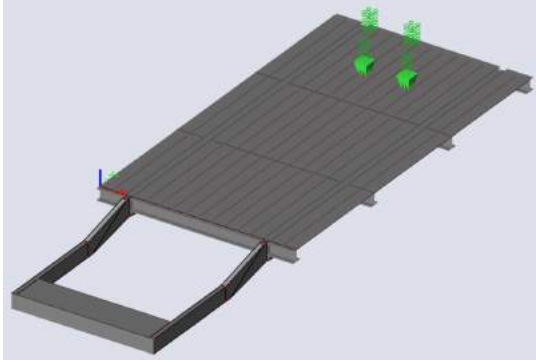


Figure 3.23: Load case thirteen.

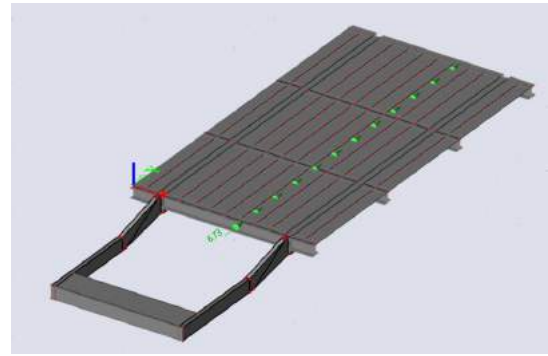


Figure 3.24: Load case fourteen.

3.4.2. Load Combinations**Traffic bridges**

To verify the structural integrity of traffic bridges, three load combinations are drawn up for both a regular traffic bridge and pedestrian- and cyclebridge. These load combinations are based on normative loading situations in the renovation of the Bullebakbrug, Berlagebrug and Elizabeth Admiraalbrug.

Load combination one appeared to be normative for the main beams, in the top flange near the intermediate part. This load combination is defined with the following equation:

$$\text{Load Combination 1 : } 1.2 \cdot (LC1 + LC2 + LC3) + 1.35 \cdot (LC5 + LC6) \quad (3.22)$$

The second load combination appeared to be governing for the cross beams, more specifically the "voorhar", which is the front-most cross beam of the bridge deck. In practice, this beam is usually designed with a slightly smaller cross-section than the other cross beams, because of the support points. In the model of this thesis, all crossbeams are modeled with the same cross-section. Load combination two is defined with the following equation:

$$\text{Load Combination 2 : } 1.2 \cdot (LC1 + LC2 + LC3) + 1.35 \cdot (LC7 + LC8) + 1.56 \cdot L12 \quad (3.23)$$

Lastly, the third load combination also describes a significant loading case. However, in this case, the highest uniformly distributed loads and tandem systems are placed in the middle of the bridge deck, at the position of the rear-most cross beam. This load combination is defined by:

$$\text{Load Combination 3 : } 1.2 \cdot (LC1 + LC2 + LC3) + 1.35 \cdot (LC9 + LC10) \quad (3.24)$$

Pedestrian and cyclebridges

The first load combination for pedestrian and cyclebridges follows from equation 6.10a, using the self weight for the structure only. This load combination appeared to be normative for the main beams of the pedestrian and cyclebridge in Elzenhagen-Zuid. The load combination is described by:

$$\text{Load Combination 4 : } 1.3 \cdot (LC1 + LC2 + LC4) \quad (3.25)$$

Load combination five follows from applying the self weight of the structure in combination with the traffic loading group 2 for pedestrian and cyclebridges, in equation 6.10b. The traffic load group describes an incidental vehicle in combination with a vertical distributed load and horizontal traffic load along the span of the bridge deck. In which the vertical distributed load is calculated with $0.8q_k$ and is not applied within 5 meters of the vehicle. For the vehicle and horizontal load, characteristic values need to be used. This load combination appeared to be normative for the cross beams in reference case one. Load combination two is described by:

$$\text{Load Combination 5} : 1.2 \cdot (LC1 + LC2 + LC4) + 1.35 \cdot (LC12 + LC14) \quad (3.26)$$

Load combination six follows from the normative load combination for the rib profiles in the bridge of reference case one. In this case, only the rear axle of the vehicle is placed on the bridge. Additionally, the distributed vertical load and horizontal load due to applying traffic group two, are left out, since these had a positive influence on the stress distribution in the ribs. Load combination three is described by:

$$\text{Load Combination 6} : 1.2 \cdot (LC1 + LC2 + LC4) + 1.35 \cdot LC13 \quad (3.27)$$

General

The normative stresses in the bridge deck plate, usually occur right underneath the wheel loads. Therefore, the stresses in the bridge deck plate need to be checked throughout all load combinations in which traffic load models are applied.

4

Validation

In this chapter, the method developed in this research is validated. Firstly, the functioning and predicting performance of the neural network is validated and evaluated. The prediction accuracy of the neural network was found to be poor, hence an improvement to the model was made, which is described in section 4.2. In paragraph 4.3, an analysis is done of the correctness of the SCIA Engineer models that the workflow generates, for five random input cases. The following sub-questions are answered in this chapter:

7. *How is the performance of the neural network described and assessed?*
8. *How is the performance of the structural analysis models verified?*

4.1. Neural network validation

4.1.1. Neural Network Configuration

Following the explanation in section 3.3, about what properties were chosen for the neural network, an analysis of the obtained error of the model was done. Based on these observations, the optimal amount of hidden neurons, iterations, learning rate and momentum were determined. The loss curves of the neural network trained with all 35 bridges, are shown in the figure below, with 2,5,10,15 and 20 neurons in the hidden layer. The loss of the model is described by the mean squared error. In this initial step, default values for the learning rate and momentum were used, which are equal to 0.1 and 0 respectively.

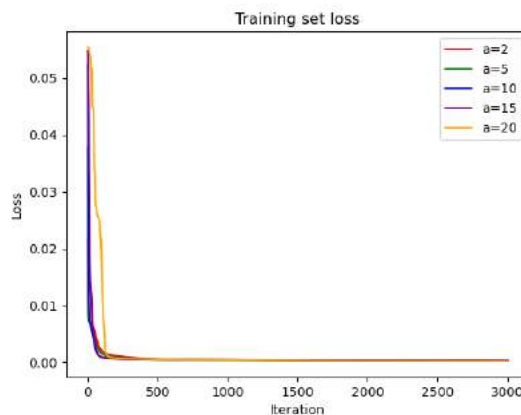


Figure 4.1: Loss curves of neural network.

It can be concluded that in all cases the model converges to about the same loss value. And after

2000 iterations, there is no significant improvement in the accuracy of the model. It can also be seen that the neural network with 20 neurons converges the slowest. It is thus more efficient to use less neurons in the network.

The following figures show the loss curves for two sets of five neurons, ranging from 2 to 11.

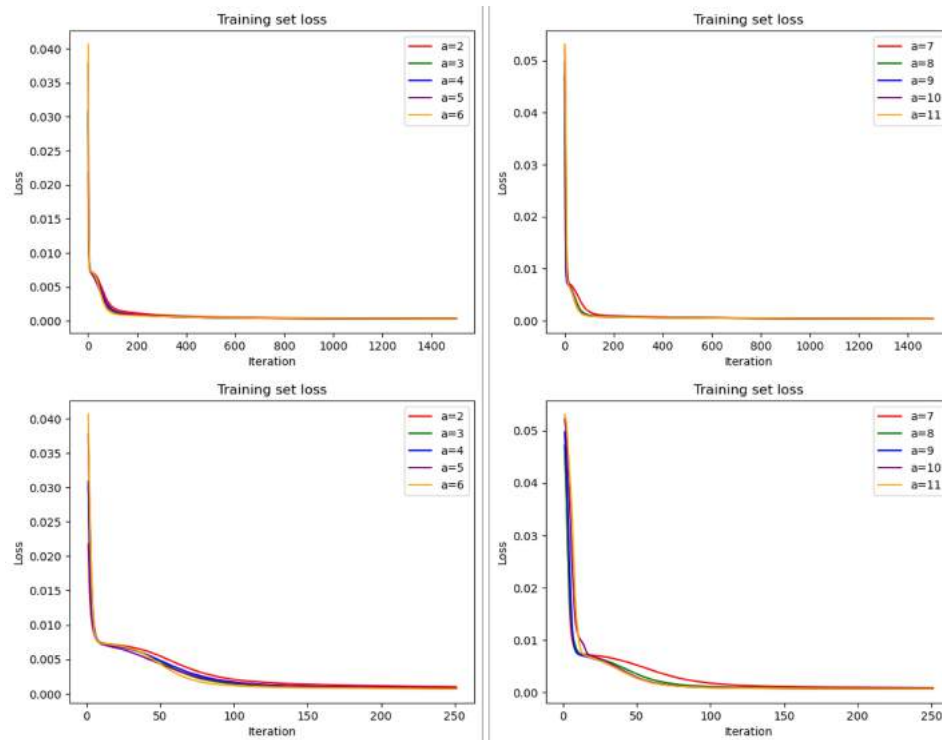


Figure 4.2: Loss curves of neural network.

Only minor differences in convergence behaviour can be seen in the early iteration steps. Table 4.1 shows the final loss to which the neural networks converge, after 3000 iterations.

Table 4.1: Model Loss

Hidden Neurons	Loss
2	0.000325
3	0.000273
4	0.000248
5	0.000248
6	0.000262
7	0.000264

Hidden Neurons	Loss
8	0.000277
9	0.000281
10	0.000273
11	0.000275
15	0.000286
20	0.000279

It can be seen that a model with four or five neurons both reach the same loss value after 3000 iteration steps. Their loss curve is also almost identical. With the obtained results it can be concluded that a neural network with four neurons performs best on the data set.

The following figures show the neural network loss convergence for different values of the learning rate and momentum, which both influence how fast the model converges to a minimal loss. The following figures show different loss curves for learning rate values between 0.001 and 0.1, and momentum values between 0 and 0.9.

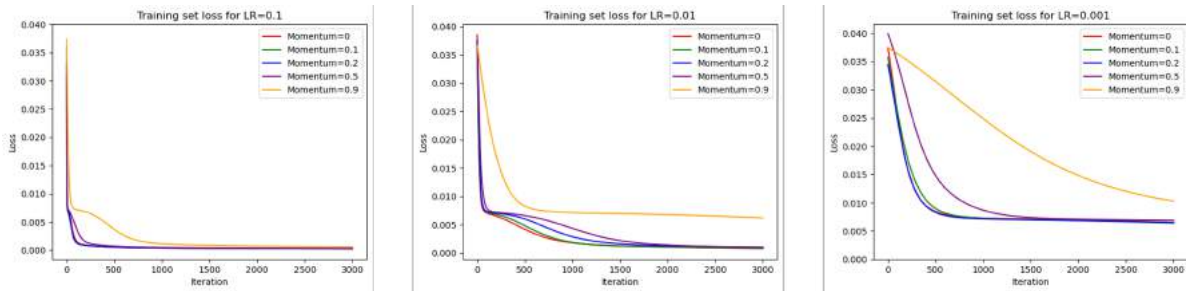


Figure 4.3: Loss curves for different learning rates and momentum.

Table 4.2: Model Loss

Momentum	Loss
0	0.000248
0.1	0.000257
0.2	0.000276
0.5	0.000305
0.9	0.000598

Momentum	Loss
0	0.000724
0.1	0.000801
0.2	0.000964
0.5	0.000989
0.9	0.00615

Momentum	Loss
0	0.006507
0.1	0.006508
0.2	0.006427
0.5	0.006895
0.9	0.010283

As the momentum increases and learning rate decreases, the model takes a longer time to reach its minimal loss. It can also be seen that for a learning rate of 0.001, the model converges to a significantly higher loss value compared to the other two situations. For this small data set, it can be concluded that introducing momentum has no benefit. It is therefore kept at its default value of zero.

Lastly, considering higher learning rate values might also be interesting. The following figures show the learning curves for the neural network with momentum equal to zero, for higher steps of learning rate up until 0.2. Choosing a high learning rate could lead to an underfit model which generates sub-optimal solutions. Therefore, the maximum learning rate chosen to be analysed is 0.2. Table 4.3 again shows the model loss after 3000 iterations.

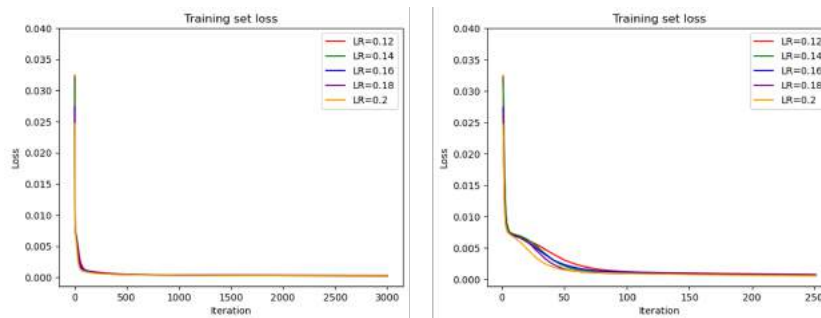


Figure 4.4: Training loss for momentum equal to zero.

Table 4.3: Training loss for momentum equal to zero.

Learning Rate	Loss
0.12	0.000269
0.14	0.000267
0.16	0.000222
0.18	0.000234
0.2	0.000217

It can again be seen that model convergence behaviour is similar between all curves, and that the model with a learning rate of 0.2 reaches the smallest loss value of 0.000217.

Summarizing, for the workflow in this thesis, the neural network is configured with the following properties:

- Hidden Neurons : 4
- Learning Algorithm: Backpropagation
- Activation Function: Sigmoid
- Iterations: 3000
- Learning Rate: 0.2
- Momentum: 0

4.1.2. 5-Fold Cross Validation

To analyze the final accuracy of the neural network, 5-Fold Cross Validation is performed. The data set is randomly divided into five groups of seven bridges each. In each step, the neural network is trained with four folds, and its accuracy evaluated with the remaining validation fold. The division of validation sets, is shown in appendix F.1. The initial parameters L_1 , W_1 and L_6 for the bridges in the validation sets, are entered into the neural network, and their predictions for said values are collected. The full predicted data set can be seen in appendix F.2. The following table summarizes the mean squared error values that were found during the iteration steps.

Table 4.4: Results from cross-validation.

	MSE 1	MSE 2	MSE 3	MSE 4	MSE 5	MSE 6	MSE 7	Average
Test fold 1	0.347599	0.020862	0.018320	0.178561	0.045721	0.240840	0.140397	0.1418
Test fold 2	0.024860	0.205327	0.061708	0.011361	0.011361	0.326310	0.076974	0.1026
Test fold 3	0.031279	0.200026	0.238801	0.046608	0.066963	0.033721	0.034954	0.0932
Test fold 4	0.046257	0.076225	0.035377	0.147259	0.028967	0.103893	0.052457	0.0701
Test fold 5	0.041097	0.073068	0.062761	0.058137	0.111448	0.044376	0.063385	0.0649
Average	0.09822	0.11510	0.08339	0.08389	0.05290	0.14983	0.07363	0.0945

The average validation MSE values for every step, their variance as well as the obtained training errors per step, are shown in table 4.5.

Table 4.5: Average MSE value per step.

	Training set loss	Validation set loss	Validation set variance
Test fold 1	0.000260	0.141757	0.141929
Test fold 2	0.000228	0.102557	0.094707
Test fold 3	0.000177	0.093193	0.086605
Test fold 4	0.000266	0.070062	0.040859
Test fold 5	0.000274	0.064896	0.000461
Average	0.000241	0.0945	0.0729122

The average training set loss value is equal to 0.000241, which is slightly higher than the model loss of when the data set is trained with all 35 bridges. The average validation set loss is equal to 0.0945, which is significantly higher than the obtained training set loss. The average validation set variance is equal to 0.0729122. It is also interesting to see that the spread in validation loss is significantly lower in the last test fold. The training set loss is significantly lower than the validation set loss. This large difference suggests that the model is memorizing the training data too well and not generalizing well to unseen data. This indicates overfitting. The validation set variance is relatively high compared to the loss, possibly indicating that the model is sensitive to small changes in the data. This can be a sign that the model is too complex or has too many parameters. Given that a neural network with only four neurons is used, it is likely the case that it is difficult to find relationships between the 24 parameters that describe the bridge leaf, with only 35 instances. The high validation set loss and variance indicate that the model might not perform well on unseen data, and could limit its capability to make correct

predictions.

Like explained in section 2.3.2, in addition to comparing the obtained loss and variance values, one would also like to plot the loss convergence of both the training data set, and validation data set, per iteration, and compare these curves, to be able to draw a conclusion about possible under- or overfitting. Here, a limitation of the lunchbox component and Grasshopper environment comes into play. The neural network can only be trained by one dataset, after which it has to be forwarded into the test component, to do predictions. It is not possible to save the learned algorithm, and apply the validation set to re-learn. It is thus only possible to analyse the loss curve of the training data set, and to compare the obtained values for the mean squared error.

4.1.3. Prediction behavior

To further determine the predicting accuracy of the neural network, the differences between the actual values and predictions done in the cross validation stage, can be analyzed. The following table shows the mean values of the percentual difference between the prediction and real value, per bridge.

Table 4.6: Prediction inaccuracy per bridge.

Bridge	Inaccuracy [%]	Bridge	Inaccuracy [%]	Bridge	Inaccuracy [%]
BRU0050	66.63	BRU0272	63.48	BRU0485	185.22
BRU0101	37.50	BRU0274	161.83	BRU0487	147.69
BRU0149	65.21	BRU0314	137.78	BRU0491	99.63
BRU0151	31.76	BRU0318	58.98	BRU1787	82.70
BRU0155	40.39	BRU0324	25.99	BRU1788	55.48
BRU0171	26.52	BRU0345	40.74	BRU1939	321.92
BRU0173	31.86	BRU0346	27.16	BRU2023	44.71
BRU0199	45.58	BRU0349	40.74	BRU2038	35.43
BRU0238	34.64	BRU0350	90.44	BRU2190	112.28
BRU0239	143.70	BRU0356	57.16	BRU5046	56.97
BRU0246	42.13	BRU0357	80.64	BRU5047	43.06
BRU0266	27.91	BRU0382	29.20		

It can be seen that differences between the real values and predicted values are high in all cases. The absolute difference in predictions range from 25.99 to 321.92%. Meaning that in the best case, the structure for an existing bridge is predicted with a 25.99% inaccuracy. Even though the loss of the model has converged to its optimal point with the configuration determined in section 3.3, its prediction performance is still far off.

The following table shows the mean prediction inaccuracy per parameter.

Table 4.7: Prediction inaccuracy per parameter.

Parameter	Inaccuracy [%]	Parameter	Inaccuracy [%]	Parameter	Inaccuracy [%]
L_2 [m]	72.23	n_{main} [—]	46.71	$I_{zz,top}$ [$\cdot 10^4$ mm ⁴]	69.95
L_3 [m]	28.31	n_{cross} [—]	28.53	$I_{zz,cross}$ [$\cdot 10^4$ mm ⁴]	276.12
L_4 [m]	34.35	n_{rib} [—]	37.48	$I_{zz,rib}$ [$\cdot 10^4$ mm ⁴]	440.36
L_5 [m]	27.46	$t_{w,1}$ [m]	40.51	H_{bottom} [mm]	15.48
L_7 [m]	65.04	$t_{w,2}$ [m]	38.24	W_{bottom} [mm]	21.80
L_8 [m]	28.65	$t_{w,3}$ [m]	26.34	$t_{w,bottom}$ [mm]	27.19
b_{main} [m]	33.71	t_{roof} [m]	27.06	$t_{f,bottom}$ [mm]	24.98

Here, prediction differences range from 15.48 to 440.36%. It can be seen that the values for parameters L_2 , L_7 and the moment of inertia parameters, are significantly higher than the rest. The neural network finds it difficult to predict these parameters accurately. For the remaining parameters, the prediction difference falls within the range of 20 to 40%. It can be seen that the dimensions of the

bottom main beam, are predicted most accurately. This indicates that there is only small fluctuation in main beam dimensions within existing bridges.

Another thing that stands out in the predicting behaviour of the model, is the acquired inaccuracy for predicting the required main beams in the bridge deck. Even though the majority of the bridges in the data set have two, three or four main beams, for which it can be assumed that these are correlated to the width of the bridge deck, the neural network predicts this value with a 46.71% inaccuracy. From testing the workflow, it was found that in especially bridges with a bridge deck width in the top range of the data set, the neural network generally does not suggest to use more than four main beams. This means that for wider bridge decks, the neural network generates a bridge deck with large cantilevers on the sides of the bridge deck. In practice, this is avoided as much as possible, and in the bridges in the data set, the maximum distances between the last main beam and side of the bridge deck, is smaller than in the bridge leaves that the neural network generates.

The inaccuracy in predicting the amount of cross beams and rib profiles is also remarkable, since it could be expected that these values are also related to the length and width of the bridge deck. Especially, considering that for the rib profiles, the same few standard profiles are used in most bridges. The inaccuracy can likely be explained by the large value range for these parameters in the data set. In newer bridges, such as the Kadoelenbridge, architectural aspects have played a more dominant role, compared to the functionality of the bridge, which stands central in older bridges within the city. This bridge has for example only two main beams and twelve cross beams in between, without rib profiles in longitudinal direction. It therefore deviates from the older bridges in the dataset, which all have a standard orthotropic bridge deck focused on functionality.

There is also a possibility that the acquired inaccuracy for predicting the L_7 variable, is somewhat skewed. Since in most bridge decks, this distance is equal to zero. As can be seen in the next table, this figure is based on only sixteen predictions.

The mean absolute inaccuracy, taken over all 735 predictions, is equal to 74.09%. When the predictions for the moments of inertia, $I_{zz,top}$, $I_{zz,cross}$ and $I_{zz,rib}$ are left out, the mean absolute inaccuracy reduces to 34.67%. The inaccuracy of predicting these three parameters thus significantly influences the overall prediction accuracy of the neural network. Therefore, they skew the prediction results. Overestimating the required moments of inertia for the structural components will lead to a more conservative structure in the first generated model, but could still work as good starting point for the structural engineer. After which he may make changes to the model. Whether the workflow generates correct structures is evaluated in the next section of this chapter.

The following table shows how often the neural network has over- or underestimated the parameter for a bridge design, and with what mean inaccuracy.

Table 4.8: Relative prediction inaccuracy per parameter.

Parameter	# Overestimated	# Underestimated	Inac. overestimated[%]	Inac. underestimated[%]
L_2 [m]	12	18	112.24	-44.42
L_3 [m]	16	14	10.08	-13.68
L_4 [m]	16	14	14.33	-14.91
L_5 [m]	12	17	7.82	-14.34
L_7 [m]	17	13	3.71	-25.22
L_8 [m]	15	16	13.73	-11.39
b_{main} [m]	20	15	20.29	-13.43
n_{main} [-]	19	16	35.26	-11.45
n_{cross} [-]	20	15	17.28	-11.25
n_{rib} [-]	14	17	15.50	-17.40
$t_{w,1}$ [m]	13	19	17.59	-17.65
$t_{w,2}$ [m]	16	17	23.24	-12.87
$t_{w,3}$ [m]	16	17	14.57	-10.02
t_{roof} [m]	16	17	14.71	-10.41
$I_{zz,top}$ [$\cdot 10^4 mm^4$]	13	17	36.66	-23.78
$I_{zz,cross}$ [$\cdot 10^4 mm^4$]	15	17	231.34	-25.43
$I_{zz,rib}$ [$\cdot 10^4 mm^4$]	16	15	373.54	-26.32
H_{bottom} [mm]	13	16	2.98	-10.34
W_{bottom} [mm]	15	14	6.61	-11.77
$t_{w,bottom}$ [mm]	12	17	8.90	-13.71
$t_{f,bottom}$ [mm]	16	13	8.19	-12.80

Each parameter gets under- or overestimated about equally as much, and the aforementioned parameters with poor prediction accuracy, can again be distinguished. The required moment of inertia for the cross beams and ribs get overestimated by sometimes three or four times as much as is needed. When an underestimation is done for these, the prediction is about 75% of what should be needed in the design. Additionally, it can be seen that most parameters, when underestimated, are done so by between 10 and 25%.

Lastly, the following table shows again the mean squared error of the different test folds, compared to the mean absolute prediction difference of the bridges in that respective test set.

Table 4.9: Test fold error and prediction difference.

	Training set loss	Validation set loss	Validation set variance	Abs. prediction diff. [[%]]
Test fold 1	0.000260	0.141757	0.141929	49.07
Test fold 2	0.000228	0.102557	0.094707	56.63
Test fold 3	0.000177	0.093193	0.086605	99.94
Test fold 4	0.000266	0.070062	0.040859	99.90
Test fold 5	0.000274	0.064896	0.000461	64.89

For this data set, which is very small compared to usual machine learning data sets, no relationships can be found between either the loss of the training and validation data set, and the obtained prediction difference of the trained algorithm within each individual test fold. Based on the results obtained, it can be concluded that indeed the high validation loss and variance also result in poor prediction performance. To increase the accuracy of the model, a remapping of the parameters is done, to reduce the amount of parameters in the model. This is described in the next paragraph.

4.2. Re-configuring the model

To further increase the accuracy of the network, there are two options. The first is to increase the amount of data points, which is very difficult in this case, since there are no more bascule bridges to easily add to the data set. The second option is to reduce the complexity of the model. At the moment,

the amount of parameters that the neural network has to predict is namely almost equal to the amount of entries in the data set. To reduce the complexity of the model, the amount of parameters that the neural network has to predict is reduced from 21 to fourteen. The following changes are made:

The values for the bascule chamber $t_{w,1}$, $t_{w,2}$, $t_{w,3}$ and t_{roof} are omitted from the data set. During the project, the focus shifted more towards the bridge leaf. The generated bascule chamber was solely for indicative reasons to obtain a sense of the dimensions of the whole structure needed for the bridge.

Secondly, an intervention is done to omit the predictions for the required moment of inertia's for the structural elements, since these have the highest inaccuracy. It can be expected that there is some form of relation between for example the amount of main beams, their moment of inertia and the bridge deck width. Choosing more main beams for a certain width, should require smaller beams to reach the same structural capacity. For the top main beams, cross beams and ribs, the following factors are defined.

$$r_{mainbeam} = \frac{I_{zz,top} \cdot n_{main}}{W_1} \left[\frac{\cdot 10^4 mm^4}{m} \right] \quad (4.1)$$

$$r_{crossbeam} = \frac{I_{zz,cross} \cdot n_{cross}}{L_1} \left[\frac{\cdot 10^4 mm^4}{m} \right] \quad (4.2)$$

$$r_{rib} = \frac{I_{zz,rib} \cdot n_{rib}}{W_1} \left[\frac{\cdot 10^4 mm^4}{m} \right] \quad (4.3)$$

These factors are calculated for all 35 bridges in the data set, after which the average for the three factors is used to calculate the required moment of inertia's for the user input parameters. By doing this, the moments of inertia are dependent on the predictions made for n_{main} , n_{cross} and n_{rib} . They are calculated inside the Grasshopper script and are thus also omitted from the data set.

The average values found for the ratios are:

$$r_{mainbeam} = 102863.5 \quad (4.4)$$

$$r_{crossbeam} = 69520.8 \quad (4.5)$$

$$r_{rib} = 4464.36 \quad (4.6)$$

In total, the complexity of the neural network is significantly reduced. It now has to predict fourteen parameters, instead of 21, with the same amount of data entries. In the following sections, the training behaviour and prediction performance is again briefly analyzed. The same test fold division is used to be able to compare the improved model with the old one.

4.2.1. Training behaviour

To evaluate the training behaviour of the new model, the same neural network properties that were described in section 4.1.1 are maintained. The following figure shows the training loss convergence of the model trained with all 35 bridges.

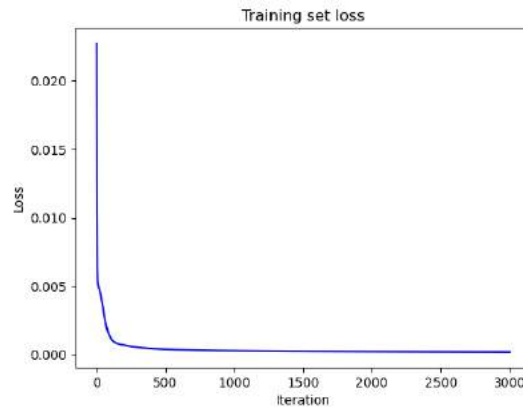


Figure 4.5: Loss curve of neural network in improved model.

The model converges to a training loss of 0.000181 after 3000 iterations. This is about 16.6% less than the value of 0.000217 that was achieved in the first model. This model thus improves to a lower training loss value.

Section F.3.1 in appendix F, shows again the predictions made per bridge in the test folds, and the mean squared error belonging to every predicted bridge. The following table shows again the mean squared errors in an overview.

Table 4.10: Cross-validation of improved model.

	MSE 1	MSE 2	MSE 3	MSE 4	MSE 5	MSE 6	MSE 7	Average
Test fold 1	0.454216	0.012051	0.017285	0.219254	0.044587	0.199773	0.135316	0.154640
Test fold 2	0.020539	0.249854	0.052735	0.014078	0.014078	0.501616	0.057821	0.130103
Test fold 3	0.034004	0.247289	0.374323	0.023621	0.086192	0.012736	0.012167	0.112904
Test fold 4	0.036291	0.066188	0.009208	0.087505	0.020524	0.124882	0.010605	0.050743
Test fold 5	0.043898	0.054856	0.024053	0.129615	0.157315	0.030314	0.031090	0.067306
Average	0.11779	0.126048	0.095521	0.094814	0.064539	0.173864	0.0494	0.10314

Table 4.11 shows the average validation MSE for every step, their variance as well the obtained training errors per step, and the difference of every value compared to the initial model presented in table 4.5.

Table 4.11: Average MSE value per step.

	Training set loss	Diff [%]	Validation set loss	Diff [%]	Validation set variance	Diff [%]
Test fold 1	0.000194	-25.38	0.154640	+9.08	0.021061	-85.16
Test fold 2	0.000162	-28.94	0.130103	+26.86	0.025313	-73.27
Test fold 3	0.000130	-26.55	0.112904	+21.15	0.017356	-79.96
Test fold 4	0.000189	-28.94	0.050743	-27.57	0.001649	-95.96
Test fold 5	0.000190	-30.66	0.067306	+3.71	0.002463	+434.27
Average	0.000173	-28.22	0.10314	+9.14	0.013568	-81.39

The trained model converges to a loss which is on average 28.22% lower than the first model. This indicates a better refinement of the model. Again, the validation set loss is significantly larger than the training set loss, meaning that the new model generalizes to new, unseen data, even less than the original one. This sign of an overfit model appears to be unavoidable with such a small data set. The variance is however on average 81.39% smaller, indicating that the improved model is more stable and is less sensitive to data changes inside the data set. This is likely the result of reducing the complexity.

4.2.2. Prediction performance

The absolute prediction differences per predicted value can be seen in section F.3.2 of appendix F.

The following table shows the prediction inaccuracy per bridge. The improvement or degradation with respect to the first model, is shown in the second column.

Table 4.12: Absolute prediction inaccuracy per bridge in improved model.

Bridge	Inaccuracy [[%]]	Diff. [%]
BRU0050	20.60	-69.08
BRU0101	38.33	+2.23
BRU0149	64.22	-1.51
BRU0151	23.92	-24.69
BRU0155	28.07	-30.50
BRU0171	18.77	-29.22
BRU0173	31.38	-1.51
BRU0199	19.30	-57.65
BRU0238	26.75	-22.77
BRU0239	36.34	-74.71
BRU0246	43.21	+2.57
BRU0266	24.48	-12.29
BRU0272	79.88	+25.84
BRU0274	50.93	-68.53
BRU0314	15.77	-88.55
BRU0318	20.74	-64.84
BRU0324	25.76	-0.88
BRU0345	17.73	-56.48

Bridge	Inaccuracy [[%]]	Diff. [%]
BRU0346	15.05	-44.60
BRU0349	17.73	-56.48
BRU0350	84.36	-6.72
BRU0356	60.98	+6.69
BRU0357	24.81	-69.23
BRU0382	23.34	-20.06
BRU0485	43.12	-76.72
BRU0487	26.53	-82.04
BRU0491	21.61	-78.31
BRU1787	42.92	-48.10
BRU1788	53.22	-4.08
BRU1939	44.29	-86.24
BRU2023	42.24	-5.52
BRU2038	36.56	+3.20
BRU2190	139.38	+24.14
BRU5046	56.21	-1.34
BRU5047	43.94	+2.05

It can be seen that for most bridges, there is a significant improvement in prediction accuracy. Improvement ranges from 0.88 to 86.24%. For seven bridges, the model predicts less accurate values compared to the first neural network. Degradation in accuracy for these bridges ranges from 2.23 to 25.84%, compared to the first model. By far the largest inaccuracy occurs for bridge 2190, which has a prediction difference of 139.38%. The first model had multiple outliers which had a severe inaccuracy. In this case, only bridge 0272, 0350 and 2190 have significantly worse prediction performance compared to the rest.

The following table shows the prediction inaccuracy of the different parameters. It also shows the improvement or degradation in prediction behavior compared to the first neural network model.

Table 4.13: Absolute prediction inaccuracy per parameter in improved model.

Parameter	Inaccuracy [[%]]	Diff. [%]
L_2 [m]	74.80	+3.56
L_3 [m]	29.58	+4.50
L_4 [m]	34.64	+0.84
L_5 [m]	29.87	+8.76
L_7 [m]	64.63	-0.62
L_8 [m]	29.22	+1.99
b_{main} [m]	35.15	+4.28

Parameter	Inaccuracy [[%]]	Diff. [%]
n_{main} [-]	45.54	-2.51
n_{cross} [-]	29.99	+5.13
n_{rib} [-]	35.34	-5.70
H_{bottom} [mm]	15.82	+2.20
W_{bottom} [mm]	21.79	-0.03
$t_{w,bottom}$ [mm]	27.97	+2.86
$t_{f,bottom}$ [mm]	25.52	+2.17

It can be seen that for most parameters, the average prediction accuracy has actually decreased compared to the first model. Differences are however very slim. The best improvement of accuracy occurs for parameter n_{rib} , which gets predicted with a 5.7% higher accuracy compared to the first model. Prediction accuracy for the L_5 parameter has degraded the most, with a loss of accuracy of 8.76% compared to the first model.

Measured over all predictions made, which are now in total 490, the mean prediction inaccuracy is equal to 38.93%. Meaning that the accuracy of the model is equal to $100\% - 38.93\% = 61.07\%$. The accuracy of the first model was equal to $100\% - 74.09\% = 25.91\%$. Relative to the first model, this is thus an improvement of 135.7% in prediction accuracy. This indicates that the neural network performs better when the amount of parameters that it has to predict, reduces. An accuracy of 61.07% is still quite poor, however, this could still lead to properly designed structures for the starting

phases of a bridge project. An explanation for the poor prediction performance could be that bridge design is also based on architectural decisions that fit the design space better, and that there do not always exist relationships between the variables describing the bridge leaf design. Further decreasing the parameters that describe the model is not a logical step to undertake, since this diminishes the legitimacy to investigate the added value of incorporating a neural network algorithm in the design process. Then, the workflow transfers into a parametric tool in which the user operates most of the buttons, which does not contribute to answering the research question.

The next table shows again how many times each parameter was over- and underestimated and by what amount on average.

Table 4.14: Relative prediction inaccuracy per parameter in improved model.

Parameter	# Overestimated	# Underestimated	Inac. overestimated[%]	Inac. underestimated[%]
L_2 [m]	13	17	43.35	-21.93
L_3 [m]	16	14	10.87	-13.92
L_4 [m]	15	15	14.46	-15.17
L_5 [m]	12	17	8.86	-15.22
L_7 [m]	18	12	3.81	-24.63
L_8 [m]	14	17	14.04	-11.64
b_{main} [m]	20	15	21.60	-13.56
n_{main} [—]	19	16	33.99	-11.55
n_{cross} [—]	20	15	18.25	-11.74
n_{rib} [—]	15	16	14.06	-16.98
H_{bottom} [mm]	13	16	3.25	-10.41
W_{bottom} [mm]	15	14	6.83	-11.64
$t_{w,bottom}$ [mm]	13	16	9.53	-13.65
$t_{f,bottom}$ [mm]	14	15	8.37	-13.10

It can be seen that the balance for each parameter has shifted lightly, but on average each parameter gets predicted lower or higher about equally. The average amount by which parameters get over- or underestimated has barely changed with respect to the first model, as already indicated by table 4.13. The only notable difference can be seen for the L_2 parameter. The average overestimation has reduced from 112.24% to 43.35% and the underestimation difference from -44.42% to -21.93%. The parameter W_{bottom} now gets predicted larger or smaller about equally, in similar trend as the other parameters describing the bottom main beam. In the previous model, the parameter W_{bottom} got underestimated seventeen times out of 29.

In general, it can be said that the new neural network and model configuration yields a higher prediction accuracy. This is likely due to omitting the moment of inertia parameters, which had the highest prediction inaccuracy. The acquired model is used to generate bridge designs in the workflow.

4.3. Validation of workflow

In this section, a short assessment is made on whether the workflow generates structurally sound bridge leaves. A comparison is done between simplified models for the main and cross beam, and results from the SCIA Engineer model, for five randomly chosen input suggestions. The differences in magnitude of occurring moments, shear forces and stresses in the main beams and crossbeams are analyzed, to validate whether the SCIA models behave correctly.

4.3.1. Calculation procedure

A simplified model of both the main beam and cross beam in an arbitrary design is constructed.

Main beam

The main beam is subjected to the following loads:

- Self-weight
- Line load due to counterweight
- Surface load on the bridge deck of 5 kN/m^2
- Point load of 300 kN

The main beam is schematized as a single statically indeterminate beam, as shown in figure 4.6. It is supported on two point supports in location A and B, similar to how a bridge leaf is supported.

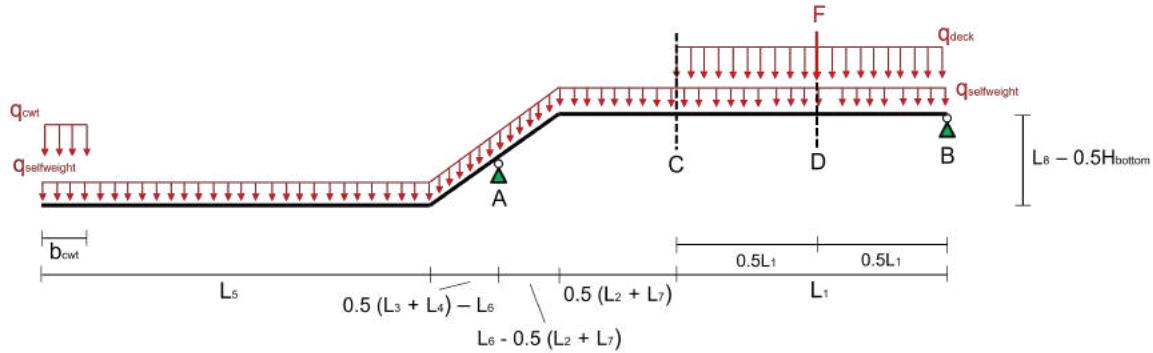


Figure 4.6: Schematization of main beam.

This simplified system of the main beam is modeled in MatrixFrame for comparison. The moment, shear force and stress distribution over the main beam is compared to the results of the SCIA model, and their magnitudes are compared in the two cross sections indicated. These are cross sections C and D, which are located at the beginning of the bridge deck and in the middle of the bridge deck respectively. The moment and shear force diagrams as result of the mentioned loading, look approximately as follows:

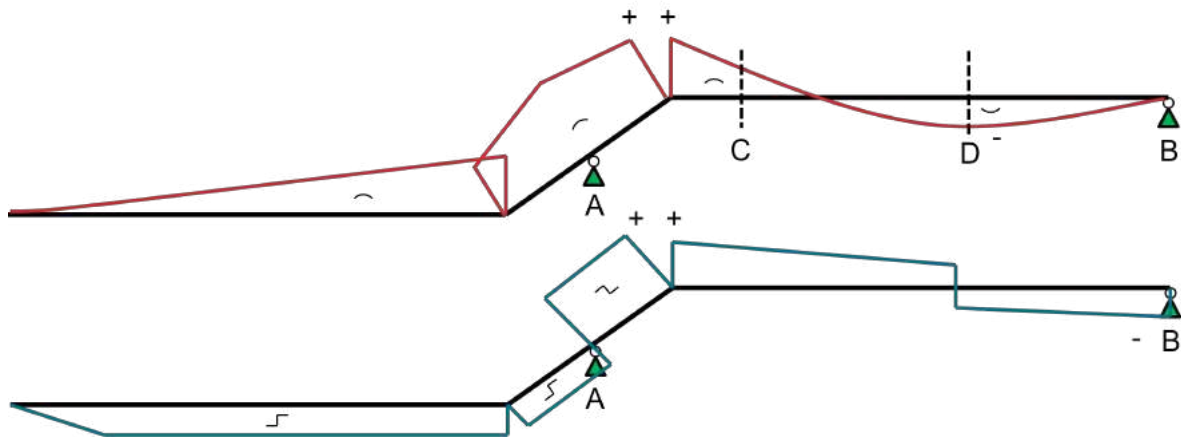


Figure 4.7: Moment diagram (top) and shear force diagram (bottom) of main beam.

The resulting moment, shear force and stress distributions from the MatrixFrame model for every validation case, can be consulted in appendix F.4.1.

In the SCIA model, the internal moment in the main beam can be approximately derived from multiplying the force in one of the two flanges with the internal lever arm z . Where $z = H - t_f$. The force n_y can be measured, which needs to be multiplied by the flange width, to obtain the total force in the bottom or top flange. The shear force in the main beam can be obtained by using the integration strips function within SCIA Engineer. With an integration strip, the forces and stresses in a plate element, can be displayed as a 1D element. To obtain the moment and shear force diagram over the main beam, integration strips are applied on the webs of the main beam. It is assumed that each web of the main beam takes approximately half of the total shear force in the beam.

Cross beam

The cross beam is subjected to the following loads:

- Self-weight
- Surface load on the bridge deck of 5 kN/m^2
- Point load of 200 kN

The cross beam is schematized as clamped beam, with length b_{main} .

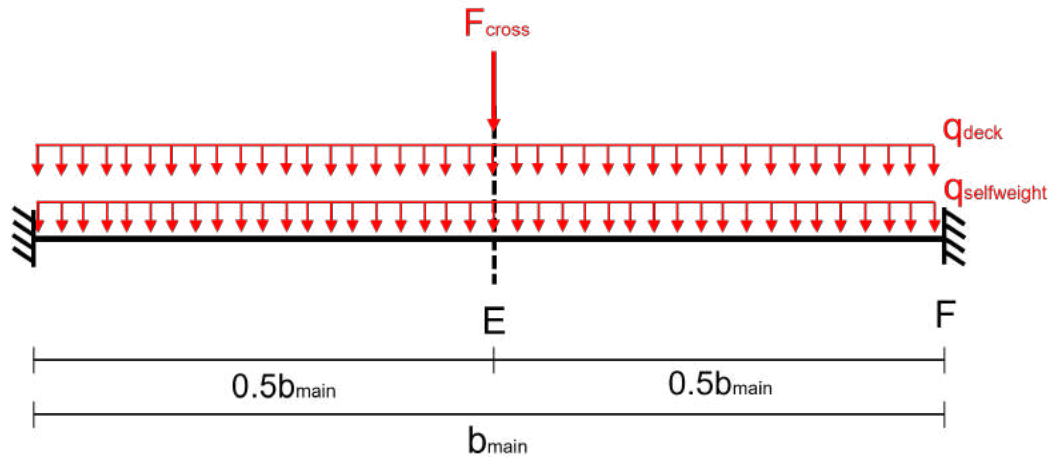


Figure 4.8: Schematization of crossbeam.

The superposition of the individual load cases leads to the following moment and shear force distribution.

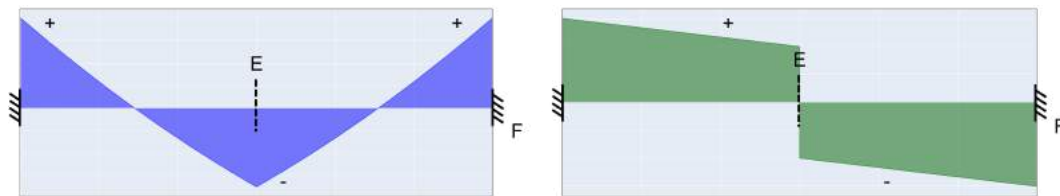


Figure 4.9: Moment diagram (left) and shear force diagram (right) of cross beam.

The schematization as a double clamped beam is a standardized case, hence, the moment, shear force and stress distribution over the beam can be easily solved with predefined equations. The magnitudes of moments, shear force and stresses in the cross beam are compared in cross sections E and F, which are in the middle and next to the welded connection with the main beam. The equations that are used to obtain the moments and shear forces in the cross-sections are shown in appendix F.4.2. Calculation of the occurring moments, shear forces and stresses in cross sections E and F is done in the Excel sheets shown in appendix F.4.3. The cross beams are modeled as line element, meaning that the bending moments, shear forces and stresses can be obtained immediately from the structural analysis results.

4.3.2. Application

The generation of bridge leaf models and the validation of their accompanying SCIA models, is done with five example cases. A combination of random values, within the range of the data set, were generated for L_1 and W_1 . For the accompanying L_6 parameter, realistic values were chosen.

Validation case one

Table 4.15 shows the input parameters that were used for this validation case. The second column shows the predicted parameters by the neural network. The third column, shows the dependent parameters, which were calculated in the Grasshopper script. These are the minimal required width of the counterweight, and the moments of inertia for the top main beam, cross beam and ribs, as calculated with the ratio determined in equations 5.1 through 5.3.

Table 4.15: Parameters for validation case one.

Input			Predictions			Dependent		
L_1	6.25	[m]	L_2	0.55	[m]	$I_{zz,top}$	615123.73	$[x10^4 mm^4]$
W_1	23.92	[m]	L_3	2.393	[m]	$I_{zz,cross}$	108626.25	$[x10^4 mm^4]$
L_6	1.94	[m]	L_4	1.921	[m]	$I_{zz,rib}$	5085.1	$[x10^4 mm^4]$
			L_5	3.387	[m]	b_{cwt}	1.1	[m]
			L_7	0.029	[m]			
			L_8	1.624	[m]			
			b_{main}	3.61	[m]			
			n_{main}	4	[-]			
			n_{cross}	4	[-]			
			n_{rib}	21	[-]			
			H_{bottom}	940	[mm]			
			W_{bottom}	290	[mm]			
			$t_{w,bottom}$	13	[mm]			
			$t_{r,bottom}$	26	[mm]			

For the above user input, the algorithm has generated a structure that is displayed in the following figures. In the right figure, the deck plate is hidden.

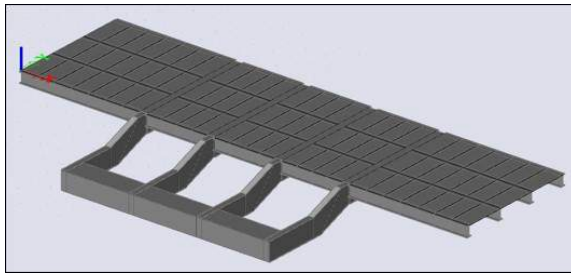


Figure 4.10: Suggested structure by workflow.

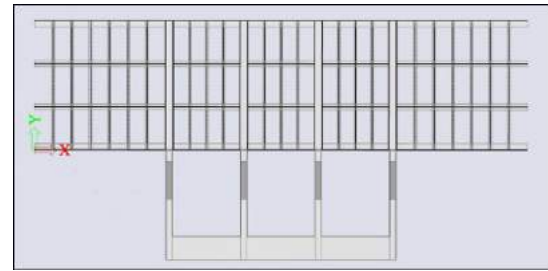


Figure 4.11: Top view of suggested structure by workflow.

What can be concluded from the suggested structure, is that it has very large cantilevers on the side. For such a wide bridge deck, it is more optimal to increase the distance between the main beams and/or increase the amount of main beams, so that the cantilevers on the side get minimized to about the width of a typical sidewalk. Purely based on the data set, the algorithm only predicts that there are four main beams needed in this design. Spacing them at a larger distance than the predicted 3.61 meters, could make it work. The amount of ribs predicted is equal to 21, which also seems like a low amount, based on the bridges in the data set. Usually, a rib is placed every 60 to 70 centimeters. In this case, the ribs are spaced apart more than a meter. The dimensions of the bottom main beam, look similar to those of the bridges in the data set. This is adequately explained by the fact that the algorithm can predict these values with the least margin of error.

For the top main beams, the calculated required moment of inertia, which is equal to $615123.73 \cdot 10^4 mm^4$, translates into a tubular profile with dimensions shown in figure 4.12. This image is not to scale. For the cross beams, the required moment of inertia results in the choice for a HE550A cross section. For the ribs, the Grasshopper script selects a "RHS 250x150x8.0" cross section.

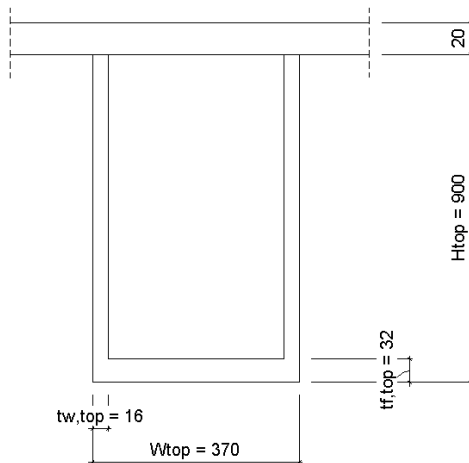


Figure 4.12: Top main beam in the design.

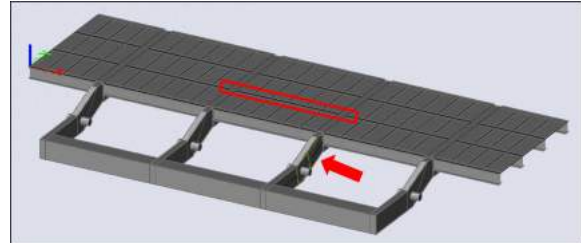


Figure 4.13: Improved structure by user.

Prior to validation of the SCIA model, a manual change to the design is made. The main beam spacing is increased to 5.6 meters, to create a somewhat realistic design. Otherwise the self-weight of the cantilevering steel elements will have a too significant influence on the stress distribution in the cross and main beams in the center of the bridge leaf. This new design is visible in figure 4.13. The correctness of occurring stresses, moments and shear forces, will be checked on the main beam and cross beam indicated in red. The loading that was described earlier, will be applied onto these two elements in the model.

Using the integration strips function within SCIA Engineer, the total distribution of moments and shear forces over the web flanges of the main beam, can be plotted as graph. The following figures show the moment distribution M_z and shear force V_y over one flange of the main beam.

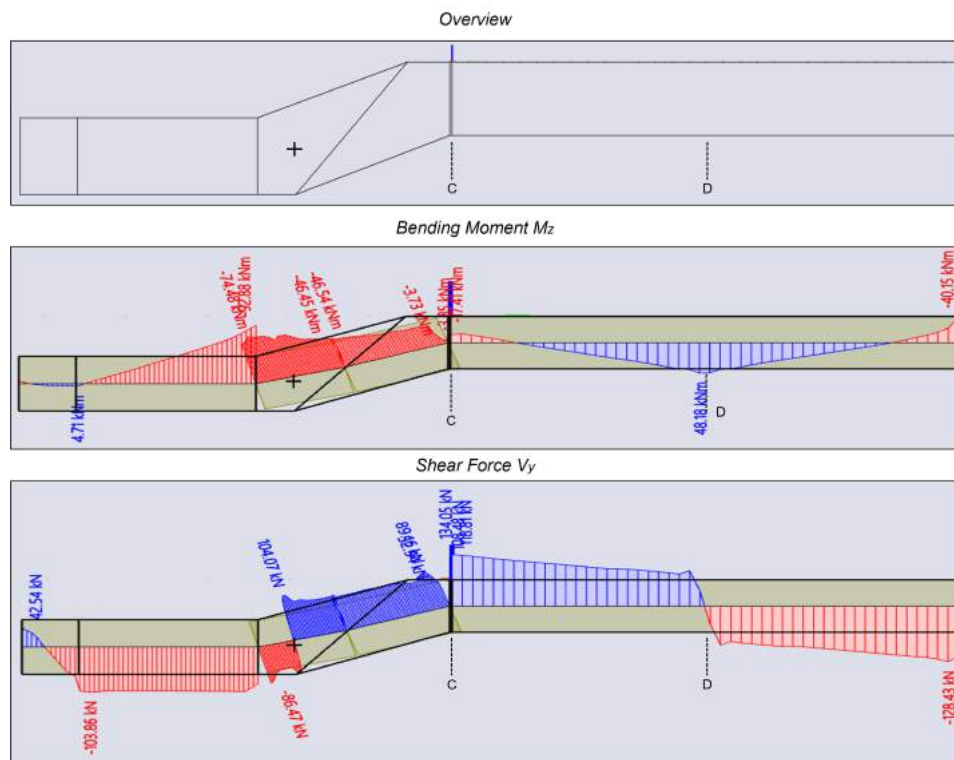


Figure 4.14: Main beam case one (top), moment diagram (middle) and shear force diagram (bottom).

The moment and shear force distribution are in line with the schematization in figure 4.7. The maximum hogging moment occurs near the support point at the rotational axis. It can also be seen that the web flanges underneath the bridge deck, are mostly subjected to a negative bending moment. In the SCIA model, the maximum occurring bending moment in the beam occurs at the connection between the intermediate part and bottom main beam, just next to the rotational axis.

The normal forces in the bottom flange of the main beam, are shown in figures F.12 and F.13. In cross section C, the normal force appears to be 600 kN/m on average. Multiplying this with the width of the flange and internal leverarm, the moment in the main beam can be estimated as 164 kNm. In cross section D, the average force in the bottom flange is equal to -712 kN/m. This leads to a negative bending moment of approximately 237 kNm. These values are significantly smaller than the calculated values in the MatrixFrame model. It can also be seen that the maximum shear force in the beam occurs at cross section C, which is equal to 119.02 kN per web. The shear force line switches signs at cross section D, and at the rotational axis, where the bending moments in the beam are maximum. The local shear force peaks around cross section D are similar in magnitude, namely 82.8 kN per web.

Figure F.22 displays the stresses σ_y+ over the top flange of the loaded main beam and the bridge deck plate.

The bridge deck plate is subjected to a small compressive stress zone near the loaded main beam, while further away, tensile zones can be found. The highest compressive stresses in the bridge deck occur right underneath the point load of 300 kN, in the middle of the span. Right underneath the point load, compressive stresses of up to 40 MPa occur. In the majority of the bridge deck, tensile and compressive stresses do not exceed a magnitude of 10 MPa. Figure 4.15 shows a more elaborated view on the stress distribution in the main beam. The second figure from the top shows again the stresses σ_y+ in the top flange and bridge deck plate. The third figure shows the stresses σ_y- over the bottom flange of the main beam. The bottom two figures show a zoomed in view of points of interest, namely where high stress concentrations occur.

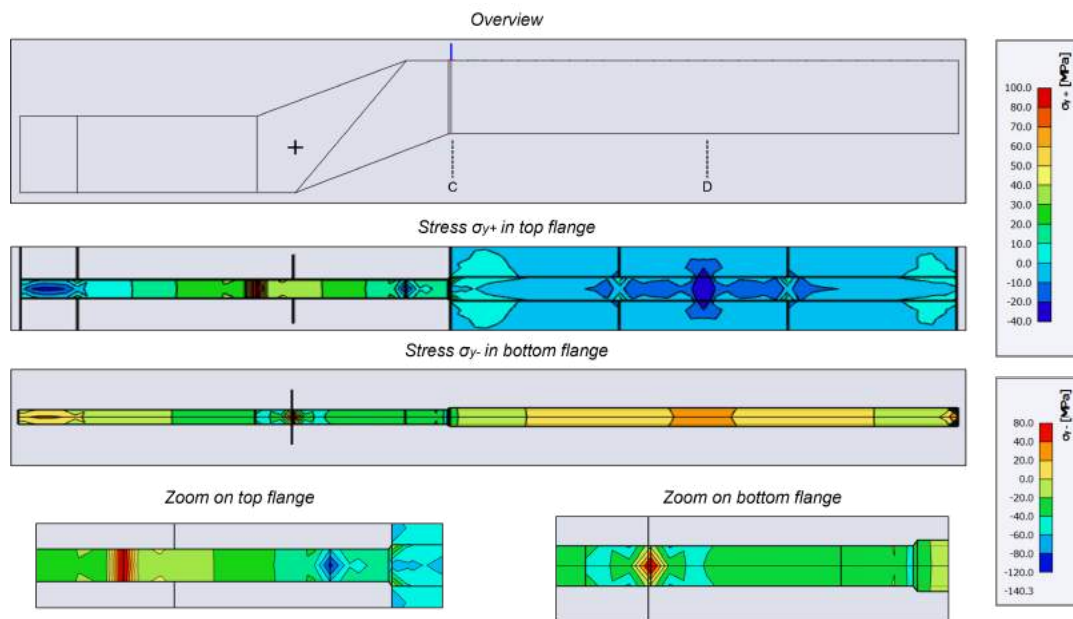


Figure 4.15: Stresses in the main beam.

In the top flange of the main beam in cross section C, the effective width of the cross section changes drastically, which the SCIA model finds hard to process. In the model, the maximum occurring stress in the top flange at cross section C is calculated to be a tensile stress of 18.8 MPa. In the bottom flange at cross section C, the maximum stress in loaded direction is a tensile stress of 38.3 MPa. In cross section D, the maximum stress in the bridge deck plate is a compressive stress of 39.7 MPa. In the bottom flange, the maximum stress occurring is a tensile stress of 22.7 MPa, and hence not normative

for this cross section. It can be seen that in the connection between the top flange of the bottom main beam and intermediate part, a tensile stress concentration occurs of up to 100 MPa. This zone is indicated in red in the bottom left figure. This zone occurs due to the fact that the two plates connect under an angle, and are not modeled as continuous plate element. In practice, the main beams are fabricated as one curved element. Similar stress concentrations occur underneath the rotational axis in the bottom flange and in the top flange at the end of the intermediate part. One can also find two local compressive stress concentrations in the bottom flange of the main beam, near their support points at the toe of the leaf. The supports are modeled in these two nodes, hence there is a stress concentration at each node which does not occur in practice. At the point where the counterweight attaches to the main beams, compressive stresses of up to 40 MPa occur in the top flange and tensile stresses of up to 40 MPa in the bottom flange. The stress distributions over the top and bottom flanges of the main beam show fitting behavior with the moment and shear force distribution in the previous figure.

The following figure shows the moment distribution M_y , shear force distribution V_z and stress distribution σ_x , over the cross beam, from top to bottom respectively.

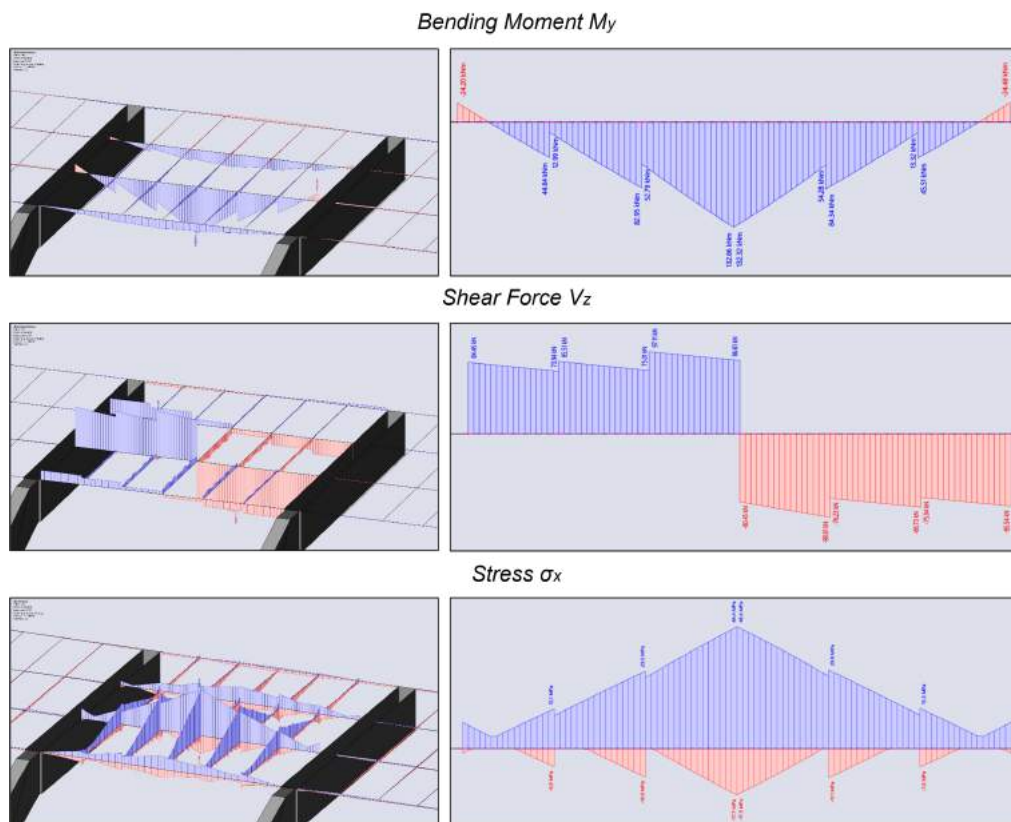


Figure 4.16: Moment (top), shear force (middle) and stress distribution over the cross beam.

From the top two figures it can be seen that the moment distribution occurring, can be expected given the structure of the bridge deck. The maximum bending moment in the cross beams happens in the middle of its span, at cross section E. Within the hand calculation, it was assumed that the cross beams would behave as a clamped beam, since they are welded in between the main beams. The rotational stiffness of the connection between the I-profile of the cross beam and tubular profile of the main beam, appears to be less stiff than expected. The moment distribution of the cross beam tends to be more like that of a simply supported beam, since the hogging moments at the connections are very small compared to the bending moment at mid-span. The small jumps in all distributions can also be explained, since the rib profiles connect to the cross beam at these locations. The shear force diagram also resembles correct structural behaviour of the crossbeam within the bridge deck. Lastly, considering the stress diagram in the bottom two figures, it can be seen that the tensile stresses, which are indicated in blue, reach higher values than the compressive stresses. Assuming a linear

distribution over the cross section height, it could be said that the majority of the cross section is under tension when the bridge deck is loaded. This can be explained by the fact that the ribs have a smaller profile height than the cross beams, and that the cross beams usually have a smaller profile height than the main beams, while they align at the top, right under the bridge deck plate. The compressive forces thus get redirected over the whole bridge deck structure, while the bottom of the crossbeam profile, has less stiffness to resist bending. Tensile forces thus automatically get redistributed over the bottom remainder of the crossbeams.

From the SCIA model, the following data can be deducted.

The maximum negative bending moment in the cross beam occurs at mid-span and is equal to -132.86 kNm. The hogging moment at the connection between the crossbeam and main beam is equal to 24.2 kNm.

The shear force right next to mid-span is equal to ± 86.61 kN. The shear force at the connection between the crossbeam and main beam is equal to 84.45 kN. The maximum tensile stress at mid span is equal to 46.4 MPa, and the maximum compressive stress -17.5 MPa. At cross section F, the maximum tensile stress is equal to 10.1 MPa and the maximum compressive stress equal to -1.8 MPa.

The comparison between the MatrixFrame model, hand calculation and SCIA model, is shown in the next table, as well as the relative difference between the two obtained values for every cross section.

Table 4.16: Comparison between MatrixFrame model, hand calculation and SCIA model for validation case one.

Main beam			
	MatrixFrame	SCIA Model	Difference [%]
Cross section C			
Bending moment M_z [kNm]	930.61	164	-82.38
Shear force V_y [kN]	379.06	238.04	-37.20
Stress σ_y [MPa]	117.79	38.3	-67.48
Cross section D			
Bending moment M_z [kNm]	-209.69	-237	+13.02
Shear force V_y [kN]	281.33	± 165.6	-41.14
Stress σ_y [MPa]	-37.61	-39.7	+5.56
Cross beam			
	Hand calculation	SCIA Model	Difference [%]
Cross section E			
Bending moment M_y [kNm]	-155.794	-132.86	-14.72
Shear force V_z [kN]	100	86.61	-13.39
Stress σ_x [MPa]	38.724	46.4	+19.82
Cross section F			
Bending moment M_y [kNm]	31.588	24.2	-23.39
Shear force V_z [kN]	-133.84	-84.45	-36.90
Stress σ_x [MPa]	7.851	10.1	+28.64

For the main beam, it can be seen that there is a significant difference in the obtained values between the 2D MatrixFrame model and the SCIA Model. The shape of the moment, shear force and stress distribution corresponds between the two models, however the magnitudes do not. This is due to the fact that in the SCIA model, the forces get redistributed over the whole bridge leaf structure, while in the 2D MatrixFrame model, only a single supported beam is considered. It is therefore a logical consequence that the moments in the simply supported beam, are significantly higher than in the SCIA model, where the effective width of the whole bridge leaf structure is taken into account. Given that the whole bridge deck plate acts as top flange of the main beam in the SCIA model, it appears that the 2D framework schematization is not a good comparison to estimate the occurring moments and shear forces in the beam. What can be concluded from the SCIA model is that the distribution of moments, shear forces and stresses appear to be correct under the applied loading. The eventual distribution and magnitudes of shear forces, moments and stresses in the SCIA model, appear to be correct.

Judging from the values obtained that describe the force and stress distribution in the cross beams, it can be said that the schematization as clamped beam, reflects the expected structural behaviour quite well. In most comparisons between the SCIA model and simplified hand calculation, a difference on average of 10 to 30 percent can be observed. Meaning that the magnitudes of bending moments, shear forces and stresses σ_x in the SCIA model are likely quite accurate to the bridge leafs real behaviour. Thus meaning that the cross beams in the model also reflect proper structural behaviour. Also, considering that the distributions shown in figure 4.16, show that the cross beam behaves more like a simply supported beam due to the weak stiffness of the connection between the main beam, the magnitudes of the considered properties, can be said to be in the same order of magnitude.

Validation case two

The input parameters and accompanying predictions made by the neural network for validation case two, can be seen in table 4.17.

Table 4.17: Parameters for validation case two.

Input			Predictions			Dependent		
L_1	12.5	[m]	L_2	1.125	[m]	$I_{zz,top}$	541747.8	$[x10^4 mm^4]$
W_1	31.6	[m]	L_3	3.467	[m]	$I_{zz,cross}$	124144.3	$[x10^4 mm^4]$
L_6	1.38	[m]	L_4	3.207	[m]	$I_{zz,rib}$	2766.152	$[x10^4 mm^4]$
			L_5	5.348	[m]	b_{cwt}	0.8	[m]
			L_7	0.266	[m]			
			L_8	2.192	[m]			
			b_{main}	5.52	[m]			
			n_{main}	6	[-]			
			n_{cross}	7	[-]			
			n_{rib}	51	[-]			
			H_{bottom}	1140	[mm]			
			W_{bottom}	370	[mm]			
			$t_{w,bottom}$	20	[mm]			
			$t_{f,bottom}$	37	[mm]			

The neural network suggests a structure like shown in the next two figures.

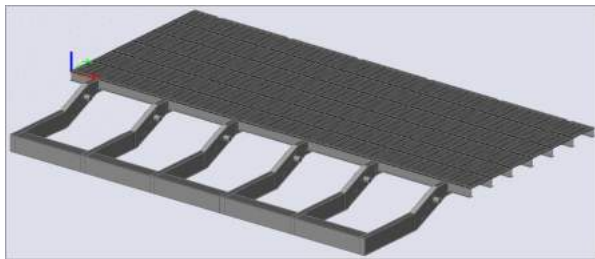


Figure 4.17: Suggested structure by workflow.

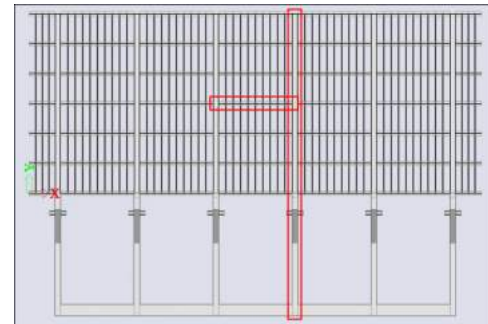


Figure 4.18: Top view of suggested structure by workflow.

Unlike the first validation case, the neural network does seem to predict a realistic structure for these input parameters. The generated structure consists of six main beams which are spaced at 5.52 meters. This means that on both sides, a small cantilevering part is present in the bridge deck with a width of two meters. The predicted size of the bottom main beams and amount of ribs necessary in the bridge deck, also appear to be a logical choice given the bridges in the data set. The top main beam, in the bridge deck structure, has a total height of 870 millimeters, and a width of 350 millimeters. The webs have a thickness of sixteen millimeters and the bottom flange thirty millimeters. The cross beams are modeled with HE600A profiles, and the ribs as "RHS 200x100x12" profiles. Once again, the bridge deck plate is twenty millimeters thick.

This structure is further used as second case for the structural validation of the SCIA model. The main beam and cross beam on which the loads were placed, are again highlighted in red in figure 4.18. Figure 4.19 shows the distribution of moments and shear forces in the main beam.

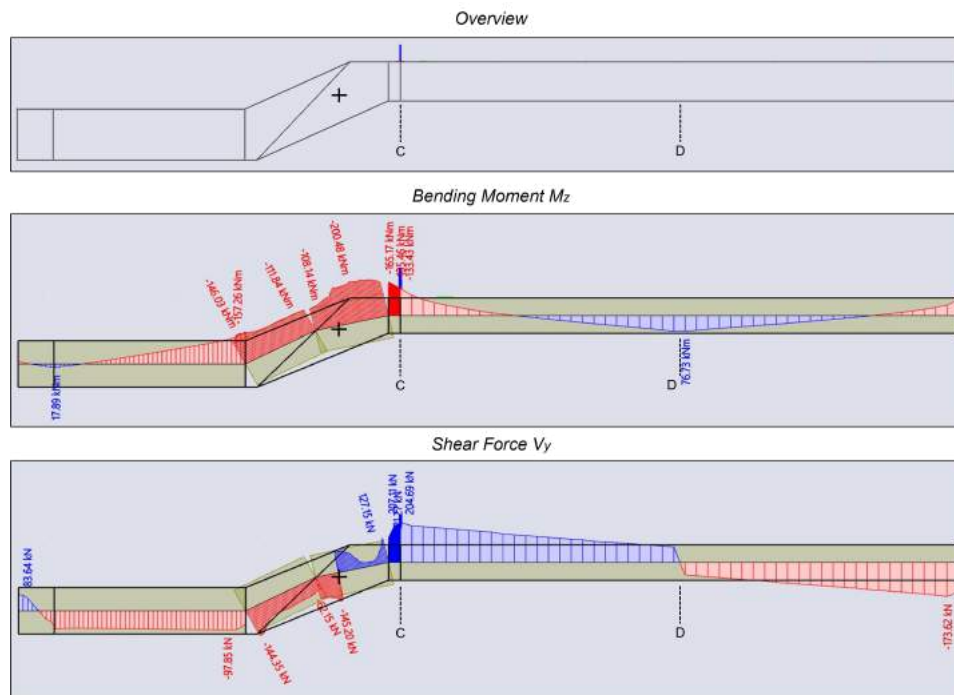


Figure 4.19: Main beam case two (top), moment diagram (middle) and shear force diagram (bottom).

The figures show similar distributions as in the first case. One difference is that the maximum moment occurs right above the rotational axis, instead of just next to it in the bottom main beam. The normal forces in the bottom flange of the respective main beam, can be seen in figures F.14 and F.15. In cross section C, the average normal force in the flange is equal to 1800 kN/m. This leads to an internal bending moment of approximately 759 kNm in cross section C. In cross section D, the average normal force in the flange appears to be around -1400 kN/m, which translates into a bending moment of -426 kNm. The maximum shear force in the main beam occurs in cross section C and is equal to 207.11 kN per web. In the local peaks right next to cross section D, the shear force is equal to ± 81.1 kN per web.

Figure F.23 shows a top view of the stress distribution σ_y over the top flange of the main beam and the bridge deck plate.

A symmetrical stress distribution can be observed due to the loading on one of the middle main beams. Again, the majority of the bridge deck plate is in a low state of stresses of up to 20 MPa. Stress concentrations occur right underneath the point load in the middle of the bridge deck, and also at the connection between the bridge deck plate and main beams. Near the connection to the main beams, the magnitude of tensile stresses increase.

Figure 4.20 shows a detailed view on the occurring stresses in the main beam for this validation case.

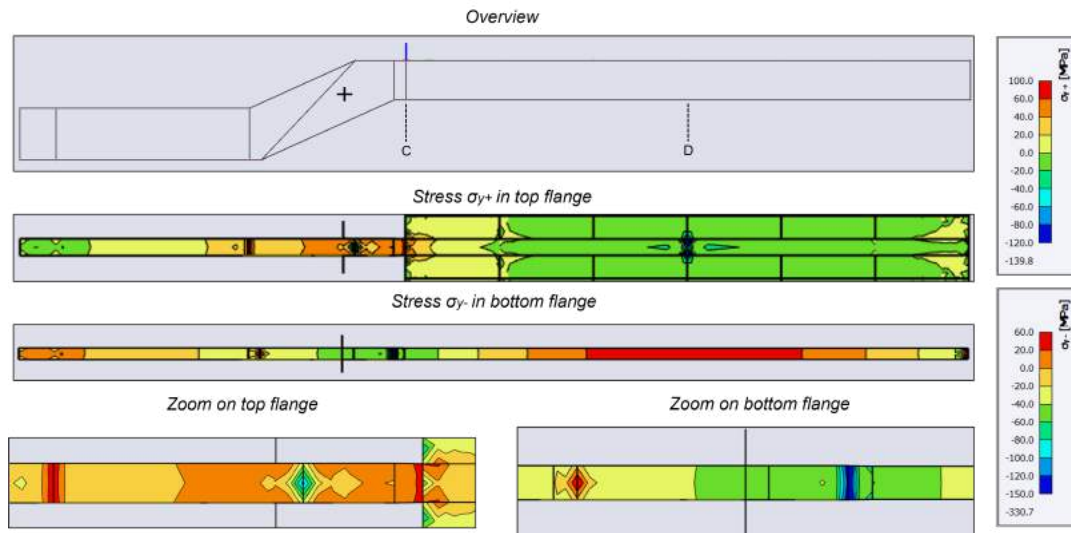


Figure 4.20: Stresses in the main beam.

The stress concentrations at the connection between the plates of the intermediate part can again be seen. In the top corner connection, shown in detail in the bottom left figure, the stresses converge to one central point in the plate, indicated in cyan. This is not correct behaviour of the stress flow between the plates. It can also be seen that SCIA cannot model the connection between the main beam and bridge deck plate well. Before the bridge deck starts, the magnitude of stresses gradually increases to a maximum stress of 100 MPa in the red zone. Suddenly, in the bridge deck three distinct points of local compression can be seen near the connection. These stress concentrations further dissipate into tensile stresses in the bridge deck plate. The distribution of stresses in the bottom flange of the main beam seems to be modeled correctly, with the exception of previous mentioned locations at the interface between the intermediate part of the main beam. Underneath the point load in cross section D, the bottom flange is in maximum tension. Moving towards both ends of the bridge deck, the bottom flange transfers to a compressive state. The peak stresses of -330.7 MPa occur in the corner points of the support nodes, which are the result of how the model is built up. The maximum stress in cross section C is measured next to the bridge deck plate, where the top flange of the main beam is still in the dark red zone. The maximum stress occurring in the center of the top flange is equal to 89.2 MPa. In the bottom flange in cross section C, the stress is equal to -64.5 MPa. In cross section D, the maximum stress in the main beam occurs in the bottom flange, which is a tensile stress of 46.5 MPa. The local stress concentration underneath the point load is disregarded, since SCIA Engineer cannot model this correctly.

Figure 4.21 shows the distribution of M_x , V_z and σ_x over the cross beam.

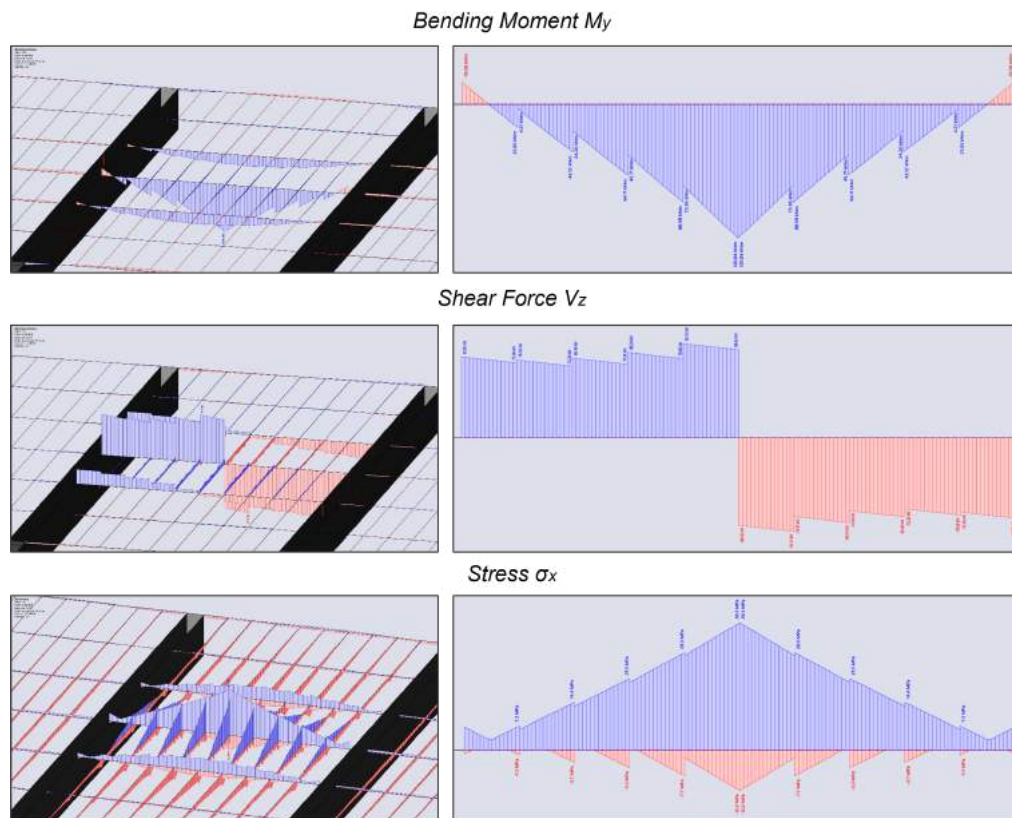


Figure 4.21: Moment (top), shear force (middle) and stress distribution over the cross beam.

The model shows similar behavior as the cross beam in the first validation case. The distributions of bending moment, shear forces and stresses look alike.

The maximum negative bending moment in cross section E is equal to -120.84 kNm. This is slightly less than in the first validation case, in which the beam span was marginally higher, namely 5.6 meters compared to 5.52 meters in this validation case. The hogging moment at cross section F is equal to 19.58 kNm. The shear force in the cross section directly next to mid-span is equal to 88.85 kN, again approaching the theoretical value of 100 kN, in which a beam was assumed without ribs attached. The shear force in cross section F is equal to 81.85 kN. The maximum tensile stress at mid span is equal to 38.3 MPa, and the maximum tensile stress in cross section F is equal to 7.0 MPa.

The following table again shows the comparison between the results from the SCIA model and simplified models.

Table 4.18: Comparison between MatrixFrame model, hand calculation and SCIA model for validation case two.

Main beam			
	MatrixFrame	SCIA Model	Difference [%]
Cross section C			
Bending moment M_z [kNm]	2616.75	759	-71
Shear force V_y [kN]	540.08	414.22	-23.30
Stress σ_y+ [MPa]	130.88	89.2	-31.84
Cross section D			
Bending moment M_z [kNm]	-475.93	-426	-10.49
Shear force V_y [kN]	329.37	± 162.2	-50.75
Stress σ_y- [MPa]	61.62	46.5	-24.54
Cross beam			
	Hand calculation	SCIA Model	Difference [%]
Cross section E			
Bending moment M_y [kNm]	-153.48	-120.84	-21.27
Shear force V_z [kN]	100	88.85	-11.15
Stress σ_x [MPa]	36.47	38.3	+5.02
Cross section F			
Bending moment M_y [kNm]	30.96	19.58	-36.76
Shear force V_z [kN]	-133.66	-81.85	-38.76
Stress σ_x [MPa]	7.36	7.0	-4.89

Again, for the main beams it can be concluded that there is a significant difference between the values obtained in the SCIA model and framework model. Both bending moments get estimated a little better. The magnitude of the stress in both cross sections get overestimated by the framework model by about 25 to 30 percent. In the SCIA model, the stresses in the flanges of the main beam are smaller since the whole bridge deck plate acts as top flange of the main beam in the bridge deck. The magnitudes of occurring stresses in the SCIA model appears to be correct, with the exception of the local stress concentrations at the plate connections and support nodes.

For the stress distribution throughout the cross beam, the differences between the simplified hand calculation and SCIA model are minor. There is namely only a five percent difference in calculated stresses. For the bending moment and shear forces, the difference is larger, namely up to approximately 35 percent. In this bridge leaf design, there are more rib profiles connecting to the cross beams, compared to the first case, that take up forces. Hence, the approximation of the hand calculation is expected to be further off the real values. Still, the cross beam in the model behaves like one would expect, and its behaviour is in line with the distributions found in the first validation case.

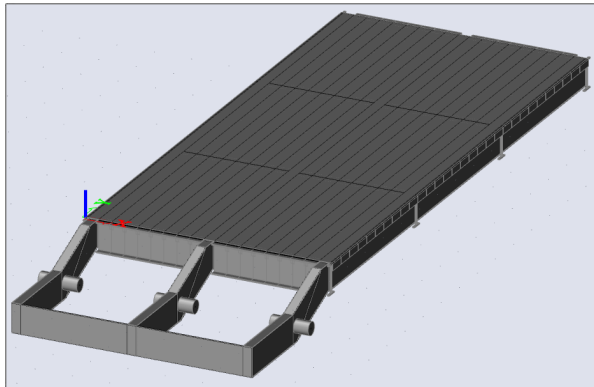
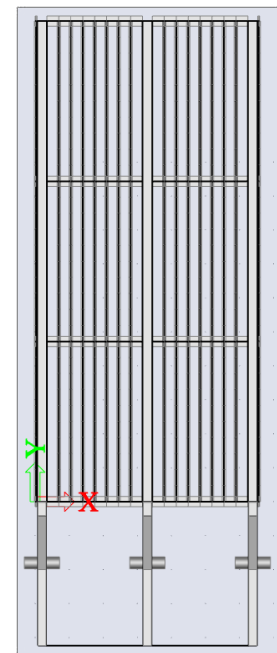
Validation case three

The input and output of the Grasshopper script for the third validation case, can be seen in the next table.

Table 4.19: Parameters for validation case three.

Input			Predictions			Dependent		
L_1	14.15	[m]	L_2	0.415	[m]	$I_{zz,top}$	225956.8	[x10 ⁴ mm ⁴]
W_1	6.59	[m]	L_3	1.97	[m]	$I_{zz,cross}$	245929.8	[x10 ⁴ mm ⁴]
L_6	1.8	[m]	L_4	1.493	[m]	$I_{zz,rib}$	1838.76	[x10 ⁴ mm ⁴]
			L_5	2.44	[m]	b_{cwt}	-	[m]
			L_7	0.019	[m]			
			L_8	1.37	[m]			
			b_{main}	3.095	[m]			
			n_{main}	3	[-]			
			n_{cross}	4	[-]			
			n_{rib}	16	[-]			
			H_{bottom}	770	[mm]			
			W_{bottom}	240	[mm]			
			$t_{w,bottom}$	10	[mm]			
			$t_{r,bottom}$	20	[mm]			

The neural network suggests a structure like shown in the figures below.

**Figure 4.22:** Suggested structure by workflow.**Figure 4.23:** Top view of suggested structure by workflow.

For this relatively long, small bridge structure, the neural network suggests a structure made out of three main beams. The main beams are spaced at 3.095 meters in between. There are several problems with the suggested structure. Firstly, the neural network suggests three main beams for this user input. The width of the bridge deck is only 6.59 meters, meaning that a good suggestion would be to use two main beams. All but one of bridges in Amsterdam, the Roskambrug, with similar width, use two main beams in the bridge leaf. This also seems to be a logical choice for a bridge this small. Secondly, with a spacing of 3.095 meters in between the main beams, there remains a very small cantilevering part next to the outer main beams. In practice, this is not achievable construction-wise. Additionally, the neural network models a rib element inside this outer part. There are namely only seven rib profiles placed in between each pair of two main beams. The cantilevering parts are too small to implement a rib profile, it conflicts with the geometry of the outer main beams. Lastly, the suggestion made for the L_5 parameter, namely the length of the bottom main beams, is too small. The given suggestion of 2.44 meters, is too short to be able to build a counterweight that can compensate for the static moment of the bridge deck. This is why there is no counterweight modeled in figures 4.22

and 4.23.

The suggested dimensions for the bottom main beam, are slightly smaller than in the previous two validation cases, which is logical since the bridge deck structure is smaller. Decreasing the amount of main beams to two, will likely increase the dimensions of them, to achieve sufficient structural capacity. What is interesting is that the model predicts that a larger profile must be chosen for the cross beams, than the top main beams. For the top main beams, a tube is modeled with height of 700 millimeters and a width of 290. The web thickness is twelve millimeters and the flange thickness 26. For the cross beams, a HE800A profile is chosen by the neural network. This is a significantly larger cross section compared to the first two cases, which is interesting since this bridge deck is smaller. For the rib profiles, a "RHS180x100x10" profile is chosen, which is quite small. This is expected, since the model predicts 16 ribs to be used in this structure, which is a lot.

It can be said that for this case study, the user will have to manually alter five parameters in the model, to create a viable structure. Before the structure is forwarded into SCIA engineer to validate the occurring stresses, the following changes are made. The amount of main beams are decreased to two, and they are spaced at 5 meters heart to heart distance. The amount of rib profiles is reduced to 12, and the distance L_5 is increased to 4.0 meters, so a suitable counterweight can be modeled. A bridge deck plate of twenty millimeters is again used. As result of these changes, the dimensions of the cross sections for the top main beam and rib profiles, increase. The top main beams are now modeled with a height of 780 millimeters and a width of 320. The web thickness increases to fourteen millimeters and the flange thickness to 28. The rib profiles increase to a "RHS 200x100x10" profile. Additionally, the parameter L_4 needs to increase to 1.7 meters to create a feasible spot for the rotational axis. The final input parameters can be seen in the calculation sheet in appendix F.4.3.

The distribution of M_z and V_y over the main beam, can be seen in figure 4.24.

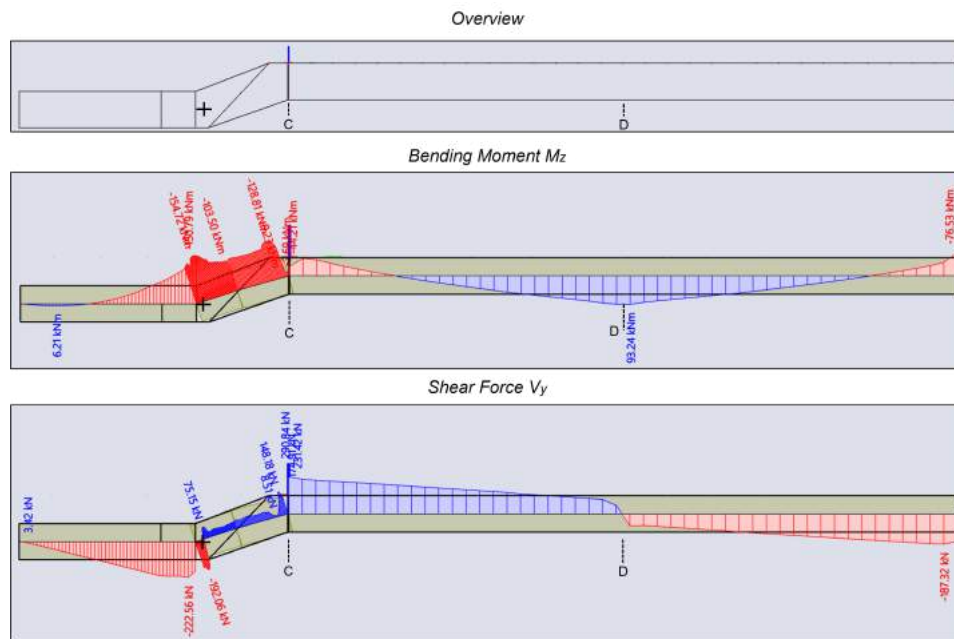


Figure 4.24: Main beam case three (top), moment diagram (middle) and shear force diagram (bottom).

It can be seen that in this design, the rotational axis is placed quite far outwards towards the bottom main beam. This also the position where the maximum bending moment in the beam occurs. There appears to be a disturbance in the moment diagram along the length of the main beam. There is namely a small peak downward, which should not occur. This is likely due to the fact that the distance L_7 is too small, which is the distance over which the profile of the main beam changes towards the profile that is present underneath the bridge deck. If there is a sudden change in beam width, the

steel plates are angled and have a different local coordinate system with respect to the beam webs. Hence, projecting the bending moment M_z in the global coordinate system, like done in the figures, leads to a disturbance of the moment and shear force lines over this connecting piece of main beam. The normal force in the bottom flange of the main beam can be seen in figures F.16 and F.17. The moment in cross section C is approximately equal to 406 kNm and is in cross section D approximately equal to -507.5 kNm. From figure 4.24, it can be deducted that the shear force in cross section C is equal to 290.84 kN per web and in cross section D it is equal to 76.27 kN per web.

Figure F.24 shows a top view of the stress distribution σ_y over the top flange of the main beam and the bridge deck plate.

Compressive stresses occur in the majority of the bridge deck due to the loading on the main beam. In this validation case, the stresses in the bridge deck seem to be of higher magnitude. Also, the peak stresses reach significantly higher values. The following figure shows a detailed view on the stresses in the main beam.

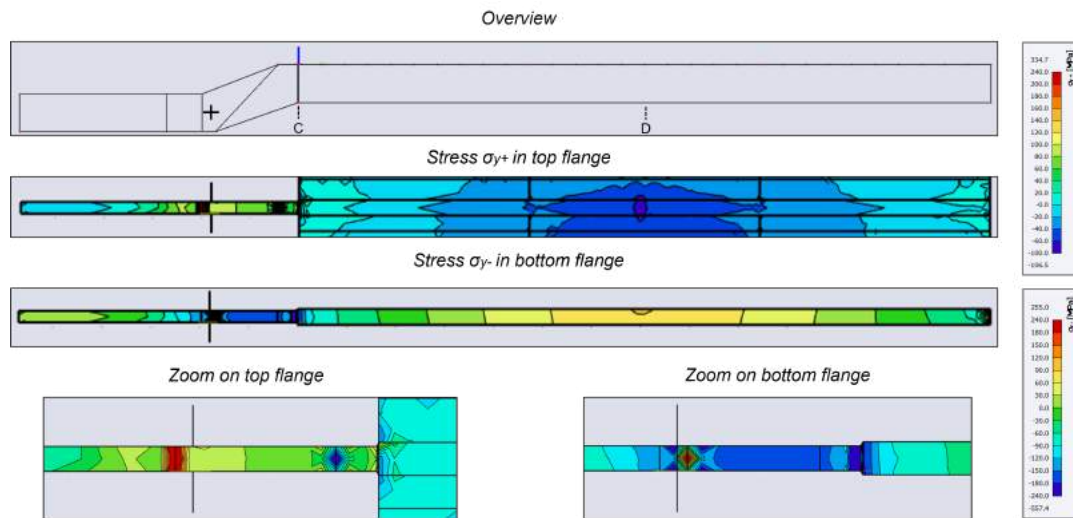


Figure 4.25: Stresses in the main beam.

It can be seen that the same stress concentrations in the main beam occur around the intermediate part. The bottom flange of the intermediate part is in significant compression, while the top flange is under tension and compression. Again, a concentration of compressive stresses in a single point occurs at the top corner of the intermediate part, which further influences the stress distribution towards the bridge deck. In the connection between the main beam and deck plate, now two stress concentrations occur, namely in both corner points where the top flange of the main beam meets the deck plate. In the bottom side, a concentration of compressive stresses occur, indicated in the dark blue zone in the bottom left figure. While on the inward side of the structure, tensile stresses gather in a single node. Again, the distribution of stresses over the bottom flange of the main beam underneath the bridge deck, appears to be normal. The normative stress in cross section C occurs in the bottom flange and is equal to -259.4 MPa. The normative stress in cross section D occurs in the bottom flange and is a tensile stress of 91.7 MPa.

Figure 4.26 shows the distribution of M_x , V_z and σ_x over the cross beam in this design.

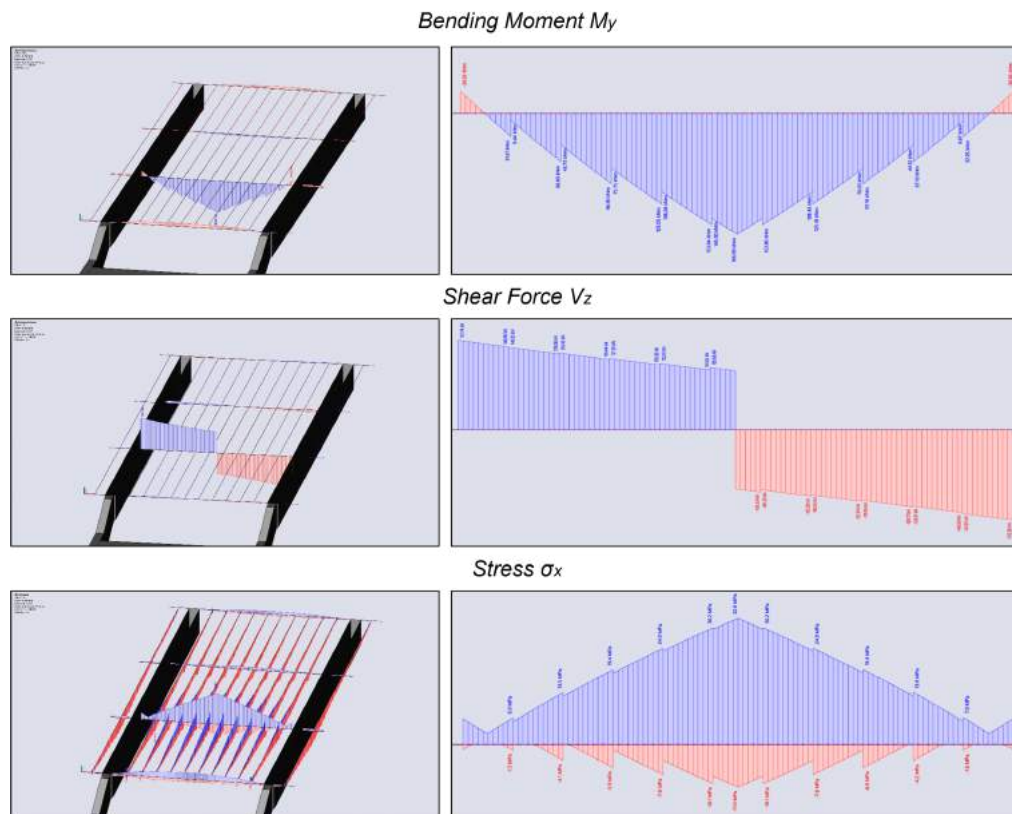


Figure 4.26: Moment (top), shear force (middle) and stress distribution over the cross beam.

The distribution of bending moments and stresses is again similar to those in the previous two validation cases. The shear force diagram appears to have shifted towards the typical, expected distribution like shown in figure 4.9. This can be explained by the fact that there are only two main beams in the bridge leaf structure of this validation case. When there are more main beams, the cross beam can be schematized as continuous beam on multiple support points. Given that a cross beam somewhere in the middle of the bridge deck was chosen for analysis in the first two validation cases, this results in a lower "reaction" force in one of the middle main beams, compared to one of the outer main beams. In general, it can be concluded that also in this validation case, the cross beams show correct structural behaviour.

The maximum negative bending moment at mid span of the cross beam is equal to -166.89 kNm. The hogging moment at cross section F is equal to 30.66 kNm. The shear force right next to mid span is equal to 100.17 kN, and the shear force at cross section F is equal to 152.90 kN. Lastly, the maximum tensile stress in the middle of the cross beam is equal to 32.6 MPa, and at cross section F it is equal to 6.7 MPa.

The following table shows again the results for the model validation for this case.

Table 4.20: Comparison between MatrixFrame model, hand calculation and SCIA model for validation case three.

Main beam			
	MatrixFrame	SCIA Model	Difference [%]
Cross section C			
Bending moment M_z [kNm]	1120.12	406	-63.75
Shear force V_y [kN]	485.85	581.68	+19.72
Stress σ_y [MPa]	-237.46	-259.4	+9.24
Cross section D			
Bending moment M_z [kNm]	-1486.79	-507.5	-65.87
Shear force V_y [kN]	221.71	152.54	-31.2
Stress σ_y [MPa]	148.32	91.7	-38.17
Cross beam			
	Hand calculation	SCIA Model	Difference [%]
Cross section E			
Bending moment M_y [kNm]	-151.90	-166.89	+9.87
Shear force V_z [kN]	100	100.17	+0.17
Stress σ_x [MPa]	24.4	32.6	+33.61
Cross section F			
Bending moment M_y [kNm]	53.81	30.66	-43.02
Shear force V_z [kN]	-164.57	-152.90	-7.09
Stress σ_x [MPa]	8.64	6.7	-22.45

Like in previous validation cases, comparing the values between the simplified framework calculation and the SCIA model for the main beam in this design, leads to significant differences for four of the six values. However, the estimations for the occurring shear forces and stresses in the two cross sections by the simplified model, approximate the real values better than in the first two cases. In both cases, the approximations for the bending moments are about 65% off, in contrast to the previous two validation cases, in which the moment in cross section D matched by 10%.

For the cross beams, true occurring shear forces, moments and stresses appear to be larger than what is predicted by the hand calculation. Again, confirming that the cross beams behave more like a simply supported beam than a clamped beam. Additionally, the hogging moment at the connection in cross section F, gets overestimated by the hand calculation. Confirming this thought. Once again, the magnitudes of occurring moments, shear forces and stresses in the cross beam indicate that the cross beam functions properly in the SCIA model of this validation case.

Validation case four

The input and output of the Grasshopper script for the fourth validation case, can be seen in the next table.

Table 4.21: Parameters for validation case four.

Input			Predictions			Dependent		
L_1	10.8	[m]	L_2	0.509	[m]	$I_{zz,top}$	367222.7	[x10 ⁴ mm ⁴]
N_1	14.28	[m]	L_3	2.276	[m]	$I_{zz,cross}$	187706.2	[x10 ⁴ mm ⁴]
L_6	2.1	[m]	L_4	1.81	[m]	$I_{zz,rib}$	3355.319	[x10 ⁴ mm ⁴]
			L_5	3.112	[m]	b_{out}	1.7	[m]
			L_7	0.024	[m]			
			L_8	1.559	[m]			
			b_{main}	3.58	[m]			
			n_{main}	4	[-]			
			n_{cross}	4	[-]			
			n_{rib}	19	[-]			
			H_{bottom}	900	[mm]			
			W_{bottom}	280	[mm]			
			$t_{w,bottom}$	12	[mm]			
			$t_{f,bottom}$	24	[mm]			

The neural network suggests a structure like shown in figure 4.27.

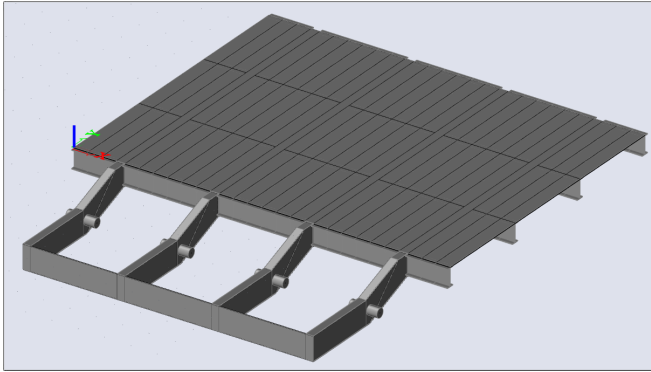


Figure 4.27: Suggested structure by workflow.

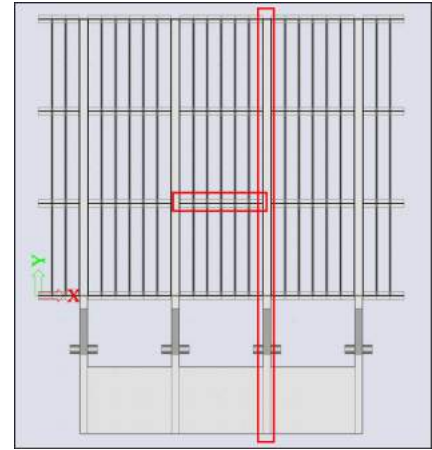
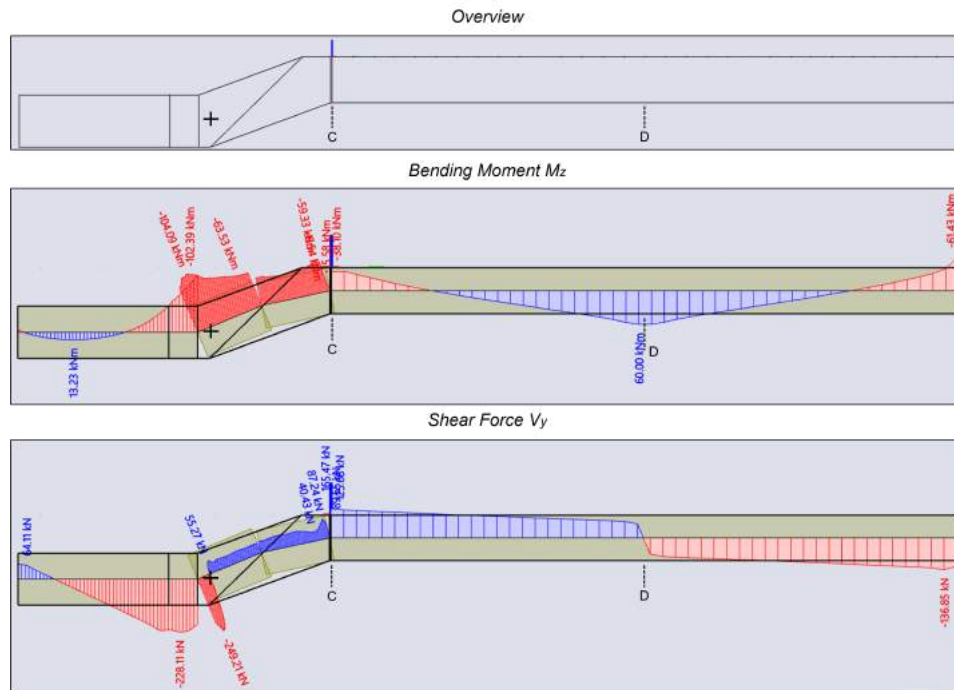


Figure 4.28: Top view of altered structure.

The neural network can give a good suggestion for a structure with these input parameters, except for one thing. The neural network again predicts a too small value for the depth of the bottom main beam, L_5 . The remainder of the bridge leaf design looks similar to bridges in the data set. The neural network predicts four main beams for this structure, which are spaced at 3.58 meters. This results in cantilevering parts of approximately 1.7 meters on each side of the bridge deck. The algorithm predicts four crossbeams and nineteen ribs, which seem to be a good fit for this design. The predictions done for the size of the main beams, also seem to be in line with the data set and previously generated bridges.

For the top main beam, the neural network predicts that a moment of inertia of $I_{zz,top} = 367223 \cdot 10^4 \text{ mm}^4$ is required. This translates into a tube profile with a height of 790 millimeters and a width of 330 millimeters. The web thickness is equal to fourteen and the flange thickness to 28 millimeters. For the cross beams, a HE700A profile is chosen and for the ribs a "RHS 200x100x16" profile.

To be able to generate a counterweight that can compensate the structure of the bridge deck, the parameter L_5 was set to 3.3 meters. The structure was then forwarded into SCIA Engineer for validation. Figure 4.29 shows the distribution of M_z and V_y over the main beam.



The diagrams have the same shape as the three cases before. Again, the maximum bending moment in the main beam occurs near the rotational axis. In cross section C, the bending moment is approximately equal to 417 kNm. In cross section D, the bending moment is equal to -376 kNm. The shear force in cross section C is equal to 165.47 kN per web and in cross section D it is equal to 62.56 kN per web.

Figure F.25 shows the stress distribution over the top flange and bridge deck.

Again, the stress distribution in the bridge deck gets modeled as expected. The compression zone around the loaded main beam dissipates into a tensile zone around. In the top flange of the main beam, a compressive zone is located where the counterweight connects onto the main beam, and in the top joint between the plates of the intermediate part and linear parts of the beam. Figure 4.30 shows an in depth view on the stresses in the main beam.

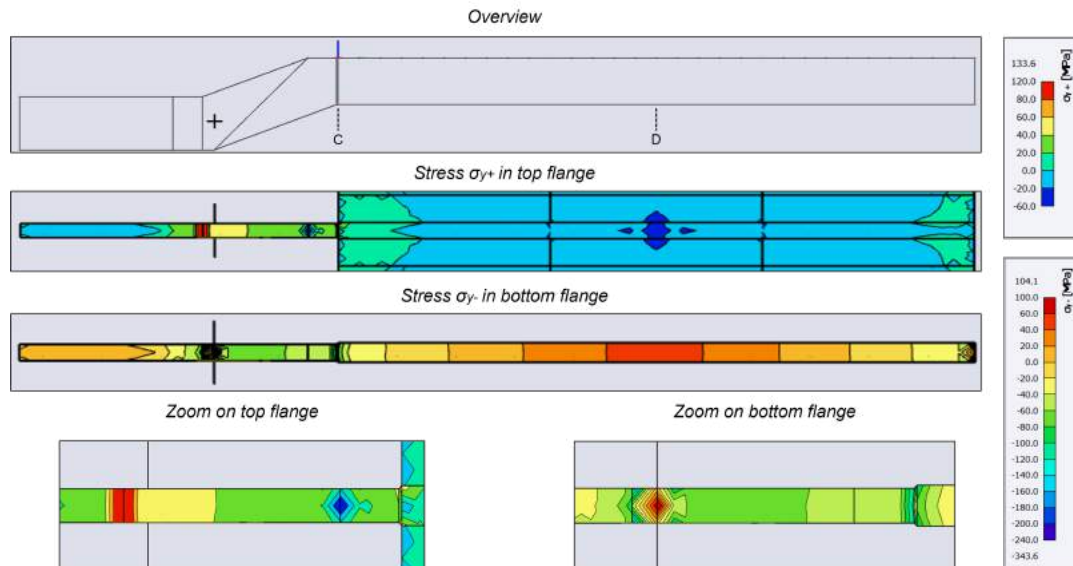


Figure 4.30: Stresses in the main beam.

The same stress concentrations in the intermediate part can be seen as in the other validation cases. In this structure, the stress disturbance between the main beam and bridge deck plate seems to be less significant compared to the other cases. The stress in the main beam just left of the bridge deck is quite constant over the beams width, and is equal to somewhere between 20 and 40 MPa in the top flange and -40 to -80 in the bottom flange. In the bottom flange at cross section C, again two points of stress concentration occur, as can be seen in the bottom right image in figure 4.30. In cross section C, the stress in the middle of the top flange of the main beam is equal to 27.4 MPa. In the bottom flange, a compressive stress concentration occurs in this transition, so no reliable value can be deducted. In cross section D, the stress in the bottom flange of the main beam is equal to 50.6 MPa and in the bridge deck plate underneath the point load it is equal to -57 MPa.

Figure 4.31 shows the distribution of M_x , V_z and σ_x over the cross beam in this design.

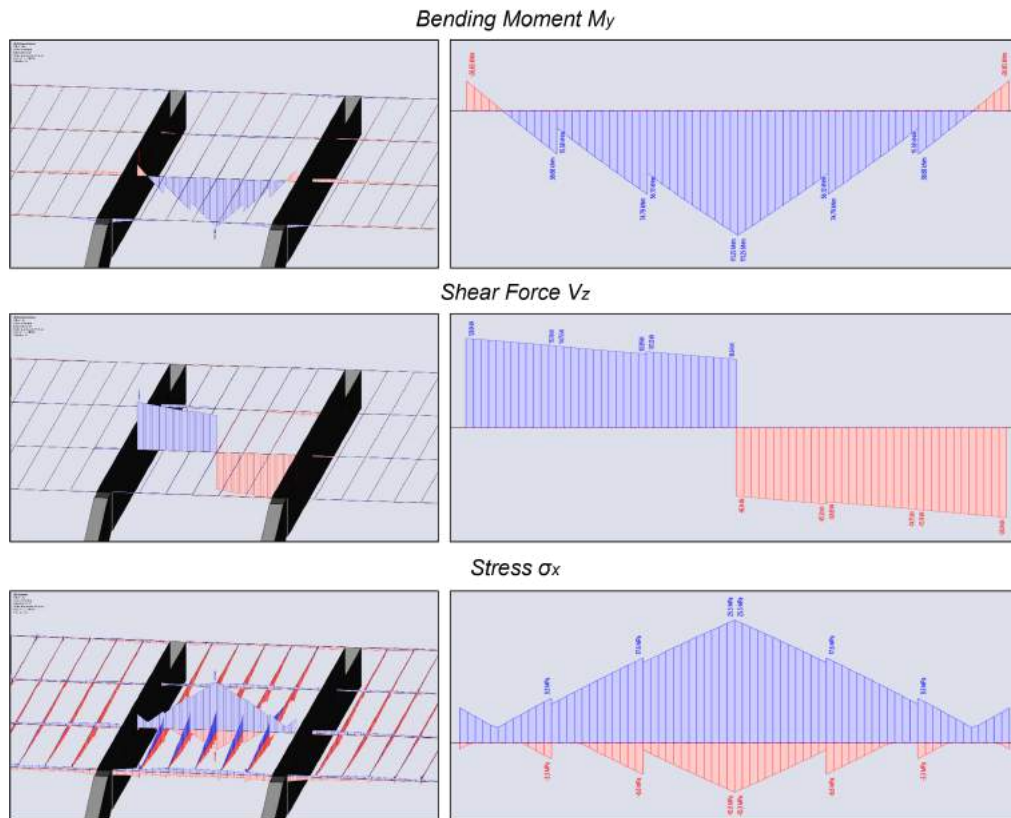


Figure 4.31: Moment (top), shear force (middle) and stress distribution over the cross beam.

The distribution of moments, shear forces and stresses is again similar to all other cases. One major distinction can be seen in the shear force diagram compared to the first two validation cases. In this case, only very small jumps in the shear force diagram occur at the positions where the ribs connect to the cross beam. These jumps are significantly larger in validation case one and two. Meaning that the rib profiles in this validation case take up less force, and play less of a role in redistributing the forces over the bridge deck. This can be confirmed by the image in the bottom left of figure 4.31. The stresses in the ribs perpendicular to the crossbeam, are significantly smaller compared to the cross beams. While in validation case one and two, the peak stress in the rib at the connection between the two elements, approached the stress in the crossbeam at that position, way closer. This behaviour can be explained by the ratio between the strength of the cross beam compared to that of the rib profile. In this case, the ratio between $I_{zz,top}$ and $I_{zz,rib}$ is approximately equal to 56. While for validation case one and two this ratio is equal to approximately 21 and 45 respectively. In this bridge leaf, the cross beams draw more of the forces to themselves.

The maximum negative bending moment in the middle of the cross beam is equal to -111.25 kNm. The maximum hogging moment in cross section F is equal to 26.65 kNm. The shear force next to mid span is equal to 96.34 kN and at cross section F it is equal to -126.04 kN. The maximum tensile stress in the cross beam occurs at mid span and is equal to 25.5 MPa. The tensile stress in cross section F is equal to 7.3 MPa.

Table 4.22 shows the comparison results.

Table 4.22: Comparison between MatrixFrame model, hand calculation and SCIA model for validation case four.

Main beam			
	MatrixFrame	SCIA Model	Difference [%]
Cross section C			
Bending moment M_z [kNm]	641.78	417.12	-35
Shear force V_y [kN]	313.42	330.94	+5.59
Stress σ_y + [MPa]	65.53	27.4	-58.19
Cross section D			
Bending moment M_z [kNm]	-830.67	-376	-54.74
Shear force V_y [kN]	201.68	125.12	-37.96
Stress σ_y - [MPa]	85.54	50.6	-40.84
Cross beam			
	Hand calculation	SCIA Model	Difference [%]
Cross section E			
Bending moment M_y [kNm]	-100.2	-111.25	+11.03
Shear force V_z [kN]	100	96.34	-3.66
Stress σ_x [MPa]	18.42	25.5	+38.44
Cross section F			
Bending moment M_y [kNm]	21.41	26.65	+24.74
Shear force V_z [kN]	-135.88	-126.04	-7.24
Stress σ_x [MPa]	3.93	7.3	+85.75

In validation case four, the relative difference in both predictions for the bending moments has been reduced, while the difference between the stress approximation has increased for both cross sections, based on the trend that could be seen in the previous cases. However, the values obtained in the SCIA model seem correct, excluding the zones of the main beam that get modeled incorrectly, which have been addressed earlier.

For the cross beams, no peculiarities can be found in the differences between the SCIA model and hand calculation. The relative difference in the stresses occurring are larger compared to the other validation cases. It is difficult to pinpoint a cause for this observation. However, the absolute difference between the stresses in both cross sections is only seven and three megapascals respectively. It could still be said that the order of magnitude of occurring stresses in the SCIA model is approximately equal to those of the hand calculations. The SCIA model behaviour of the cross beam is identical to the other three models.

Validation case five

The input and output of the Grasshopper script for the fifth validation case, can be seen in the next table.

Table 4.23: Parameters for validation case five.

Input			Predictions			Dependent		
L_1	13.5	[m]	L_2	0.738	[m]	$I_{zz,top}$	380595	[x10 ⁴ mm ⁴]
W_1	18.5	[m]	L_3	2.771	[m]	$I_{zz,cross}$	187706.2	[x10 ⁴ mm ⁴]
L_6	1.85	[m]	L_4	2.381	[m]	$I_{zz,rib}$	2753.022	[x10 ⁴ mm ⁴]
			L_5	4.186	[m]	b_{cwt}	1.6	[m]
			L_7	0.07	[m]			
			L_8	1.857	[m]			
			b_{main}	4.14	[m]			
			n_{main}	5	[-]			
			n_{cross}	5	[-]			
			n_{rib}	30	[-]			
			H_{bottom}	1020	[mm]			
			W_{bottom}	320	[mm]			
			$t_{w,bottom}$	15	[mm]			
			$t_{t,bottom}$	30	[mm]			

The generated structure can be seen in the next two figures.

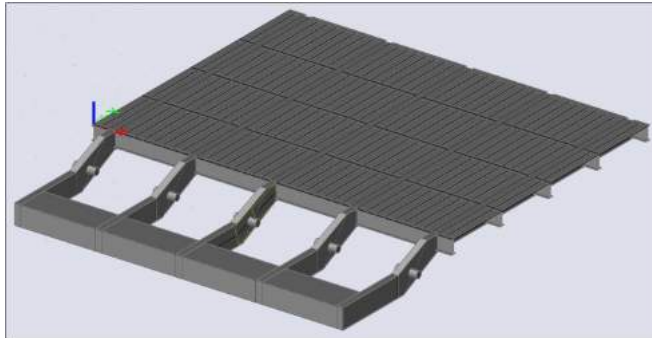


Figure 4.32: Suggested structure by workflow.

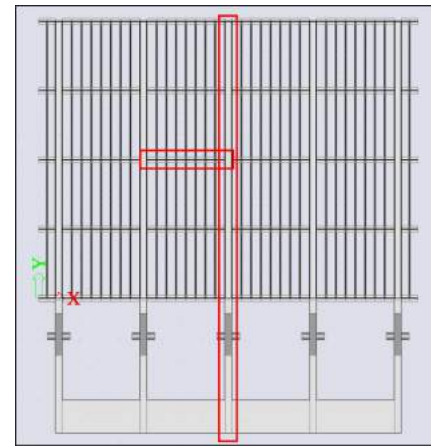


Figure 4.33: Top view of suggested structure by workflow.

The suggested structure consists of five main beams, which are spaced at 4.14 meters apart. The amount of main beams, cross beams and ribs that are predicted, appear to be a good choice for a bridge deck of this size. The height on the top main beam is predicted to be 800 millimeters, and its width 330 millimeters. The web thickness for the top main beam is predicted to be fourteen and the flange thickness 28 millimeters. The cross beams are modeled as HE700A beams and the ribs as "RHS 200x100x12". Again, the neural network appears to do a good suggestion directly, without needing user interference.

The following figure shows the moment and shear force distribution over the main beam for this validation case.

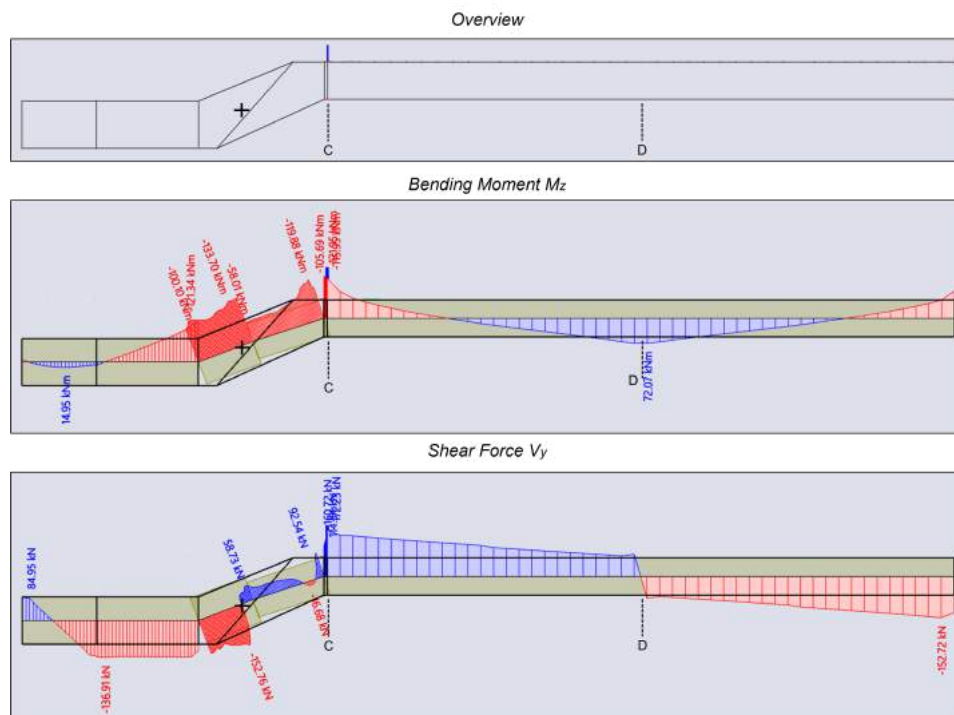


Figure 4.34: Main beam case five (top), moment diagram (middle) and shear force diagram (bottom).

The maximum moment in cross section C is approximately equal to 475 kNm and in cross section D

the maximum moment is equal to approximately -449 kNm. There is also an odd jump in the moment line at the position just right of the rotational axis. This looks to be the result of the transition between the integration strips. Here, the limitations of the integration strip function come into play. Although this jump is present in the moment lines of all validation cases, the jump in this case is more significant. In the shear force line, a local sag can be seen just left of cross section C, where the shear force line reaches the opposite direction. This is also odd, and not in line with the other shear force diagrams shown. The maximum shear force in cross section C is equal to 172.23 kN per web, and the shear force in the local peaks around cross section D is equal to ± 78.35 kN per web. The peculiar behavior of the moment and shear force line in the discussed section is likely the result of the inaccuracy in the integration strips and incorrectly modeled piece between the bridge deck plate and main beam, more specifically the location where the main beam profile transitions over the length L_7 .

Figure F.26 shows an overview of the stresses in the bridge deck plate and top flange of the main beam, that result from the loading on the main beam.

It can be seen that the majority of the top flange of the loaded main beam is under tensile stress, up until where the counterweight begins. The bridge deck plate around the loaded main beam is under compression, the stresses transform into tensile stresses further away from the loaded main beam, similar as in the other validation cases. The majority of the bridge deck plate is in no stress state larger than 40 MPa. The stress distribution over both the deck plate and top flange of the main beam is symmetrical, indicating that there are no model or geometry inconsistencies in the transverse direction. The following figure shows an in-depth view on the stresses in the structure.

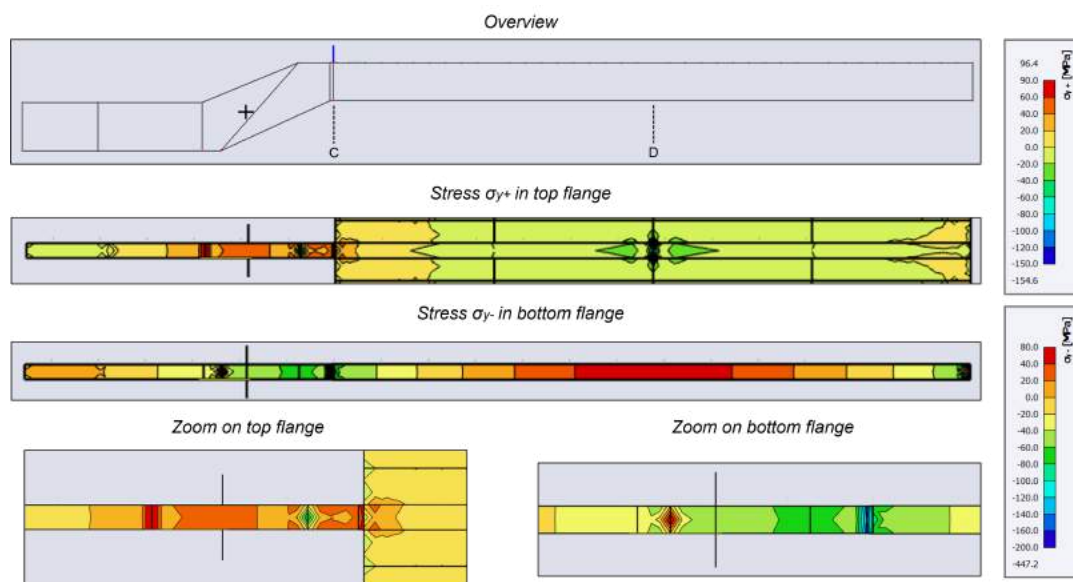


Figure 4.35: Stresses in the main beam.

The same patterns in stress distribution over the top and bottom flange can be seen as in the other validation cases. In cross section C, a central point of stress concentration occurs in the transition from the main beam to the deck plate. The peak tensile stress of 96.4 MPa occurs here in the middle of the flange, in the small, dark red zone next to the bridge deck, as can be seen in the bottom left figure. In the bottom flange, two stress concentration occurs in both joints between the straight parts of the main beam and the intermediate part, which were also present in the previous models. The peak stress in this bottom joint, indicated by the blue strip in the bottom right figure, is a compressive stress of 96.8 MPa. The remainder of the stress distribution over the bottom flange looks correct and similar to the other validation cases. The peak stress occurring at cross section D in the bottom flange is a tensile stress equal to 62.2 MPa.

Figure 4.36 shows the distribution of M_x , V_z and σ_x over the cross beam in this design.

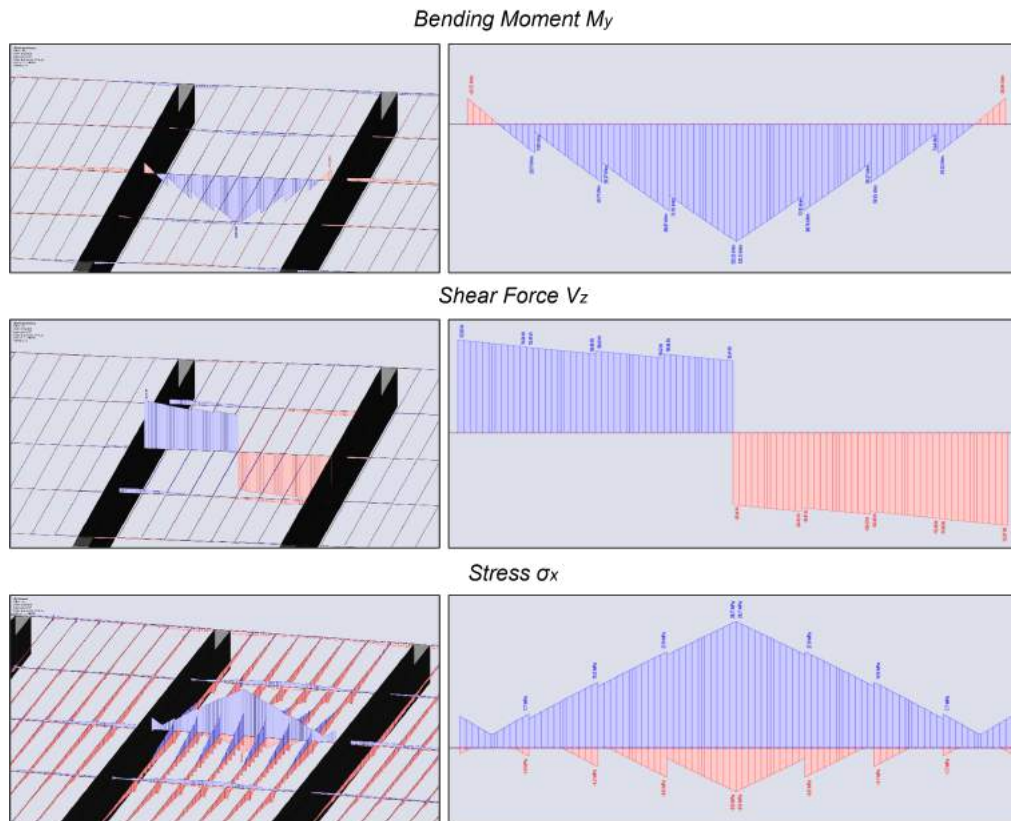


Figure 4.36: Moment (top), shear force (middle) and stress distribution over the cross beam.

The distribution of bending moments, shear force and stresses throughout the cross beam show logical behaviour. No peculiarities can be found in the diagrams shown, which have not already been mentioned in the previous validation cases.

The maximum negative bending moment in the cross beam is equal to -120.55 kNm and the moment in cross section F is equal to 26.94 kNm. The shear force at mid span is equal to 95.44 kN and in cross section F it is equal to 123.07 kN. The tensile stress at mid span is equal to 28.7 MPa, and the tensile stress at cross section F is equal to 7.3 MPa.

Table 4.24: Comparison between MatrixFrame model, hand calculation and SCIA model for validation case five.

Main beam			
	MatrixFrame	SCIA Model	Difference [%]
Cross section C			
Bending moment M_z [kNm]	1868.68	475	-74.58
Shear force V_y [kN]	441.9	344.46	-22.05
Stress σ_y [MPa]	-120.59	-96.8	-19.73
Cross section D			
Bending moment M_z [kNm]	-724.68	-449	-38.04
Shear force V_y [kN]	275.22	156.7	-43.06
Stress σ_y [MPa]	103.89	62.2	-40.13
Cross beam			
	Hand calculation	SCIA Model	Difference [%]
Cross section E			
Bending moment M_y [kNm]	-117	-120.55	+3.03
Shear force V_z [kN]	100	95.44	-4.56
Stress σ_x [MPa]	21.51	28.7	+33.43
Cross section F			
Bending moment M_y [kNm]	27.02	26.94	-0.30
Shear force V_z [kN]	-139.16	-123.07	-11.56
Stress σ_x [MPa]	4.97	7.3	+46.88

There are large differences between the MatrixFrame model of the main beam and what occurs in the SCIA model. The bending moment gets overestimated by 38 to 75 percent, and the shear force in the range of 20 to 40 percent. The occurring stresses in the cross section are smaller in the SCIA model by 20 to 40 percent. Minor differences between the models for the cross beam can be observed. The order of magnitude of both values are similar, and the distribution of forces and stresses over the cross beam, indicate correct structural behaviour, the same that could be concluded from the previous four validation cases.

Conclusion

Concluding about the predicting behaviour of the neural network, the neural network directly predicts a viable structure in only two out of five cases. In two cases, the user had to alter only one parameter in the model, namely the main beam spacing and length of the bottom main beam. In the remaining one, the user had to alter five of fourteen predicted parameters, to create a realistic structure. Which, undermines the use of a neural network to predict the structure for the user. However, the Grasshopper script is organised in such a way that parameters are changed very quickly, meaning that the user can still generate a viable structure with assistance of the neural network, easily. In two cases, the neural network predicted a structure in which it was not possible to create a significantly large enough counterweight. Apparently, it is difficult for the neural network to find a relationship between the length of the bottom main beam and steel mass used in the bridge deck. In the future, this could be solved by incorporating the size of the counterweight as model parameter, or making it dependent on the static moment of the steel structure of the bridge deck.

Extending the findings within these five cases to a broader scope, it can be said that the neural network likely has difficulties predicting a correct structure when the user input reaches the border of the data set. Even though there are bridges in the data set with a similar width, that use two main beams, the neural network does not recognize this, because it always tries to find relationships between bridges in the whole data set. Similarly when a user wants to generate a very wide bridge deck.

With regards to the structural behaviour of the SCIA models that the Grasshopper script generates, the following key takeaway points can be concluded.

- For the main beams, the shape of the moment and shear force line, and direction of moments and shear forces align between the MatrixFrame model and SCIA model, indicating that the distribution of forces and stresses in the main beam appears to be correct. No trend however can

be found in the comparison between the magnitude of occurring bending moments and shear forces. In some cases the values are of similar magnitude, i.e. in the range of 10 to 30 percent difference, while in other cases the differences are significantly larger. The bending moments in the SCIA model in both cross sections C and D are consistently lower by 35 to 80 percent, and the shear forces by 20 to 50 percent.

- The stresses throughout the main beam show logical behaviour following the moment and shear force distributions, but are still 20 to 40 percent lower than in the MatrixFrame model. This over-estimation seems to be consistent over every validation case, indicating that there is consistency in the modeling of stresses in the SCIA models.
- For the cross beams, the conclusion can be drawn that they behave properly and as expected within the SCIA model. The distribution and magnitude of occurring bending moments, shear forces and stresses are of similar magnitude in every validation case. The only minor difference that has been noted is that the cross beams do not fully act as clamped beam, due to the rotational stiffness of the joint with the main beams.
- The overall stress distribution throughout the SCIA model appears to be correct, despite the modeling errors encountered. Based on the SCIA models for the five validation cases, seven modeling errors can be found which may influence the stress distribution throughout the structure. These zones of modeling inaccuracy are present in almost every model the Grasshopper script has generated, and are the result of how the model has been built up or about how SCIA Engineer interprets the .xml file from which it imports geometry. Hence, this is difficult to solve without changing the buildup of the whole model. The zones where wrong stress concentrations occur are highlighted in the figure below.

1. In the transition between the top flange of the bottom main beam and intermediate part.
2. In the transition between the intermediate part and top flange of the top main beam.
3. In both bottom corners of the intermediate part.
4. In the transition between the top flange of the main beam and bridge deck plate.
5. In the transition element in the bottom flange, where the profile of the main beam changes.
6. At the support points at the toe of the leaf, where the structure is supported in the two bottom nodes of every main beam.
7. Right underneath the point load in the bridge deck plate.

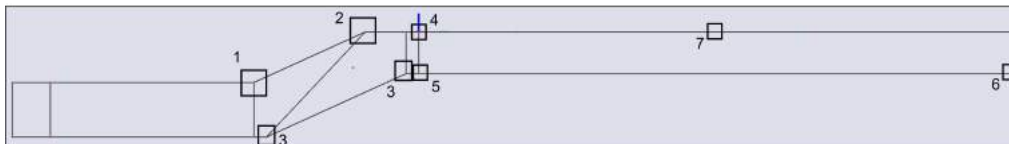


Figure 4.37: Locations of stress concentrations in the SCIA model.

5

Results

This chapter presents the results of this research. In the first paragraph, the structural performance of two design alternatives generated by the workflow, and of two reference projects, is evaluated and compared. For the same input parameters as these two bridges, structures are generated by the workflow, so an assessment can be made whether the workflow generates viable structures. This comparison is based on the stress distribution and eventual unity check of the different elements in the structure, which is a similar analysis of what has been done in the previous chapter. This comparison is done using the load combinations that were discussed in section 3.4.2. The goal of this paragraph is to provide quantitative grounds, on which a conclusion to the research question can be formulated, hence also the material use is taken into account. In the second paragraph, a short theoretical description is given on what the created workflow in this thesis can contribute to the bridge design process, based on the experiences that were gained during this project. Paragraph 5.3 contains the evaluation of the obtained results.

5.1. Design Comparison

The comparison between the reference project and generated structural design by the workflow, is done based on output from the respective SCIA models. For the reference projects, the structural verification of the bridge leaf is established in definitive design reports, in which a concise description is given of the normative load combinations and occurring forces, stresses and unity checks of the different elements in the structure. Figures and values shown in this chapter are extracted from these project documents. Based on the experiences obtained from the validation stage in this research, and calculation reports from the firm, the following starting points must be noted regarding the SCIA model output.

- Local stress distribution in the bridge deck plate, right underneath axle loads and point loads, and near support nodes are disregarded, since SCIA Engineer cannot model these correctly. In design projects, separate models are constructed for these structural details, in more elaborate FEA software. To be able to properly analyze the stress flow from the bridge deck plate to the other structural components.
- The stress flow in the transition between the top flange of the main beam and the bridge deck plate, is also incorrectly modeled by SCIA Engineer. The software cannot process the sudden change in effective width of the cross section correctly. Hence, the normative stress occurring in the top flange of the main beam, is assumed to be right before the transitional element with length L_7 . This position is indicated in figure 5.1.
- Structural verification is done based on the occurring Von Mises stresses σ_E in SCIA Engineer. In order for the structure to suffice, these should not exceed the yield stress of S355 steel, under ultimate limit state conditions.

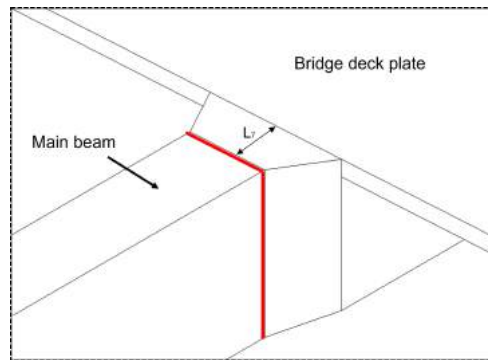


Figure 5.1: Normative cross section for stresses in the main beam near the bridge deck.

5.1.1. Renovation Berlagebrug

The Berlagebrug is a traffic bridge located in the city center of Amsterdam, that crosses over the Amstel river. The bridge leaf of this bridge has recently been renovated. A description of this reference project is given in section G.1 in appendix G.

The main dimensions of the Berlagebrug are as follows.

- $L_1 = 13$ meters
- $W_1 = 23.18$ meters
- $L_6 = 1.285$ meters

For these input parameters, the Grasshopper script suggests a bridge leaf with the following parameters.

Table 5.1: Parameters for alternative design Berlagebrug.

Input			Predictions			Dependent		
L_1	13	[m]	L_2	0.842	[m]	$I_{zz,top}$	476875.2	[$\times 10^4 \text{ mm}^4$]
W_1	23.18	[m]	L_3	2.91	[m]	$I_{zz,cross}$	180754.1	[$\times 10^4 \text{ mm}^4$]
L_6	1.285	[m]	L_4	2.596	[m]	$I_{zz,rib}$	2874.552	[$\times 10^4 \text{ mm}^4$]
			L_5	4.648	[m]	b_{cwt}	0.9	[m]
			L_7	0.103	[m]			
			L_8	1.939	[m]			
			b_{main}	4.35	[m]			
			n_{main}	5	[-]			
			n_{cross}	5	[-]			
			n_{rib}	36	[-]			
			H_{bottom}	1060	[mm]			
			W_{bottom}	330	[mm]			
			$t_{w,bottom}$	16	[mm]			
			$t_{t,bottom}$	32	[mm]			

The design is shown in figure 5.2.

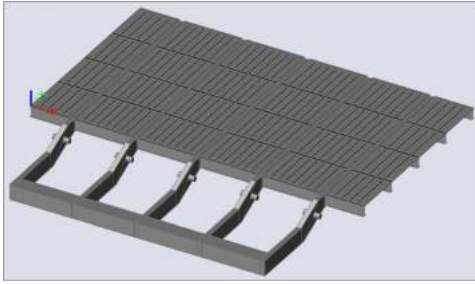


Figure 5.2: Suggestion by the neural network for the Berlagebrug.

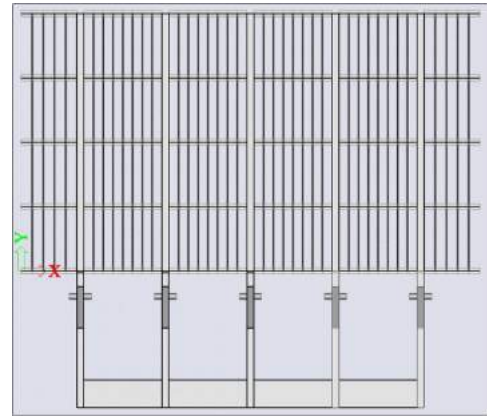


Figure 5.3: Top view of suggestion by the neural network for the Berlagebrug.

The neural network appears to do a good suggestion immediately. The suggested design has five main beams, instead of six in the original design. However, they are spaced at a larger distance from each other, ultimately spanning about the same width as in the original design. The neural network also predicts that five cross beams can be used instead of six. The amount of rib elements to be used is 36, which is very close to the 34 in the original design. The size of the main beam is similar in height, the major difference being that the parametric model is built using a tubular cross section instead of an I-section that has been used in the renovation of the Berlagebrug. The predicted moment of inertia for the top main beam results in a tubular section with a height of 840 millimeters and width of 350 millimeters. The web thickness is equal to sixteen millimeters and flange thickness thirty millimeters. For the cross beams, the design uses HE700A profiles, which are of similar dimension as the cross beams used in the renovated bridge leaf of the Berlagebrug. For the ribs, the Grasshopper script chooses a "RHS 200x100x12" cross section. The neural network also predicts a long enough bottom main beam to be able to construct a suitable counterweight, which is not often the case as has been found in the validation stage of the research.

The total steel mass used in this structure is equal to 234647 kilograms, of which 120421.5 kilograms is from the counterweight.

Comparison of structural behavior

The structural performance of the generated design is evaluated with load combinations one to three, to compare its performance to the new bridge leaf of the Berlagebrug. The resulting Von Mises stress in the structure for each load combination, can be found in figures G.17 to G.20.

The structural analysis of load combination one leaves the bridge in a stress state which far exceeds the yield stress of S355. In figure G.17, it can be seen that the stresses in the deck plate exceed 355 MPa along the axis of the first main beam. Peak concentrations of stresses occur along the outermost interface between the bridge deck plate and web of the main beam. Next to this line, the stress in the bridge deck quickly dissipates into a stress state of below 120 MPa. From the figure, it can also be concluded that stress concentrations occur in the intermediate part of the main beam, namely between the support node at the rotational axis, and the bottom corner, underneath the start of the bridge deck. It can also be seen that such a stress concentration occurs above the left most main beam in the bridge deck, which is not under significant loading in this load combination. This indicates a model error in the interface between the bridge deck plate and outermost main beams, where the bridge deck cantilevers. The effect of this error could not be further investigated during the project. In the top flange of the main beam, the stress increases to a magnitude of 249.9 MPa, just before the bridge deck plate starts. This plate element is highlighted in pink in the next figure.

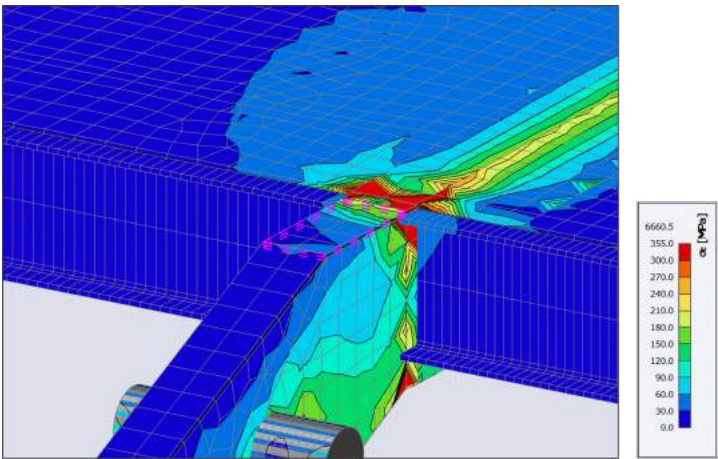


Figure 5.4: Von Mises stress in plate element S87.

For load combination two, the stresses in the fore-most cross beam should be observed, to make a comparison to the structural performance of the real Berlagebrug. Figure 5.5 shows the Von Mises stress over the fore-most cross beam of the bridge leaf. Here, the highest tandem loads are placed on the left of the bridge deck, in the view shown.

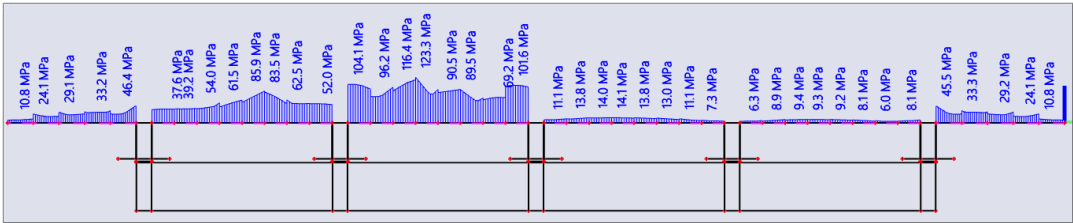


Figure 5.5: Von Mises stress in the governing cross beam.

It can be seen that the maximum stress is equal to 123.3 MPa. Which translates into a unity check of 0.35.

For load combination three, the stress in the rear most cross beam is governing. Figure 5.6 shows the stress distribution over this cross beam under the loading defined by load combination three. Here, the cross beam is shown from the opposite side of the bridge deck.

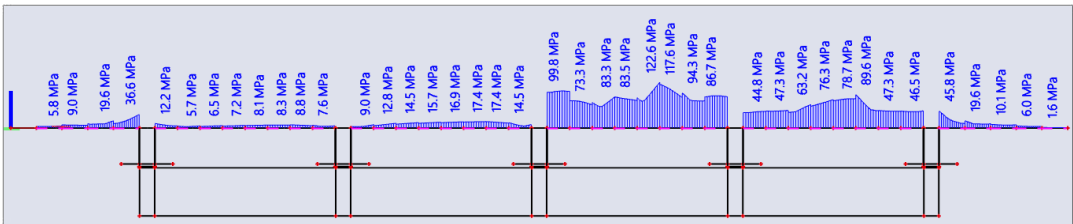


Figure 5.6: Von Mises stress in the governing cross beam.

The maximum stress is equal to 122.6 MPa. Which is equal to a unity check of 0.35.

The structural analysis results of the generated design and the definitive design of the Berlagebrug, have been summarized in the next table.

Table 5.2: Structural performance comparison Berlagebrug.

Generated design by neural network			
Mass [kg]	234647 kg		
Load combination	Norm. element	$\sigma_{E,max}$	U.C.
LC1	Main beam	249.9	0.70
LC2	Cross beam	123.3	0.35
LC3	Cross beam	122.6	0.35
Berlagebrug			
Mass [kg]	447020 kg		
Load combination	Norm. element	$\sigma_{E,max}$	U.C.
LC1	Main beam	268	0.75
LC2	Cross beam	179	0.5
LC3	Cross beam	237	0.67

The neural network generates a structure which is significantly smaller in weight, yet scores lower unity checks on the given normative load combinations one to three, when comparing the same elements in the structure. The occurring stresses in the main beams of the two designs are comparable, even though the real design of the Berlagebrug uses one more main beam. The stresses in the cross beams of the generated designs, are about 50 to 60 percent lower, than in the real case. This could be due to the fact that the HE700A are more heavy profiles. It is however odd that these stresses are significantly lower than in the real design, since in the design of the Berlagebrug extra stiffening elements and plates are applied, to further reinforce the orthotropic deck, and further dissipate the stresses over the whole structure. Even still, the cross beams are subjected to stresses of 179 and 237 MPa in load combinations two and three, in which traffic load models are applied at two different positions.

Purely based on the dimensions and elements used in the design suggested by the neural network, it could be said that this design is similar to the real design. However, combining the structural analysis results with the conclusion that the neural network generates a structure that uses almost twice less steel and scores better on the normative load combinations, it is highly likely that the calculated SCIA model is disturbed by the interface between the bridge deck plate and underlying elements. The improper FEA calculation of the stresses in the bridge deck plate, likely influences the stress distribution in the whole structure. When the calculation would be done properly, it is likely that stresses in the main beams and cross beams will exceed the yield stress of 355 MPa, given that the generated design uses one less main beam and cross beam, while they have roughly the same dimensions.

5.1.2. Elizabeth Admiraalbrug

The Elizabeth Admiraalbrug, bridge 0925, is a new pedestrian and cycle bridge that will be built in the neighborhood of Elzenhagen-Zuid. The bridge is designed by the firm, and is currently in the definitive design phase. A description of the bridge can be found in section G.2.

Bridge 0925 has the following input properties:

- $L_1 = 15.88$ meters
- $W_1 = 7.4$ meters
- $L_6 = 2.145$ meters

For these input parameters, the Grasshopper script suggests a bridge leaf as shown in figure 5.7.

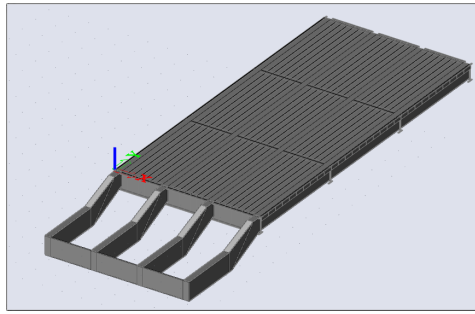


Figure 5.7: Suggestion by the neural network for the Elizabeth Admiraalbrug.

What can be concluded is that the neural network cannot predict a good structure for these input parameters. There is no use for four main beams in such a small bridge deck. The network also predicts four cross beams and twenty ribs. Using twenty ribs in this structure, also seems excessive. Additionally, it can again be seen that the parameter L_5 is too short, to accommodate a suitable counterweight. To create an alternative structure for the Elizabeth Admiraalbrug, the amount of main beams is reduced to two, and they are spaced at 5.7 meters. The amount of ribs is reduced to ten and the length of the bottom main beam L_5 is increased to 5.0 meters. The distance L_7 is extended to 0.32 meters, equal to the definitive design. The parameters of the eventual design are shown in table 5.3. The design is shown in figures 5.8 and 5.9.

Table 5.3: Parameters for alternative design Elizabeth Admiraalbrug.

Input			Predictions			Dependent		
L_1	15.88	[m]	L_2	0.558	[m]	$I_{zz,top}$	380595	[$\times 10^4 \text{ mm}^4$]
W_1	7.4	[m]	L_3	2.361	[m]	$I_{zz,cross}$	275997.6	[$\times 10^4 \text{ mm}^4$]
L_6	2.145	[m]	L_4	1.924	[m]	$I_{zz,rib}$	3303.626	[$\times 10^4 \text{ mm}^4$]
			L_5	5	[m]	b_{cwt}	1.7	[m]
			L_7	0.32	[m]			
			L_8	1.615	[m]			
			b_{main}	5.7	[m]			
			n_{main}	2	[-]			
			n_{cross}	4	[-]			
			n_{rib}	10	[-]			
			H_{bottom}	930	[mm]			
			W_{bottom}	290	[mm]			
			$t_{w,bottom}$	13	[mm]			
			$t_{b,bottom}$	26	[mm]			

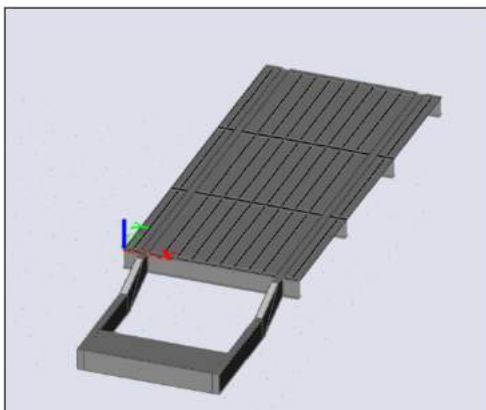


Figure 5.8: 3D view of the generated design alternative.

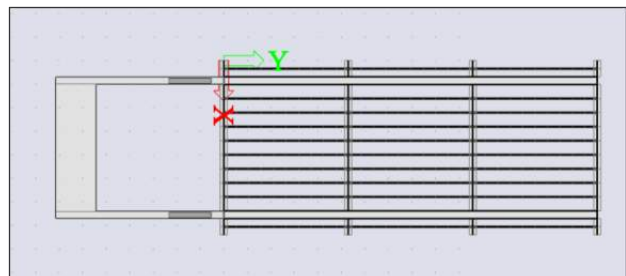


Figure 5.9: Top view of the design alternative.

Difference between the designs can be found in the robustness of the system. The generated design

uses larger, more slender main beams, while the design for the Elizabeth Admiraalbrug uses more rectangular shaped main beams. The flange and web thicknesses of the main beams are quite similar. For the bottom main beam, the generated model consists of a rectangular cross section with height 930 millimeters and width 290 millimeters. In the real design, the bottom main beams are significantly larger in size. They are namely 1300 millimeters in height and 500 millimeters in width. The largest difference between the two structures can be found in the modeled cross beams. The workflow generates a structural design which uses only four cross beams, which are modeled as HE800A profiles. These are significantly larger than the steel sheets applied in the original design, which have a thickness of only 25 millimeters. The ribs of the design are made out of "RHS 200x100x16" profiles. Which are of similar size as the rib profiles shown in figure G.5.

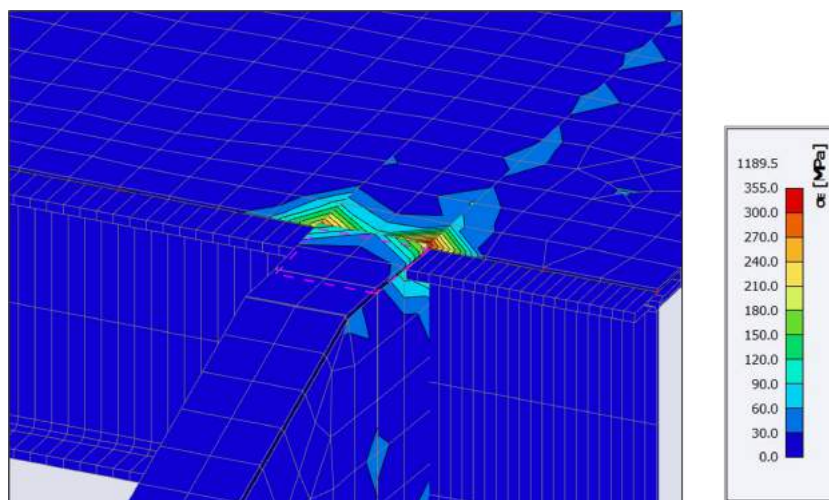
The total weight of the structure generated by the workflow is equal to approximately 97602.65 kilograms, of which 57330.12 kg is from the counterweight. The total weight of the structure is more than double the amount of the Elizabeth Admiraalbrug.

Comparison of structural behavior

The structural performance of the generated design is evaluated with load combinations four to six, to be able to compare its performance to the Elizabeth Admiraalbrug. The resulting Von Mises stresses in the structure for each load combination, can be found in figures G.22 to G.26.

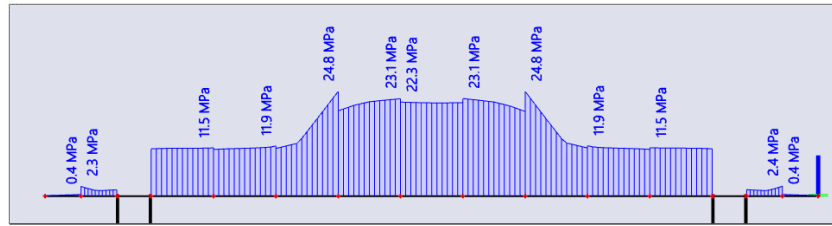
For load combination four, the maximum stress in the structure occurs in the top flange of the main beam, right before the bridge deck. The stresses in this surface element are shown in figure 5.10. The plate element is highlighted in pink.

Figure 5.10: Von Mises stresses in governing plate element S26.



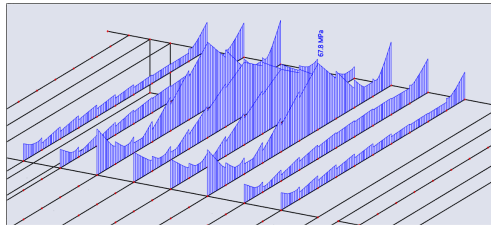
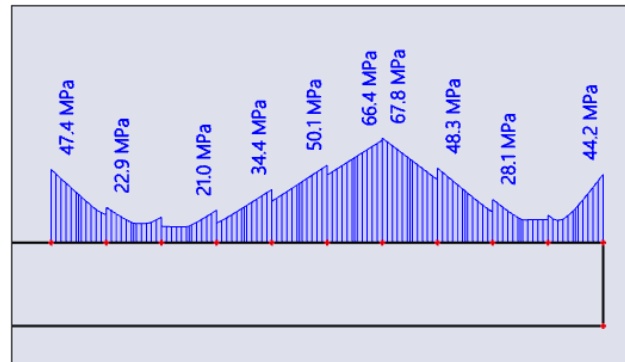
The maximum Von Mises stress occurs in the top right corner, and is equal to 245.4 MPa, as shown in the results table in figure G.23. This stress translates to a unity check of 0.69 for the structure under load combination four. It must be noted that the real stress occurring in this position is lower than calculated by the model, due to the stress concentrations occurring in the transition between the top flange and deck plate, which SCIA cannot process.

For load combination five, the maximum stress occurs in the foremost crossbeam. The Von Mises stress in this beam is shown in figure 5.11.

Figure 5.11: Von Mises stresses in foremost crossbeam.

The maximum stress in the beam under this loading combination is equal to 24.8 MPa, leading to a unity check of 0.07. Indicating that the structure is severely over-designed for this load combination. The results table as output from the SCIA model, is shown in figure G.25.

For load combination six, the governing stresses occur in the rib elements right near the axle loads of the incidental vehicle, which are placed two meters inwards of the bridge deck. The stress distribution over the rib elements due to this load combination can be seen in figure 5.12. Figure 5.13 shows the normative rib element.

**Figure 5.12:** Stress distribution in rib elements under axle loads.**Figure 5.13:** Normative rib element in load combination six.

The normative stress for this load combination is equal to 67.8 MPa. This results in a unity check of 0.19.

The structural analysis results of the generated design and the definitive design of the Elizabeth Admiraalbrug, have been summarized in the next table.

Table 5.4: Structural performance comparison Elizabeth Admiraalbrug

Generated design by neural network			
Mass [kg]	97603 kg		
Load combination	Norm. element	$\sigma_{E,max}$	U.C.
LC4	Main beam	245.4	0.69
LC5	Cross beam	24.8	0.07
LC6	Rib	67.8	0.19
Elizabeth Admiraalbrug			
Mass [kg]	46325 kg		
Load combination	Norm. element	$\sigma_{E,max}$	U.C.
LC4	Main beam	150.1	0.42
LC5	Cross beam	248	0.7
LC6	Rib	137	0.39

The results show that the neural network, in assistance with the user, generates a structure which is way over-designed compared to the definitive design of the Elizabeth Admiraalbrug. It uses more than twice as much steel. In load combination four, the occurring stresses in the main beams are

comparable in both designs, since the dimensions of the main beams are approximately equal. The stresses obtained in load combination four are likely influenced by the inconsistency around the bridge deck plate, indicating that for a correct working model, one would obtain a stress in the top flange of the main beam which is of a similar magnitude as 150 MPa found in the definitive design of the Elizabeth Admiraalbrug. What has also been found is that the cross beam and rib elements are significantly over-designed compared to the Elizabeth Admiraalbrug. Unity checks of 0.07 and 0.19 respectively, indicate that the bridge leaf design is designed far from optimal. The generated design can however be used as good starting point in the design procedure. Improvements can mainly be made to the design of the cross beam elements.

It must be noted that the real design of the Elizabeth Admiraalbrug consists of more types of stiffening elements than the basic components in the parametric model. The parametric model only differentiates between main beams, cross beams and rib elements, while in practice stiffening elements are used throughout the bridge leaf structure. These elements influence the stress distribution and have different normative load combinations that should also be considered in a fair comparison. This leads to the fact that other structural elements such as the main beams and cross beams can be designed more slender, because the force distribution is organized in a better way. .

5.2. Integration in design process

Based on the experiences gained during the project, the following advantages and disadvantages can be named when incorporating the AI-powered workflow into the structural design process, compared to the traditional design process which is currently followed. This is assuming that the created workflow works consistently accurate and contains no errors, which is not yet the case in the current workflow.

Advantages

- The main advocate for implementing the created workflow into the design process is that a significant amount of time can be saved. Even though the validation and research step have shown that the neural network algorithm does not generate a viable structure immediately in most cases. The suggestion that it does, is often a good step in the right direction, and is alike similar structures in the data set. Meaning that the structural engineer will have to change only few parameters to be able to create a suitable design. Time can be saved in two design scenarios that are relevant within the firm.
 1. Firstly, for new bridge projects to come, for which the tool is designed. With the created Grasshopper script, a design alternative can be easily generated already in the early phase of a bascule bridge project. This can instigate a discussion about the trade-offs between architectural design and structural performance way earlier in the design process than what currently happens, since an elaborate SCIA Engineer model of the structure can be generated immediately.
 2. The intended goal of the tool is to be able to flow through the design process for new bascule bridges more quickly. Hence, the parametric model of the bridge leaf is tuned to how new bascule bridges are built. However, the firm is also facing a major renovation task in which current bridge decks, not only of bascule bridges, need to be reassessed, to judge whether the bridge leaf is up for repairs or renovation. The orthotropic bridge decks of these other movable bridges are quite similar. With minor changes, the created parametric model can be used to evaluate the structural performance of existing bridges in the city.
 3. Once acquainted with the created tool, structural engineers can become more time efficient within future bridge projects, since the suggestions that the neural network does are based on the existing bridges in the city. Meaning that the engineer can spend less time manually searching for reference projects. This was already mentioned in the introduction of this project.
- As mentioned as vision point in the beginning of the report, with the created tool incorporated in the bridge design process, it is likely that the different project members can become more aware of design choices in the structure of the bridge leaf. The tool can provide a platform in which a project team can collaborate and evaluate the bridge design together. Changes in the parametric model,

done by either the neural network or manually, can be seen immediately, and their changes to the structural performance can be assessed quickly after. This is a significant advantage over the current design process, in which the structural engineers handle the structural design themselves. They construct their own models and make decisions based on their own experience. When the workflow is applied within a project, other project members can also experiment with different design alternatives, since the neural network suggests the structural design for them, provided that the design alternative is realistic. Which should be assessed by a structural engineer.

- Lastly, because the workflow generates an accompanying structural analysis in SCIA Engineer, for every design alternative generated, the structural performance of a design alternative can be adopted in the design evaluation in the conceptual phase of a project. In the current design process, trade-offs are made based on qualitative assessments on different design criteria. Within a new workflow with the AI-powered model, the structural performance can also be taken up as design criterion.

Disadvantages

- The biggest disadvantage of the workflow is that it is near impossible to gain understandable insight into the working of the neural network, namely how it learns the data set and on what grounds the predictions are made. The neural network namely only does a suggestion based on data, while in bridge design a lot of design aspects play a role. During the project, different structural engineers made it clear that the tool would become significantly more useful when the workflow would textually describe the properties of the suggested design. About their possible flaws and challenges that have a significant chance of occurring during its lifetime, and on what designs in the data set the suggestion is based. For every bridge in the city, multiple flaws or difficulties can be named, that have appeared during their design lifetime. Meaning that not every bridge design in the city is a good design or is up to today's structural design standards. An example is fatigue loading due to increased vehicle traffic and weights. The only way to incorporate this into the neural network is by manually adding a score metric for the structural design aspects that are found important. However, still after doing this, no qualitative insight will be gained on the suggestions done by the neural network. Additionally, as appeared in this project, the designs and models generated by the workflow do not consistently work correctly. Meaning that in the current form, generated results should still be evaluated by structural engineers, to determine whether the model works correctly. This is almost unavoidable.
- A second disadvantage could be the knowledge gap that is introduced when this piece of software is introduced within the firm. Rhino and Grasshopper are not currently used in the firm, meaning that time will have to be invested for structural engineers to understand the software. Additionally, it takes a significant amount of time to understand (visual) programming scripts that someone else has constructed. This introduces an extra barrier before reaching good collaboration between people in the firm, that can use this tool.
- Applying this workflow in practice could prove to be difficult, since at first a strategy must be constructed, which defines how the parametric model of an orthotropic bridge deck is built up. In this project, the main beams are constructed using 2D plate elements, which leads to classic calculation problems in SCIA Engineer, at the interfaces between the plates. In other projects, the main beams can for example be built up using 1D line elements with a tapered profile. Within the firm, the method of how a model is built up is usually chosen by the responsible structural engineer. However, the way a parametric model is built up, defines what parameters need to be collected in the data set. If a general solution is not made up, it could mean that each time, a new data set will have to be constructed, that will each time consist of different parameters describing the bridge leaf. Having to recollect different bridge dimensions from the archives for a specific parametric model, contradicts the purpose of the workflow.

This general solution must also be tailored to the possibilities/limitations that are present in Grasshopper and the Koala plug-in. Since there are no engineers with knowledge of the software, it will take time to map this. Time and effort will need to be spent to create a general strategy on how to implement this AI-powered workflow in the structural design process, which cannot be spend on projects and will not be profitable in the beginning.

- Lastly, it is uncertain whether the Koala plug-in will be continuously developed in the future. There might be a risk involved when a project team fully depends on this tool in the future.

5.3. Evaluation

In this section, the accuracy and usefulness of the obtained results is evaluated. A concise description of factors is given, that possibly limit the scope of applicability of the Grasshopper workflow.

Firstly, it is disputable to what extent a machine learning algorithm can be applied on bridge data, or in general, to what extent it can create good structural bridge designs, purely based on the data used in thesis. There are namely so many factors, like architecture, constructability, costs and maintainability, that play a role in movable bridge design. Not every design choice is motivated by the fact that the structural performance of the bridge leaf should be central. In the improved model presented in section 4.2, there are only fourteen parameters left, out of which seven describe something directly related to the structural performance of the bridge leaf, namely the size of the bottom main beam and amount of structural elements used in the bridge deck. The remaining parameters left, describe the geometry of the main beams L_2 to L_8 . These do not necessarily influence the structural performance of the bridge leaf, but are rather influenced by boundary conditions, like the size and positioning of the support axis and bascule chamber. Moreover, the predictions done for $I_{zz,top}$, $I_{zz,cross}$ and $I_{zz,rib}$ were internalized in the second step. They were simply assumed as a constant ratio based on the bridges in the data set, and made dependent on n_{main} , n_{cross} and n_{rib} . It could thus be questioned to what extent the neural network in the application developed in this thesis, actually predicts the structure well. Especially, considering that a structural engineer would probably be able to tell how many main beams, cross beams and rib profiles he should use for a certain bridge deck, pretty easily. To form a better conclusion on the accuracy of predicting the structural design of the bridge leaf, one would probably have to evaluate bridge designs that the initial model, described in chapter 3 would generate, or construct new parameters to describe the bridge deck. The parameters predicting the required moment of inertia were removed in the second step, since their prediction inaccuracy was high, this does not however have to mean that the initial model would generate improper structures. By comparing results generated by the original neural network and improved model presented in section 4.2, a more extensive conclusion can be formed on how well a neural network can predict the structural properties of the bridge leaf. After the accuracy assessment in paragraph 4.1, the decision to create an improved model was simply made based on the poor accuracy of 25.91%.

This continues into a second point of attention, namely that it is difficult to assess what prediction accuracy is needed to formally conclude whether the neural network and whole workflow, work well or good enough for its purpose. As was concluded in section 4.1.3, the prediction performance was poor, since the average prediction inaccuracy was high. It is however difficult to assess what the prediction error is in absolute terms, in this application. In regular machine learning problems, there is usually a single goal, namely to optimize the output of the model. By doing a sensitivity analysis, one can then investigate what the influence of every parameter is on the outcome of the model. However, in this application on bridge leaves, most parameters that describe the bridge are design choices and are not directly related to optimizing the structural performance of the bridge leaf. Meaning that regular methods applied in machine learning, to determine the absolute accuracy of parameters, are not applicable. It is thus difficult to further assess what consequences the accuracy of the predictions made, have, with other metrics than the mean squared error and relative inaccuracy. Additionally, it is also difficult to determine how the prediction inaccuracy translates into inaccuracies in structural performance of generated bridge designs. This is something that could not be investigated further in this thesis. An additional point is that the neural network operates based on bridges in the city, for which it cannot be said that these are all optimal designs. To properly steer the neural network and reach better design suggestions, one should aim to implement an objective score metric that describes the structural performance.

The usefulness of the whole workflow was only assessed with a comparison to two realistic design cases. Where the inaccuracy of predicting the amount of main beams and cross beams became apparent. In the first reference case, the neural network suggested one main beam and one cross

beam fewer than in the original design. Which led to a structure that had a less optimal structure. For the design alternative for the Elizabeth Admiraalbrug, three main beams were generated. After a manual correction of this fact, it became apparent that the neural network had generated a design which was significantly over-designed compared to the definitive design. This could be expected given that the majority of the bridges in the data set are traffic bridges. This leads to the fact that the application of this workflow on the design of pedestrian- and cyclebridges is disputable. What can be concluded from the pedestrian- and cyclebridges that are taken up in the data set, is that most of these have a peculiar design, which deviates from the standard orthotropic bridge deck as defined in chapter 3. In these bridges, the architectural aspect plays a more dominant role compared to structural performance, examples are the Kadoelenbrug and Solitudobrug. For these types of bridges, it can thus be discussed whether it is useful to divide these structures into the described parameters of the parametric model, and to add them to the data base, since they also negatively influence the predicting performance of the model for regular traffic bridges.

The question must also be asked to what accuracy it is actually needed to predict every parameter. Judging from the validation and result steps, it could be said that it is most important to be able to predict the amount of needed main beams, cross beams and ribs, and the main beam spacing, the most accurate. Since these have the most influence on the structural performance of the bridge. It is simply crucial, that the neural network suggests a suitable amount of main beams, cross beams and ribs, which are in line with the existing bridges in the city. The other parameters, such as the dimensions L_2 to L_8 that describe the main beam, need not to be predicted with such a high accuracy, since deviating from the optimal solutions for these parameters, does not influence the structural performance significantly. Based on the results of this research, it could be said that the obtained prediction inaccuracy of the parameters other than n_{main} , n_{cross} , n_{rib} and b_{main} , is sufficient enough to conclude that the neural network works well. However, in the total of seven design alternatives generated throughout the validation and results phase of this project, an improper amount of main beams, cross beams and rib, or spacing of main beams was predicted in the majority of cases. Especially, when the user inputs values that reach the border of the range of the data set, the neural network finds it hard to predict the correct amount of main beams and cross beams.

Taking into account the previously named points, it is difficult to assess the performance of the total workflow and about how it can contribute to the structural design process. The usefulness of the workflow can in the future be increased by incorporating other design aspects of movable bridges such as costs, maintainability, constructability, sustainability and structural performance into the data set and neural network.

6

Discussion

This chapter describes the discussion in paragraph 6.1 and lessons learned from the project in paragraph 6.2.

6.1. Discussion

This section describes a discussion about possible inaccuracies, flaws and shortcomings of the research, as well as things learned during the process of performing this research. Four concrete topics are discussed. Firstly, shortcomings in the application of the neural network that may influence the results, are discussed. Secondly, shortcomings in the parametric model are discussed. Thirdly, a short notice of the encountered SCIA model errors is given. Lastly, the legitimacy and usefulness of obtained observations and results in the validation and results phases of the research, is discussed in section 6.1.4.

6.1.1. Application of neural network

In the application of the neural network, the following inaccuracies and shortcomings have influenced the outcomes of this research.

- At the core of the model stands the data set with gathered information on all parameters per bridge. This information was gathered manually by consulting old technical drawings and inspection reports. This could have led to mistakes in the following aspects:
 1. The parametric model assumes straight plate elements with corners near the intermediate part of the main beam. They are modeled between nodes. In practice, the main beams are often curved and continuously welded for architectural reasons and to improve stress distribution. They do not have sharp angles. This means that corner points had to be assumed at certain positions, possibly leading to inaccuracies in measured dimensions L_2 to L_7 .
 2. Technical drawings of old bridges were consulted in the online city archives. Measurement errors in the dimensions can occur due to technical drawings that have not been scanned correctly, i.e. were skewed or shifted during scanning.
 3. Not all dimensions that describe the parametric model were indicated in technical drawings. A general measurement error can occur due to incorrect measuring of distance from a digital screen.

These measurements could lead to incorrect predictions done by the neural network, that do not reflect the existing bridge designs. This is however impossible to assess afterwards.

- The data set only consists of 35 bridges. It was known beforehand that the data set was limited. A normal machine learning task uses thousands of data entries to predict a few parameters. In this case there is a low amount of data present, with which a high amount of parameters is predicted. Such a complex machine learning model with a small data set could lead to large inaccuracies in predicting behavior in case there is no clear trend in the data.

- As mentioned in the validation stage, the neural network component within Grasshopper has limited capabilities. The normal cross-validation procedure in machine learning, in which a neural network is trained, then saved and evaluated with a testing data set, cannot be followed in this thesis. Since, the trained algorithm cannot be saved locally. Every time the Grasshopper script is opened, the neural network algorithm is trained from scratch again. This can lead to discrepancies in predicting behaviour every time the model is opened. Entering the same input parameters could lead to a different bridge design every time the script is used. This shortcoming of Grasshopper and its lunchbox plug-in has limited the possibility for validation of the neural network and assessment of its accuracy. This could question the legitimacy of the results obtained in this research.
- Lastly, the neural network component within Grasshopper is a pre-defined module. No insight other than the obtained mean squared error of the trained model can be acquired into its performance or behavior. The settings that can be configured by the user are also limited. In a normal neural network application, one can select the amount of hidden layers, neurons per hidden layer and activation function per layer. In the Grasshopper component, the architecture of the neural network is set to one hidden layer and one type of activation function for the whole algorithm. The user can only change the amount of hidden neurons in the only hidden layer that is available.

6.1.2. Shortcomings of parametric model

The parametric model is a simplified version of a real orthotropic bridge deck. Simplifications in the design could influence the moments, shear force and stress distribution throughout the bridge leaf, on which conclusions were drawn later on in the project. Shortcomings in the parametric model due to time constraints of the project are:

- The parametric model lacks a side member along the outermost edge of the bridge deck plate. This is usually a rib-type element of slightly smaller dimensions, which helps stress distribution and stiffens the cantilevering part of the bridge deck.
- The parametric model lacks proper modeling of the support points of the bridge leaf. In a regular model, time is spent to model the trunnion at the rotational axis, with accompanying thickness and stiffness that fits the bridge leaf. In the parametric model in this research, the trunnion is modeled as solid steel shaft of 350 millimeter in diameter, that extends to 400 millimeters outward of the main beam on both sides. It is connected into a single node in the plate, meaning that here stress concentrations occur. At the toe of the leaf, each main beam is supported in both its bottom nodes as point support. This means that stress concentrations occur in these locations in the SCIA model, which do not occur in a real bridge.
- The parametric model lacks custom cross beam and rib profiles. As explained, a choice is made out of the HEA profile library for the cross beams, and out of the RHS profile library for the rib elements, based on the required moment of inertia. This does not influence the structural behavior of the model, but is only visual.
- As mentioned in the previous section, the parametric model uses a schematization of a typical main beam. The intermediate part of the main beams is modeled with sharp angles between the plate elements, while in practice the main beams are continuous and have corners with radii.
- The counterweight is not modeled as steel mass but rather as distributed load that acts on the main beams. It was not possible within time to model the steel counterweight as solid mass within Grasshopper. Therefore, an easier solution was to model its weight as distributed load as part of load case two. This has the same loading effect and does not influence the structural behavior of the bridge leaf.
- In the parametric model, all of the cross beams have the same cross section. In practice, the rear-most and fore-most cross beam, called the "achterhar" and "voorhar" have a slightly smaller cross section than the other cross beams to accommodate for the supports and abutments. This does not significantly influence the structural behavior of the bridge leaf.

Shortcomings in the parametric model due to limitations of Grasshopper and the Koala plug-in are:

- In practice, all line elements in the bridge deck are directly welded to the bridge deck plate. Meaning that their top flange is removed and that the bridge deck plate acts also as top flange of the

cross beams and ribs. Within the Koala plug-in, line elements must be assigned a standard cross-section which cannot be altered. In this case a HEA profile for the cross beams and RHS profile for the rib elements. This means that the cross beams and ribs in the structural model have slightly more capacity than what is correct.

- The eccentricity function of line elements within the Koala plug-in does not work. The foremost and rear most cross beam are modeled at the outer center-line of the bridge deck in Grasshopper, meaning that they should be moved inwards to be completely underneath the bridge deck. This should in theory be possible with the eccentricity property, which can be assigned to every line element in a FEA model. However, this function does not correctly in the Koala plug-in, hence the cross beams are all modeled at their center line, meaning that half of the rear-most and fore-most cross beams stick out underneath the bridge deck. This does not have a significant influence on the structural behavior of the model. During the project, the support team of SCIA Engineer was contacted multiple times about this issue but no response was received.

6.1.3. Error in SCIA model

In the results of section 5.1.1, it became apparent that there is an error in the SCIA model at the interface between the outer web of the main beam and bridge deck plate. Significant stress concentrations occur along this axis, which may influence the stress distribution around in the bridge deck plate.

This issue was presented to structural engineers in the firm, who acknowledged that this is a well-known issue in SCIA Engineer. The root of the problem is that SCIA Engineer faces difficulties with plate models, specifically where two plate elements come together. Either as a perpendicular connection like in this case, as parallel connection like the connection between the top flange of the main beam and bridge deck plate, or when two plate elements are modeled on top of each other. The problem that arises is that SCIA Engineer does not acknowledge the connection between the two plates, meaning that there is no official connection. The software then interprets it as a joint without stiffness, meaning that the bridge deck plate does not function as top flange of the effective width of the whole orthotropic bridge deck. This explains why peak stresses occur along this axis. This often occurring problem is usually manually fixed by placing a line element without mass, inside this axis. This line element then draws both plates towards its center of gravity, meaning that afterwards the two plates are connected.

In the generated design alternative for the Berlagebrug, the stress concentrations in the bridge deck are such significant that they should be fixed to be able to say something about the stresses in the main beams. To what extent it influences the stress distribution over the system of cross beams and ribs, is difficult to say.

This notion implies that every SCIA model that the Grasshopper workflow generates, has this connectivity issue. It was only noticed late in the project, in the results phase, since the validation phase only used small load cases, which did not animate this model issue, since the stresses were too low. Therefore, the conclusions drawn from the validation phase are valid. An alteration to the model should be made when traffic bridges with complete loading combinations are generated and analyzed.

6.1.4. Obtained results

The validation step of the research had two objectives. Firstly, to analyze the accuracy and predicting behavior of the neural network algorithm. Secondly, to evaluate whether the SCIA models show correct structural behavior.

In the first validation step, the inaccuracy of the predicting behavior of the neural network was assessed in the cross-validation. It appeared that the neural network algorithm had poor prediction accuracy. The majority of parameters were predicted with relative differences of 20 to 40 percent to their original value. These values found were rather remarkable. Even though it was known beforehand that the model was complex and had a small data set to run with, it was not expected that predictions for certain parameters would be that far off. By eliminating the parameters describing the bascule chamber and moments of inertia, the overall prediction accuracy increased from 25.91% to

61.07%, which is significantly better. However, this still is poor performance. Indicating that the model is either too complex or has too few data points.

In the next step, five validation cases were introduced to analyze whether the neural network could predict good bridge designs. In only two out of the five cases, a good bridge design was generated. Which translates into an accuracy of 40% for the workflow. In the other three cases, parameters had to be altered by the user. The parameters that had to be altered, were the main beam spacing b_{main} and bottom main beam length L_5 . For validation case one, the spacing b_{main} had to be changed from 3.61 meters to 5.6 meters, indicating a relative prediction inaccuracy of 35.5%. In the third validation case, five parameters had to be altered to create a viable structure. These are shown in table 5.5, as well as the inaccuracy. In the fourth validation case, the parameter L_5 had to be increased from 3.112 meters to 3.3 meters, which translates into an inaccuracy of 5.7%.

Table 6.1: Prediction inaccuracy for validation case three.

Parameter	Predicted value	User input	Inaccuracy [%]
L_4	1.493	1.7	12.18
L_5	2.44	4.0	39
b_{main}	3.095	5	38.1
n_{main}	3	2	50
n_{rib}	16	12	33.3

The next table shows again the average inaccuracy per parameter, from the cross-validation step.

Table 6.2: Prediction inaccuracy per relevant parameter.

Parameter	Inaccuracy [%]
L_4	34.64
L_5	29.87
b_{main}	35.15
n_{main}	45.54
n_{rib}	35.34

It can be seen that for new data, the algorithm approximately achieves similar inaccuracy values. The magnitude of inaccuracy between the cross-validation step and within the validation cases, is approximately the same. Indicating that the model behavior is consistent also on new data. With the exception of the fourth validation case, in which the parameter L_5 only had to be changed by a small amount. Looking back at the prediction inaccuracies, it was found that on average the values n_{main} , n_{cross} and n_{rib} , were predicted with an inaccuracy of 30 to 40 percent. On an integer in the range of 3 to 6, it is thus very much explainable that the neural network misses the amount of main beams or cross beams by one, or even more, consistently. To evaluate the prediction behavior of the neural network properly, one should investigate more randomly chosen cases. However, due to time restraints only five could be tested.

This has lead to the fact that no predictions for the full input range of the parameters L_1 , W_1 and L_6 have been tested. Most of the validation cases have input parameters that fall somewhere in the middle of the dataset, in which the most amount of similar bridges are. To fully evaluate the predicting behavior of the neural network, one should also test inputs that lie on the borders of the data set.

In the next step of validation, it was checked whether the SCIA models behaved correctly based on the distribution of stresses, moments and shear forces in two cross sections. In hindsight, the selection of the two cross sections C and D might not have been the best cross sections to perform this check on, but these were chosen randomly at the time the validation procedure was constructed. What can be concluded from the model validation step is that there are often significant differences between the 2D framework model in MatrixFrame and the estimated bending moments and shear forces in the SCIA model. There appears to be no distinctive pattern or consistency in the difference in magnitude

between the cases. It is likely that an orthotropic bridge deck behaves significantly different than a single beam supported on two point supports. Hence, estimating the bending moment in the beam in the SCIA model at locations C and D is difficult. It is likely that if a position had been chosen outside of the bridge deck, there would be less significant differences between the bending moments in the SCIA and framework model. For the cross beams, the differences in magnitude of all moments, shear forces and stresses is constant throughout all five validation cases, indicating that the simplified model is a decent approximation of how the crossbeam behaves in the SCIA model. All SCIA models showed similar stress behavior, and it was concluded that their behavior was accurate based on the five cases. Investigating more validation cases would have likely landed the same conclusion, but for the research itself it would have been better to at least investigate more cases that covered the full range of the input parameters in the data set.

The results section sees two completely different design cases, in which for the Berlagebrug an under-designed structure is generated by the workflow, and for the Elizabeth Admiraalbrug a severely over-designed structure. The identified inaccuracies in predicting the amount of necessary main beams and cross beams, also continue forward in this phase. Where, in the case of the Berlagebrug, one main beam and one cross beam too few is generated with respect to the optimal solution and in the Elizabeth Admiraalbrug case study two main beams too many, one cross beam too few and too many ribs are predicted. The cross beams are also predicted to be of a significantly stronger profile than in the real design, ultimately leading to a structure which is significantly larger in steel mass.

Even though the validation step did not prove any difficulties or problems in the SCIA models, a significant problem occurred in the structural model for the Berlagebrug design alternative. This could have been avoided by testing the models with higher amounts of loading on the bridge, in an earlier phase. The obtained error in the model, likely influences the stress distribution around both main beams to such an extent that no good comparison could be done between the structural performance. The neural network generates a structure which is about twice as small in mass, yet the unity checks in all considered positions are smaller than in the definitive design of the Berlagebrug, on which a design team has worked for years. This is not a logical observation and it likely means that due to the error at the interface between the web of the main beam and bridge deck plate, stresses are not correctly transferred to the underlying system of cross beams and rib elements, but rather get cropped up in the faulty nodes. The structural performance results for this case comparison are not reliable enough to be used in forming a conclusion to the research question.

Regarding the structural performance of the design alternative for the Elizabeth Admiraalbrug, it can be said that it behaves as expected. The mass of the structure is more than twice as much, and the obtained unity checks for the cross beams and ribs under the same load combinations are also significantly smaller compared to the real design, which is a logical consequence. The unity checks for the main beam are similar, this is logical since their dimensions are also similar in both cases.

To further increase the strength of the structural performance comparison, one should investigate the behavior under all possible loading combinations for movable bridges, and one should take into account the highest occurring stresses at any point in the structure, instead of specifically comparing stresses in a single element.

6.2. Lessons learned

This section gives a short insight into points of attention that could be done better or differently in future work continuing on this topic, and into what was learned from this project.

Defining objective score metrics

Probably the most important lesson that has been learned from performing this research, is that it is important to define objective targets/indicators with which the structural performance of a design can be scored. With this in place, there is an objective metric in place to which the functioning of the neural network can be optimized and evaluated. These scores must be included in the data set for all bridges, as well. With such a metric, it is easier to evaluate the correctness of generated design alternatives,

and to form an answer to the research question posed in this thesis.

Simpler parameter definition

In future research, it is advisable to reduce the complexity of the parametric model. The focus should be more on predicting the amount of structural elements and their required strength, and less on the exact geometry of for example the main beams. It would be more beneficial to construct some ground rules based on the geometry of the existing bridges, with which the shapes of the main beams are formed inside the parametric model. The machine learning algorithm can then be focused on predicting the required strength of the elements. Creating a model with less parameters also means that it takes less time to collect all required information, meaning that in the same time frame, more bridges could be added to the data set.

Choice of machine learning algorithm

This goes hand in hand with the previous point. In this thesis, a neural network algorithm was chosen because 21 parameters needed to be predicted. An advantage of the architecture of a neural network algorithm is that it can easily be applied onto a data set of arbitrary shape. In the future, when a simpler parametric model is made, which is steered by less parameters, it is advised to use a less complex regression algorithm to do predictions. A benefit is that it is easier to gain insight into the prediction performance of such a simpler algorithm and that it is controlled by less variables.

Comparison with ground rules

To further validate the design alternatives generated by the neural network algorithm, it can be interesting to investigate manually, whether there are relationships between parameters in the data set. If ratio's between parameters can be found, it might be possible to draw up design rules based on the data set. One can then create a design alternative based on these rules, and compare it to both the real case, and the design alternative generated by the neural network, meaning a three-way comparison, instead of a two-way comparison like was done in this research. Doing this further strengthens the validity and conclusion of the research.

Conclusion & Recommendations

7.1. Conclusion

The main research question that was posed in this research is: *How can machine learning be used to improve the structural design process of bascule bridges?*

This research aimed to investigate the possibility of applying a neural network algorithm into the structural design process of bascule bridges, by creating a workflow in Grasshopper and SCIA Engineer. Based on the quantitative results obtained in the validation and results phase of the research, it can be concluded that the machine learning algorithm in the application developed in its current form, will not significantly improve the structural design process, due to a lack of consistency in generated results. There are two main reasons why the created workflow will not improve the structural design process of bascule bridges at this moment. Firstly, there is a lack of consistency in predicting behavior of the neural network. In three out of seven design cases considered in this study, a viable structural design was suggested by the neural network. In the results section, it appeared that for a cycle and pedestrian bridge, a severely over-dimensioned structure was generated. Indicating that the workflow is not suitable in predicting designs for this typology. Secondly, it was found in the results section that there are still errors in the SCIA models that the workflow generates. Important in the structural design process is a realistic finite element analysis model that shows correct behavior. This thesis has showed that at this point, the workflow that forwards a structural design via a ".xml" file into SCIA Engineer, does not generate correctly working models, consistently.

However, taking into account the scope of this assignment, which was focused on the conceptual and preliminary design phase of bascule bridge projects, it can be said that the developed workflow, in which the power of the neural network and parametric model are combined, can improve the design process in general because of two main points. Firstly, it appeared in the validation phase of this research that in two of the five cases, the neural network predicted a good structure except for one parameter. Being able to create a realistic design based on having to change only one parameter as user, means one can generate design alternatives quickly. The parametric model defined in Grasshopper, which is combined with the power of a neural network, which indirectly contains information about existing bridges, provides a platform in which the user can quickly generate different design alternatives. Secondly, changes to the model are visible immediately, meaning that the Grasshopper environment can possibly facilitate more engaged discussions about design choices between different stakeholders and project members. The fact that the neural network can assist with generating designs in four out of five cases in the validation stage, indicates that an orthotropic bridge deck can be standardized and divided into parameters effectively, and that such a bridge deck is suitable to be predicted by a machine learning algorithm. Regarding the type of bridge data in the data set, this thesis has shown that it is possible to apply a neural network algorithm onto an arbitrary parameter definition, as long as the data is normalized before it is fed into the algorithm. The choice for parameters, and their different value ranges, does not matter.

The approach taken in this thesis shows that the application of a machine learning algorithm onto a data set of such a structure typology, can be very useful when worked out properly. When a more simple model is constructed, with a less complex architecture and more data points, it is very much possible that a neural network algorithm can be applied in civil engineering applications of which the structural design is more data-driven. Bridge design is one of the disciplines within civil engineering that is influenced by a lot of factors and subjective design choices, it is not purely driven by optimal structural performance. Therefore, the results of this research indicate that applying a machine learning algorithm into other design processes which are purely driven by structural performance efficiency, is very much possible. The created workflow in this thesis does illustrate the power and advantages of parametric modeling, which partly solves the problems and difficulties named in the introduction, and already helps the firm a great deal in the exploration of design alternatives.

7.2. Recommendations

Further research is needed to investigate not only the application of machine learning in bridge design, but also in terms of how and with what data it is possible to describe civil engineering structures to a machine learning algorithm, so the structural design process can be automated and sped up. To further analyze the possibilities of applying a neural network algorithm into bascule bridge design, the following steps are recommended:

- Re-evaluating the created parametric model of an orthotropic bridge deck. During the project, a better understanding of the working of such a bridge deck was conceived, however, the parameters were already defined earlier in the project. The parameter definition functions as base of the whole workflow, and it is therefore important to divide the structure in useful parameters.
- Decrease the model complexity. What has already been addressed is that the neural network is too complex, which leads to poor prediction accuracy. The model only contains 35 data entries, with which fourteen parameters need to be predicted. New research can investigate the influences of adding more bascule bridges to the data set and reducing the amount of parameters that the neural network has to predict.
- Constructing a model strategy. Further research should investigate what the most optimal way is to define a finite-element analysis model of an orthotropic bridge deck, which yields no geometrical errors like encountered in this thesis. Only when such a strategy is defined firm-wide, the created Grasshopper workflow can help save time in future bridge projects.

To further investigate the possibilities of applying machine learning within the structural design process of civil engineering structures, the following points should be investigated:

- Choice for a machine learning algorithm. It is possible that an artificial neural network has been too complex of an algorithm, to base the created Grasshopper workflow on. Research should be done on what type of algorithms can be best applied on what type of data that describes a structure. It is likely best to start with simple, classifying algorithms.
- Determine what data to describe a structure with. This goes hand in hand with the previous point. In order to successfully apply a machine learning algorithm into a structural design procedure, it must be trained with suitable data. As was encountered in this thesis, because different types of parameters were inserted, such as the profile height and required moment of inertia, different magnitudes of inaccuracy were measured. Because of this, it has been difficult to assess what the influence of every parameter was on the model accuracy.

References

- Alzubi, J. & Nayyar, A. & Kumar, A. (2018). Machine Learning from Theory to Algorithms: An Overview. *Journal of Physics:Conference Series*, 1142. <https://doi.org/10.1088/1742-6596/1142/1/012012>
- Beck, A.D. & Kurz, M. (2020). A Perspective On Machine Learning Methods in Turbulence Modeling. <https://doi.org/10.13140/RG.2.2.17469.69608>
- Brownlee, J. (2020). *Understand the Impact of Learning Rate on Neural Network Performance*. Deep Learning Performance. Obtained from <https://machinelearningmastery.com/understand-the-dynamics-of-learning-rate-on-deep-learning-neural-networks/>
- Brownlee, J. (2019). *How to use Learning Curves to Diagnose Machine Learning Model Performance*. Deep Learning Performance. Retrieved from <https://machinelearningmastery.com/learning-curves-for-diagnosing-machine-learning-model-performance/>
- Brownlee, J. (2018). *How to Avoid Overfitting in Deep Learning Neural Networks*. Deep Learning Performance. Obtained from <https://machinelearningmastery.com/introduction-to-regularization-to-reduce-overfitting-and-improve-generalization-error/>
- Connor, R. et al. (2012). Manual for Design, Construction, and Maintenance of Orthotropic Steel Deck Bridges.
- Davidson, S. (2023). *About Grasshopper....* Retrieved from <https://www.grasshopper3d.com/>
- Detweiler, W.H.(2008). Selecting and Specifying Bearings for Movable Bridges. *SKF USA Inc..* Obtained from <https://heavymovablestructures.org/wp-content/uploads/2017/12/Selecting-and-Specifying-Bearings-for-Movable-Bridges.pdf>
- Dhage, S.N. & Raina, C.K. (2016). A review on Machine Learning Techniques. *International Journal on Recent and Innovation Trends in Computing and Communication*, 4(3).395-399. ISSN:2321-8169
- DigitalSreeni. (2020, September 1). *154 - Understanding the training and validation loss curves*[Video]. YouTube. <https://www.youtube.com/watch?v=p3CcfljycBA>
- EPC-Groep. (n.d.). *Amaliabrug in Gouda*. Retrieved from <https://www.epc-groep.nl/amaliabrug-in-gouda>
- Goodfellow, I. & Bengio, Y. & Courville, A. (2016). *Deep Learning*. The MIT Press.
- Gupta, N. (2013). Artificial Neural Network. *Network and Complex Systems*, 3(1). 24-28.
- Heaton, J. (2008). *Introduction to Neural Networks in Java* (Second edition). Heaton Research Inc.
- Igel, C. & Hüsken, M. (2003). Empirical evaluation of the improved Rprop learning algorithms. *Neurocomputing*, 50.105-123. [https://doi.org/10.1016/S0925-2312\(01\)00700-7](https://doi.org/10.1016/S0925-2312(01)00700-7)
- Keen, M.(2022). *Supervised vs. Unsupervised learning*[Video].IBM Technology on YouTube. Retrieved from https://www.youtube.com/watch?v=W01tIRP_Rqs
- Kohavi, R. (1995). A Study of Cross-Validation and Bootstrap for Accuracy Estimation and Model

Selection. *IJCAI*, 14(2).1137-1145. Retrieved from https://link.springer.com/content/pdf/10.1007/978-3-540-76917-0_9.pdf

Kuhn, M. & Johnson, K. (2018). *Applied Predictive Modeling*(2nd Corr. edition). Springer.

LeCun, Y. & Bengio, Y. & Hinton, G. (2015). Deep Learning. *Nature*, 521. 436-444.
<https://doi.org/10.1038/nature14539>

LeCun, Y. et al. (2002). Efficient BackProp. *Neural Networks: Tricks of the trade*.9-50.Berlin, Heidelberg: Springer Berlin Heidelberg.

Mahesh, B. (2018). Machine Learning Algorithms - A Review. *International Journal of Science and Research*, 9(1).<https://doi.org/10.21275/ART20203995>

McNeel & Associates. (2023). *Rhino - Features*. Retrieved from <https://www.rhino3d.com/features/>

Miller, Nathan. (2017). *Machine Learning with LunchboxML*. Provingground. Retrieved from <https://provingground.io/2017/08/01/machine-learning-with-lunchboxml/>

Mitchell, T.M.(1997).*Machine Learning*. McGraw-Hill Science/Engineering/Math.

Mobilis(2023, September 22).*Monumentale Berlagebrug weer toekomstbestendig: 'Mooi draaiboek'*. Mobilis | TBI. Retrieved from <https://www.mobilis.nl/nieuws/monumentale-berlagebrug-weer-toekomstbestendig-mooi-draaiboek>

Moen, J.C.(2014). Feasibility Study on Heavy-Traffic FRP Bascule Bridges. *Master thesis TU Delft*. Obtained from repository.tudelft.nl

Movares. (2016, March). *Bewegingswerken: Vervangen of laten zitten?*. Obtained from <https://movares.nl/wp-content/uploads/2016/07/Artikel-herberekenen-bewegingswerken-in-blad-Bruggen-maart-2016.pdf>

Nasteski, V. (2017). An overview of the supervised machine learning methods. *Horizons*. b4.51-62.
<https://doi.org/10.20544/horizons.b.04.1.17.p05>

Natsheh, S.H. & Menzemer, C.C. (2022). Built-Up Closed-Rib Steel Orthotropic Bridge Decks. *CivilEng*, 3(4).960-978. <https://doi.org/10.3390/civileng3040054>

Nemetschek Group. (2024).*KOALA - GRASSHOPPER PLUGIN FOR SCIA ENGINEER*.
<https://www.scia.net/en/support/addons/koala-grasshopper-scia-engineer>

Olson, D.L. et al.(2008). Performance evaluation for predictive modeling. *Advanced data mining techniques*.137-147. Retrieved from https://link.springer.com/content/pdf/10.1007/978-3-540-76917-0_9.pdf

Osisanwo, F.Y. (2017). Supervised Machine Learning Algorithms:Classification and Comparison. *International Journal of Computer Trends and Technology*, 48(3). 128-138. ISSN: 2231-2803.

Pannell, J.J. & Rigby, S.E. & Panoutsos, G. (2022). Physics-informed regularisation procedure in neural networks: An application in blast protection engineering. *International Journal of Protective Structures*, 13(3). 555-578.<https://doi.org/10.1177/20414196211073501>

Parke, G. & Hewson, N. (2008). *ICE manual of bridge engineering* (Second edition). Thomas Telford Limited.

Payne, A. (2009).*Using a wii to control Grasshopper*.Lift architects. Retrieved from

<http://www.liftarchitects.com/blog/2009/9/9/using-a-wii-to-control-grasshopper>

Prasad, A. (2021). *Feed Forward Neural Networks - Intuition on Forward Propagation*. Analytics Vidhya. Retrieved from <https://www.analyticsvidhya.com/blog/2021/10/feed-forward-neural-networks-intuition-on-forward-propagation/>

Scikit-learn. (2024). 3.1. *Cross-validation: evaluating estimator performance*. Retrieved from https://scikit-learn.org/stable/modules/cross_validation.html

Sharma, G. (2022). *5 Regression algorithms you should know - Introductory Guide!*. Analytics Vidhya. Retrieved from <https://www.analyticsvidhya.com/blog/2021/05/5-regression-algorithms-you-should-know-introductory-guide/>

Sutskever, I. (2013). On the importance of initialization and momentum in deep learning. *Proceedings of Machine Learning Research*, 28(3).1139-1147. Retrieved from <https://proceedings.mlr.press/v28/sutskever13.html>

Van der Zwaag, B.J. & Spaanenburg, L. (2004). Translating Feedforward Neural Maps to SOM-like Maps.

Van Hattum en Blankevoort. (n.d.). *N522 Vervanging brug Ouderkerk*. Retrieved from <https://www.vhbinfra.nl/nl/projecten/detail/n522-vervanging-brug-ouderkerk>

Van Zantvliet, P.S. (2015). Analysis of the force distribution on operating mechanisms in a bascule bridge. *Master Thesis TU Delft*. Obtained from <https://repository.tudelft.nl>

Viik, L. D. (2019). StructuralComponents 6: An early-stage design tool for flexible topologies of mid-rise concrete buildings. *Master thesis Delft University of Technology*. Obtained from <https://repository.tudelft.nl>

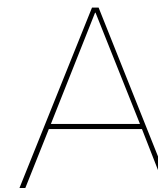
Vilhjálmsón, T. (2023). A Methodology for Damage Detection Using Unsupervised Learning in the Field of Structural Health Monitoring. *Master Thesis TU Delft*. Obtained from <https://repository.tudelft.nl>

Wang, S.-C.(2003). *Interdisciplinary Computing in Java Programming*. Kluwer Academic Publishers. Obtained from <https://link.springer.com/book/10.1007/978-1-4615-0377-4>

Willemsen, R.(2020). Towards BIM-based automation of the vertical load calculation. *Master thesis TU Delft*. <https://repository.tudelft.nl>

WisDOT. (August, 2017). *WisDOT Structure Inspection Manual, Part 3.2 Bascule Bridges*. Obtained from <https://wisconsindot.gov/dtsdManuals/strct/inspection/insp-fm-pt3ch2.pdf>

Wood, W.H.,III, and Agogino, A.M.(1996). Case-Based Conceptual Design Information Server for Concurrent Engineering. *Computer-Aided Design*, 28(25).361-369. [https://doi.org/10.1016/0010-4485\(95\)00055-0](https://doi.org/10.1016/0010-4485(95)00055-0)



Bridge overview

There are 41 bascule bridges in the municipality of Amsterdam. These are named in the following table. Five bridges are disregarded in this thesis, these are highlighted in red.

Table A.1: Bascule bridges in Amsterdam.

Object number	Name	Construction year	Typology	Construction material	Operating mechanism	Traffic function
BRU0050	Latjesbrug	1968	Single	Steel/concrete	Electro-Mechanical	Vehicle traffic
BRU0101	Nieuwe Amstelbrug	1986	Double	Steel/concrete	Electro-Mechanical	Vehicle traffic + tram
BRU0149	Bullebak	2023	Double	Steel/concrete	Electro-Mechanical	Vehicle traffic + tram
BRU0151	Willemsbrug	1928	Single	Steel/concrete	Electro-Mechanical	Vehicle traffic
BRU0155	Kattenslootbrug	1954	Single	Steel/concrete	Electro-Mechanical	Vehicle traffic + tram
BRU0171		1931	Single	Steel/concrete	Electro-Mechanical	Vehicle traffic
BRU0173	Wiegbrug	1988	Single	Steel/concrete	Electro-Mechanical	Vehicle traffic + tram
BRU0199	Overtoomsesluis	1948	Single	Steel/concrete	Electro-Mechanical	Vehicle traffic + tram
BRU0238	M.S.Vaz Diasbrug	1962	Single	Steel/concrete	Electro-Mechanical	Vehicle traffic
BRU0239	Hortusbrug	1960	Single	Steel/concrete	Electro-Mechanical	Vehicle traffic + tram
BRU0246	Hogesluis	2011	Double	Steel/concrete	Electro-Mechanical	Vehicle traffic + tram
BRU0266	Kinkerbrug	2003	Single	Steel/concrete	Electro-Mechanical	Vehicle traffic + tram
BRU0272	Mariniersbrug	1935	Single	Steel/concrete	Electro-Mechanical	Vehicle traffic
BRU0274	Kattenburgerbrug	1965	Single	Steel/concrete	Electro-Mechanical	Vehicle traffic
BRU0314	Westerdoksluis	1960	Single	Steel/concrete	Electro-Mechanical	Vehicle traffic
BRU0318	Zoutkeetsbrug	1965	Single	Steel/concrete	Electro-Mechanical	Vehicle traffic
BRU0324	Beltbrug	2007	Single	Steel/concrete	Electro-Mechanical	Vehicle traffic
BRU0345		1964	Single	Steel/concrete	Electro-Mechanical	Vehicle traffic
BRU0346	Westerkeersluis	1962	Single	Steel/concrete	Electro-Mechanical	Vehicle traffic
BRU0349	Cor Thesingbrug	1964	Single	Steel/concrete	Electro-Mechanical	Vehicle traffic
BRU0350	Torontobrug	1968	Double	Steel/concrete	Electro-Mechanical	Vehicle traffic
BRU0356	NSM-brug	2018	Single	Steel/concrete	Electro-Mechanical	Vehicle traffic
BRU0357	Gerben Wagenaarbrug	1964	Single	Steel/concrete	Electro-Mechanical	Vehicle traffic
BRU0382		1936	Single	Steel/concrete	Electro-Mechanical	Vehicle traffic
BRU0423	Berlagebrug	2024	Single	Steel/concrete	Hydraulic	Vehicle traffic + tram
BRU0485	Dees Postmabrug	1970	Single	Steel/concrete	Electro-Mechanical	Vehicle traffic + tram
BRU0487	Kortjewantsbrug	1967	Single	Steel/concrete	Electro-Mechanical	Vehicle traffic
BRU0491	Meeuwenpleinbrug	1967	Single	Steel/concrete	Electro-Mechanical	Vehicle traffic
BRU1647	Schinkelmetrobrug	1995	Single	Steel/concrete	Electro-Mechanical	Metro
BRU1787	Kadoelenbrug	2012	Single	FRP+steel/concrete	Electro-Mechanical	Pedestrian- and cyclebridge
BRU1788	Theo Fransmanbrug	2013	Single	Steel/concrete	Hydraulic	Pedestrian- and cyclebridge
BRU1797	Bongerdbrug	2018	Single	Steel/concrete	Hydraulic	Pedestrian- and cyclebridge
BRU1939	Mr. J.J. van der Veldebrug	1992	Single	Steel/concrete	Electro-Mechanical	Pedestrian- and cyclebridge
BRU2023		2008	Single	Steel/concrete	Hydraulic	Vehicle traffic
BRU2038	Steigereilandbrug	2003	Single	Steel/concrete	Hydraulic	Vehicle traffic
BRU2190	Solitudobrug	2023	Single	Cortensteel/concrete	Hydraulic	Pedestrian- and cyclebridge
BRU2202	Han Lammersbrug	2003	Single	Aluminium/concrete	Hydraulic	Pedestrian- and cyclebridge
BRU2208	Uiverbrug	2004	Single	Aluminium/concrete	Hydraulic	Vehicle traffic
BRU5046	Roskambrug	1970	Single	Steel/concrete	Electro-Mechanical	Vehicle traffic
BRU5047	De Uitkomst	1970	Single	Steel/concrete	Electro-Mechanical	Vehicle traffic
BRU55P	Schellingwouderbrug	2013	Double	Steel/concrete	Electro-Mechanical	Vehicle traffic

B

SBS Bascule bridge

The following figure shows the system breakdown structure of a typical bascule bridge.

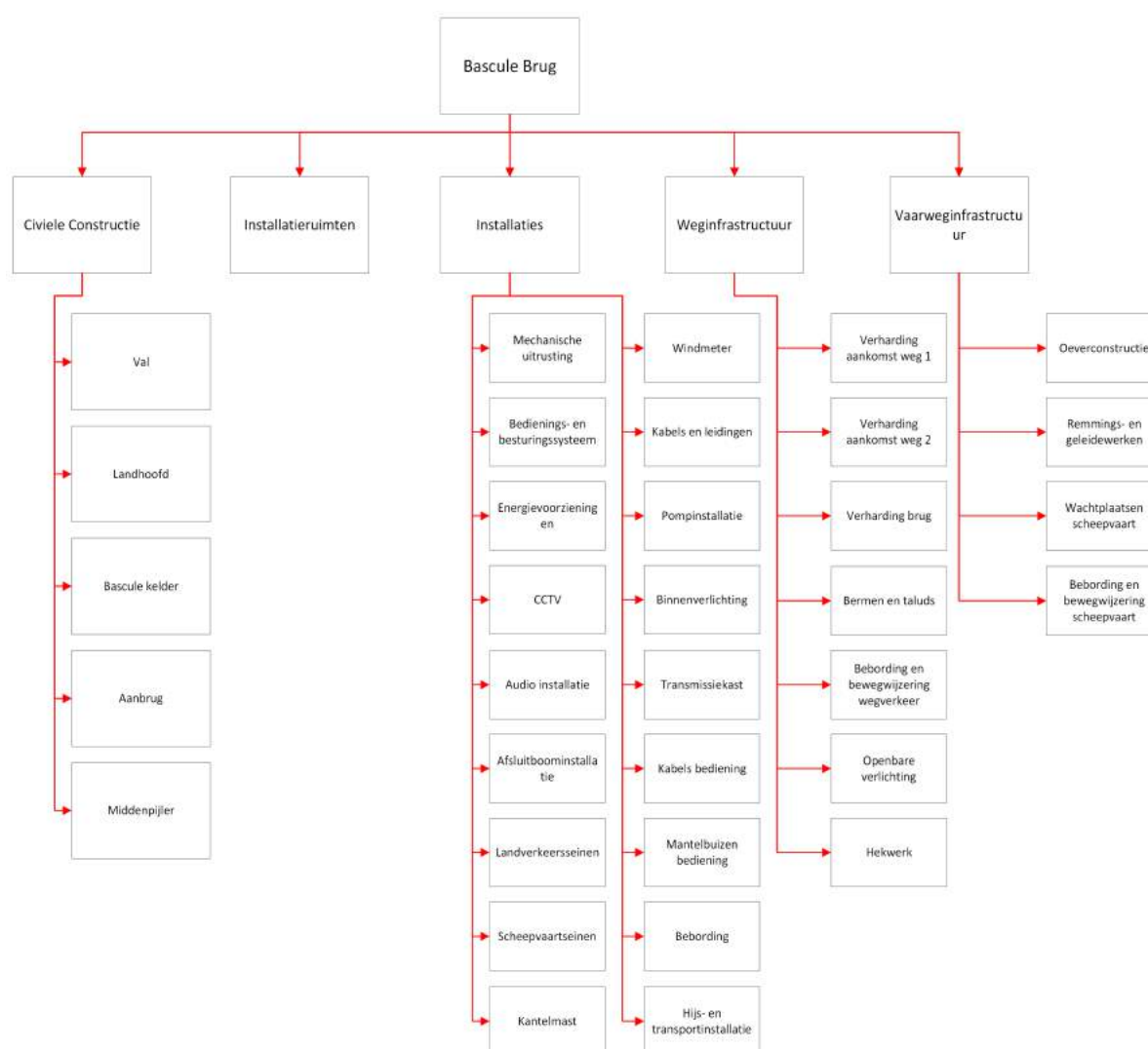
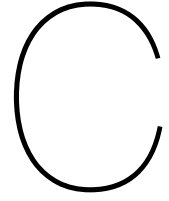


Figure B.1: System Breakdown Structure of Bascule bridge.



Calculation procedure loading on bridge deck

C.1. Wind loading

For a closed bridge deck, the Eurocode defines directions as shown in figure C.1.

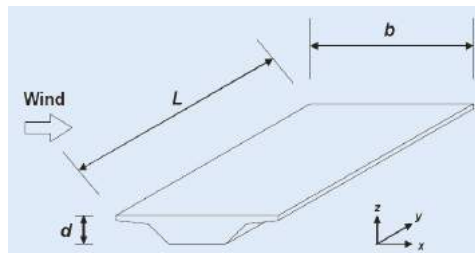


Figure C.1: Local axis system for wind loading on a bridge deck.(NEN-EN1991-1-4:2005+C2:2011+NB:2019)

Wind loading in transverse direction

For wind loading on a closed bridge deck in x-direction, one can use a simplified function to determine the wind loading, when a dynamic response calculation is not necessary. Dynamic response calculations are not considered in this thesis. The simplified wind load in transverse direction onto the bridge is modeled by:

$$F_w = \frac{1}{2} \rho \cdot v_b^2 \cdot C \cdot A_{ref,x} \quad (C.1)$$

where

ρ is the air density during stormy conditions in the region.

$\rho = 1.25 \text{ kg/m}^3$ according to section 4.5 of NEN1991-1-4.

v_b is the base wind speed, calculated according to $v_b = c_{dir} \cdot c_{season} \cdot v_{b,0}$ (NEN-EN1991-1-4:2005).

$v_{b,0}$ is the characteristic 10-min average wind speed at 10 meters above ground level.

For the different zones in the Netherlands, values are shown in the next table.

Table C.1: Windspeeds per area.(NEN-EN1991-1-4:2005)

Windgebied	I	II	III
$v_{b,0}$ [m/s]	29.5	27.0	24.5

Amsterdam is located in zone II, so $v_{b,0} = 27.0 \text{ m/s}$.

$c_{dir} = c_{season} = 1$, so $v_b = v_{b,0}$, according to NEN-EN1991-1-4.

C is the wind loading factor, which is calculated by $C = c_e \cdot c_{f,x}$. Where c_e is the exposure factor, as

calculated by section 4.5 of NEN-EN1991-1-4 and NB:2019.

$c_{f,x}$ is the force coefficient which is dependent on the shape of the bridge deck and accompanying height of traffic over the bridge. This value can be deducted from figure 8.3 in NEN-EN1991-1-4:2005. C can also be deducted from table NB.18.

$A_{ref,x}$ is the reference surface area of the bridge normal to the wind direction. This value is determined using section 8.3.1 of above mentioned code.

Wind loading in vertical plane

For wind loading in z-direction, the uplifting force of wind is of interest, since it must be prevented that the bridge deck lifts from its support pier due to wind. The downward force on the support pier must be larger than the uplifting force, to prevent loading on the locking mechanism and possibly bouncing movements of the bridge leaf. The vertical force on the bridge leaf in closed position, is calculated similarly to equation 3.1, namely by:

$$F_{w,z} = \frac{1}{2} \rho \cdot v_b^2 \cdot C_z \cdot A_{ref,z} \quad (C.2)$$

The coefficient C_z is in this case calculated by $C = c_e \cdot c_{f,z}$. In this equation, c_e is the same as mentioned before, and $c_{f,z}$ is determined from figure NB.8 in NEN-EN1991-1-4:2005+NB:2019. This value is dependent on the slope of the bridge deck and wind angle relative to the horizontal axis. For flat terrain, a wind angle of five degrees can be assumed due to turbulence, this results in $c_{f,z} = \pm 0.9$. $A_{ref,z}$ is the area at which the uplifting force acts, which is calculated by $A_{ref,z} = b \cdot L$.

Wind loading in parallel direction

In longitudinal direction, which is parallel to the span of the bridge, the wind loading can be assumed to be 40% of the transverse wind loading(NEN-EN1991-1-4). In closed position, this force always acts simultaneously as the unfavourable transverse wind loading. The uplifting force must be taken into account simultaneously, only when it leads to unfavourable conditions.

Load situations

When the bridge is stationary in opened stance, thus outside of the operation cycle, the wind loading must be applied onto the bridge leaf in perpendicular and transverse direction. For the wind load perpendicular to the bridge leaf, in z-direction of the local axis system, the wind pressure must be calculated according to section 4.5 in NEN-EN1991-1-4. Where $q_p(z_e)$ must be determined with a height z_e as the height between the average water level and the highest point of the bridge leaf. For transverse wind loading, the same procedure needs to be followed as described earlier, where the surface area is determined as function of the leaf thickness and attributes on the bridge deck. These two wind loading cases must be checked separately as well as in the following combinations(NEN 6786-1):

- Wind loading perpendicular to the bridge leaf with 40% of calculated transverse wind loading.
- Wind loading transverse to the bridge leaf with 40% of calculated perpendicular wind loading.

Lastly, the wind loading during the operational cycle of a bascule bridge should be considered. The wind loading during the operational cycle is dependent on the type of fairway and the amount of hours that the bridge is allowed to be nonoperational due to high wind loading.

Table C.2: Maximum hours non-operational due to high wind loads(NEN 6786-1:2017+C1:2021).

Type vaarweg	Maximaal aantal uren per jaar niet-bedienbaar
Zeevaart	12
Hoofdtransportas	
Doorvaarthoogte ≥ 9.10 m	24
Doorvaarthoogte < 9.10 m	6
Hoofdvaarweg	
Doorvaarthoogte ≥ 6.00 m	48
Doorvaarthoogte < 6.00 m	12
Overige vaarwegen	72

For newly constructed bascule bridges, maximum non-operational hours are set at 72 hours, unless specified differently in the bridge's program of requirements. It must also be at least equal to the hours of other bridges in the same fairway. NEN 6786-1 states two equations to calculate the maximum wind pressure on the bridge leaf during the opening or closing cycle. The most easy applicable equations is:

$$q_p(z_e) = \left(\frac{q_p(z_e)}{v_{m,10}^2} \right) \cdot v_{m,10}^2 \quad (C.3)$$

$\frac{q_p(z_e)}{v_{m,10}^2}$ is a value dependent on height z_e , which can be determined from table 2 in section 2.3.2.2 of NEN 6786-1. Here, z_e is again the distance between the average water level and the highest point of the bridge leaf.

$v_{m,10}$ is the 10 minute average wind speed at 10 meters above ground level. Its value can be deducted from table 3 in NEN-EN 6786-1, using the acquired information about the wind area that the bridge is placed in and maximum non-operational hours per year.

It must be assumed that wind loading can work in both directions when both opening and closing the bridge, as well as in opened position. The wind loading must therefore always be considered as acting moment around the rotational axis, so that the forces on the supports and operational system of the bascule bridge can be checked. It must be assumed that the maximum wind pressure is always perpendicular to the bridge leaf, regardless of its angle. The maximum moment around the rotational axis due to wind loading is described by:

$$M_{w,bridge} = 1.05 \cdot c_s \cdot c_d \cdot C_t \cdot \Sigma(q_p(z_e)) \cdot S \quad (C.4)$$

Where $c_s = 0.95$ and $c_d = 1.15$.

C_t is a wind form factor which is determined with figure C.2 shown below. In this graph, $\frac{l}{b}$ is the ratio between the length and width of the bridge leaf that is susceptible to wind loading.

S is the static moment with respect to the rotational axis, of the part of the bridge leaf at which wind loading is present.

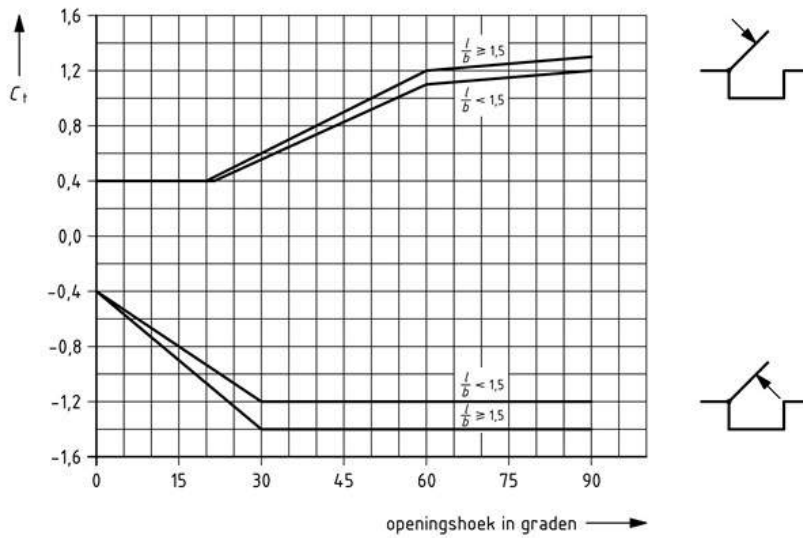


Figure C.2: Wind form factor(NEN 6786-1:2017+C1:2021).

C.2. Traffic loading

Traffic load model 1

Load model 1 is used to simulate vehicles driving over the bridge deck. The bridge deck is divided into notional lanes, which have a decreasing significance of axis loading, to simulate asymmetric loading. The bridge is divided in lanes of equal width, between the permanent road restraining systems. The

width of the notional lane depends on the total width of the drivable part of the bridge, as illustrated in table C.3.

Table C.3: Division of notional lanes.(NEN-EN1991-2:2003+C1:2015+NB:2019)

Breedte van de rijweg w	Aantal theoretische rijstroken	Breedte van een theoretische rijstrook w_l	Breedte van het resterende oppervlak
$w < 5.4 \text{ m}$	$n_l = 1$	3 m	$w - 3 \text{ m}$
$5.4 \text{ m} \leq w < 6.0 \text{ m}$	$n_l = 2$	$\frac{w}{2}$	0
$6.0 \text{ m} \leq w$	$n_l = \text{Int}(\frac{w}{3})$	3 m	$w - 3 \times n_l$

The notional lanes are counted from one side of the drivable part, as shown in figure C.4. Figure C.3 shows examples of carriageway widths of different bridge configurations. Elevated footpaths on the side of the bridge that have kerbs of at least 100 mm, are not part of the carriageway width.

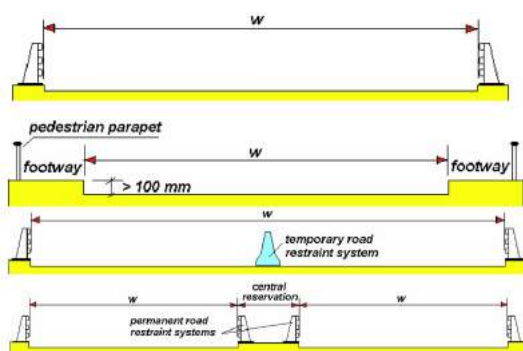


Figure C.3: Examples of carriageway widths and restraint systems.(Pavlovic, 2022)

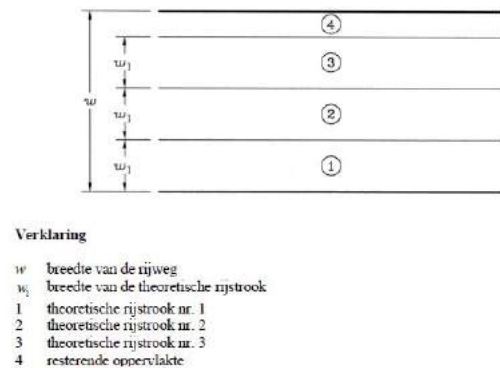


Figure C.4: Division of notional lanes.(NEN-EN1991-2:2003+C1:2015+NB:2019)

Load model 1 uses both concentrated and distributed loads, to simulate car and heavy traffic. The tandem loads are defined per axle, and are given by the following equation:

$$\alpha_{Qi} \cdot Q_{ik} \quad (\text{C.5})$$

Each wheel thus exerts a force of $0.5 \cdot \alpha_{Qi} \cdot Q_{ik}$, which should be applied onto a contact area of 0.4 x 0.4 meters, in a grid of 2 x 1.2 meters. Such a tandem system of four loads, should be applied on the center of every notional lane. Every notional lane should only have a maximum of one, complete tandem system applied.

In addition to the tandem system, load model one also includes uniformly distributed loads, which are given by:

$$\alpha_{qi} \cdot q_{ik} \quad (\text{C.6})$$

Which can be applied onto notional lanes and the remaining part of the bridge deck. In the previously named equations, α_{Qi} and α_{qi} are correction factors, which are dependent on the amount of heavy traffic over the bridge and the bridge's span. These factors can be deducted from table NB.1 in the national annex accompanying NEN-EN1991-2. Characteristic values of the loads Q_{ik} and q_{ik} that should be applied onto every notional lane, can be found in table 4.2 (NEN-EN1991-2:2003+C1:2015+NB:2019).

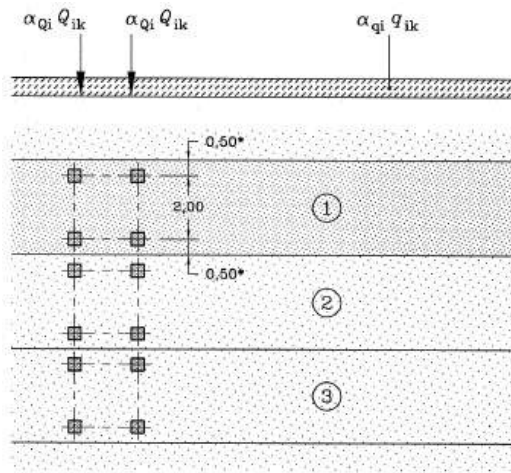


Figure C.5: Load model
1.(NEN-EN1991-2:2003+C1:2015+NB:2019)

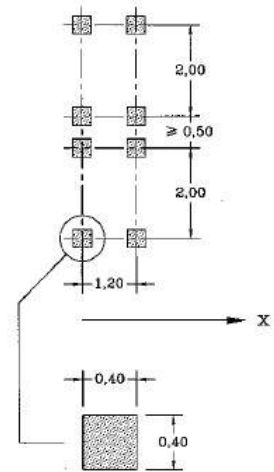


Figure C.6: Parallel vehicles in
load model 1.(NEN-EN1991-
2:2003+C1:2015+NB:2019)

Traffic load model 2

Load model 2 consists of a single axis load of $\beta_Q \cdot Q_{ak}$, in which $\beta_Q = \alpha_{Q1}$ and $Q_{ak} = 400$ kN. This load can be placed at an arbitrary position on the drivable part of the bridge deck. Wheels are spaced at 2 meters, and have a contact area of 0.6 x 0.35 meters, as can be seen in figure C.7.

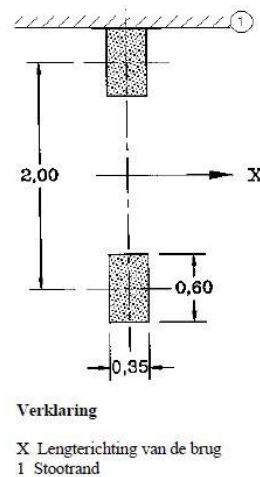


Figure C.7: Load model 2.(NEN-EN1991-2:2003+C1:2015+NB:2019)

Traffic load model 3

Load model 3 depicts loading for special vehicles, for which specific requirements can be recorded in a project's program of requirements. Its requirements are specified in the national annex. Special vehicles with a maximum width of 3.0 meters and maximum axle load of 200 kN should be applied on notional lane 1. Special vehicles with a width or loading higher than previously named values should be applied on two neighboring lanes, as shown in the right of figure C.9. The remainder of the notional lanes should be loaded with the frequent loading as defined in load model 1.

If special vehicles drive faster than 5 km/h, a dynamic loading factor ϕ should be applied onto the characteristic values of the vertical axle loads. An equation for ϕ is given in section 4.3.4.2 of NEN-EN1991-2. Additional rules regarding calculations for special transport can be found in section 4.3.4.3.

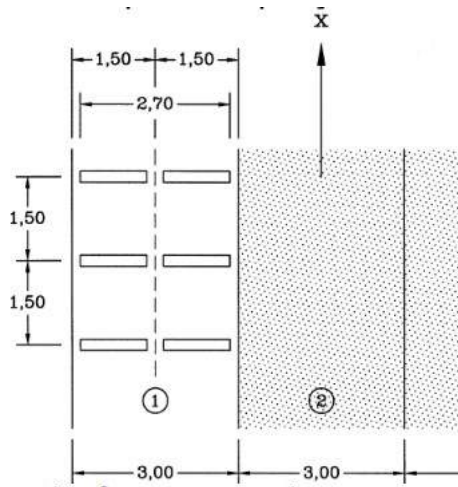


Figure C.8: Example of axle loads of special vehicle.(Pavlovic,2022)

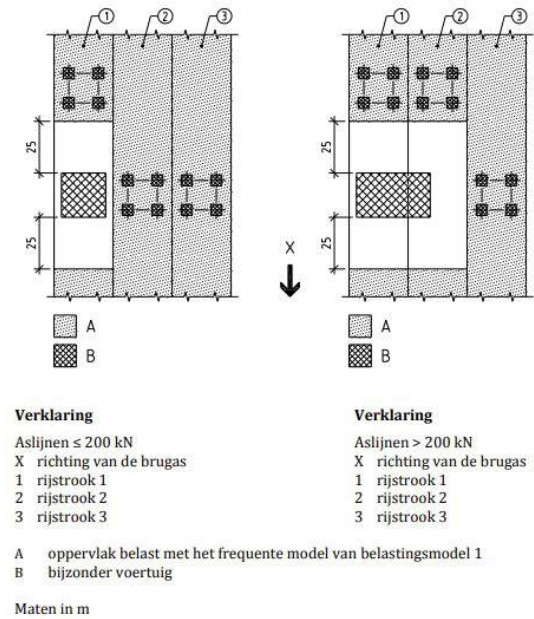


Figure C.9: Deck loading around special vehicle.(NEN-EN1991-2:2003+C1:2015+NB:2019)

Traffic load model 4

Load model 4 represents a crowd loading with uniformly distributed load of 5 kN/m^2 . This should be applied on all accessible parts of the bridge deck. This load case is meant for general assessments and should be regarded as temporary load.

Horizontal loading due to braking and accelerating, have been defined in the Eurocode, as a fraction of the occurring vertical loading on notional lane 1 in load model 1. A horizontal force should be assumed in longitudinal direction of the bridge, which takes place at the top of the bridge deck. This load is calculated by:

$$0.6 \cdot \alpha_{Q,1} \cdot (2Q_{1,k}) + 0.1 \cdot \alpha_{q,1} \cdot q_{1,k} \cdot w_1 \cdot L \quad (\text{C.7})$$

Eurocode specifies a maximum value of 900 kN. The Dutch national annex specifies a maximum value of 800 kN for this force.

In transverse direction, centrifugal forces can occur when a bridge has curved lanes, and due to slip movements of traffic. This is disregarded in this thesis. Firstly, an assessment must be made for which traffic category the bridge is built. This is dependent on the amount of lorries that pass the bridge per year per notional lane. According to the Dutch national annex, every notional lane should be assumed as heavy traffic lane. This assessment is made using table NB.5, which is shown below.

Table C.4: Definition of traffic categories.(NEN-EN1991-2:2003+C1:2015+NB:2019)

Verkeerscategorie	$N_{obs,a,sl}$ per jaar en per rijstrook voor zwaar verkeer
1 Autosnelwegen (A-wegen) en wegen met twee of meer rijstroken per rijrichting en met intensief vrachtverkeer	$2,0 \times 10^6$
2 (Auto)wegen met gemiddeld vrachtverkeer (zoals N-wegen)	$0,5 \times 10^6$
3 Wegen met weinig vrachtverkeer	$0,125 \times 10^6$
4 Wegen met weinig vrachtverkeer en bovendien uitsluitend bestemmingsverkeer	$0,05 \times 10^6$
OPMERKING De aantallen zware voertuigen per jaar en per rijstrook voor zwaar verkeer $N_{obs,a,sl}$ zijn inclusief de trend.	

C.3. Fatigue

Fatigue model 1

Fatigue model 1 is similar to load model 1 described earlier. In this fatigue calculation, reduced traffic loads of $0.7Q_{ik}$, $0.3q_{ik}$ and $0.3q_{rk}$ may be used. These loads are used to determine the maximum and minimum occurring stresses in the structure, which are denoted as $\sigma_{FLM,max}$ and $\sigma_{FLM,min}$ respectively. For bridges determined to be traffic category 3 or 4, a multiplication factor of 0.85 may be applied onto the loading.

Fatigue model 2

Fatigue model 2 is a similar analysis. In this model, a set of frequent trucks is applied onto the structure. These trucks have their own specifications including the number of axles and their spacing, axle loads and contact surface area per wheel. The maximum and minimum occurring stresses for fatigue, must be determined using the least favourable combination of different trucks onto the bridge. A description of the trucks to be considered is given in table 4.6 in NEN-EN1991-2:2003+C1:2015+NB:2019.

Fatigue model 3

Fatigue model 3 consists of a single vehicle with four axles, spread as shown in figure x. The axle load is equal to 120 kN, and the contact area per wheel is again 0.4×0.4 meters. Where applicable, two vehicles should be applied in one lane. In this case, the axle load is equal to 36 kN, and the vehicles should be more than 40 meters apart heart-to-heart. This is in general not relevant for bridge leafs of bascule bridges.

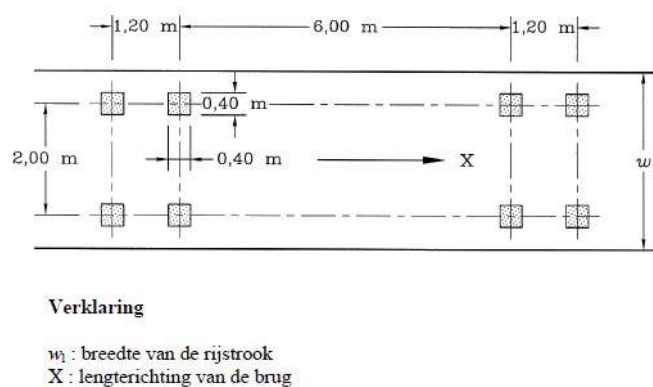


Figure C.10: Fatigue load model 3.(NEN-EN1991-2:2003+C1:2015+NB:2019)

Fatigue model 4

Fatigue model 4 simulates fatigue loading due to traffic, as measured by a set of standard trucks that make up a certain percentage of traffic. A further distinction is made between model 4a and 4b. Model 4a is used when only the stress range is of influence on the fatigue strength of the structural material. Model 4b is used when the fatigue strength is also dependent on the magnitude of the occurring stress. For both load models, a table with standard trucks is given in the Eurocode. A reduction factor may be applied in case the structure falls in traffic category 2,3 or 4 and when additional requirements specified in section 4.6.5.1 are met.

Fatigue model 5

Fatigue model 5 is based on the application of measured traffic data, that is possibly extended with extrapolated data and statistical information. More information about the application of this fatigue model is described in annex B of NEN-EN1991-2:2003+C1:2015+NB:2019.

C.4. Friction and roll resistance

The loading that occurs due to friction is firstly determined by the friction factor μ_r . This friction factor is dependent on the type of bearing used, and must thus be delivered by the manufacturer. Table 4 and 5 in section 2.3.6 of the VOBB give exemplary values for μ_R , for common construction materials.

The occurring friction moment, which is assumed to be a uniformly distributed loading over the length of the trunnion, is given by:

$$M_R = \mu_r \cdot F_{Ed}^{(2/3)} \cdot r \quad (C.8)$$

where:

r is the radius of the trunnion.

μ_r is the bearing friction factor.

F_{Ed} is the value of the force on the trunnion.

C.5. Thermal loading

A distinction can be made between two types of thermal loading on the structure. Firstly, the uniformly distributed temperature component. This is dependent on the minimum and maximum temperature that the bridge can reach. For buildings constructed outdoor, the atmospheric temperature in shadow, will vary from $T_{max} = 30^\circ$ to $T_{min} = -25^\circ$ (NEN-EN 1991-1-5:2003+C1:2009+NB:2019). The maximum uniform temperature range that a bridge in the Netherlands can then be subject to, can be deducted from the graph in figure NB.1 of section 6.1.3 of the Dutch national annex to NEN-EN1991-1-5:2003. In this case:

$$T_{e,max} = T_{max} + 16 = 46^\circ$$

$$T_{e,min} = T_{min} - 3 = -28^\circ$$

With respect to the actual temperature of the bridge T_0 , the characteristic values for the maximum range of uniformly distributed temperature are given by:

$$\Delta T_{N,con} = T_0 - T_{e,min}$$

$$\Delta T_{N,exp} = T_{e,max} - T_0$$

The second type of thermal loading that should be considered is the temperature difference component over the height of the structure. Due to weather influences, one side of the structure can become hotter or colder than the other side, resulting in a temperature gradient. This temperature component can be approached with a linear or non-linear method.

In case of a linear approach, values for the maximum temperature differences when one side is warmer than the other, should be deducted from table NB.1 in section 6.1.4.1 of the same national annex. Here, values of $\Delta T_{M,heat} = 18^\circ$ and $\Delta T_{M,cool} = 13^\circ$ are used for steel bridges. If the deck finishing is of different thickness than 50 mm, this value needs to be multiplied with a coefficient k_{sur} , for which values can be found in table NB.2 in the same section.

In case a non-linear approach is used, temperature differences should be deducted from tables and figures in section 6.4.1.2 of NEN-EN 1991-1-5.

If it is necessary to take into account the two mentioned types of temperature loading, they must be taken into account together in a loading combination. These are given with the following equations:

$$\Delta T_{M,heat}(or \Delta T_{M,cool}) + \omega_N \cdot \Delta T_{N,exp}(or \Delta T_{N,con})$$

$$\omega_M \cdot \Delta T_{M,heat}(or \Delta T_{M,cool}) + \Delta T_{N,exp}(or \Delta T_{N,con})$$

Where $\omega_N = 0.35$ and $\omega_M = 0.75$. The most unfavourable situation must be used.

Lastly, differences in the uniformly distributed temperature component of different structural elements must also be taken into account, with a maximum difference of 15° .

C.6. Accidental loading

For a collision between a vehicle and hard shoulder or bumper of the pedestrian path, a transverse force of 100 kN, should be taken into account. This force takes place at 0,05 meters below the point of contact and must be assumed to be a uniformly distributed line load over 0.5 meters. This force is then transferred to the underlying structural elements. With stiff structural elements, this force dissipates over an angle of 45° and must be combined with a vertical traffic load of $0.75 \cdot \alpha_{Q1} \cdot Q_{1k}$, if this appears to be an unfavourable load combination(NEN-EN 1991-2:2003+C1:2015+NB:2019).

For collisions between vehicles and structural elements, a distinction in the Eurocode is made between stiff and flexible structures. Section 4.7.3.4 states what forces should be taken into account for collisions on both highways and other roads. No further dependency on vehicle speed is defined. The point of engagement of such an accidental force is located at 1.2 meters above the road surface. The contact area is defined with a height of 0.25 meters and a width equal to that of the structural element that is hit, with a maximum of 1,0 meter(NEN-EN 1991-2:2003+C1:2015+NB:2019). This form of loading should not be combined with other variable loading cases.

In case there is no hard shoulder separating the foot- and cycle paths from the traffic lanes, vehicles can accidentally end up on them. In this case one axle load of $\alpha_{(Q2)} \cdot Q_{2,k}$ should be placed in the most unfavourable position. As shown in figure 4.9 in section 4.7.3.1 of NEN-EN 1991-2:2003+C1:2015+NB:2019. Again, this type of loading should not be combined with other variable loading on the deck.

Additionally, vessels on the fairway could also collide with either the bridge leaf or substructure of the bascule bridge. Collision forces with support piers and other elements of the substructure are defined in section 4.6 of NEN-EN 1991-1-7+C1+A1. For a collision between a vessel and the bridge leaf, the collision must be decomposed in a force $F_{d,x}$, which acts in the sailing direction, perpendicular onto the bridge leaf, accompanied with a friction force F_R . Also a transverse force $F_{d,y}$ must be taken into account. The friction force is given by:

$$F_R = \mu F_{d,y} \quad (C.9)$$

where μ is equal to 0.4(NEN-EN 1991-1-7:2006+A1:2014+NB:2019). For collisions with the substructure, the force should be applied at a height of 1.5 meters above the relevant water level of the fairway. For the contact area holds:

- $b = b_{pier}$ and $h = 0.5$ meters for a frontal collision.
- $b = 0.5$ meters and $h = 1.0$ meters for a sideways collision.

For collision with the bridge leaf, force of 1 MN should be taken into account. Which has a contact area of 0.25 (h) x 3.0 (b) meters.

Lastly, an emergency stop of the operating mechanism of the bridge leaf, can lead to substantial forces in the bridge deck. This corresponds to stop category 0 or 1. Section 2.3.9 of the VOB describes the time limits for stopping movement of the bridge leaf in case of an emergency stop.

C.7. Pedestrian and cycle paths

C.7.1. Traffic loading

Vertical loading

Separate traffic models are used for loading on footpaths, cycle paths and dedicated pedestrian and cyclebridges which are not accessible for regular vehicle traffic. For vertical loading, three load models can be distinguished. Firstly, a load model for a uniformly distributed load. For traffic bridges that have foot and cycle paths, a uniformly distributed load $q_{fk} = 5 \text{ kN/m}^2$, should be applied on the accessible surfaces of the foot and cycle paths, as can be seen in figure C.11.

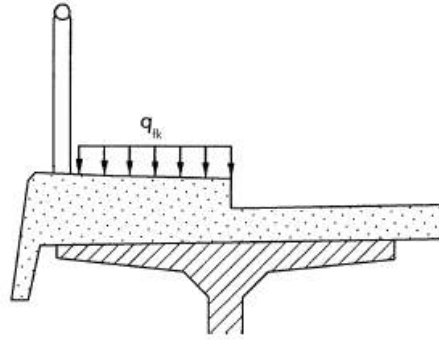


Figure C.11: Uniformly distributed load on sidewalk.(NEN-EN1991-2:2003+C1:2015+NB:2019)

For dedicated pedestrian and cyclebridges, a vertical uniformly distributed load of:

$$q_{fk} = 2.0 + \frac{120}{L + 30} \quad (\text{C.10})$$

should be applied on the unfavourable parts of the bridge. For which holds that $2.5 \text{ kN/m}^2 \leq q_{f,k} \leq 5.0 \text{ kN/m}^2$. In this equation, L is equal to the smallest continuous part of the influence line, with the same sign(NEN-EN 1991-2:2003+C1:2015+NB:2019). This load should only be applied in case the crowd loading described in traffic load model 4 is not required for the project.

Secondly, a vertical concentrated load of $Q_{fvd} = 7 \text{ kN}$ should be applied on the unfavourable part of the structure. This force has a contact area of 0.1 x 0.1 meters.

If service vehicles can use the bridge, a force of Q_{serv} must be taken into account, which substitutes Q_{fvd} . This force consists of two axles with a wheelbase of 3 meters. The characteristic value of every axle load is 25 kN. Each axle has two wheels spaced at 1.75 meters apart and each wheel has a contact area of 0.25 x 0.25 meters. Different types of service vehicles could be described in a project's program of requirements.

Horizontal loading

Only for separate pedestrian and cyclebridges, a horizontal force Q_{flk} should be taken into account. This force is the maximum of the following two values:

- 10% of the total load taking into account the uniformly distributed load $q_{f,k}$.
- 30% of the total weight of the service vehicle, if applicable.

This force acts on the central axis of the bridge, at the top of the bridge deck layer.

C.7.2. Accidental loading

An accidental loading case should be taken into account in the form of an incidental vehicle, which is represented by the tandem loads shown in figure C.12.

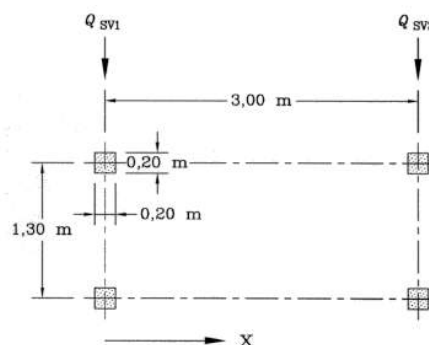


Figure C.12: Accidental vehicle on a pedestrianbridge.(NEN-EN1991-2:2003+C1:2015+NB:2019)

where:

$$Q_{sv1} = 80kN$$

$$Q_{sv2} = 40kN$$

This vehicle has a wheelbase of 1.3 meters and two axles spaced 3.0 meters apart. The contact area of the forces is 0.2 x 0.2 meters.

C.7.3. Dynamic loading

The harmonic load model for regular pedestrian traffic is described by the following equation:

$$p(t) = P \cdot \cos(2 \cdot \pi \cdot f_s \cdot t) \cdot n' \cdot \psi \quad (C.11)$$

where:

$p(t)$ is the uniformly distributed harmonic loading, expressed in N/m^2 .

P is the force exerted by a single pedestrian in vertical, longitudinal or lateral direction.

f_s is the stepfrequency, assumed to be equal to the eigenfrequency of the bridge that is considered.

t is the time unit.

n' is the equivalent amount of pedestrians on the loadable area.

ψ is a reduction coefficient representing the probability that the stepfrequency approaches the critical area around the eigenfrequency.

The force components of the force P , exerted by a pedestrian are shown in the next table.

Table C.5: Table NB.I.1(NEN-EN 1991-2:2003+C1:2015+NB:2019)

Verticaal	Longitudinaal	Zijdelings
280 N	140 N	35 N

Values for the reduction coefficient ψ can be deducted from figure NB.I.1.

Determining the value for n' is done using table NB.I.1, in which equations are given for n' . For TC3, n' is calculated using:

$$n' = \frac{10.8 \cdot \sqrt{\epsilon \cdot n}}{S} \quad (C.12)$$

where:

ϵ is the logarithmic decline of structural dampening, to be deducted from table F.2 in NEN-EN 1991-1-4+A1+C2:2011.

n is the amount of pedestrians on the loaded area S . Calculated with $n = S \cdot d$.

S is the loaded area.

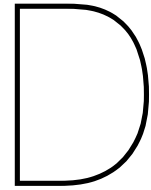
d is the amount of pedestrians per square meter.

The load model for joggers is constructed similarly, it assumes a single load which moves over the bridge deck. This loading is calculated with:

$$p(t, v) = P \cdot \cos(2 \cdot \pi \cdot f \cdot t) \cdot n' \cdot \psi \quad (C.13)$$

The force P exerted by a single jogger consists of only a vertical component, which is equal to 1250 N. The value for n' depends on the joggersclass and length of the bridge span.

For further rules of application, section 5.7 and annex NB.I of NEN-EN 1991-2:2003+C1:2015+NB:2019 can be consulted.



Interview Documentation

The following questions were asked during an interview and talks with engineers. Some additional technical questions about structural design, were asked regarding the person's specific field of expertise.

Could you introduce yourself?

What is your function within the firm? And within projects that you currently work on?

Which steps do you roughly undertake in the design process of a movable bridge/bridge leaf/basculer chamber?

How would you describe your knowledge on parametric design? And at what level is it prevalent within the firm?

How would you describe your knowledge on artificial intelligence and machine learning?

Is it already being used within the firm, and if so, in which applications?

What software do you use in the design process?

Do you think that this tool would be useful for a structural engineer in the firm's design process? What is important to take into account?

What parameters would be desirable as input for the tool?

What type of information and output would be useful to obtain from the tool?

What rules and requirements are applicable to a basculer bridge?

How have design rules in for example the Eurocode, changed over the last few decades?

How does the steel bridge leaf influence the design of the basculer chamber? Is there a standard design that you opt to reach?

Could you elaborate more on the design of the connection between the bridge leaf and the basculer chamber, at the rotational axis?

What does a typical operating system look like? And how is it fitted into the basculer chamber?

What are functional requirements to take into account in the design of a basculer chamber?



Bridge Database

E.1. Data set

The following figures show the data that was used as input for the algorithm. Table E.1 and E.2 show the geometrical properties for the bridges. The figure in section D.2 shows the structural properties that were used as input.

Brug ID	Name	Column1	L ₁ [m]	W ₁ [m]	L ₂ [m]	L ₃ [m]	L ₄ [m]	L ₅ [m]	L ₆ [m]	L ₇ [m]	L ₈ [m]	b _{main} [m]	n _{main} [-]	n _{cross} [-]	n _{rib} [-]	t _{w1} [m]	t _{w2} [m]	t _{w3} [m]
BRU0050	Latjesbrug		12.71	24.12	0.471	2.481	2.311	5.515	2	0	2.41	4.3	5	6	60	0.35	0.85	0.8
BRU0101	Nieuwe Amstelbrug		7	16	1.275	4.078	1.35	4.269	1.35	0	1.977	2.84	6	3	23	0.4	0.4	0.4
BRU0149	Bullebak		5.16	12.09	0.485	2.242	1.53	3.92	1.15	0	1.628	3.266	4	3	13	0.65	0.65	1.05
BRU0151	Willemsbrug		13.78	19.6	1.05	2.665	1.041	3.981	1.5	0.25	1.469	4.08	6	5	27	2.275	0.25	0.75
BRU0155	Kattenslootbrug		11.88	26.4	1.223	2.868	2.788	3.794	1.6	0.606	1.548	3.055	8	5	34	0.52	0.25	0.75
BRU0171			12.3	16	0.88	2.33	2.33	4.035	1.3	0.23	1.61	4.135	4	5	19	0.65	0.25	0.65
BRU0173	Wiegbrug		12.5	22.4	0.48	2.3	2.16	6.04	2.2	0.26	3.09	5.435	4	4	29	0.625	0.9	0.72
BRU0199	Overtoomse sluis		12.8	25.3	1.04	2.986	2.07	4.8125	1.5	0	1.78	3.6	6	5	27	0.85	0.5	0.6
BRU0238	M.S. Vaz Diasbrug		10.327	30.176	1.21	3.72	3.53	3.9	2.25	0.45	1.52	3.675	8	4	42	1	0.5	0.6
BRU0239	Hortusbrug		12.2	31.709	1.16	2.522	2.328	4.125	1.693	0.4	1.33	3.675	8	4	66	0.55	0.55	0.75
BRU0246	Hogesluis		4.25	16.2	0.876	2.628	0.876	2.8	1	0	1.034	2.87	6	3	29		0.68	0.6375
BRU0266	Kinkerbrug		12.245	20	2.33	3.028	2.64	3.785	1.725	0.472	1.851	3.07	6	4	25	0.58	0.5	0.63
BRU0272	Mariniersbrug		24.4	16.7	n.a.	n.a.	n.a.	n.a.	n.a.	n.a.	n.a.	12.04	2	7	30	2.5	1.17	0.972
BRU0274	Kattenburgerbrug		15.4	29.402	0.35	3.191	3.107	5.743	2.25	0.277	2.633	3.8	7	7	85	0.9	0.9	1.3
BRU0314	Westerdoks sluis		14.13	22.6	0.917	3.045	3.045	4.93	2	0.355	1.89	4.125	5	5	24	0.4	0.5	1.4
BRU0318	Zoutkeetsbrug		12.5	17.4	0.388	2.173	1.975	5.66	1.95	0	2.18	4.33	4	6	44	0.6	0.95	1.2
BRU0324	Beltbrug		15.129	23.16	1.05	2.893	2.474	4.673	1.945	0.134	1.834	3.6	6	5	22	0.5	0.6	0.6
BRU0345			12.52	16.4	0.388	2.173	1.975	5.66	1.95	0	2.18	4.33	4	6	40	0.525	0.55	0.7
BRU0346	Westerkeersluis		14.838	27.1	0.737	2.217	3.292	5.218	1.374	0	1.846	4.14	6	5	35	0.38	0.5	1.3
BRU0349	Cor Thesingbrug		12.52	16.4	0.388	2.173	1.975	5.66	1.95	0	2.18	4.33	4	6	40	0.525	0.55	0.7
BRU0350	Torontobrug		5.975	35.6	0.143	1.786	1.786	2.218	0.75	0	1.34	2.685	13	3	82	0.6	0.6	0.6
BRU0356	NSM-brug		13.075	7.51	0.44	3.035	2.82	4.475	2.1	0.26	2.1	5.5	2	6	10	0.5	0.6	0.525
BRU0357	Gerben Wagenaarbrug		15.15	20.68	0.855	3.887	4.11	5.301	2.4	0.377	2.05	4.32	4	7	54	0.65	0.7	1.2
BRU0382			15.129	23.16	1.05	2.893	2.474	4.673	1.945	0.134	1.834	3.6	6	5	22	0.5	0.6	0.6
BRU0485	Dees Postmabrug		20.614	28.58	0.525	4.44	3.75	7.455	2.175	0	2.7	4.08	7	9	73	0.8	1.05	0.8
BRU0487	Kortjewantsbrug		12.8	27.76	1	2.4	2.13	6.07	2.6	0.65	2.386	4.15	7	6	72	0.7	0.7	0.85
BRU0491	Meeuwenpleinbrug		15.918	20.88	0.665	4.41	4.313	5.112	2.4	0	2.106	4.32	4	7	44	0.65	0.7	1.2
BRU1787	Kadoelenbrug		14.632	5.8	n.a.	n.a.	n.a.	n.a.	0.8	n.a.	n.a.	5.3	2	12	0	0.4	0.4	0.4
BRU1788	Theo Fransmanbrug		15.6	5.9	n.a.	n.a.	n.a.	n.a.	1.1	n.a.	n.a.	5.7	2	7	0	n.a.	n.a.	n.a.
BRU1939	Mr. J.J. van der Veldebrug		9.5	5	n.a.	n.a.	n.a.	n.a.	0.5	n.a.	n.a.	5.65	2	15	0	n.a.	n.a.	n.a.
BRU2023			6.89	20.5	1.041	2.934	2.76	2.35	1.56	0.11	2.15	11.1	2	3	32	0.5	0.73	0.7
BRU2038	Steigereilandbrug		9.66	15.248	1.62	3.532	3.411	2.011	1.62	0	1.982	6.88	2	4	21	0.5	0.75	0.5
BRU2190	Solitudobrug		10.785	9.326	n.a.	n.a.	n.a.	n.a.	10.5	n.a.	1.221	7.3	2	14	0	0.3	0.4	0.8
BRU5046	Roskambrug		8.8	12	0.93	3.82	3.82	1.7	1.2	0	0.475	4.45	3	4	16	0.35	0.65	0.35
BRU5047	De Uitkomst		13	10.2	2	6.15	6.15	0	2	0	2	6.9	2	5	15	0.5	0.5	0.6

Figure E.1: Dataset in Excel.

Brug ID	Name	Column1	t _{roof} [m]	H _{top} [mm]	W _{top} [mm]	t _{w,top} [mm]	t _{r,top} [mm]	H _{bottom} [mm]	W _{bottom} [mm]	t _{w,bottom} [mm]	t _{r,bottom} [mm]	t _{deck} [mm]
BRU0050	Latjesbrug		0.5	1070	288	19	33	1041	288	19	33	12
BRU0101	Nieuwe Amstelbrug		0.25	900.5	350	15	40	1000	350	20	40	12
BRU0149	Bullebak		0.39	690	390	20	40	864	390	20	40	8
BRU0151	Willemsbrug		0.25	802	350	12	26	1040	350	12	26	12
BRU0155	Kattenslootbrug		0.38	748	350	12	12	1013	350	12	24	12
BRU0171			0.52	780	450	15	25	1000	450	15	25	12
BRU0173	Wiegbrug		0.35	1090	400	15	40	1420	400	15	40	12
BRU0199	Overtoomsesluis		0.5	1072	300	12	36	1060	300	12	36	12
BRU0238	M.S. Vaz Diasbrug		0.4	650	300	16	31	900	300	16	31	12
BRU0239	Hortusbrug		0.35	650	300	16	31	900	300	16	31	12
BRU0246	Hogesluis		0.2125									
BRU0266	Kinkerbrug		0.42	1000	400	15	25	931	400	15	25	12
BRU0272	Mariniersbrug		0.38	n.a.	n.a.	n.a.	n.a.	n.a.	n.a.	n.a.	n.a.	n.a.
BRU0274	Kattenburgerbrug		0.57	900	300	18.5	35	1200	310	19	39	12
BRU0314	Westerdoksuis		0.45	900	300	19	36	1130	300	19	36	12
BRU0318	Zoutkeetsbrug		0.45	638	297	14	26	1000	297	14	26	12
BRU0324	Beltbrug		0.4	709	350	12	26	1100	350	12	26	10
BRU0345			0.5	638	297	14	26	1000	297	14	26	12
BRU0346	Westerkeersluis		0.4	700	300	18	34	1000	300	18	34	12
BRU0349	Cor Thesingbrug		0.5	638	297	14	26	1000	297	14	26	12
BRU0350	Torontobrug		0.5	700	310	16	39	1000	310	35	50	12
BRU0356	NSM-brug		0.525	1000	500	20	20	1160	500	20	20	10
BRU0357	Gerben Wagenaarbrug		0.53	1000	300	16	20	1200	300	16	20	12
BRU0382			0.4	709	350	12	26	1100	350	12	26	12
BRU0485	Dees Postmabrug		0.75	1430	300	16	26	1400	310	19	39	12
BRU0487	Kortjewantsbrug		0.5	640	300	13.5	26	1000	310	19	39	12
BRU0491	Meeuwenpleinbrug		0.53	1078	300	16	50	1200	310	19	39	12
BRU1787	Kadoelenbrug		0.45	800	500	12	15	n.a.	n.a.	n.a.	n.a.	12
BRU1788	Theo Fransmanbrug		n.a.	n.a.	n.a.	n.a.	n.a.	n.a.	n.a.	n.a.	n.a.	n.a.
BRU1939	Mr. J.J. van der Veldebrug		n.a.	n.a.	n.a.	n.a.	n.a.	n.a.	n.a.	n.a.	n.a.	12
BRU2023			0.84	1070	300	12	30	1000	300	40	30	10
BRU2038	Steigereilandbrug		0.4	972	400	12	40	1200	400	12	40	10
BRU2190	Solitudobrug		0.4	n.a.	n.a.	n.a.	n.a.	n.a.	n.a.	n.a.	n.a.	12
BRU5046	Roskambrug		0.45	792	298	16	30	920	298	16	30	12
BRU5047	De Uitkomst		0.6	1100	400	18	30	800	400	18	30	12

Figure E.2: Dataset in Excel.



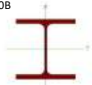

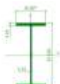













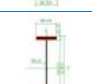

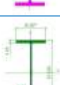

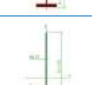



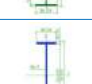

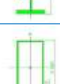
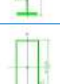
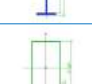
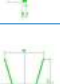
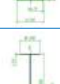
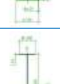
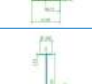

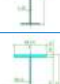
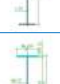
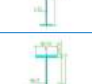

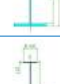
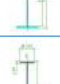
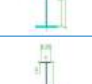

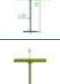

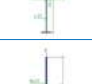

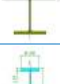

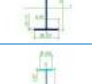

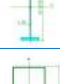
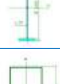
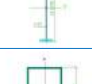
Brug ID	Name	Column1	$I_{zz,top}$ [$\times 10^4$ mm ⁴]	$I_{zz,cross}$ [$\times 10^4$ mm ⁴]	$I_{zz,rib}$ [$\times 10^4$ mm ⁴]
BRU0050	Latjesbrug		671430	329300	426.52
BRU0101	Nieuwe Amstelbrug		219980	85271	3156.2
BRU0149	Bullebak		367800	18417	5873.2
BRU0151	Willemsbrug		316280	164970	3015.2
BRU0155	Kattenslootbrug		151720	102960	2662.3
BRU0171			369380	128280	3015.2
BRU0173	Wiegbrug		1011200	267730	5598.3
BRU0199	Overtoomesluis		679810	23130	3143.5
BRU0238	M.S. Vaz Diasbrug		210600	95292	3015.2
BRU0239	Hortusbrug		210600	10640	3015.2
BRU0246	Hogesluis				
BRU0266	Kinkerbrug		689760	264390	6252.1
BRU0272	Mariniersbrug			668810	11447
BRU0274	Kattenburgerbrug		494100	121500	307.2
BRU0314	Westerdoksuis		494100	5696	7845.1
BRU0318	Zoutkeetsbrug		169240	41562	307.2
BRU0324	Beltbrug		240710	153660	3150
BRU0345			169240	41984	307.2
BRU0346	Westerkeersluis		256900	191250	3226.1
BRU0349	Cor Thesingbrug		169240	41984	307.2
BRU0350	Torontobrug		297710	151710	307.2
BRU0356	NSM-brug		775180	266460	6001.1
BRU0357	Gerben Wagenaarbrug		356260	283060	307.2
BRU0382			240710	153660	3150
BRU0423	Berlagebrug				
BRU0485	Dees Postmabrug		1096700	842820	307.2
BRU0487	Kortjewantsbrug		175200	27303	307.2
BRU0491	Meeuwenpleinbrug		923210	400040	307.2
BRU1787	Kadoelenbrug		322420	9877	
BRU1788	Theo Fransmanbrug				
BRU1939	Mr. J.J. van der Veldebrug			1562.6	
BRU1979	Bongerdbrug				
BRU2023			589890	231900	6990.5
BRU2038	Steigereilandbrug		236650	178440	7197.5
BRU2190	Solitudobrug				13087
BRU5046	Roskambrug		313640	108320	3880.6
BRU5047	De Uitkomst		855850	128030	4414.3















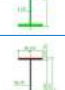
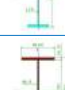


Figure E.3: Dataset in Excel.

E.2. Cross section properties

This table shows the properties of the structural elements of bridges in the data set.

Bridge	Name	Main beam top	Main beam bottom	Crossbeam	Rib
BRU0050	Latjesbrug			HE700M 	
BRU0101	Nieuwe Amstelbrug				
BRU0149	Bullebak				
BRU0151	Willemsbrug				
BRU0155	Kattenslootbrug				
BRU0171					
BRU0173	Wiegbrug				
BRU0199	Overtoomsesluis			IPE400 	
BRU0238	M.S. Vaz Diasbrug	HE650B 	HE650B 		
BRU0239	Hortusbrug	HE650B 	HE650B 	HE200M 	
BRU0246	Hogesluis	No information available	No information available	No information available	No information available
BRU0266	Kinkerbrug				
BRU0272	Mariniersbrug	Not applicable	Not applicable		
BRU0274	Kattenburgerbrug	HE900B 			

BRU0314	Westerdoks-luis	HE900B			HE200B		
BRU0318	Zoutkeetsbrug						
BRU0324	Beltbrug						
BRU0345							
BRU0346	Westerkeersluis	HE700B					
BRU0349	Cor Thesingbrug						
BRU0350	Torontobrug						
BRU0356	NSM-brug						
BRU0357	Gerben Wagenaarbrug						
BRU0382							
BRU0485	Dees Postmabrug						
BRU0487	Kortjewantsbrug	HE650A					
BRU0491	Meeuwenpleinbrug						
BRU1787	Kadoelenbrug						Not applicable

BRU1788	Theo Fransmanbrug	No information available	No information available	No information available	No information available
BRU1939	Mr. J.J. van der Veldebrug	Not applicable	Not applicable		Not applicable
BRU2023					
BRU2038	Steigereilandbrug				
BRU2190	Solitudobrug	Not applicable	Not applicable	Not applicable	
BRU5046	Roskambrug				
BRU5047	De Uitkomst				



Validation

F.1. Cross-Validation Test sets

Test Set 1	
BRU0149	Bullebak
BRU0199	Overtoomsesluis
BRU0324	Beltbrug
BRU5047	De Uitkomst
BRU1788	Theo Fransmanbrug
BRU0272	Mariniersbrug
BRU2023	

Test Set 2	
BRU0382	
BRU5046	Roskambrug
BRU0239	Hortusbrug
BRU0345	
BRU0349	Cor Thesingbrug
BRU0356	NSM-Brug
BRU0266	Kinkerbrug

Test Set 3	
BRU0246	Hogesluis
BRU1939	Mr. J.J. van der Veldebrug
BRU2190	Solitudobrug
BRU0491	Meeuwenpleinbrug
BRU0101	Nieuwe Amstelbrug
BRU0318	Zoutkeetsbrug
BRU0346	Westerkeersluis

Test Set 4	
BRU0357	Gerben Wagenaarbrug
BRU0274	Kattenburgerbrug
BRU0314	Westerdoksuis
BRU0485	Dees Postmabrug
BRU0050	Latjesbrug
BRU2038	Steigereilandbrug
BRU0151	Willemsbrug

Test Set 5	
BRU0171	
BRU0173	Wiegbrug
BRU0155	Kattenslootbrug
BRU1787	Kadoelenbrug
BRU0350	Torontobrug
BRU0238	M.S. Vaz Diasbrug
BRU0497	Kortjewantsbrug

Figure F.1: Test sets.

F.2. Cross-Validation Results

F.2.1. Fold 1

BRU0149	Parameter	Real value	Prediction	Norm. real value	Norm. prediction	$(y-\hat{y})^2$	MSE
				y	\hat{y}		
	L ₂ [m]	0.485	0.145022	0.156379	0.000925	0.024166	0.347599
	L ₃ [m]	2.242	0.743477	0.104491	-0.238892	0.117912	
	L ₄ [m]	1.53	0.405298	0.124005	-0.089250	0.045477	
	L ₅ [m]	3.92	0.677038	0.525822	0.090817	0.189229	
	L ₇ [m]	0	0.011334	0.000000	0.017437	0.000304	
	L ₈ [m]	1.628	0.513717	0.440918	0.014806	0.181571	
	b _{main} [m]	3.266	3.037536	0.062106	0.037684	0.000596	
	n _{main} [-]	4	2.523706	0.181818	0.047610	0.018012	
	n _{cross} [-]	3	3.575218	0.000000	0.047935	0.002298	
	n _{rib} [-]	13	6.155197	0.152941	0.072414	0.006485	
	t _{w1} [m]	0.65	0.221566	0.159091	-0.035652	0.037925	
	t _{w2} [m]	0.65	0.227549	0.434783	-0.024403	0.210852	
	t _{w3} [m]	1.05	0.331202	0.666667	-0.017903	0.468635	
	t _{roof} [m]	0.39	0.212308	0.282869	-0.000306	0.080188	
	I _{zz,top} [x10 ⁴ mm ⁴]	367800	69294.42914	0.228661	-0.087225	0.099784	
	I _{zz,cross} [x10 ⁴ mm ⁴]	18417	30111.74195	0.020035	0.033936	0.000193	
	I _{zz,rib} [x10 ⁴ mm ⁴]	5873.2	406.268152	0.435531	0.007752	0.182995	
	H _{bottom} [mm]	864	150.583608	0.103226	-1.047446	1.324045	
	W _{bottom} [mm]	390	54.923005	0.481132	-1.099420	2.498144	
	t _{w,bottom} [mm]	20	2.828255	0.285714	-0.327562	0.376108	
	t _{f,bottom} [mm]	40	4.066727	0.666667	-0.531109	1.434667	

BRU0199	Parameter	Real value	Prediction	Norm. real value	Norm. prediction	$(y-\hat{y})^2$	MSE
				y	\hat{y}		
	L ₂ [m]	1.04	0.839658	0.410151	0.318545	0.008392	0.020862
	L ₃ [m]	2.986	3.09026	0.274977	0.298868	0.000571	
	L ₄ [m]	2.07	2.806476	0.226394	0.366036	0.019500	
	L ₅ [m]	4.8125	4.872833	0.645540	0.653633	0.000065	
	L ₇ [m]	0	0.16168	0.000000	0.248738	0.061871	
	L ₈ [m]	1.78	2.02714	0.499044	0.593553	0.008932	
	b _{main} [m]	3.6	4.415304	0.097809	0.184960	0.007595	
	n _{main} [-]	6	5.439457	0.363636	0.312678	0.002597	
	n _{cross} [-]	5	5.777311	0.166667	0.231443	0.004196	
	n _{rib} [-]	27	41.811381	0.317647	0.491899	0.030364	
	t _{w1} [m]	0.85	0.566008	0.250000	0.120913	0.016664	
	t _{w2} [m]	0.5	0.656102	0.271739	0.441415	0.028790	
	t _{w3} [m]	0.6	0.83674	0.238095	0.463562	0.050835	
	t _{roof} [m]	0.5	0.466794	0.458167	0.405249	0.002800	
	I _{zz,top} [x10 ⁴ mm ⁴]	679810	379664.0023	0.558837	0.241216	0.100883	
	I _{zz,cross} [x10 ⁴ mm ⁴]	23130	138439.4988	0.025637	0.162705	0.018788	
	I _{zz,rib} [x10 ⁴ mm ⁴]	3143.5	2520.650337	0.221936	0.173199	0.002375	
	H _{bottom} [mm]	1060	1092.417328	0.419355	0.471641	0.002734	
	W _{bottom} [mm]	300	338.08761	0.056604	0.236262	0.032277	
	t _{w,bottom} [mm]	12	16.539257	0.000000	0.162116	0.026282	
	t _{f,bottom} [mm]	36	32.769262	0.533333	0.425642	0.011597	

BRU0324	Parameter	Real value	Prediction	Norm. real value	Norm. prediction	$(y-\hat{y})^2$	MSE
				y	\hat{y}		
	L ₂ [m]	1.05	0.905512	0.414723	0.348657	0.004365	0.010917
	L ₃ [m]	2.893	3.209366	0.253666	0.326161	0.005255	
	L ₄ [m]	2.474	2.956726	0.302996	0.394525	0.008378	
	L ₅ [m]	4.673	5.080868	0.626828	0.681538	0.002993	
	L ₇ [m]	0.134	0.197618	0.206154	0.304028	0.009579	
	L ₈ [m]	1.834	2.107223	0.519694	0.624177	0.010917	

	b_{main} [m]	3.6	4.553724	0.097809	0.199757	0.010393
	n_{main} [-]	6	5.718721	0.363636	0.338066	0.000654
	n_{cross} [-]	5	6.200701	0.166667	0.266725	0.010012
	n_{rib} [-]	22	45.953862	0.258824	0.540634	0.079417
	t_{w1} [m]	0.5	0.605624	0.090909	0.138920	0.002305
	t_{w2} [m]	0.6	0.687453	0.380435	0.475492	0.009036
	t_{w3} [m]	0.6	0.88191	0.238095	0.506581	0.072085
	t_{roof} [m]	0.4	0.479186	0.298805	0.424998	0.015925
	I_{zz,top} [x10⁴ mm⁴]	240710	430476.3563	0.094171	0.294987	0.040327
	I_{zz,ross} [x10⁴ mm⁴]	153660	157907.9698	0.180798	0.185847	0.000025
	I_{zz,rib} [x10⁴ mm⁴]	3150	2921.066058	0.222445	0.204531	0.000321
	H_{bottom} [mm]	1100	1110.021021	0.483871	0.500034	0.000261
	W_{bottom} [mm]	350	344.91716	0.292453	0.268477	0.000575
	t_{w,bottom} [mm]	12	17.054297	0.000000	0.180511	0.032584
	t_{f,bottom} [mm]	26	33.898208	0.200000	0.463274	0.069313
						0.018320

BRU5047	Parameter	Real value	Prediction	Norm. real value y	Norm. prediction ŷ	(y-ŷ) ²	MSE
	L₂ [m]	2	0.465509	0.849108	0.147466	0.492301	
	L₃ [m]	6.15	2.129438	1.000000	0.078698	0.848797	
	L₄ [m]	6.15	1.673571	1.000000	0.151227	0.720416	
	L₅ [m]	0	3.259501	0.000000	0.437223	0.191164	
	L₇ [m]	0	0.037721	0.000000	0.058032	0.003368	
	L₈ [m]	2	1.461464	0.583174	0.377233	0.042412	
	b_{main} [m]	6.9	3.631976	0.450561	0.101227	0.122035	
	n_{main} [-]	2	3.871732	0.000000	0.170157	0.028954	
	n_{cross} [-]	5	4.10842	0.166667	0.092368	0.005520	
	n_{rib} [-]	15	19.493183	0.176471	0.229332	0.002794	
	t_{w1} [m]	0.5	0.401517	0.090909	0.046144	0.002004	
	t_{w2} [m]	0.5	0.445257	0.271739	0.212236	0.003541	
	t_{w3} [m]	0.6	0.544304	0.238095	0.185051	0.002814	
	t_{roof} [m]	0.6	0.383293	0.617530	0.272180	0.119266	
	I_{zz,top} [x10⁴ mm⁴]	855850	157123.7812	0.745127	0.005718	0.546725	
	I_{zz,ross} [x10⁴ mm⁴]	128030	64027.40656	0.150331	0.074252	0.005788	
	I_{zz,rib} [x10⁴ mm⁴]	4414.3	981.626345	0.321374	0.052773	0.072147	
	H_{bottom} [mm]	800	872.490957	0.000000	0.116921	0.013670	
	W_{bottom} [mm]	400	263.900789	0.528302	-0.113676	0.412135	
	t_{w,bottom} [mm]	18	12.180325	0.214286	0.006440	0.043200	
	t_{f,bottom} [mm]	30	22.021879	0.333333	0.067396	0.070723	0.178561

BRU1788	Parameter	Real value	Prediction	Norm. real value y	Norm. prediction ŷ	(y-ŷ) ²	MSE
	L₂ [m]		0.433452		0.132808		
	L₃ [m]		2.015263		0.052535		
	L₄ [m]		1.55129		0.128041		
	L₅ [m]		3.060071		0.410472		
	L₇ [m]		0.032938		0.050674		
	L₈ [m]		1.398407		0.353119		
	b_{main} [m]	5.7	3.562394	0.322288	0.093789	0.052212	
	n_{main} [-]	2	3.727563	0.000000	0.157051	0.024665	
	n_{cross} [-]	7	4.021739	0.333333	0.085145	0.061597	
	n_{rib} [-]	0	17.912878	0.000000	0.210740	0.044411	
	t_{w1} [m]		0.385924		0.039056		
	t_{w2} [m]		0.425424		0.190678		
	t_{w3} [m]		0.518071		0.160068		
	t_{roof} [m]		0.372572		0.255095		

$I_{zz,top}$ [x10 ⁴ mm ⁴]	144067.0791	-0.008099	0.045721
$I_{zz,cross}$ [x10 ⁴ mm ⁴]	59904.2174	0.069350	
$I_{zz,rib}$ [x10 ⁴ mm ⁴]	898.22323	0.046247	
H_{bottom} [mm]	828.083459	0.045296	
W_{bottom} [mm]	249.670582	-0.180799	
$t_{w,bottom}$ [mm]	11.444948	-0.019823	
$t_{f,bottom}$ [mm]	20.465602	0.015520	

BRU0272	Parameter	Real value	Prediction	Norm. real value y	Norm. prediction \hat{y}	$(y-\hat{y})^2$	MSE
	L_2 [m]		1.043339		0.411678		0.240840
	L_3 [m]		3.422326		0.374960		
	L_4 [m]		3.22902		0.446155		
	L_5 [m]		5.499215		0.737655		
	L_7 [m]		0.277501		0.426925		
	L_8 [m]		2.273377		0.687716		
	b_{main} [m]	12.04	4.814814	1.000000	0.227666	0.596500	
	n_{main} [-]	2	6.287872	0.000000	0.389807	0.151949	
	n_{cross} [-]	7	7.139135	0.333333	0.344928	0.000134	
	n_{rib} [-]	30	54.133894	0.352941	0.636869	0.080615	
	t_{w1} [m]	2.5	0.698608	1.000000	0.181185	0.670457	
	t_{w2} [m]	1.17	0.746439	1.000000	0.539608	0.211961	
	t_{w3} [m]	0.972	0.961531	0.592381	0.582410	0.000099	
	t_{roof} [m]	0.38	0.504516	0.266932	0.465364	0.039375	
	$I_{zz,top}$ [x10 ⁴ mm ⁴]		535827.1425		0.406471		
	$I_{zz,cross}$ [x10 ⁴ mm ⁴]	668810	205678.7345	0.793155	0.242632	0.303075	
	$I_{zz,rib}$ [x10 ⁴ mm ⁴]	11447	3840.744913	0.871672	0.276495	0.354237	
	H_{bottom} [mm]		1141.372576		0.550601		
	W_{bottom} [mm]		356.966112		0.325312		
	$t_{w,bottom}$ [mm]		18.041227		0.215758		
	$t_{f,bottom}$ [mm]		35.850589		0.528353		

BRU0233	Parameter	Real value	Prediction	Norm. real value y	Norm. prediction \hat{y}	$(y-\hat{y})^2$	MSE
	L_2 [m]	1.041	0.499694	0.410608	0.163097	0.061262	0.140397
	L_3 [m]	2.934	2.252867	0.263061	0.106981	0.024361	
	L_4 [m]	2.76	1.804708	0.357224	0.176092	0.032809	
	L_5 [m]	2.35	3.423171	0.315225	0.459178	0.020723	
	L_7 [m]	0.11	0.044694	0.169231	0.068760	0.010094	
	L_8 [m]	2.15	1.507181	0.640535	0.394715	0.060427	
	b_{main} [m]	11.1	3.7256	0.899519	0.111235	0.621392	
	n_{main} [-]	2	4.040752	0.000000	0.185523	0.034419	
	n_{cross} [-]	3	4.225715	0.000000	0.102143	0.010433	
	n_{rib} [-]	32	21.221213	0.376471	0.249661	0.016081	
	t_{w1} [m]	0.5	0.414652	0.090909	0.052115	0.001505	
	t_{w2} [m]	0.73	0.466774	0.521739	0.235624	0.081862	
	t_{w3} [m]	0.7	0.579895	0.333333	0.218948	0.013084	
	t_{roof} [m]	0.84	0.392936	1.000000	0.287547	0.507589	
	$I_{zz,top}$ [x10 ⁴ mm ⁴]	589890	174266.2807	0.463682	0.023859	0.193444	
	$I_{zz,cross}$ [x10 ⁴ mm ⁴]	231900	68166.04676	0.273801	0.079171	0.037881	
	$I_{zz,rib}$ [x10 ⁴ mm ⁴]	6990.5	1088.64311	0.522958	0.061147	0.213270	
	H_{bottom} [mm]	1000	914.392433	0.322581	0.184504	0.019065	
	W_{bottom} [mm]	300	278.255579	0.056604	-0.045964	0.010520	
	$t_{w,bottom}$ [mm]	40	12.932147	1.000000	0.033291	0.934526	
	$t_{f,bottom}$ [mm]	30	23.737011	0.333333	0.124567	0.043583	

F.2.2. Fold 2

BRU0382	Parameter	Real value	Prediction	Norm. real value	Norm. prediction	$(y-\hat{y})^2$	MSE
				y	\hat{y}		
	L_2 [m]	1.05	0.954286	0.414723	0.370958	0.001915	
	L_3 [m]	2.893	3.250023	0.253666	0.335477	0.006693	
	L_4 [m]	2.474	2.878158	0.302996	0.379628	0.005872	
	L_5 [m]	4.673	4.916218	0.626828	0.659452	0.001064	
	L_7 [m]	0.134	0.142095	0.206154	0.218608	0.000155	
	L_8 [m]	1.834	2.090274	0.519694	0.617696	0.009604	
	b_{main} [m]	3.6	5.094776	0.097809	0.257592	0.025531	
	n_{main} [-]	6	5.629951	0.363636	0.329996	0.001132	
	n_{cross} [-]	5	6.514685	0.166667	0.292890	0.015932	
	n_{rib} [-]	22	43.107113	0.258824	0.507143	0.061662	
	t_{w1} [m]	0.5	0.696979	0.090909	0.180445	0.008017	
	t_{w2} [m]	0.6	0.724967	0.380435	0.516268	0.018451	
	t_{w3} [m]	0.6	0.941242	0.238095	0.563088	0.105620	
	t_{roof} [m]	0.4	0.502046	0.298805	0.461428	0.026446	
	$I_{zz,top}$ [x10 ⁴ mm ⁴]	240710	485388.7	0.094171	0.353096	0.067042	
	$I_{zz,cross}$ [x10 ⁴ mm ⁴]	153660	178795.55	0.180798	0.210676	0.000893	
	$I_{zz,rib}$ [x10 ⁴ mm ⁴]	3150	3852.3405	0.222445	0.277402	0.003020	
	H_{bottom} [mm]	1100	1117.2992	0.483871	0.511773	0.000779	
	W_{bottom} [mm]	350	347.91755	0.292453	0.282630	0.000096	
	$t_{w,bottom}$ [mm]	12	18.341466	0.000000	0.226481	0.051294	
	$t_{f,bottom}$ [mm]	26	35.987913	0.200000	0.532930	0.110843	0.024860

BRU5046	Parameter	Real value	Prediction	Norm. real value	Norm. prediction	$(y-\hat{y})^2$	MSE
				y	\hat{y}		
	L_2 [m]	0.93	0.172824	0.359854	0.013637	0.119866	
	L_3 [m]	3.82	0.977551	0.466086	-0.185254	0.424244	
	L_4 [m]	3.82	0.644611	0.558210	-0.043874	0.362505	
	L_5 [m]	1.7	0.720236	0.228035	0.096611	0.017272	
	L_7 [m]	0	0.005167	0.000000	0.007949	0.000063	
	L_8 [m]	0.475	0.815397	0.000000	0.130171	0.016944	
	b_{main} [m]	4.45	3.154973	0.188669	0.050238	0.019163	
	n_{main} [-]	3	2.61944	0.090909	0.056313	0.001197	
	n_{cross} [-]	4	3.623501	0.083333	0.051958	0.000984	
	n_{rib} [-]	16	10.017762	0.188235	0.117856	0.004953	
	t_{w1} [m]	0.35	0.243616	0.022727	-0.025629	0.002338	
	t_{w2} [m]	0.65	0.299461	0.434783	0.053762	0.145177	
	t_{w3} [m]	0.35	0.423866	0.000000	0.070349	0.004949	
	t_{roof} [m]	0.45	0.262309	0.378486	0.079377	0.089466	
	$I_{zz,top}$ [x10 ⁴ mm ⁴]	313640	79674.117	0.171348	-0.076241	0.061300	
	$I_{zz,cross}$ [x10 ⁴ mm ⁴]	108320	27033.821	0.126902	0.030278	0.009336	
	$I_{zz,rib}$ [x10 ⁴ mm ⁴]	3880.6	379.99976	0.279613	0.005696	0.075030	
	H_{bottom} [mm]	920	246.72528	0.193548	-0.892379	1.179237	
	W_{bottom} [mm]	298	86.440767	0.047170	-0.950751	0.995846	
	$t_{w,bottom}$ [mm]	16	4.178543	0.142857	-0.279338	0.178249	
	$t_{f,bottom}$ [mm]	30	6.689792	0.333333	-0.443674	0.603740	0.205327

BRU0239	Parameter	Real value	Prediction	Norm. real value	Norm. prediction	$(y-\hat{y})^2$	MSE
				y	\hat{y}		
	L_2 [m]	1.16	1.054033	0.465021	0.416567	0.002348	
	L_3 [m]	2.522	3.499144	0.168653	0.392563	0.050136	
	L_4 [m]	2.328	3.202783	0.275313	0.441180	0.027512	

	n_{cross} [-]	6	4.633759	0.250000	0.136147	0.012963	0.011361
	n_{rib} [-]	40	23.861835	0.470588	0.280727	0.036047	
	t_{w1} [m]	0.525	0.41398	0.102273	0.051809	0.002547	
	t_{w2} [m]	0.55	0.530914	0.326087	0.305341	0.000430	
	t_{w3} [m]	0.7	0.666816	0.333333	0.301730	0.000999	
	t_{roof} [m]	0.5	0.410493	0.458167	0.315527	0.020346	
	$I_{zz,top}$ [x10 ⁴ mm ⁴]	169240	230140.44	0.018540	0.082986	0.004153	
	$I_{zz,cross}$ [x10 ⁴ mm ⁴]	41984	80250.595	0.048049	0.093536	0.002069	
	$I_{zz,rib}$ [x10 ⁴ mm ⁴]	307.2	1550.9169	0.000000	0.097319	0.009471	
	H_{bottom} [mm]	1000	960.99345	0.322581	0.259667	0.003958	
	W_{bottom} [mm]	297	300.57974	0.042453	0.059338	0.000285	
	$t_{w,bottom}$ [mm]	14	13.323277	0.071429	0.047260	0.000584	
	$t_{f,bottom}$ [mm]	26	28.425942	0.200000	0.280865	0.006539	

BRU0356	Parameter	Real value	Prediction	Norm. real value	Norm. prediction	$(y-\hat{y})^2$	MSE
				y	\hat{y}		
	L_2 [m]	0.44	0.248693	0.135802	0.048328	0.007652	0.326310
	L_3 [m]	3.035	1.270129	0.286205	-0.118211	0.163552	
	L_4 [m]	2.82	0.878133	0.368601	0.000404	0.135568	
	L_5 [m]	4.475	1.151335	0.600268	0.154438	0.198765	
	L_7 [m]	0.26	0.008252	0.400000	0.012695	0.150005	
	L_8 [m]	2.1	1.010757	0.621415	0.204878	0.173503	
	b_{main} [m]	5.5	3.285043	0.300909	0.064141	0.056059	
	n_{main} [-]	2	2.881243	0.000000	0.080113	0.006418	
	n_{cross} [-]	6	3.811874	0.250000	0.067656	0.033249	
	n_{rib} [-]	10	12.711163	0.117647	0.149543	0.001017	
	t_{w1} [m]	0.5	0.283196	0.090909	-0.007638	0.009712	
	t_{w2} [m]	0.6	0.350308	0.380435	0.109030	0.073660	
	t_{w3} [m]	0.525	0.480924	0.166667	0.124690	0.001762	
	t_{roof} [m]	0.525	0.29793	0.498008	0.136143	0.130946	
	$I_{zz,top}$ [x10 ⁴ mm ⁴]	775180	106054.57	0.659760	-0.048324	0.501383	
	$I_{zz,cross}$ [x10 ⁴ mm ⁴]	266460	36430.051	0.314883	0.041447	0.074767	
	$I_{zz,rib}$ [x10 ⁴ mm ⁴]	6001.1	557.10425	0.445539	0.019555	0.181463	
	H_{bottom} [mm]	1160	387.89409	0.580645	-0.664687	1.550852	
	W_{bottom} [mm]	500	129.99863	1.000000	-0.745289	3.046035	
	$t_{w,bottom}$ [mm]	20	5.833509	0.285714	-0.220232	0.255981	
	$t_{f,bottom}$ [mm]	20	10.505672	0.000000	-0.316478	0.100158	

BRU0266	Parameter	Real value	Prediction	Norm. real value	Norm. prediction	$(y-\hat{y})^2$	MSE
				y	\hat{y}		
	L_2 [m]	2.33	0.701017	1.000000	0.255152	0.554799	
	L_3 [m]	3.028	2.672976	0.284601	0.203248	0.006618	
	L_4 [m]	2.64	2.196214	0.334471	0.250325	0.007081	
	L_5 [m]	3.785	3.916879	0.507713	0.525403	0.000313	
	L_7 [m]	0.472	0.041891	0.726154	0.064448	0.437855	
	L_8 [m]	1.851	1.806408	0.526195	0.509143	0.000291	
	b_{main} [m]	3.07	4.028153	0.041154	0.143576	0.010490	
	n_{main} [-]	6	4.579682	0.363636	0.234517	0.016672	
	n_{cross} [-]	4	4.923958	0.083333	0.160330	0.005928	
	n_{rib} [-]	25	27.412042	0.294118	0.322495	0.000805	
	t_{w1} [m]	0.58	0.458967	0.127273	0.072258	0.003027	
	t_{w2} [m]	0.5	0.574074	0.271739	0.352254	0.006483	
	t_{w3} [m]	0.63	0.723357	0.266667	0.355578	0.007905	

	t_{roof} [m]	0.42	0.431609	0.330677	0.349178	0.000342	
	$I_{zz,\text{top}}$ [$\times 10^4 \text{ mm}^4$]	689760	273698.79	0.569367	0.129081	0.193852	
	$I_{zz,\text{cross}}$ [$\times 10^4 \text{ mm}^4$]	264390	95129.256	0.312422	0.111222	0.040481	
	$I_{zz,\text{rib}}$ [$\times 10^4 \text{ mm}^4$]	6252.1	1903.6565	0.465179	0.124920	0.115776	
	H_{bottom} [mm]	931	1017.4793	0.211290	0.350773	0.019455	
	W_{bottom} [mm]	400	317.70592	0.528302	0.140122	0.150683	
	$t_{w,\text{bottom}}$ [mm]	15	14.584931	0.107143	0.092319	0.000220	
	$t_{f,\text{bottom}}$ [mm]	25	30.800746	0.166667	0.360025	0.037387	0.076974

F.2.3. Fold 3

BRU0246	Parameter	Real value	Prediction	Norm. real value	Norm. prediction	$(y-\hat{y})^2$	MSE
				y	\hat{y}		
	L ₂ [m]	0.876	0.350684	0.335162	0.094963	0.057696	
	L ₃ [m]	2.628	2.055523	0.192942	0.061761	0.017209	
	L ₄ [m]	0.876	1.57828	0.000000	0.133159	0.017731	
	L ₅ [m]	2.8	1.95424	0.375587	0.262138	0.012871	
	L ₇ [m]	0	0.012859	0.000000	0.019783	0.000391	
	L ₈ [m]	1.034	1.22009	0.213767	0.284929	0.005064	
	b _{main} [m]	2.87	3.373527	0.019776	0.073600	0.002897	
	n _{main} [-]	6	2.769818	0.363636	0.069983	0.086232	
	n _{cross} [-]	3	4.01398	0.000000	0.084498	0.007140	
	n _{rib} [-]	29	12.588304	0.341176	0.148098	0.037279	
	t _{w1} [m]		0.449866		0.068121		
	t _{w2} [m]	0.68	0.420931	0.467391	0.185795	0.079297	
	t _{w3} [m]	0.6375	0.546011	0.273810	0.186677	0.007592	
	t _{roof} [m]	0.2125	0.384616	0.000000	0.274288	0.075234	
	I _{zz,top} [x10 ⁴ mm ⁴]		138380.8238		-0.014116		
	I _{zz,cross} [x10 ⁴ mm ⁴]		43980.74927		0.050422		
	I _{zz,rib} [x10 ⁴ mm ⁴]		661.443758		0.027719		
	H _{bottom} [mm]		863.804929		0.102911		
	W _{bottom} [mm]		282.188274		-0.027414		
	t _{w,bottom} [mm]		11.99431		-0.000203		
	t _{f,bottom} [mm]		21.038718		0.034624		0.031279

BRU1939	Parameter	Real value	Prediction	Norm. real value	Norm. prediction	$(y-\hat{y})^2$	MSE
				y	\hat{y}		
	L ₂ [m]		0.13266		-0.004728		
	L ₃ [m]		0.956784		-0.190013		
	L ₄ [m]		0.687673		-0.035709		
	L ₅ [m]		0.494701		0.066358		
	L ₇ [m]		0.002422		0.003726		
	L ₈ [m]		0.404661		-0.026898		
	b _{main} [m]	5.65	3.067352	0.316943	0.040871	0.076215	
	n _{main} [-]	2	2.262193	0.000000	0.023836	0.000568	
	n _{cross} [-]	15	3.4994	1.000000	0.041617	0.918499	
	n _{rib} [-]	0	5.632813	0.000000	0.066268	0.004391	
	t _{w1} [m]		0.344733		0.020333		
	t _{w2} [m]		0.261528		0.012530		
	t _{w3} [m]		0.377169		0.025875		
	t _{roof} [m]		0.283498		0.113144		
	I _{zz,top} [x10 ⁴ mm ⁴]		59964.80472		-0.097097		
	I _{zz,cross} [x10 ⁴ mm ⁴]	1562.6	19566.62155	0.000000	0.021401	0.000458	
	I _{zz,rib} [x10 ⁴ mm ⁴]		208.332022		-0.007736		
	H _{bottom} [mm]		384.166695		-0.670699		
	W _{bottom} [mm]		131.513771		-0.738143		
	t _{w,bottom} [mm]		6.116296		-0.210132		
	t _{f,bottom} [mm]		8.761289		-0.374624		0.200026

BRU2190	Parameter	Real value	Prediction	Norm. real value	Norm. prediction	$(y-\hat{y})^2$	MSE
				y	\hat{y}		
	L ₂ [m]		1.631519		0.680621		
	L ₃ [m]		4.037122		0.515839		
	L ₄ [m]		3.93207		0.579460		

	L ₅ [m]		6.535341		0.876639	
	L ₇ [m]		0.562979		0.866122	
	L ₈ [m]	1.221	2.608781	0.285277	0.815977	0.281643
	b _{main} [m]	7.3	7.496118	0.493319	0.514283	0.000439
	n _{main} [-]	2	9.329304	0.000000	0.666300	0.443956
	n _{cross} [-]	14	7.869468	0.916667	0.405789	0.260996
	n _{rib} [-]	0	71.658935	0.000000	0.843046	0.710727
	t _{w1} [m]	0.3	1.027189	0.000000	0.330540	0.109257
	t _{w2} [m]	0.4	0.896685	0.163043	0.702918	0.291465
	t _{w3} [m]	0.8	1.045138	0.428571	0.662036	0.054506
	t _{roof} [m]	0.4	0.608698	0.298805	0.631391	0.110614
	I _{zz,top} [x10 ⁴ mm ⁴]		849063.4204		0.737945	
	I _{zz,cross} [x10 ⁴ mm ⁴]		427784.5987		0.506649	
	I _{zz,rib} [x10 ⁴ mm ⁴]	13087	8579.304956	1.000000	0.647280	0.124412
	H _{bottom} [mm]		1220.359116		0.677999	
	W _{bottom} [mm]		407.732424		0.564776	
	t _{w,bottom} [mm]		23.240984		0.401464	
	t _{f,bottom} [mm]		41.477462		0.715915	
						0.238801

BRU0491	Parameter	Real value	Prediction	Norm. real value y	Norm. prediction ŷ	(y-ŷ) ²	MSE
	L ₂ [m]	0.665	1.152795	0.238683	0.461726	0.049748	
	L ₃ [m]	4.41	3.347376	0.601283	0.357786	0.059291	
	L ₄ [m]	4.313	3.150215	0.651688	0.431213	0.048609	
	L ₅ [m]	5.112	5.387083	0.685714	0.722613	0.001362	
	L ₇ [m]	0	0.315654	0.000000	0.485622	0.235828	
	L ₈ [m]	2.106	2.230538	0.623709	0.671334	0.002268	
	b _{main} [m]	4.32	5.382218	0.174773	0.288318	0.012893	
	n _{main} [-]	4	6.466688	0.181818	0.406063	0.050286	
	n _{cross} [-]	7	6.220714	0.333333	0.268393	0.004217	
	n _{rib} [-]	44	51.620345	0.517647	0.607298	0.008037	
	t _{w1} [m]	0.65	0.765464	0.159091	0.211575	0.002755	
	t _{w2} [m]	0.7	0.747471	0.489130	0.540729	0.002662	
	t _{w3} [m]	1.2	0.86955	0.809524	0.494810	0.099045	
	t _{roof} [m]	0.53	0.527979	0.505976	0.502755	0.000010	
	I _{zz,top} [x10 ⁴ mm ⁴]	923210	595637.5432	0.816409	0.469764	0.120163	
	I _{zz,cross} [x10 ⁴ mm ⁴]	400040	225036.1354	0.473669	0.265642	0.043275	
	I _{zz,rib} [x10 ⁴ mm ⁴]	307.2	5155.361533	0.000000	0.379361	0.143915	
	H _{bottom} [mm]	1200	1129.754246	0.645161	0.531862	0.012837	
	W _{bottom} [mm]	310	366.364481	0.103774	0.369644	0.070687	
	t _{w,bottom} [mm]	19	18.90064	0.250000	0.246451	0.000013	
	t _{f,bottom} [mm]	39	35.872368	0.633333	0.529079	0.010869	0.046608

BRU0101	Parameter	Real value	Prediction	Norm. real value y	Norm. prediction ŷ	(y-ŷ) ²	MSE
	L ₂ [m]	1.275	0.358884	0.517604	0.098712	0.175470	
	L ₃ [m]	4.078	2.041724	0.525206	0.058599	0.217723	
	L ₄ [m]	1.35	1.602592	0.089875	0.137769	0.002294	
	L ₅ [m]	4.269	2.078522	0.572636	0.278809	0.086334	
	L ₇ [m]	0	0.014085	0.000000	0.021669	0.000470	
	L ₈ [m]	1.977	1.237595	0.574379	0.291623	0.079951	
	b _{main} [m]	2.84	3.328691	0.016569	0.068807	0.002729	
	n _{main} [-]	6	2.848639	0.363636	0.077149	0.082075	

	n_{cross} [-]	3	4.023164	0.000000	0.085264	0.007270	0.066963
	n_{rib} [-]	23	12.127302	0.270588	0.142674	0.016362	
	t_{w1} [m]	0.4	0.403419	0.045455	0.047009	0.000002	
	t_{w2} [m]	0.4	0.413772	0.163043	0.178013	0.000224	
	t_{w3} [m]	0.4	0.521034	0.047619	0.162890	0.013287	
	t_{roof} [m]	0.25	0.373113	0.059761	0.255957	0.038493	
	$I_{zz,\text{top}}$ [x10 ⁴ mm ⁴]	219980	138854.7105	0.072234	-0.013614	0.007370	
	$I_{zz,\text{cross}}$ [x10 ⁴ mm ⁴]	85271	43212.9896	0.099504	0.049510	0.002499	
	$I_{zz,\text{rib}}$ [x10 ⁴ mm ⁴]	3156.2	726.645324	0.222930	0.032821	0.036141	
	H_{bottom} [mm]	1000	867.621915	0.322581	0.109068	0.045588	
	W_{bottom} [mm]	350	278.403195	0.292453	-0.045268	0.114055	
	$t_{w,\text{bottom}}$ [mm]	20	11.509414	0.285714	-0.017521	0.091952	
	$t_{f,\text{bottom}}$ [mm]	40	21.362869	0.666667	0.045429	0.385936	

BRU0318	Parameter	Real value	Prediction	Norm. real value	Norm. prediction	$(y-\hat{y})^2$	MSE
				y	\hat{y}		
	L_2 [m]	0.388	0.672105	0.112026	0.241932	0.016876	0.033721
	L_3 [m]	2.173	2.620343	0.088680	0.191188	0.010508	
	L_4 [m]	1.975	2.287885	0.208381	0.267707	0.003520	
	L_5 [m]	5.66	3.757156	0.759222	0.503978	0.065149	
	L_7 [m]	0	0.07722	0.000000	0.118800	0.014113	
	L_8 [m]	2.18	1.741738	0.652008	0.484412	0.028088	
	b_{main} [m]	4.33	3.919134	0.175842	0.131922	0.001929	
	n_{main} [-]	4	4.14453	0.181818	0.194957	0.000173	
	n_{cross} [-]	6	4.82178	0.250000	0.151815	0.009640	
	n_{rib} [-]	44	26.343338	0.517647	0.309922	0.043150	
	t_{w1} [m]	0.6	0.498441	0.136364	0.090200	0.002131	
	t_{w2} [m]	0.95	0.559351	0.760870	0.336251	0.180301	
	t_{w3} [m]	1.2	0.658347	0.809524	0.293664	0.266112	
	t_{roof} [m]	0.45	0.436088	0.378486	0.356316	0.000492	
	$I_{zz,\text{top}}$ [x10 ⁴ mm ⁴]	169240	301835.6733	0.018540	0.158856	0.019689	
	$I_{zz,\text{cross}}$ [x10 ⁴ mm ⁴]	41562	95838.56124	0.047547	0.112066	0.004163	
	$I_{zz,\text{rib}}$ [x10 ⁴ mm ⁴]	307.2	2172.225016	0.000000	0.145935	0.021297	
	H_{bottom} [mm]	1000	1005.635639	0.322581	0.331670	0.000083	
	W_{bottom} [mm]	297	320.318867	0.042453	0.152447	0.012099	
	$t_{w,\text{bottom}}$ [mm]	14	14.282247	0.071429	0.081509	0.000102	
	$t_{f,\text{bottom}}$ [mm]	26	28.769205	0.200000	0.292307	0.008521	

BRU0346	Parameter	Real value	Prediction	Norm. real value	Norm. prediction	$(y-\hat{y})^2$	MSE
				y	\hat{y}		
	L_2 [m]	0.737	1.026128	0.271605	0.403808	0.017478	0.0204310
	L_3 [m]	2.217	3.175974	0.098763	0.318509	0.048289	
	L_4 [m]	3.292	2.943411	0.458096	0.392001	0.004369	
	L_5 [m]	5.218	4.986187	0.699933	0.668838	0.000967	
	L_7 [m]	0	0.237883	0.000000	0.365974	0.133937	
	L_8 [m]	1.846	2.115066	0.524283	0.627176	0.010587	
	b_{main} [m]	4.14	4.97152	0.155532	0.244417	0.007901	
	n_{main} [-]	6	5.748897	0.363636	0.340809	0.000521	
	n_{cross} [-]	5	5.841779	0.166667	0.236815	0.004921	
	n_{rib} [-]	35	45.430393	0.411765	0.534475	0.015058	
	t_{w1} [m]	0.38	0.714501	0.036364	0.188410	0.023118	
	t_{w2} [m]	0.5	0.706277	0.271739	0.495953	0.050272	
	t_{w3} [m]	1.3	0.825393	0.904762	0.452755	0.204310	

t_{roof} [m]	0.4	0.508437	0.298805	0.471613	0.029863	
$I_{zz,\text{top}}$ [$\times 10^4 \text{ mm}^4$]	256900	522336.4841	0.111304	0.392195	0.078900	
$I_{zz,\text{cross}}$ [$\times 10^4 \text{ mm}^4$]	191250	185869.608	0.225481	0.219085	0.000041	
$I_{zz,\text{rib}}$ [$\times 10^4 \text{ mm}^4$]	3226.1	4235.313773	0.228400	0.307369	0.006236	
H_{bottom} [mm]	1000	1103.277808	0.322581	0.489158	0.027748	
W_{bottom} [mm]	300	355.878801	0.056604	0.320183	0.069474	
$t_{w,\text{bottom}}$ [mm]	18	17.924937	0.214286	0.211605	0.000007	
$t_{f,\text{bottom}}$ [mm]	34	34.189897	0.466667	0.472997	0.000040	0.034954

F.2.4. Fold 4

BRU0357	Parameter	Real value	Prediction	Norm. real value	Norm. prediction	$(y-\hat{y})^2$	MSE
				y	\hat{y}		
	L_2 [m]	0.855	0.989339	0.325560	0.386986	0.003773	
	L_3 [m]	3.887	2.932604	0.481439	0.262742	0.047829	
	L_4 [m]	4.11	2.625338	0.613197	0.331691	0.079246	
	L_5 [m]	5.301	4.874387	0.711066	0.653841	0.003275	
	L_7 [m]	0.377	0.136672	0.580000	0.210265	0.136704	
	L_8 [m]	2.05	1.971575	0.602294	0.572304	0.000899	
	b_{main} [m]	4.32	4.785871	0.174773	0.224572	0.002480	
	n_{main} [-]	4	5.65767	0.181818	0.332515	0.022710	
	n_{cross} [-]	7	5.692845	0.333333	0.224404	0.011866	
	n_{rib} [-]	54	35.16857	0.635294	0.413748	0.049083	
	t_{w1} [m]	0.65	0.55219	0.159091	0.114632	0.001977	
	t_{w2} [m]	0.7	0.62336	0.489130	0.405826	0.006940	
	t_{w3} [m]	1.2	0.761958	0.809524	0.392341	0.174042	
	t_{roof} [m]	0.53	0.462398	0.505976	0.398244	0.011606	
	$I_{zz,\text{top}}$ [x10 ⁴ mm ⁴]	356260	403953.59	0.216449	0.266919	0.002547	
	$I_{zz,\text{cross}}$ [x10 ⁴ mm ⁴]	283060	145801.81	0.334615	0.171457	0.026621	
	$I_{zz,\text{rib}}$ [x10 ⁴ mm ⁴]	307.2	3981.4656	0.000000	0.287506	0.082660	
	H_{bottom} [mm]	1200	1051.8694	0.645161	0.406241	0.057083	
	W_{bottom} [mm]	300	350.60334	0.056604	0.295299	0.056975	
	$t_{w,\text{bottom}}$ [mm]	16	17.261843	0.142857	0.187923	0.002031	
	$t_{f,\text{bottom}}$ [mm]	20	33.11269	0.000000	0.437090	0.191047	0.046257

BRU0274	Parameter	Real value	Prediction	Norm. real value	Norm. prediction	$(y-\hat{y})^2$	MSE
				y	\hat{y}		
	L_2 [m]	0.35	1.467402	0.094650	0.605579	0.261049	
	L_3 [m]	3.191	3.925698	0.321952	0.490307	0.028343	
	L_4 [m]	3.107	3.714607	0.423019	0.538227	0.013273	
	L_5 [m]	5.743	5.643896	0.770355	0.757062	0.000177	
	L_7 [m]	0.277	0.488193	0.426154	0.751066	0.105568	
	L_8 [m]	2.633	2.294224	0.825239	0.695688	0.016783	
	b_{main} [m]	3.8	7.715929	0.119188	0.537780	0.175219	
	n_{main} [-]	7	7.816652	0.454545	0.528787	0.005512	
	n_{cross} [-]	7	9.960689	0.333333	0.580057	0.060873	
	n_{rib} [-]	85	56.33323	1.000000	0.662744	0.113742	
	t_{w1} [m]	0.9	0.907684	0.272727	0.276220	0.000012	
	t_{w2} [m]	0.9	0.820278	0.706522	0.619867	0.007509	
	t_{w3} [m]	1.3	1.041307	0.904762	0.658388	0.060700	
	t_{roof} [m]	0.57	0.561018	0.569721	0.555407	0.000205	
	$I_{zz,\text{top}}$ [x10 ⁴ mm ⁴]	494100	815862.59	0.362315	0.702811	0.115938	
	$I_{zz,\text{cross}}$ [x10 ⁴ mm ⁴]	121500	298827.45	0.142569	0.353358	0.044432	
	$I_{zz,\text{rib}}$ [x10 ⁴ mm ⁴]	307.2	7826.8913	0.000000	0.588404	0.346220	
	H_{bottom} [mm]	1200	1145.3607	0.645161	0.557033	0.007767	
	W_{bottom} [mm]	310	405.10119	0.103774	0.552364	0.201233	
	$t_{w,\text{bottom}}$ [mm]	19	24.27028	0.250000	0.438224	0.035428	
	$t_{f,\text{bottom}}$ [mm]	39	39.81425	0.633333	0.660475	0.000737	0.076225

BRU0314	Parameter	Real value	Prediction	Norm. real value	Norm. prediction	$(y-\hat{y})^2$	MSE
				y	\hat{y}		
	L_2 [m]	0.917	0.993697	0.353909	0.388979	0.001230	
	L_3 [m]	3.045	2.957243	0.288497	0.268387	0.000404	
	L_4 [m]	3.045	2.646366	0.411263	0.335678	0.005713	

	L ₅ [m]	4.93	4.880209	0.661301	0.654622	0.000045	0.035377
	L ₇ [m]	0.355	0.14232	0.546154	0.218954	0.107060	
	L ₈ [m]	1.89	1.975216	0.541109	0.573696	0.001062	
	b _{main} [m]	4.125	4.84516	0.153928	0.230910	0.005926	
	n _{main} [-]	5	5.662635	0.272727	0.332967	0.003629	
	n _{cross} [-]	5	5.779892	0.166667	0.231658	0.004224	
	n _{rib} [-]	24	35.627054	0.282353	0.419142	0.018711	
	t _{w1} [m]	0.4	0.5619	0.045455	0.119045	0.005416	
	t _{w2} [m]	0.5	0.629483	0.271739	0.412482	0.019808	
	t _{w3} [m]	1.4	0.771989	1.000000	0.401894	0.357730	
	t _{roof} [m]	0.45	0.465629	0.378486	0.403393	0.000620	
	I _{zz,top} [x10 ⁴ mm ⁴]	494100	414898.19	0.362315	0.278501	0.007025	
	I _{zz,cross} [x10 ⁴ mm ⁴]	5696	147472.28	0.004913	0.173442	0.028402	
	I _{zz,rib} [x10 ⁴ mm ⁴]	7845.1	4036.496	0.589829	0.291812	0.088814	
	H _{bottom} [mm]	1130	1052.2562	0.532258	0.406865	0.015723	
	W _{bottom} [mm]	300	351.66792	0.056604	0.300320	0.059398	
t _{w,bottom} [mm]	19	17.4029	0.250000	0.192961	0.003253		
t _{r,bottom} [mm]	36	33.198171	0.533333	0.439939	0.008722		

BRU0485	Parameter	Real value	Prediction	Norm. real value	Norm. prediction	$(\hat{y}-y)^2$	MSE
				y	\hat{y}		
	L_2 [m]	0.525	1.658761	0.174668	0.693078	0.268748	
	L_3 [m]	4.44	4.341587	0.608158	0.585607	0.000509	
	L_4 [m]	3.75	4.169771	0.544937	0.624530	0.006335	
	L_5 [m]	7.455	5.809319	1.000000	0.779251	0.048730	
	L_7 [m]	0	0.585091	0.000000	0.900140	0.810252	
	L_8 [m]	2.7	2.41905	0.850860	0.743423	0.011543	
	b_{main} [m]	4.08	9.116017	0.149118	0.687442	0.289792	
	n_{main} [-]	7	8.753284	0.454545	0.613935	0.025405	
	n_{cross} [-]	9	11.860282	0.500000	0.738357	0.056814	
	n_{rib} [-]	73	64.093176	0.858824	0.754037	0.010980	
	t_{w1} [m]	0.8	1.099503	0.227273	0.363410	0.018533	
	t_{w2} [m]	1.05	0.894038	0.869565	0.700041	0.028738	
	t_{w3} [m]	0.8	1.125894	0.428571	0.738947	0.096333	
	t_{roof} [m]	0.75	0.601624	0.856574	0.620118	0.055911	
	$I_{zz,\text{top}}$ [x10 ⁴ mm ⁴]	1096700	915657.83	1.000000	0.808417	0.036704	
	$I_{zz,\text{cross}}$ [x10 ⁴ mm ⁴]	842820	376741.2	1.000000	0.445974	0.306945	
	$I_{zz,\text{rib}}$ [x10 ⁴ mm ⁴]	307.2	9405.2227	0.000000	0.711907	0.506811	
	H_{bottom} [mm]	1400	1179.0274	0.967742	0.611335	0.127026	
	W_{bottom} [mm]	310	423.89586	0.103774	0.641018	0.288632	
	$t_{w,\text{bottom}}$ [mm]	19	27.263613	0.250000	0.545129	0.087101	
	$t_{r,\text{bottom}}$ [mm]	39	42.089071	0.633333	0.736302	0.010603	0.147259

BRU0050	Parameter	Real value	Prediction	Norm. real value	Norm. prediction	$(y-\hat{y})^2$	MSE
				y	\hat{y}		
	L ₂ [m]	0.471	1.000011	0.149977	0.391866	0.058510	
	L ₃ [m]	2.481	2.990623	0.159258	0.276036	0.013637	
	L ₄ [m]	2.311	2.676207	0.272089	0.341336	0.004795	
	L ₅ [m]	5.515	4.889185	0.739772	0.655826	0.007047	
	L ₇ [m]	0	0.150728	0.000000	0.231889	0.053773	
	L ₈ [m]	2.41	1.98003	0.739962	0.575537	0.027035	
	b _{main} [m]	4.3	4.930587	0.172635	0.240041	0.004544	
	n _{main} [-]	5	5.673504	0.272727	0.333955	0.003749	

	n_{cross} [-]	6	5.90605	0.250000	0.242171	0.000061	0.028967
	n_{rib} [-]	60	36.272952	0.705882	0.426741	0.077920	
	t_{w1} [m]	0.35	0.575757	0.022727	0.125344	0.010530	
	t_{w2} [m]	0.85	0.638241	0.652174	0.422001	0.052980	
	t_{w3} [m]	0.8	0.786125	0.428571	0.415357	0.000175	
	t_{roof} [m]	0.5	0.470131	0.458167	0.410567	0.002266	
	$I_{zz,top}$ [x10 ⁴ mm ⁴]	671430	430684.36	0.549969	0.295207	0.064904	
	$I_{zz,cross}$ [x10 ⁴ mm ⁴]	329300	150018.77	0.389580	0.176469	0.045416	
	$I_{zz,rib}$ [x10 ⁴ mm ⁴]	426.52	4119.0934	0.009337	0.298275	0.083485	
	H_{bottom} [mm]	1041	1052.8977	0.388710	0.407900	0.000368	
	W_{bottom} [mm]	288	353.16082	0.000000	0.307362	0.094472	
	$t_{w,bottom}$ [mm]	19	17.595083	0.250000	0.199824	0.002518	
	$t_{f,bottom}$ [mm]	33	33.317904	0.433333	0.443930	0.000112	

BRU2038	Parameter	Real value	Prediction	Norm. real value	Norm. prediction	$(y-\hat{y})^2$	MSE
				y	\hat{y}		
	L_2 [m]	1.62	0.455312	0.675354	0.142804	0.283610	0.103893
	L_3 [m]	3.532	2.134532	0.400092	0.079865	0.102545	
	L_4 [m]	3.411	1.651414	0.480660	0.147026	0.111312	
	L_5 [m]	2.011	2.48306	0.269752	0.333073	0.004010	
	L_7 [m]	0	0.025564	0.000000	0.039329	0.001547	
	L_8 [m]	1.982	1.438001	0.576291	0.368260	0.043277	
	b_{main} [m]	6.88	3.72199	0.448423	0.110849	0.113957	
	n_{main} [-]	2	3.332351	0.000000	0.121123	0.014671	
	n_{cross} [-]	4	4.238627	0.083333	0.103219	0.000395	
	n_{rib} [-]	21	19.33898	0.247059	0.227517	0.000382	
	t_{w1} [m]	0.5	0.435967	0.090909	0.061803	0.000847	
	t_{w2} [m]	0.75	0.503107	0.543478	0.275116	0.072018	
	t_{w3} [m]	0.5	0.602451	0.142857	0.240430	0.009520	
	t_{roof} [m]	0.4	0.406616	0.298805	0.309348	0.000111	
	$I_{zz,top}$ [x10 ⁴ mm ⁴]	236650	164680.09	0.089875	0.013715	0.005800	
	$I_{zz,cross}$ [x10 ⁴ mm ⁴]	178440	53830.832	0.210254	0.062131	0.021940	
	$I_{zz,rib}$ [x10 ⁴ mm ⁴]	7197.5	1474.0805	0.539156	0.091307	0.200569	
	H_{bottom} [mm]	1200	809.81804	0.645161	0.015836	0.396051	
	W_{bottom} [mm]	400	263.17218	0.528302	-0.117112	0.416560	
	$t_{w,bottom}$ [mm]	12	11.102499	0.000000	-0.032054	0.001027	
	$t_{f,bottom}$ [mm]	40	21.467528	0.666667	0.048918	0.381614	

BRU0151	Parameter	Real value	Prediction	Norm. real value	Norm. prediction	$(y-\hat{y})^2$	MSE
				y	\hat{y}		
	L_2 [m]	1.05	0.826481	0.414723	0.312520	0.010446	
	L_3 [m]	2.665	2.679738	0.201421	0.204798	0.000011	
	L_4 [m]	1.041	2.32167	0.031286	0.274113	0.058965	
	L_5 [m]	3.981	4.385231	0.534004	0.588227	0.002940	
	L_7 [m]	0.25	0.07877	0.384615	0.121185	0.069396	
	L_8 [m]	1.469	1.847304	0.380115	0.524782	0.020929	
	b_{main} [m]	4.08	4.294006	0.149118	0.171994	0.000523	
	n_{main} [-]	6	4.909453	0.363636	0.264496	0.009829	
	n_{cross} [-]	5	4.999489	0.166667	0.166624	0.000000	
	n_{rib} [-]	27	29.491324	0.317647	0.346957	0.000859	
	t_{w1} [m]	2.275	0.494286	0.897727	0.088312	0.655153	
	t_{w2} [m]	0.25	0.576165	0.000000	0.354527	0.125690	
	t_{w3} [m]	0.75	0.691091	0.380952	0.324849	0.003148	

t_{roof} [m]	0.25	0.440873	0.059761	0.363941	0.092526	
$I_{zz,\text{top}}$ [$\times 10^4 \text{ mm}^4$]	316280	299001.04	0.174141	0.155856	0.000334	
$I_{zz,\text{cross}}$ [$\times 10^4 \text{ mm}^4$]	164970	110325.27	0.194242	0.129286	0.004219	
$I_{zz,\text{rib}}$ [$\times 10^4 \text{ mm}^4$]	3015.2	3018.7401	0.211897	0.212174	0.000000	
H_{bottom} [mm]	1040	1008.1063	0.387097	0.335655	0.002646	
W_{bottom} [mm]	350	330.54179	0.292453	0.200669	0.008424	
$t_{w,\text{bottom}}$ [mm]	12	15.358784	0.000000	0.119957	0.014390	
$t_{f,\text{bottom}}$ [mm]	26	30.365829	0.200000	0.345528	0.021178	0.052457

F.2.5. Fold 5

BRU0171	Parameter	Real value	Prediction	Norm. real value	Norm. prediction	$(y-\hat{y})^2$	MSE
				y	\hat{y}		
	L ₂ [m]	0.88	0.578094	0.336991	0.198946	0.019057	0.041097
	L ₃ [m]	2.33	2.572436	0.124656	0.180210	0.003086	
	L ₄ [m]	2.33	2.031727	0.275692	0.219137	0.003199	
	L ₅ [m]	4.035	3.624159	0.541247	0.486138	0.003037	
	L ₇ [m]	0.23	0.015559	0.353846	0.023937	0.108840	
	L ₈ [m]	1.61	1.752998	0.434034	0.488718	0.002990	
	b _{main} [m]	4.135	3.810075	0.154997	0.120265	0.001206	
	n _{main} [-]	4	3.707718	0.181818	0.155247	0.000706	
	n _{cross} [-]	5	4.693071	0.166667	0.141089	0.000654	
	n _{rib} [-]	19	22.261275	0.223529	0.261897	0.001472	
	t _{w1} [m]	0.65	0.378475	0.159091	0.035670	0.015233	
	t _{w2} [m]	0.25	0.544779	0.000000	0.320412	0.102664	
	t _{w3} [m]	0.65	0.634287	0.285714	0.270750	0.000224	
	t _{roof} [m]	0.52	0.406604	0.490040	0.309329	0.032656	
	I _{zz,top} [x10 ⁴ mm ⁴]	369380	228090.427	0.230333	0.080817	0.022355	
	I _{zz,cross} [x10 ⁴ mm ⁴]	128280	80833.8021	0.150629	0.094229	0.003181	
	I _{zz,rib} [x10 ⁴ mm ⁴]	3015.2	1784.23063	0.211897	0.115575	0.009278	
	H _{bottom} [mm]	1000	962.794042	0.322581	0.262571	0.003601	
	W _{bottom} [mm]	450	296.07099	0.764151	0.038071	0.527193	
	t _{w,bottom} [mm]	15	13.947054	0.107143	0.069538	0.001414	
	t _{f,bottom} [mm]	25	25.944913	0.166667	0.198164	0.000992	
BRU0173	Parameter	Real value	Prediction	Norm. real value	Norm. prediction	$(y-\hat{y})^2$	MSE
				y	\hat{y}		
	L ₂ [m]	0.48	0.825174	0.154092	0.311922	0.024910	0.073068
	L ₃ [m]	2.3	3.036563	0.117782	0.286563	0.028487	
	L ₄ [m]	2.16	2.642004	0.243458	0.334851	0.008353	
	L ₅ [m]	6.04	4.573427	0.810195	0.613471	0.038700	
	L ₇ [m]	0.26	0.058521	0.400000	0.090032	0.096080	
	L ₈ [m]	3.09	1.983119	1.000000	0.576719	0.179167	
	b _{main} [m]	5.435	4.490755	0.293960	0.193026	0.010188	
	n _{main} [-]	4	4.877892	0.181818	0.261627	0.006369	
	n _{cross} [-]	4	5.53977	0.083333	0.211648	0.016465	
	n _{rib} [-]	29	32.278886	0.341176	0.379752	0.001488	
	t _{w1} [m]	0.625	0.525526	0.147727	0.102512	0.002044	
	t _{w2} [m]	0.9	0.651009	0.706522	0.435879	0.073247	
	t _{w3} [m]	0.72	0.830743	0.352381	0.457850	0.011124	
	t _{roof} [m]	0.35	0.46798	0.219124	0.407139	0.035350	
	I _{zz,top} [x10 ⁴ mm ⁴]	1011200	392941.689	0.909522	0.255266	0.428050	
	I _{zz,cross} [x10 ⁴ mm ⁴]	267730	137804.194	0.316392	0.161950	0.023852	
	I _{zz,rib} [x10 ⁴ mm ⁴]	5598.3	3261.63491	0.414021	0.231180	0.033431	
	H _{bottom} [mm]	1420	1062.44653	1.000000	0.423301	0.332582	
	W _{bottom} [mm]	400	329.707285	0.528302	0.196732	0.109938	
	t _{w,bottom} [mm]	15	16.406097	0.107143	0.157361	0.002522	
	t _{f,bottom} [mm]	40	31.946138	0.666667	0.398205	0.072072	
BRU0155	Parameter	Real value	Prediction	Norm. real value	Norm. prediction	$(y-\hat{y})^2$	MSE
				y	\hat{y}		
	L ₂ [m]	1.223	0.869811	0.493827	0.332332	0.026081	

	L ₃ [m]	2.868	3.091748	0.247938	0.299209	0.002629
	L ₄ [m]	2.788	2.725823	0.362533	0.350744	0.000139
	L ₅ [m]	3.794	4.690087	0.508920	0.629120	0.014448
	L ₇ [m]	0.606	0.074681	0.932308	0.114894	0.668165
	L ₈ [m]	1.548	2.01608	0.410325	0.589323	0.032040
	b _{main} [m]	3.055	4.635698	0.039551	0.208519	0.028550
	n _{main} [-]	8	5.100215	0.545455	0.281838	0.069494
	n _{cross} [-]	5	5.68038	0.166667	0.223365	0.003215
	n _{rib} [-]	34	34.792047	0.400000	0.409318	0.000087
	t _{w1} [m]	0.52	0.541977	0.100000	0.109990	0.000100
	t _{w2} [m]	0.25	0.672109	0.000000	0.458814	0.210510
	t _{w3} [m]	0.75	0.879762	0.380952	0.504535	0.015273
	t _{roof} [m]	0.38	0.476976	0.266932	0.421476	0.023884
	I _{zz,top} [x10 ⁴ mm ⁴]	151720	433470.332	0.000000	0.298155	0.088896
	I _{zz,cross} [x10 ⁴ mm ⁴]	102960	148737.831	0.120531	0.174947	0.002961
	I _{zz,rib} [x10 ⁴ mm ⁴]	2662.3	3572.83101	0.184283	0.255531	0.005076
	H _{bottom} [mm]	1013	1070.3753	0.343548	0.436089	0.008564
	W _{bottom} [mm]	350	332.482279	0.292453	0.209822	0.006828
	t _{w,bottom} [mm]	12	16.309482	0.000000	0.153910	0.023688
	t _{f,bottom} [mm]	24	32.867023	0.133333	0.428901	0.087360
	0.062761					

BRU1787	Parameter	Real value	Prediction	Norm. real value y	Norm. prediction ŷ	(y-ŷ) ²	MSE
	L ₂ [m]		0.401528		0.118211		0.058137
	L ₃ [m]		2.001378		0.049353		
	L ₄ [m]		1.398161		0.099007		
	L ₅ [m]		2.192756		0.294132		
	L ₇ [m]		0.006561		0.010094		
	L ₈ [m]		1.365974		0.340717		
	b _{main} [m]	5.3	3.549396	0.279530	0.092399	0.035018	
	n _{main} [-]	2	2.831781	0.000000	0.075616	0.005718	
	n _{cross} [-]	12	4.283094	0.750000	0.106925	0.413546	
	n _{rib} [-]	0	16.647206	0.000000	0.195849	0.038357	
	t _{w1} [m]	0.4	0.324368	0.045455	0.011076	0.001182	
	t _{w2} [m]	0.4	0.463725	0.163043	0.232310	0.004798	
	t _{w3} [m]	0.4	0.519175	0.047619	0.161119	0.012882	
	t _{roof} [m]	0.45	0.344285	0.378486	0.210016	0.028382	
	I _{zz,top} [x10 ⁴ mm ⁴]	322420	136821.959	0.180639	-0.015765	0.038575	
	I _{zz,cross} [x10 ⁴ mm ⁴]	9877	55264.7341	0.009883	0.063836	0.002911	
	I _{zz,rib} [x10 ⁴ mm ⁴]		1042.55261		0.057540		
	H _{bottom} [mm]		696.954223		-0.166203		
	W _{bottom} [mm]		218.492264		-0.327867		
	t _{w,bottom} [mm]		9.672077		-0.083140		
	t _{f,bottom} [mm]		17.630451		-0.078985		

BRU0350	Parameter	Real value	Prediction	Norm. real value y	Norm. prediction ŷ	(y-ŷ) ²	MSE
	L ₂ [m]	0.143	0.708483	0.000000	0.258566	0.066856	
	L ₃ [m]	1.786	2.775417	0.000000	0.226723	0.051403	
	L ₄ [m]	1.786	2.377613	0.172545	0.284720	0.012583	
	L ₅ [m]	2.218	4.299348	0.297518	0.576707	0.077946	
	L ₇ [m]	0	0.033638	0.000000	0.051751	0.002678	

	L_8 [m]	1.34	1.903494	0.330784	0.546269	0.046434	
	b_{main} [m]	2.685	4.090042	0.000000	0.150192	0.022558	
	n_{main} [-]	13	4.455877	1.000000	0.223262	0.603323	
	n_{cross} [-]	3	4.952751	0.000000	0.162729	0.026481	
	n_{rib} [-]	82	27.663977	0.964706	0.325459	0.408637	
	t_{w1} [mm]	0.6	0.409062	0.136364	0.049574	0.007533	
	t_{w2} [mm]	0.6	0.599508	0.380435	0.379900	0.000000	
	t_{w3} [mm]	0.6	0.76594	0.238095	0.396133	0.024976	
	t_{roof} [mm]	0.5	0.436176	0.458167	0.356456	0.010345	
	$I_{zz,\text{top}}$ [$\times 10^4 \text{ mm}^4$]	297710	326413.791	0.154490	0.184865	0.000923	
	$I_{zz,\text{cross}}$ [$\times 10^4 \text{ mm}^4$]	151710	102971.186	0.178480	0.120544	0.003357	
	$I_{zz,\text{rib}}$ [$\times 10^4 \text{ mm}^4$]	307.2	2532.65425	0.000000	0.174138	0.030324	
	H_{bottom} [mm]	1000	1031.1949	0.322581	0.372895	0.002532	
	W_{bottom} [mm]	310	315.807986	0.103774	0.131170	0.000751	
	$t_{w,\text{bottom}}$ [mm]	35	15.115247	0.821429	0.111259	0.504341	
	$t_{f,\text{bottom}}$ [mm]	50	30.181003	1.000000	0.339367	0.436436	0.111448

BRU0238	Parameter	Real value	Prediction	Norm. real value	Norm. prediction	$(y-\hat{y})^2$	MSE
				y	\hat{y}		
	L_2 [m]	1.21	0.941771	0.487883	0.365236	0.015042	
	L_3 [m]	3.72	3.200877	0.443171	0.324216	0.014150	
	L_4 [m]	3.53	2.868401	0.503223	0.377778	0.015737	
	L_5 [m]	3.9	4.86235	0.523139	0.652227	0.016664	
	L_7 [m]	0.45	0.104043	0.692308	0.160066	0.283281	
	L_8 [m]	1.52	2.062735	0.399618	0.607164	0.043076	
	b_{main} [m]	3.675	4.896849	0.105826	0.236435	0.017059	
	n_{main} [-]	8	5.409713	0.545455	0.309974	0.055451	
	n_{cross} [-]	4	5.972013	0.083333	0.247668	0.027006	
	n_{rib} [-]	42	38.331184	0.494118	0.450955	0.001863	
	t_{w1} [mm]	1	0.587302	0.318182	0.130592	0.035190	
	t_{w2} [mm]	0.5	0.702811	0.271739	0.492186	0.048597	
	t_{w3} [mm]	0.6	0.938078	0.238095	0.560074	0.103671	
	t_{roof} [mm]	0.4	0.492307	0.298805	0.445908	0.021639	
	$I_{zz,\text{top}}$ [$\times 10^4 \text{ mm}^4$]	210600	490358.795	0.062308	0.358356	0.087644	
	$I_{zz,\text{cross}}$ [$\times 10^4 \text{ mm}^4$]	95292	169697.804	0.111416	0.199862	0.007823	
	$I_{zz,\text{rib}}$ [$\times 10^4 \text{ mm}^4$]	3015.2	4090.78111	0.211897	0.296059	0.007083	
	H_{bottom} [mm]	900	1084.5087	0.161290	0.458885	0.088563	
	W_{bottom} [mm]	300	338.03764	0.056604	0.236027	0.032193	
	$t_{w,\text{bottom}}$ [mm]	16	16.5233	0.142857	0.161546	0.000349	
	$t_{f,\text{bottom}}$ [mm]	31	33.971413	0.366667	0.465714	0.009810	0.044376

BRU0487	Parameter	Real value	Prediction	Norm. real value	Norm. prediction	$(y-\hat{y})^2$	MSE
				y	\hat{y}		
	L_2 [m]	1	1.126438	0.391861	0.449674	0.003342	
	L_3 [m]	2.4	3.514168	0.140697	0.396005	0.065183	
	L_4 [m]	2.13	3.24629	0.237770	0.449429	0.044800	
	L_5 [m]	6.07	5.261213	0.814219	0.705729	0.011770	
	L_7 [m]	0.65	0.197316	1.000000	0.303563	0.485024	
	L_8 [m]	2.386	2.164508	0.730784	0.646083	0.007174	
	b_{main} [m]	4.15	5.681527	0.156601	0.320313	0.026802	
	n_{main} [-]	7	6.06658	0.454545	0.369689	0.007201	
	n_{cross} [-]	6	6.911343	0.250000	0.325945	0.005768	

n_{rib} [-]	72	46.182459	0.847059	0.543323	0.092255	
t_{w1} [m]	0.7	0.751508	0.181818	0.205231	0.000548	
t_{w2} [m]	0.7	0.771775	0.489130	0.567147	0.006087	
t_{w3} [m]	0.85	1.040907	0.476190	0.658007	0.033057	
t_{roof} [m]	0.5	0.53183	0.458167	0.508892	0.002573	
$I_{zz,top}$ [$\times 10^4$ mm ⁴]	175200	615654.587	0.024847	0.490946	0.217249	
$I_{zz,cross}$ [$\times 10^4$ mm ⁴]	27303	236300.555	0.030598	0.279032	0.061720	
$I_{zz,rib}$ [$\times 10^4$ mm ⁴]	307.2	5506.24024	0.000000	0.406817	0.165500	
H_{bottom} [mm]	1000	1122.53072	0.322581	0.520211	0.039058	
W_{bottom} [mm]	310	354.144344	0.103774	0.312002	0.043359	
$t_{w,bottom}$ [mm]	19	17.825387	0.250000	0.208050	0.001760	
$t_{f,bottom}$ [mm]	39	35.873666	0.633333	0.529122	0.010860	0.063385

Fold 1

BRU0149	Parameter	Real value	Prediction	Norm. real value y	Norm. prediction \hat{y}	$(y-\hat{y})^2$	MSE
	L ₂ [m]	0.485	0.126611	0.156379	-0.007494	0.026854	0.454216
	L ₃ [m]	2.242	0.729545	0.104491	-0.242084	0.120115	
	L ₄ [m]	1.53	0.373289	0.124005	-0.095319	0.048103	
	L ₅ [m]	3.92	0.67806	0.525822	0.090954	0.189110	
	L ₇ [m]	0	0.00312	0.000000	0.000297	0.000000	
	L ₈ [m]	1.628	0.518982	0.440918	0.016819	0.179860	
	b _{main} [m]	3.266	2.987767	0.062106	0.032364	0.000885	
	n _{main} [-]	4	2.458077	0.181818	0.041643	0.019649	
	n _{cross} [-]	3	3.283344	0.000000	0.023612	0.000558	
	n _{rib} [-]	13	4.859999	0.152941	0.057176	0.009171	
	H _{bottom} [mm]	864	136.165049	0.103226	-1.070702	1.378105	
	W _{bottom} [mm]	390	50.943182	0.481132	-1.118193	2.557839	
t _{w,bottom} [mm]	20	2.701045	0.285714	-0.332106	0.381701		
t _{f,bottom} [mm]	40	3.911674	0.666667	-0.536278	1.447075		
BRU0199	Parameter	Real value	Prediction	Norm. real value y	Norm. prediction \hat{y}	$(y-\hat{y})^2$	MSE
	L ₂ [m]	1.04	0.855996	0.410151	0.326016	0.007079	0.012051
	L ₃ [m]	2.986	3.122543	0.274977	0.306266	0.000979	
	L ₄ [m]	2.07	2.846933	0.226394	0.373707	0.021701	
	L ₅ [m]	4.8125	4.918326	0.645540	0.569735	0.000202	
	L ₇ [m]	0	0.171058	0.000000	0.016291	0.000265	
	L ₈ [m]	1.78	2.044347	0.499044	0.600133	0.010219	
	b _{main} [m]	3.6	4.473213	0.097809	0.191151	0.008713	
	n _{main} [-]	6	5.528872	0.363636	0.320807	0.001834	
	n _{cross} [-]	5	5.931254	0.166667	0.244271	0.006022	
	n _{rib} [-]	27	43.02016	0.317647	0.506120	0.035522	
	H _{bottom} [mm]	1060	1093.991678	0.419355	0.474180	0.003006	
	W _{bottom} [mm]	300	339.792041	0.056604	0.244302	0.035231	
t _{w,bottom} [mm]	12	16.724567	0.000000	0.168735	0.028471		
t _{f,bottom} [mm]	36	33.079595	0.533333	0.435987	0.009476		
BRU0324	Parameter	Real value	Prediction	Norm. real value y	Norm. prediction \hat{y}	$(y-\hat{y})^2$	MSE
	L ₂ [m]	1.05	0.908097	0.414723	0.349839	0.004210	0.017285
	L ₃ [m]	2.893	3.214337	0.253666	0.327300	0.005422	
	L ₄ [m]	2.474	2.961377	0.302996	0.395407	0.008540	
	L ₅ [m]	4.673	5.081006	0.626828	0.681557	0.002995	
	L ₇ [m]	0.134	0.201566	0.012762	0.019197	0.000041	
	L ₈ [m]	1.834	2.104214	0.519694	0.623026	0.010678	
	b _{main} [m]	3.6	4.588534	0.097809	0.203478	0.011166	
	n _{main} [-]	6	5.779436	0.363636	0.343585	0.000402	
	n _{cross} [-]	5	6.252169	0.166667	0.271014	0.010888	
	n _{rib} [-]	22	46.176555	0.258824	0.543254	0.080900	
	H _{bottom} [mm]	1100	1108.233246	0.483871	0.497150	0.000176	
	W _{bottom} [mm]	350	344.825402	0.292453	0.268044	0.000596	
t _{w,bottom} [mm]	12	17.178243	0.000000	0.184937	0.034202		
t _{f,bottom} [mm]	26	34.036798	0.200000	0.467893	0.071767		
BRU5047	Parameter	Real value	Prediction	Norm. real value y	Norm. prediction \hat{y}	$(y-\hat{y})^2$	MSE
	L ₂ [m]	2	0.443048	0.849108	0.137196	0.506819	
	L ₃ [m]	6.15	2.087511	1.000000	0.069091	0.866592	
	L ₄ [m]	6.15	1.613417	1.000000	0.139821	0.739908	
	L ₅ [m]	0	3.171832	0.000000	0.425464	0.181019	
	L ₇ [m]	0	0.027993	0.000000	0.002666	0.000007	
	L ₈ [m]	2	1.431492	0.583174	0.365771	0.047264	
	b _{main} [m]	6.9	3.568544	0.450561	0.094446	0.126818	
	n _{main} [-]	2	3.734029	0.000000	0.157639	0.024850	
	n _{cross} [-]	5	3.966396	0.166667	0.080533	0.007419	
	n _{rib} [-]	15	18.023151	0.176471	0.212037	0.001265	
	H _{bottom} [mm]	800	866.043108	0.000000	0.106521	0.011347	
	W _{bottom} [mm]	400	261.362729	0.528302	-0.125648	0.427650	

$t_{w,bottom}$ [mm]	18	11.861014	0.214286	-0.004964	0.048070	
$t_{f,bottom}$ [mm]	30	21.48652	0.333333	0.049551	0.080533	0.219254

BRU1788	Parameter	Real value	Prediction	Norm. real value y	Norm. prediction \hat{y}	$(y-\hat{y})^2$	MSE
	L_2 [m]		0.383924		0.110162		
	L_3 [m]		1.881206		0.021816		
	L_4 [m]		1.392065		0.097851		
	L_5 [m]		2.806351		0.376439		
	L_7 [m]		0.019618		0.001868		
	L_8 [m]		1.304351		0.317151		
	b_{main} [m]	5.7	3.448598	0.322288	0.081625	0.057919	
	n_{main} [-]	2	3.48476	0.000000	0.134978	0.018219	
	n_{cross} [-]	7	3.785813	0.333333	0.065484	0.071743	
	n_{rib} [-]	0	14.836239	0.000000	0.174544	0.030466	
	H_{bottom} [mm]		801.047		0.001689		
	W_{bottom} [mm]		241.49921		-0.219343		
	$t_{w,bottom}$ [mm]		10.796861		-0.042969		
	$t_{f,bottom}$ [mm]		19.047914		-0.031736		0.044587

BRU0272	Parameter	Real value	Prediction	Norm. real value y	Norm. prediction \hat{y}	$(y-\hat{y})^2$	MSE
	L_2 [m]		0.908491		0.350019		
	L_3 [m]		3.218265		0.328200		
	L_4 [m]		2.964429		0.395986		
	L_5 [m]		5.125731		0.687556		
	L_7 [m]		0.202077		0.019245		
	L_8 [m]		2.123125		0.630258		
	b_{main} [m]	12.04	4.576823	1.000000	0.202226	0.636444	
	n_{main} [-]	2	5.817511	0.000000	0.347046	0.120441	
	n_{cross} [-]	7	6.171557	0.333333	0.264296	0.004766	
	n_{rib} [-]	30	46.447188	0.352941	0.546438	0.037441	
	H_{bottom} [mm]		1104.105688		0.490493		
	W_{bottom} [mm]		341.672849		0.253174		
	$t_{w,bottom}$ [mm]		17.149178		0.183899		
	$t_{f,bottom}$ [mm]		33.985085		0.466170		0.199773

BRU2023	Parameter	Real value	Prediction	Norm. real value y	Norm. prediction \hat{y}	$(y-\hat{y})^2$	MSE
	L_2 [m]	1.041	0.503713	0.410608	0.164935	0.060355	
	L_3 [m]	2.934	2.281262	0.263061	0.113488	0.022372	
	L_4 [m]	2.76	1.8308	0.357224	0.181039	0.031041	
	L_5 [m]	2.35	3.482765	0.315225	0.467172	0.023088	
	L_7 [m]	0.11	0.039351	0.010476	0.003748	0.000045	
	L_8 [m]	2.15	1.53946	0.640535	0.407059	0.054511	
	b_{main} [m]	11.1	3.700537	0.899519	0.108556	0.625623	
	n_{main} [-]	2	3.980195	0.000000	0.180018	0.032406	
	n_{cross} [-]	3	4.196658	0.000000	0.099722	0.009944	
	n_{rib} [-]	32	21.500393	0.376471	0.252946	0.015258	
	H_{bottom} [mm]	1000	917.163146	0.322581	0.188973	0.017851	
	W_{bottom} [mm]	300	278.404958	0.056604	-0.045260	0.010376	
	$t_{w,bottom}$ [mm]	40	12.745919	1.000000	0.026640	0.947430	
	$t_{f,bottom}$ [mm]	30	23.698253	0.333333	0.123275	0.044124	0.135316

Fold 2

BRU0382	Parameter	Real value	Prediction	Norm. real value y	Norm. prediction \hat{y}	$(y-\hat{y})^2$	MSE
	L_2 [m]	1.05	0.95676	0.414723	0.372090	0.001818	0.020539
	L_3 [m]	2.893	3.245588	0.253666	0.334461	0.006528	
	L_4 [m]	2.474	2.905424	0.302996	0.384798	0.006692	
	L_5 [m]	4.673	4.950057	0.626828	0.663992	0.001381	
	L_7 [m]	0.134	0.142482	0.012762	0.013570	0.000001	
	L_8 [m]	1.834	2.090389	0.519694	0.617740	0.009613	
	b_{main} [m]	3.6	5.060104	0.097809	0.253886	0.024360	
	n_{main} [-]	6	5.671904	0.363636	0.333809	0.000890	
	n_{cross} [-]	5	6.482735	0.166667	0.290228	0.015267	
	n_{rib} [-]	22	42.962705	0.258824	0.505444	0.060821	
	H_{bottom} [mm]	1100	1113.070758	0.483871	0.504953	0.000444	
	W_{bottom} [mm]	350	347.173001	0.292453	0.279118	0.000178	
	$t_{w,bottom}$ [mm]	12	18.020438	0.000000	0.215016	0.046232	
	$t_{f,bottom}$ [mm]	26	36.099101	0.200000	0.536637	0.113324	
BRU5046	Parameter	Real value	Prediction	Norm. real value y	Norm. prediction \hat{y}	$(y-\hat{y})^2$	MSE
	L_2 [m]	0.93	0.181448	0.359854	0.017580	0.117151	0.249854
	L_3 [m]	3.82	1.100801	0.466086	-0.157012	0.388251	
	L_4 [m]	3.82	0.681809	0.558210	-0.036820	0.354061	
	L_5 [m]	1.7	0.816497	0.228035	0.109523	0.014045	
	L_7 [m]	0	0.005734	0.000000	0.000546	0.000000	
	L_8 [m]	0.475	0.894113	0.000000	0.160273	0.025687	
	b_{main} [m]	4.45	3.279112	0.188669	0.063507	0.015665	
	n_{main} [-]	3	2.61778	0.090909	0.056162	0.001207	
	n_{cross} [-]	4	3.653539	0.083333	0.054462	0.000834	
	n_{rib} [-]	16	10.912033	0.188235	0.128377	0.003583	
	H_{bottom} [mm]	920	297.600683	0.193548	-0.810321	1.007755	
	W_{bottom} [mm]	298	101.884259	0.047170	-0.877904	0.855762	
	$t_{w,bottom}$ [mm]	16	4.965285	0.142857	-0.251240	0.155312	
	$t_{f,bottom}$ [mm]	30	7.577184	0.333333	-0.414094	0.558647	
BRU0239	Parameter	Real value	Prediction	Norm. real value y	Norm. prediction \hat{y}	$(y-\hat{y})^2$	MSE
	L_2 [m]	1.16	1.094692	0.465021	0.435159	0.000892	0.052735
	L_3 [m]	2.522	3.537219	0.168653	0.401288	0.054119	
	L_4 [m]	2.328	3.285088	0.275313	0.456786	0.032932	
	L_5 [m]	4.125	5.36815	0.553320	0.720074	0.027807	
	L_7 [m]	0.4	0.25111	0.038095	0.023915	0.000201	
	L_8 [m]	1.33	2.231334	0.326960	0.671638	0.118803	
	b_{main} [m]	3.675	5.913882	0.105826	0.345150	0.057276	
	n_{main} [-]	8	6.328327	0.545455	0.393484	0.023095	
	n_{cross} [-]	4	7.6779	0.083333	0.389825	0.093937	
	n_{rib} [-]	66	52.571156	0.776471	0.618484	0.024960	
	H_{bottom} [mm]	900	1147.384401	0.161290	0.560297	0.159207	
	W_{bottom} [mm]	300	357.13676	0.056604	0.326117	0.072637	
	$t_{w,bottom}$ [mm]	16	19.728172	0.142857	0.276006	0.017729	
	$t_{f,bottom}$ [mm]	31	38.015855	0.366667	0.600529	0.054691	
BRU0345	Parameter	Real value	Prediction	Norm. real value y	Norm. prediction \hat{y}	$(y-\hat{y})^2$	MSE
	L_2 [m]	0.388	0.612072	0.112026	0.214482	0.010497	0.000353
	L_3 [m]	2.173	2.459059	0.088680	0.154230	0.004297	
	L_4 [m]	1.975	1.937208	0.208381	0.201215	0.000051	
	L_5 [m]	5.66	3.487643	0.759222	0.467826	0.084912	
	L_7 [m]	0	0.029069	0.000000	0.002768	0.000008	
	L_8 [m]	2.18	1.69478	0.652008	0.466455	0.034430	
	b_{main} [m]	4.33	3.816483	0.175842	0.120950	0.003013	
	n_{main} [-]	4	4.155238	0.181818	0.195931	0.000199	
	n_{cross} [-]	6	4.662722	0.250000	0.138560	0.012419	
	n_{rib} [-]	40	23.767591	0.470588	0.279619	0.036469	
	H_{bottom} [mm]	1000	963.201085	0.322581	0.263228	0.003523	
	W_{bottom} [mm]	297	302.17074	0.042453	0.066843	0.000595	
	$t_{w,bottom}$ [mm]	14	13.473984	0.071429	0.052642	0.000353	

	$t_{f, \text{bottom}}$ [mm]	26	28.386161	0.200000	0.279539	0.006326	0.014078
--	-----------------------------	----	-----------	----------	----------	----------	----------

BRU0349	Parameter	Real value	Prediction	Norm. real value y	Norm. prediction \hat{y}	$(y-\hat{y})^2$	MSE
	L_2 [m]	0.388	0.612072	0.112026	0.214482	0.010497	0.014078
	L_3 [m]	2.173	2.459059	0.088680	0.154230	0.004297	
	L_4 [m]	1.975	1.937208	0.208381	0.201215	0.000051	
	L_5 [m]	5.66	3.487643	0.759222	0.467826	0.084912	
	L_7 [m]	0	0.029069	0.000000	0.002768	0.000008	
	L_8 [m]	2.18	1.69478	0.652008	0.466455	0.034430	
	b_{main} [m]	4.33	3.816483	0.175842	0.120950	0.003013	
	n_{main} [-]	4	4.155238	0.181818	0.195931	0.000199	
	n_{cross} [-]	6	4.662722	0.250000	0.138560	0.012419	
	n_{rib} [-]	40	23.767591	0.470588	0.279619	0.036469	
	H_{bottom} [mm]	1000	963.201085	0.322581	0.263228	0.003523	
	W_{bottom} [mm]	297	302.17074	0.042453	0.066843	0.000595	
	$t_{w, \text{bottom}}$ [mm]	14	13.473984	0.071429	0.052642	0.000353	
	$t_{f, \text{bottom}}$ [mm]	26	28.386161	0.200000	0.279539	0.006326	

BRU0356	Parameter	Real value	Prediction	Norm. real value y	Norm. prediction \hat{y}	$(y-\hat{y})^2$	MSE
	L_2 [m]	0.44	0.179956	0.135802	0.016898	0.014138	0.501616
	L_3 [m]	3.035	1.092371	0.286205	-0.158943	0.198157	
	L_4 [m]	2.82	0.68033	0.368601	-0.037101	0.164594	
	L_5 [m]	4.475	0.801608	0.600268	0.107526	0.242795	
	L_7 [m]	0.26	0.006332	0.024762	0.000603	0.000584	
	L_8 [m]	2.1	0.885899	0.621415	0.157132	0.215559	
	b_{main} [m]	5.5	3.306317	0.300909	0.066415	0.054987	
	n_{main} [-]	2	2.619821	0.000000	0.056347	0.003175	
	n_{cross} [-]	6	3.668874	0.250000	0.055740	0.037737	
	n_{rib} [-]	10	11.223576	0.117647	0.132042	0.000207	
	H_{bottom} [mm]	1160	281.567202	0.580645	-0.836182	2.007399	
	W_{bottom} [mm]	500	97.038669	1.000000	-0.900761	3.612892	
	$t_{w, \text{bottom}}$ [mm]	20	4.863659	0.285714	-0.254869	0.292231	
	$t_{f, \text{bottom}}$ [mm]	20	7.337076	0.000000	-0.422097	0.178166	

BRU0266	Parameter	Real value	Prediction	Norm. real value y	Norm. prediction \hat{y}	$(y-\hat{y})^2$	MSE
	L_2 [m]	2.33	0.704245	1.000000	0.256628	0.552602	0.057821
	L_3 [m]	3.028	2.681778	0.284601	0.205265	0.006294	
	L_4 [m]	2.64	2.196751	0.334471	0.250427	0.007063	
	L_5 [m]	3.785	3.958955	0.507713	0.531047	0.000544	
	L_7 [m]	0.472	0.042227	0.044952	0.004022	0.001675	
	L_8 [m]	1.851	1.81249	0.526195	0.511468	0.000217	
	b_{main} [m]	3.07	4.020724	0.041154	0.142782	0.010328	
	n_{main} [-]	6	4.52938	0.363636	0.229944	0.017874	
	n_{cross} [-]	4	4.989621	0.083333	0.165802	0.006801	
	n_{rib} [-]	25	27.692441	0.294118	0.325793	0.001003	
	H_{bottom} [mm]	931	1025.410816	0.211290	0.363566	0.023188	
	W_{bottom} [mm]	400	320.820709	0.528302	0.154815	0.139493	
	$t_{w, \text{bottom}}$ [mm]	15	14.789586	0.107143	0.099628	0.000056	
	$t_{f, \text{bottom}}$ [mm]	25	31.173827	0.166667	0.372461	0.042351	

Fold 3

BRU0246	Parameter	Real value	Prediction	Norm. real value y	Norm. prediction \hat{y}	$(y-\hat{y})^2$	MSE
	L_2 [m]	0.876	0.248292	0.335162	0.048144	0.082379	0.034004
	L_3 [m]	2.628	1.711379	0.192942	-0.017099	0.044117	
	L_4 [m]	0.876	1.280363	0.000000	0.076671	0.005878	
	L_5 [m]	2.8	1.209839	0.375587	0.162286	0.045497	
	L_7 [m]	0	0.008321	0.000000	0.000792	0.000001	
	L_8 [m]	1.034	0.916743	0.213767	0.168927	0.002011	
	b_{main} [m]	2.87	3.325821	0.019776	0.068500	0.002374	
	n_{main} [-]	6	2.480185	0.363636	0.043653	0.102389	
	n_{cross} [-]	3	3.828319	0.000000	0.069027	0.004765	
	n_{rib} [-]	29	9.875073	0.341176	0.116177	0.050625	
	H_{bottom} [mm]		761.423436		-0.062220		
	W_{bottom} [mm]		249.723807		-0.180548		
	$t_{w,bottom}$ [mm]		10.223986		-0.063429		
	$t_{f,bottom}$ [mm]		17.623155		-0.079228		
BRU1939	Parameter	Real value	Prediction	Norm. real value y	Norm. prediction \hat{y}	$(y-\hat{y})^2$	MSE
	L_2 [m]		0.138799		-0.001921		0.247289
	L_3 [m]		0.92955		-0.196253		
	L_4 [m]		0.672239		-0.038635		
	L_5 [m]		0.504112		0.067621		
	L_7 [m]		0.004501		0.000429		
	L_8 [m]		0.401943		-0.027938		
	b_{main} [m]	5.65	3.182995	0.316943	0.053233	0.069543	
	n_{main} [-]	2	2.255503	0.000000	0.023228	0.000540	
	n_{cross} [-]	15	3.533281	1.000000	0.044440	0.913095	
	n_{rib} [-]	0	6.571553	0.000000	0.077312	0.005977	
	H_{bottom} [mm]		385.864546		-0.667960		
	W_{bottom} [mm]		134.761403		-0.722824		
	$t_{w,bottom}$ [mm]		5.957507		-0.215803		
	$t_{f,bottom}$ [mm]		8.950947		-0.368302		
BRU2190	Parameter	Real value	Prediction	Norm. real value y	Norm. prediction \hat{y}	$(y-\hat{y})^2$	MSE
	L_2 [m]		1.732109		0.726616		0.374323
	L_3 [m]		3.985527		0.504016		
	L_4 [m]		4.061152		0.603935		
	L_5 [m]		6.616239		0.887490		
	L_7 [m]		0.614963		0.058568		
	L_8 [m]	1.221	2.687356	0.285277	0.846025	0.314438	
	b_{main} [m]	7.3	8.340483	0.493319	0.604541	0.012370	
	n_{main} [-]	2	9.651784	0.000000	0.695617	0.483883	
	n_{cross} [-]	14	8.319657	0.916667	0.443305	0.224072	
	n_{rib} [-]	0	77.757647	0.000000	0.914796	0.836851	
	H_{bottom} [mm]		1274.196031		0.764832		
	W_{bottom} [mm]		416.310668		0.605239		
	$t_{w,bottom}$ [mm]		21.658918		0.344961		
	$t_{f,bottom}$ [mm]		44.155898		0.805197		
BRU0491	Parameter	Real value	Prediction	Norm. real value y	Norm. prediction \hat{y}	$(y-\hat{y})^2$	MSE
	L_2 [m]	0.665	1.139453	0.238683	0.455626	0.047064	
	L_3 [m]	4.41	3.265178	0.601283	0.338950	0.068819	
	L_4 [m]	4.313	3.085535	0.651688	0.418949	0.054167	
	L_5 [m]	5.112	5.417931	0.685714	0.726751	0.001684	
	L_7 [m]	0	0.308462	0.000000	0.029377	0.000863	
	L_8 [m]	2.106	2.212418	0.623709	0.664405	0.001656	
	b_{main} [m]	4.32	5.117202	0.174773	0.259990	0.007262	
	n_{main} [-]	4	6.545333	0.181818	0.413212	0.053543	
	n_{cross} [-]	7	6.111513	0.333333	0.259293	0.005482	
	n_{rib} [-]	44	49.528983	0.517647	0.582694	0.004231	
	H_{bottom} [mm]	1200	1114.179631	0.645161	0.506741	0.019160	
	W_{bottom} [mm]	310	357.867963	0.103774	0.329566	0.050982	
	$t_{w,bottom}$ [mm]	19	18.080803	0.250000	0.217172	0.001078	

	$t_{f, \text{bottom}}$ [mm]	39	35.362967	0.633333	0.512099	0.014698	0.023621
--	-----------------------------	----	-----------	----------	----------	----------	----------

BRU0101	Parameter	Real value	Prediction	Norm. real value y	Norm. prediction \hat{y}	$(y-\hat{y})^2$	MSE
	L_2 [m]	1.275	0.360572	0.517604	0.099484	0.174824	0.086192
	L_3 [m]	4.078	2.110975	0.525206	0.074467	0.203166	
	L_4 [m]	1.35	1.664827	0.089875	0.149569	0.003563	
	L_5 [m]	4.269	1.999387	0.572636	0.268194	0.092685	
	L_7 [m]	0	0.016682	0.000000	0.001589	0.000003	
	L_8 [m]	1.977	1.252812	0.574379	0.297442	0.076694	
	b_{main} [m]	2.84	3.44901	0.016569	0.081669	0.004238	
	n_{main} [-]	6	2.82362	0.363636	0.074875	0.083383	
	n_{cross} [-]	3	4.095658	0.000000	0.091305	0.008337	
	n_{rib} [-]	23	13.399325	0.270588	0.157639	0.012758	
	H_{bottom} [mm]	1000	891.570672	0.322581	0.147695	0.030585	
	W_{bottom} [mm]	350	288.071432	0.292453	0.000337	0.085332	
	$t_{w, \text{bottom}}$ [mm]	20	12.098591	0.285714	0.003521	0.079633	
	$t_{f, \text{bottom}}$ [mm]	40	22.214158	0.666667	0.073805	0.351485	

BRU0318	Parameter	Real value	Prediction	Norm. real value y	Norm. prediction \hat{y}	$(y-\hat{y})^2$	MSE
	L_2 [m]	0.388	0.713733	0.112026	0.260966	0.022183	0.012736
	L_3 [m]	2.173	2.658815	0.088680	0.200003	0.012393	
	L_4 [m]	1.975	2.350271	0.208381	0.279536	0.005063	
	L_5 [m]	5.66	4.069222	0.759222	0.545838	0.045533	
	L_7 [m]	0	0.09321	0.000000	0.008877	0.000079	
	L_8 [m]	2.18	1.795175	0.652008	0.504847	0.021656	
	b_{main} [m]	4.33	3.919877	0.175842	0.132002	0.001922	
	n_{main} [-]	4	4.445644	0.181818	0.222331	0.001641	
	n_{cross} [-]	6	4.909798	0.250000	0.159150	0.008254	
	n_{rib} [-]	44	26.911102	0.517647	0.316601	0.040419	
	H_{bottom} [mm]	1000	1001.416093	0.322581	0.324865	0.000005	
	W_{bottom} [mm]	297	317.455387	0.042453	0.138941	0.009310	
	$t_{w, \text{bottom}}$ [mm]	14	14.360334	0.071429	0.084298	0.000166	
	$t_{f, \text{bottom}}$ [mm]	26	28.950982	0.200000	0.298366	0.009676	

BRU0346	Parameter	Real value	Prediction	Norm. real value y	Norm. prediction \hat{y}	$(y-\hat{y})^2$	MSE
	L_2 [m]	0.737	0.942731	0.271605	0.365675	0.008849	0.012167
	L_3 [m]	2.217	3.094147	0.098763	0.299759	0.040399	
	L_4 [m]	3.292	2.817146	0.458096	0.368060	0.008107	
	L_5 [m]	5.218	4.618504	0.699933	0.619518	0.006467	
	L_7 [m]	0	0.190071	0.000000	0.018102	0.000328	
	L_8 [m]	1.846	2.033365	0.524283	0.595933	0.005134	
	b_{main} [m]	4.14	4.807378	0.155532	0.226871	0.005089	
	n_{main} [-]	6	5.2411	0.363636	0.294645	0.004760	
	n_{cross} [-]	5	5.627174	0.166667	0.218931	0.002732	
	n_{rib} [-]	35	42.125024	0.411765	0.495589	0.007026	
	H_{bottom} [mm]	1000	1087.303989	0.322581	0.463394	0.019828	
	W_{bottom} [mm]	300	352.216894	0.056604	0.302910	0.060667	
	$t_{w, \text{bottom}}$ [mm]	18	17.677024	0.214286	0.202751	0.000133	
	$t_{f, \text{bottom}}$ [mm]	34	33.143119	0.466667	0.438104	0.000816	

Fold 4

BRU0357	Parameter	Real value	Prediction	Norm. real value y	Norm. prediction \hat{y}	$(y-\hat{y})^2$	MSE
	L_2 [m]	0.855	0.953504	0.325560	0.370601	0.002029	0.036291
	L_3 [m]	3.887	2.976961	0.481439	0.272906	0.043486	
	L_4 [m]	4.11	2.616952	0.613197	0.330101	0.080143	
	L_5 [m]	5.301	4.830537	0.711066	0.647959	0.003982	
	L_7 [m]	0.377	0.140567	0.035905	0.013387	0.000507	
	L_8 [m]	2.05	1.966029	0.602294	0.570183	0.001031	
	b_{main} [m]	4.32	4.8701	0.174773	0.233576	0.003458	
	n_{main} [-]	4	5.41689	0.181818	0.310626	0.016592	
	n_{cross} [-]	7	5.840571	0.333333	0.236714	0.009335	
	n_{rib} [-]	54	35.436185	0.635294	0.416896	0.047698	
	H_{bottom} [mm]	1200	1046.332304	0.645161	0.397310	0.061430	
	W_{bottom} [mm]	300	348.881602	0.056604	0.287177	0.053164	
	$t_{w,bottom}$ [mm]	16	17.278938	0.142857	0.188534	0.002086	
	$t_{f,bottom}$ [mm]	20	32.838012	0.000000	0.427934	0.183127	
BRU0274	Parameter	Real value	Prediction	Norm. real value y	Norm. prediction \hat{y}	$(y-\hat{y})^2$	MSE
	L_2 [m]	0.35	1.477429	0.094650	0.610164	0.265755	0.066188
	L_3 [m]	3.191	3.954246	0.321952	0.496848	0.030589	
	L_4 [m]	3.107	3.734606	0.423019	0.542019	0.014161	
	L_5 [m]	5.743	5.694976	0.770355	0.763914	0.000041	
	L_7 [m]	0.277	0.488904	0.026381	0.046562	0.000407	
	L_8 [m]	2.633	2.308128	0.825239	0.701005	0.015434	
	b_{main} [m]	3.8	7.7258	0.119188	0.538835	0.176104	
	n_{main} [-]	7	7.848619	0.454545	0.531693	0.005952	
	n_{cross} [-]	7	9.93152	0.333333	0.577627	0.059679	
	n_{rib} [-]	85	56.404613	1.000000	0.663584	0.113176	
	H_{bottom} [mm]	1200	1140.295818	0.645161	0.548864	0.009273	
	W_{bottom} [mm]	310	404.45347	0.103774	0.549309	0.198502	
	$t_{w,bottom}$ [mm]	19	24.340584	0.250000	0.440735	0.036380	
	$t_{f,bottom}$ [mm]	39	40.030954	0.633333	0.667698	0.001181	
BRU0314	Parameter	Real value	Prediction	Norm. real value y	Norm. prediction \hat{y}	$(y-\hat{y})^2$	MSE
	L_2 [m]	0.917	0.955576	0.353909	0.371548	0.000311	0.009208
	L_3 [m]	3.045	2.989629	0.288497	0.275809	0.000161	
	L_4 [m]	3.045	2.631158	0.411263	0.332794	0.006157	
	L_5 [m]	4.93	4.811254	0.661301	0.645373	0.000254	
	L_7 [m]	0.355	0.141284	0.033810	0.013456	0.000414	
	L_8 [m]	1.89	1.96385	0.541109	0.569350	0.000798	
	b_{main} [m]	4.125	4.900889	0.153928	0.236867	0.006879	
	n_{main} [-]	5	5.419503	0.272727	0.310864	0.001454	
	n_{cross} [-]	5	5.885333	0.166667	0.240444	0.005443	
	n_{rib} [-]	24	35.608245	0.282353	0.418921	0.018651	
	H_{bottom} [mm]	1130	1045.923022	0.532258	0.396650	0.018390	
	W_{bottom} [mm]	300	349.979346	0.056604	0.292355	0.055579	
	$t_{w,bottom}$ [mm]	19	17.380332	0.250000	0.192155	0.003346	
	$t_{f,bottom}$ [mm]	36	32.843451	0.533333	0.428115	0.011071	
BRU0485	Parameter	Real value	Prediction	Norm. real value y	Norm. prediction \hat{y}	$(y-\hat{y})^2$	MSE
	L_2 [m]	0.525	1.686028	0.174668	0.705545	0.281830	
	L_3 [m]	4.44	4.332399	0.608158	0.583501	0.000608	
	L_4 [m]	3.75	4.179532	0.544937	0.626381	0.006633	
	L_5 [m]	7.455	5.871833	1.000000	0.787637	0.045098	
	L_7 [m]	0	0.585231	0.000000	0.055736	0.003107	
	L_8 [m]	2.7	2.442956	0.850860	0.752564	0.009662	
	b_{main} [m]	4.08	9.00576	0.149118	0.675656	0.277242	
	n_{main} [-]	7	8.971728	0.454545	0.633793	0.032130	
	n_{cross} [-]	9	11.654657	0.500000	0.721221	0.048939	
	n_{rib} [-]	73	63.883136	0.858824	0.751566	0.011504	
	H_{bottom} [mm]	1400	1177.020678	0.967742	0.608098	0.129344	
	W_{bottom} [mm]	310	422.470969	0.103774	0.634297	0.281455	
	$t_{w,bottom}$ [mm]	19	27.126783	0.250000	0.540242	0.084241	

	$t_{f,bottom}$ [mm]	39	42.457592	0.633333	0.748586	0.013283	0.087505
--	---------------------	----	-----------	----------	----------	----------	----------

BRU0050	Parameter	Real value	Prediction	Norm. real value y	Norm. prediction \hat{y}	$(y-\hat{y})^2$	MSE
	L_2 [m]	0.471	0.965495	0.149977	0.376084	0.051124	0.020524
	L_3 [m]	2.481	3.016108	0.159258	0.281876	0.015035	
	L_4 [m]	2.311	2.660679	0.272089	0.338392	0.004396	
	L_5 [m]	5.515	4.815712	0.739772	0.645971	0.008799	
	L_7 [m]	0	0.146334	0.000000	0.013937	0.000194	
	L_8 [m]	2.41	1.967498	0.739962	0.570745	0.028634	
	b_{main} [m]	4.3	4.965699	0.172635	0.243795	0.005064	
	n_{main} [-]	5	5.455898	0.272727	0.314173	0.001718	
	n_{cross} [-]	6	5.978617	0.250000	0.248218	0.000003	
	n_{rib} [-]	60	36.103582	0.705882	0.424748	0.079037	
	H_{bottom} [mm]	1041	1046.833208	0.388710	0.398118	0.000089	
	W_{bottom} [mm]	288	351.831724	0.000000	0.301093	0.090657	
	$t_{w,bottom}$ [mm]	19	17.576463	0.250000	0.199159	0.002585	
	$t_{f,bottom}$ [mm]	33	32.972468	0.433333	0.432416	0.000001	

BRU2038	Parameter	Real value	Prediction	Norm. real value y	Norm. prediction \hat{y}	$(y-\hat{y})^2$	MSE
	L_2 [m]	1.62	0.522487	0.675354	0.173519	0.251838	0.124882
	L_3 [m]	3.532	2.092647	0.400092	0.070267	0.108784	
	L_4 [m]	3.411	1.690794	0.480660	0.154493	0.106385	
	L_5 [m]	2.011	2.755102	0.269752	0.369564	0.009963	
	L_7 [m]	0	0.026168	0.000000	0.002492	0.000006	
	L_8 [m]	1.982	1.471049	0.576291	0.380898	0.038178	
	b_{main} [m]	6.88	3.701708	0.448423	0.108681	0.115425	
	n_{main} [-]	2	3.671044	0.000000	0.151913	0.023078	
	n_{cross} [-]	4	4.2004	0.083333	0.100033	0.000279	
	n_{rib} [-]	21	19.984334	0.247059	0.235110	0.000143	
	H_{bottom} [mm]	1200	829.341158	0.645161	0.047324	0.357409	
	W_{bottom} [mm]	400	267.725101	0.528302	-0.095636	0.389299	
	$t_{w,bottom}$ [mm]	12	11.302222	0.000000	-0.024921	0.000621	
	$t_{f,bottom}$ [mm]	40	22.329671	0.666667	0.077656	0.346934	

BRU0151	Parameter	Real value	Prediction	Norm. real value y	Norm. prediction \hat{y}	$(y-\hat{y})^2$	MSE
	L_2 [m]	1.05	0.794381	0.414723	0.297842	0.013661	0.010605
	L_3 [m]	2.665	2.689177	0.201421	0.206961	0.000031	
	L_4 [m]	1.041	2.30418	0.031286	0.270796	0.057365	
	L_5 [m]	3.981	4.237035	0.534004	0.568348	0.001180	
	L_7 [m]	0.25	0.074233	0.023810	0.007070	0.000280	
	L_8 [m]	1.469	1.828125	0.380115	0.517447	0.018860	
	b_{main} [m]	4.08	4.306321	0.149118	0.173311	0.000585	
	n_{main} [-]	6	4.744567	0.363636	0.249506	0.013026	
	n_{cross} [-]	5	5.044059	0.166667	0.170338	0.000013	
	n_{rib} [-]	27	29.192267	0.317647	0.343438	0.000665	
	H_{bottom} [mm]	1040	1006.53772	0.387097	0.333125	0.002913	
	W_{bottom} [mm]	350	330.308478	0.292453	0.199568	0.008628	
	$t_{w,bottom}$ [mm]	12	15.32469	0.000000	0.118739	0.014099	
	$t_{f,bottom}$ [mm]	26	29.930866	0.200000	0.331029	0.017169	

Fold 5

BRU0171	Parameter	Real value	Prediction	Norm. real value y	Norm. prediction \hat{y}	$(y-\hat{y})^2$	MSE
	L_2 [m]	0.88	0.566493	0.336991	0.193641	0.020549	0.043898
	L_3 [m]	2.33	2.500674	0.124656	0.163766	0.001530	
	L_4 [m]	2.33	1.998059	0.275692	0.212753	0.003961	
	L_5 [m]	4.035	3.63764	0.541247	0.487946	0.002841	
	L_7 [m]	0.23	0.019199	0.021905	0.001828	0.000403	
	L_8 [m]	1.61	1.748435	0.434034	0.486973	0.002803	
	b_{main} [m]	4.135	3.777143	0.154997	0.116744	0.001463	
	n_{main} [-]	4	3.74664	0.181818	0.158785	0.000531	
	n_{cross} [-]	5	4.575988	0.166667	0.131332	0.001249	
	n_{rib} [-]	19	21.972772	0.223529	0.258503	0.001223	
	H_{bottom} [mm]	1000	958.564459	0.322581	0.255749	0.004466	
	W_{bottom} [mm]	450	290.238817	0.764151	0.010560	0.567899	
	$t_{w,bottom}$ [mm]	15	13.162012	0.107143	0.041500	0.004309	
	$t_{f,bottom}$ [mm]	25	26.100982	0.166667	0.203366	0.001347	
BRU0173	Parameter	Real value	Prediction	Norm. real value y	Norm. prediction \hat{y}	$(y-\hat{y})^2$	MSE
	L_2 [m]	0.48	0.854275	0.154092	0.325229	0.029288	0.054856
	L_3 [m]	2.3	3.126845	0.117782	0.307251	0.035899	
	L_4 [m]	2.16	2.73903	0.243458	0.353248	0.012054	
	L_5 [m]	6.04	4.706313	0.810195	0.631296	0.032005	
	L_7 [m]	0.26	0.074435	0.024762	0.007089	0.000312	
	L_8 [m]	3.09	2.01966	1.000000	0.590692	0.167533	
	b_{main} [m]	5.435	4.539256	0.293960	0.198210	0.009168	
	n_{main} [-]	4	5.065562	0.181818	0.278687	0.009384	
	n_{cross} [-]	4	5.649951	0.083333	0.220829	0.018905	
	n_{rib} [-]	29	33.668842	0.341176	0.396104	0.003017	
	H_{bottom} [mm]	1420	1084.267187	1.000000	0.458495	0.293227	
	W_{bottom} [mm]	400	336.553556	0.528302	0.229026	0.089566	
	$t_{w,bottom}$ [mm]	15	16.734369	0.107143	0.169085	0.003837	
	$t_{f,bottom}$ [mm]	40	32.422653	0.666667	0.414088	0.063796	
BRU0155	Parameter	Real value	Prediction	Norm. real value y	Norm. prediction \hat{y}	$(y-\hat{y})^2$	MSE
	L_2 [m]	1.223	0.920009	0.493827	0.355285	0.019194	0.024053
	L_3 [m]	2.868	3.228732	0.247938	0.330599	0.006833	
	L_4 [m]	2.788	2.854995	0.362533	0.375236	0.000161	
	L_5 [m]	3.794	4.822624	0.508920	0.646898	0.019038	
	L_7 [m]	0.606	0.095473	0.057714	0.009093	0.002364	
	L_8 [m]	1.548	2.054449	0.410325	0.603996	0.037508	
	b_{main} [m]	3.055	4.78877	0.039551	0.224882	0.034348	
	n_{main} [-]	8	5.249657	0.545455	0.295423	0.062516	
	n_{cross} [-]	5	5.945639	0.166667	0.245470	0.006210	
	n_{rib} [-]	34	36.654882	0.400000	0.431234	0.000976	
	H_{bottom} [mm]	1013	1095.047537	0.343548	0.475883	0.017512	
	W_{bottom} [mm]	350	341.852418	0.292453	0.254021	0.001477	
	$t_{w,bottom}$ [mm]	12	17.049412	0.000000	0.180336	0.032521	
	$t_{f,bottom}$ [mm]	24	33.299126	0.133333	0.443304	0.096082	
BRU1787	Parameter	Real value	Prediction	Norm. real value y	Norm. prediction \hat{y}	$(y-\hat{y})^2$	MSE
	L_2 [m]		0.327081		0.084171		
	L_3 [m]		1.655343		-0.029940		
	L_4 [m]		1.124617		0.047140		
	L_5 [m]		1.7311		0.232207		
	L_7 [m]		0.00518		0.000493		
	L_8 [m]		1.17554		0.267893		
	b_{main} [m]	5.3	3.438086	0.279530	0.080501	0.039612	
	n_{main} [-]	2	2.529431	0.000000	0.048130	0.002317	
	n_{cross} [-]	12	3.940119	0.750000	0.078343	0.451123	
	n_{rib} [-]	0	13.548583	0.000000	0.159395	0.025407	
	H_{bottom} [mm]		581.415151		-0.352556		
	W_{bottom} [mm]		180.352465		-0.507771		
	$t_{w,bottom}$ [mm]		7.638053		-0.155784		

	$t_{f, \text{bottom}}$ [mm]	14.495087	-0.183497	0.129615
--	-----------------------------	-----------	-----------	----------

BRU0350	Parameter	Real value	Prediction	Norm. real value y	Norm. prediction \hat{y}	$(y-\hat{y})^2$	MSE
	L_2 [m]	0.143	0.800881	0.000000	0.300814	0.090489	0.157315
	L_3 [m]	1.786	3.002133	0.000000	0.278674	0.077659	
	L_4 [m]	1.786	2.575778	0.172545	0.322294	0.022425	
	L_5 [m]	2.218	4.509683	0.297518	0.604921	0.094496	
	L_7 [m]	0	0.057285	0.000000	0.005456	0.000030	
	L_8 [m]	1.34	1.971605	0.330784	0.572315	0.058337	
	b_{main} [m]	2.685	4.390247	0.000000	0.182282	0.033227	
	n_{main} [-]	13	4.747982	1.000000	0.249817	0.562775	
	n_{cross} [-]	3	5.423355	0.000000	0.201946	0.040782	
	n_{rib} [-]	82	31.667124	0.964706	0.372554	0.350643	
	H_{bottom} [mm]	1000	1065.418163	0.322581	0.428094	0.011133	
	W_{bottom} [mm]	310	329.060445	0.103774	0.193681	0.008083	
	$t_{w, \text{bottom}}$ [mm]	35	15.72364	0.821429	0.132987	0.473952	
	$t_{f, \text{bottom}}$ [mm]	50	31.546171	1.000000	0.384872	0.378382	

BRU0238	Parameter	Real value	Prediction	Norm. real value y	Norm. prediction \hat{y}	$(y-\hat{y})^2$	MSE
	L_2 [m]	1.21	1.049097	0.487883	0.414310	0.005413	0.030314
	L_3 [m]	3.72	3.442639	0.443171	0.379615	0.004039	
	L_4 [m]	3.53	3.114275	0.503223	0.424398	0.006213	
	L_5 [m]	3.9	5.082214	0.523139	0.681719	0.025148	
	L_7 [m]	0.45	0.149959	0.042857	0.014282	0.000817	
	L_8 [m]	1.52	2.125603	0.399618	0.631206	0.053633	
	b_{main} [m]	3.675	5.304456	0.105826	0.280006	0.030339	
	n_{main} [-]	8	5.678587	0.545455	0.334417	0.044537	
	n_{cross} [-]	4	6.566101	0.083333	0.297175	0.045728	
	n_{rib} [-]	42	42.225934	0.494118	0.496776	0.000007	
	H_{bottom} [mm]	900	1118.866552	0.161290	0.514301	0.124616	
	W_{bottom} [mm]	300	353.060582	0.056604	0.306890	0.062643	
	$t_{w, \text{bottom}}$ [mm]	16	18.081831	0.142857	0.217208	0.005528	
	$t_{f, \text{bottom}}$ [mm]	31	34.763137	0.366667	0.492105	0.015735	

BRU0487	Parameter	Real value	Prediction	Norm. real value y	Norm. prediction \hat{y}	$(y-\hat{y})^2$	MSE
	L_2 [m]	1	1.200454	0.391861	0.483518	0.008401	0.031090
	L_3 [m]	2.4	3.685665	0.140697	0.435304	0.086793	
	L_4 [m]	2.13	3.41502	0.237770	0.481422	0.059366	
	L_5 [m]	6.07	5.363188	0.814219	0.719408	0.008989	
	L_7 [m]	0.65	0.229054	0.061905	0.021815	0.001607	
	L_8 [m]	2.386	2.200496	0.730784	0.659846	0.005032	
	b_{main} [m]	4.15	5.990998	0.156601	0.353394	0.038727	
	n_{main} [-]	7	6.145235	0.454545	0.376840	0.006038	
	n_{cross} [-]	6	7.365448	0.250000	0.363787	0.012948	
	n_{rib} [-]	72	48.592198	0.847059	0.571673	0.075837	
	H_{bottom} [mm]	1000	1144.118276	0.322581	0.555029	0.054032	
	W_{bottom} [mm]	310	365.267143	0.103774	0.364468	0.067961	
	$t_{w, \text{bottom}}$ [mm]	19	19.336078	0.250000	0.262003	0.000144	
	$t_{f, \text{bottom}}$ [mm]	39	36.094767	0.633333	0.536492	0.009378	

F.3.2. Prediction inaccuracy

Fold 1

BRU0149	Parameter	Real value	Prediction	Inaccuracy [%]
	L ₂ [m]	0.485	0.126611	73.89
	L ₃ [m]	2.242	0.729545	67.46
	L ₄ [m]	1.53	0.373289	75.60
	L ₅ [m]	3.92	0.67806	82.70
	L ₇ [m]	0	0.00312	
	L ₈ [m]	1.628	0.518982	68.12
	b _{main} [m]	3.266	2.987767	8.52
	n _{main} [-]	4	2.458077	38.55
	n _{cross} [-]	3	3.283344	9.44
	n _{rib} [-]	13	4.859999	62.62
	H _{bottom} [mm]	864	136.165049	84.24
	W _{bottom} [mm]	390	50.943182	86.94
	t _{w, bottom} [mm]	20	2.701045	86.49
	t _{f, bottom} [mm]	40	3.911674	90.22

BRU0199	Parameter	Real value	Prediction	Inaccuracy [%]
	L ₂ [m]	1.04	0.855996	17.69
	L ₃ [m]	2.986	3.122543	4.57
	L ₄ [m]	2.07	2.846933	37.53
	L ₅ [m]	4.8125	4.918326	2.20
	L ₇ [m]	0	0.171058	
	L ₈ [m]	1.78	2.044347	14.85
	b _{main} [m]	3.6	4.473213	24.26
	n _{main} [-]	6	5.528872	7.85
	n _{cross} [-]	5	5.931254	18.63
	n _{rib} [-]	27	43.02016	59.33
	H _{bottom} [mm]	1060	1093.991678	3.21
	W _{bottom} [mm]	300	339.792041	13.26
	t _{w, bottom} [mm]	12	16.724567	39.37
	t _{f, bottom} [mm]	36	33.079595	8.11

BRU0324	Parameter	Real value	Prediction	Inaccuracy [%]
	L ₂ [m]	1.05	0.908097	13.51
	L ₃ [m]	2.893	3.214337	11.11
	L ₄ [m]	2.474	2.961377	19.70
	L ₅ [m]	4.673	5.081006	8.73
	L ₇ [m]	0.134	0.201566	50.42
	L ₈ [m]	1.834	2.104214	14.73
	b _{main} [m]	3.6	4.588534	27.46
	n _{main} [-]	6	5.779436	3.68
	n _{cross} [-]	5	6.252169	25.04
	n _{rib} [-]	22	46.176555	109.89
	H _{bottom} [mm]	1100	1108.233246	0.75
	W _{bottom} [mm]	350	344.825402	1.48
	t _{w, bottom} [mm]	12	17.178243	43.15

	$t_{f,bottom}$ [mm]	26	34.036798	30.91
--	---------------------	----	-----------	-------

BRU5047	Parameter	Real value	Prediction	Inaccuracy [%]
	L_2 [m]	2	0.443048	77.85
	L_3 [m]	6.15	2.087511	66.06
	L_4 [m]	6.15	1.613417	73.77
	L_5 [m]	0	3.171832	
	L_7 [m]	0	0.027993	
	L_8 [m]	2	1.431492	28.43
	b_{main} [m]	6.9	3.568544	48.28
	n_{main} [-]	2	3.734029	86.70
	n_{cross} [-]	5	3.966396	20.67
	n_{rib} [-]	15	18.023151	20.15
	H_{bottom} [mm]	800	866.043108	8.26
	W_{bottom} [mm]	400	261.362729	34.66
	$t_{w,bottom}$ [mm]	18	11.861014	34.11
	$t_{f,bottom}$ [mm]	30	21.48652	28.38

BRU1788	Parameter	Real value	Prediction	Inaccuracy [%]
	L_2 [m]		0.383924	
	L_3 [m]		1.881206	
	L_4 [m]		1.392065	
	L_5 [m]		2.806351	
	L_7 [m]		0.019618	
	L_8 [m]		1.304351	
	b_{main} [m]	5.7	3.448598	39.50
	n_{main} [-]	2	3.48476	74.24
	n_{cross} [-]	7	3.785813	45.92
	n_{rib} [-]	0	14.836239	
	H_{bottom} [mm]		801.047	
	W_{bottom} [mm]		241.49921	
	$t_{w,bottom}$ [mm]		10.796861	
	$t_{f,bottom}$ [mm]		19.047914	

BRU0272	Parameter	Real value	Prediction	Inaccuracy [%]
	L_2 [m]		0.908491	
	L_3 [m]		3.218265	
	L_4 [m]		2.964429	
	L_5 [m]		5.125731	
	L_7 [m]		0.202077	
	L_8 [m]		2.123125	
	b_{main} [m]	12.04	4.576823	61.99
	n_{main} [-]	2	5.817511	190.88
	n_{cross} [-]	7	6.171557	11.83
	n_{rib} [-]	30	46.447188	54.82
	H_{bottom} [mm]		1104.105688	

	W_{bottom} [mm]	341.672849	
	$t_{w,\text{bottom}}$ [mm]	17.149178	
	$t_{f,\text{bottom}}$ [mm]	33.985085	

BRU2023	Parameter	Real value	Prediction	Inaccuracy [%]
	L_2 [m]	1.041	0.503713	51.61
	L_3 [m]	2.934	2.281262	22.25
	L_4 [m]	2.76	1.8308	33.67
	L_5 [m]	2.35	3.482765	48.20
	L_7 [m]	0.11	0.039351	64.23
	L_8 [m]	2.15	1.53946	28.40
	b_{main} [m]	11.1	3.700537	66.66
	n_{main} [-]	2	3.980195	99.01
	n_{cross} [-]	3	4.196658	39.89
	n_{rib} [-]	32	21.500393	32.81
	H_{bottom} [mm]	1000	917.163146	8.28
	W_{bottom} [mm]	300	278.404958	7.20
	$t_{w,\text{bottom}}$ [mm]	40	12.745919	68.14
	$t_{f,\text{bottom}}$ [mm]	30	23.698253	21.01

Fold 2

BRU0382	Parameter	Real value	Prediction	Inaccuracy [%]
	L ₂ [m]	1.05	0.95676	8.88
	L ₃ [m]	2.893	3.245588	12.19
	L ₄ [m]	2.474	2.905424	17.44
	L ₅ [m]	4.673	4.950057	5.93
	L ₇ [m]	0.134	0.142482	6.33
	L ₈ [m]	1.834	2.090389	13.98
	b _{main} [m]	3.6	5.060104	40.56
	n _{main} [-]	6	5.671904	5.47
	n _{cross} [-]	5	6.482735	29.65
	n _{rib} [-]	22	42.962705	95.29
	H _{bottom} [mm]	1100	1113.070758	1.19
	W _{bottom} [mm]	350	347.173001	0.81
	t _{w,bottom} [mm]	12	18.020438	50.17
	t _{f,bottom} [mm]	26	36.099101	38.84

BRU5046	Parameter	Real value	Prediction	Inaccuracy [%]
	L ₂ [m]	0.93	0.181448	80.49
	L ₃ [m]	3.82	1.100801	71.18
	L ₄ [m]	3.82	0.681809	82.15
	L ₅ [m]	1.7	0.816497	51.97
	L ₇ [m]	0	0.005734	
	L ₈ [m]	0.475	0.894113	88.23
	b _{main} [m]	4.45	3.279112	26.31
	n _{main} [-]	3	2.61778	12.74
	n _{cross} [-]	4	3.653539	8.66
	n _{rib} [-]	16	10.912033	31.80
	H _{bottom} [mm]	920	297.600683	67.65
	W _{bottom} [mm]	298	101.884259	65.81
	t _{w,bottom} [mm]	16	4.965285	68.97
	t _{f,bottom} [mm]	30	7.577184	74.74

BRU0239	Parameter	Real value	Prediction	Inaccuracy [%]
	L ₂ [m]	1.16	1.094692	5.63
	L ₃ [m]	2.522	3.537219	40.25
	L ₄ [m]	2.328	3.285088	41.11
	L ₅ [m]	4.125	5.36815	30.14
	L ₇ [m]	0.4	0.25111	37.22
	L ₈ [m]	1.33	2.231334	67.77
	b _{main} [m]	3.675	5.913882	60.92
	n _{main} [-]	8	6.328327	20.90
	n _{cross} [-]	4	7.6779	91.95
	n _{rib} [-]	66	52.571156	20.35
	H _{bottom} [mm]	900	1147.384401	27.49
	W _{bottom} [mm]	300	357.13676	19.05
	t _{w,bottom} [mm]	16	19.728172	23.30

	$t_{f,bottom}$ [mm]	31	38.015855	22.63
--	---------------------	----	-----------	-------

BRU0345	Parameter	Real value	Prediction	Inaccuracy [%]
	L_2 [m]	0.388	0.612072	57.75
	L_3 [m]	2.173	2.459059	13.16
	L_4 [m]	1.975	1.937208	1.91
	L_5 [m]	5.66	3.487643	38.38
	L_7 [m]	0	0.029069	
	L_8 [m]	2.18	1.69478	22.26
	b_{main} [m]	4.33	3.816483	11.86
	n_{main} [-]	4	4.155238	3.88
	n_{cross} [-]	6	4.662722	22.29
	n_{rib} [-]	40	23.767591	40.58
	H_{bottom} [mm]	1000	963.201085	3.68
	W_{bottom} [mm]	297	302.17074	1.74
	$t_{w,bottom}$ [mm]	14	13.473984	3.76
	$t_{f,bottom}$ [mm]	26	28.386161	9.18

BRU0349	Parameter	Real value	Prediction	Inaccuracy [%]
	L_2 [m]	0.388	0.612072	57.75
	L_3 [m]	2.173	2.459059	13.16
	L_4 [m]	1.975	1.937208	1.91
	L_5 [m]	5.66	3.487643	38.38
	L_7 [m]	0	0.029069	
	L_8 [m]	2.18	1.69478	22.26
	b_{main} [m]	4.33	3.816483	11.86
	n_{main} [-]	4	4.155238	3.88
	n_{cross} [-]	6	4.662722	22.29
	n_{rib} [-]	40	23.767591	40.58
	H_{bottom} [mm]	1000	963.201085	3.68
	W_{bottom} [mm]	297	302.17074	1.74
	$t_{w,bottom}$ [mm]	14	13.473984	3.76
	$t_{f,bottom}$ [mm]	26	28.386161	9.18

BRU0356	Parameter	Real value	Prediction	Inaccuracy [%]
	L_2 [m]	0.44	0.179956	59.10
	L_3 [m]	3.035	1.092371	64.01
	L_4 [m]	2.82	0.68033	75.87
	L_5 [m]	4.475	0.801608	82.09
	L_7 [m]	0.26	0.006332	97.56
	L_8 [m]	2.1	0.885899	57.81
	b_{main} [m]	5.5	3.306317	39.89
	n_{main} [-]	2	2.619821	30.99
	n_{cross} [-]	6	3.668874	38.85
	n_{rib} [-]	10	11.223576	12.24
	H_{bottom} [mm]	1160	281.567202	75.73

	W_{bottom} [mm]	500	97.038669	80.59
	$t_{w,\text{bottom}}$ [mm]	20	4.863659	75.68
	$t_{f,\text{bottom}}$ [mm]	20	7.337076	63.31

BRU0266	Parameter	Real value	Prediction	Inaccuracy [%]
	L_2 [m]	2.33	0.704245	69.77
	L_3 [m]	3.028	2.681778	11.43
	L_4 [m]	2.64	2.196751	16.79
	L_5 [m]	3.785	3.958955	4.60
	L_7 [m]	0.472	0.042227	91.05
	L_8 [m]	1.851	1.81249	2.08
	b_{main} [m]	3.07	4.020724	30.97
	n_{main} [-]	6	4.52938	24.51
	n_{cross} [-]	4	4.989621	24.74
	n_{rib} [-]	25	27.692441	10.77
	H_{bottom} [mm]	931	1025.410816	10.14
	W_{bottom} [mm]	400	320.820709	19.79
	$t_{w,\text{bottom}}$ [mm]	15	14.789586	1.40
	$t_{f,\text{bottom}}$ [mm]	25	31.173827	24.70

Fold 3

BRU0246	Parameter	Real value	Prediction	Inaccuracy [%]
	L ₂ [m]	0.876	0.248292	71.66
	L ₃ [m]	2.628	1.711379	34.88
	L ₄ [m]	0.876	1.280363	46.16
	L ₅ [m]	2.8	1.209839	56.79
	L ₇ [m]	0	0.008321	
	L ₈ [m]	1.034	0.916743	11.34
	b _{main} [m]	2.87	3.325821	15.88
	n _{main} [-]	6	2.480185	58.66
	n _{cross} [-]	3	3.828319	27.61
	n _{rib} [-]	29	9.875073	65.95
	H _{bottom} [mm]		761.423436	
	W _{bottom} [mm]		249.723807	
	t _{w,bottom} [mm]		10.223986	
	t _{f,bottom} [mm]		17.623155	

BRU1939	Parameter	Real value	Prediction	Inaccuracy [%]
	L ₂ [m]		0.138799	
	L ₃ [m]		0.92955	
	L ₄ [m]		0.672239	
	L ₅ [m]		0.504112	
	L ₇ [m]		0.004501	
	L ₈ [m]		0.401943	
	b _{main} [m]	5.65	3.182995	43.66
	n _{main} [-]	2	2.255503	12.78
	n _{cross} [-]	15	3.533281	76.44
	n _{rib} [-]	0	6.571553	
	H _{bottom} [mm]		385.864546	
	W _{bottom} [mm]		134.761403	
	t _{w,bottom} [mm]		5.957507	
	t _{f,bottom} [mm]		8.950947	

BRU2190	Parameter	Real value	Prediction	Inaccuracy [%]
	L ₂ [m]		1.732109	
	L ₃ [m]		3.985527	
	L ₄ [m]		4.061152	
	L ₅ [m]		6.616239	
	L ₇ [m]		0.614963	
	L ₈ [m]	1.221	2.687356	120.09
	b _{main} [m]	7.3	8.340483	14.25
	n _{main} [-]	2	9.651784	382.59
	n _{cross} [-]	14	8.319657	40.57
	n _{rib} [-]	0	77.757647	
	H _{bottom} [mm]		1274.196031	
	W _{bottom} [mm]		416.310668	
	t _{w,bottom} [mm]		21.658918	

	$t_{f,bottom}$ [mm]	44.155898	
--	---------------------	-----------	--

BRU0491	Parameter	Real value	Prediction	Inaccuracy [%]
	L_2 [m]	0.665	1.139453	71.35
	L_3 [m]	4.41	3.265178	25.96
	L_4 [m]	4.313	3.085535	28.46
	L_5 [m]	5.112	5.417931	5.98
	L_7 [m]	0	0.308462	
	L_8 [m]	2.106	2.212418	5.05
	b_{main} [m]	4.32	5.117202	18.45
	n_{main} [-]	4	6.545333	63.63
	n_{cross} [-]	7	6.111513	12.69
	n_{rib} [-]	44	49.528983	12.57
	H_{bottom} [mm]	1200	1114.179631	7.15
	W_{bottom} [mm]	310	357.867963	15.44
	$t_{w,bottom}$ [mm]	19	18.080803	4.84
	$t_{f,bottom}$ [mm]	39	35.362967	9.33

BRU0101	Parameter	Real value	Prediction	Inaccuracy [%]
	L_2 [m]	1.275	0.360572	71.72
	L_3 [m]	4.078	2.110975	48.24
	L_4 [m]	1.35	1.664827	23.32
	L_5 [m]	4.269	1.999387	53.16
	L_7 [m]	0	0.016682	
	L_8 [m]	1.977	1.252812	36.63
	b_{main} [m]	2.84	3.44901	21.44
	n_{main} [-]	6	2.82362	52.94
	n_{cross} [-]	3	4.095658	36.52
	n_{rib} [-]	23	13.399325	41.74
	H_{bottom} [mm]	1000	891.570672	10.84
	W_{bottom} [mm]	350	288.071432	17.69
	$t_{w,bottom}$ [mm]	20	12.098591	39.51
	$t_{f,bottom}$ [mm]	40	22.214158	44.46

BRU0318	Parameter	Real value	Prediction	Inaccuracy [%]
	L_2 [m]	0.388	0.713733	83.95
	L_3 [m]	2.173	2.658815	22.36
	L_4 [m]	1.975	2.350271	19.00
	L_5 [m]	5.66	4.069222	28.11
	L_7 [m]	0	0.09321	
	L_8 [m]	2.18	1.795175	17.65
	b_{main} [m]	4.33	3.919877	9.47
	n_{main} [-]	4	4.445644	11.14
	n_{cross} [-]	6	4.909798	18.17
	n_{rib} [-]	44	26.911102	38.84
	H_{bottom} [mm]	1000	1001.416093	0.14

	W_{bottom} [mm]	297	317.455387	6.89
	$t_{w,\text{bottom}}$ [mm]	14	14.360334	2.57
	$t_{f,\text{bottom}}$ [mm]	26	28.950982	11.35

BRU0346	Parameter	Real value	Prediction	Inaccuracy [%]
	L_2 [m]	0.737	0.942731	27.91
	L_3 [m]	2.217	3.094147	39.56
	L_4 [m]	3.292	2.817146	14.42
	L_5 [m]	5.218	4.618504	11.49
	L_7 [m]	0	0.190071	
	L_8 [m]	1.846	2.033365	10.15
	b_{main} [m]	4.14	4.807378	16.12
	n_{main} [-]	6	5.2411	12.65
	n_{cross} [-]	5	5.627174	12.54
	n_{rib} [-]	35	42.125024	20.36
	H_{bottom} [mm]	1000	1087.303989	8.73
	W_{bottom} [mm]	300	352.216894	17.41
	$t_{w,\text{bottom}}$ [mm]	18	17.677024	1.79
	$t_{f,\text{bottom}}$ [mm]	34	33.143119	2.52

Fold 4

BRU0357	Parameter	Real value	Prediction	Inaccuracy [%]
	L ₂ [m]	0.855	0.953504	11.52
	L ₃ [m]	3.887	2.976961	23.41
	L ₄ [m]	4.11	2.616952	36.33
	L ₅ [m]	5.301	4.830537	8.87
	L ₇ [m]	0.377	0.140567	62.71
	L ₈ [m]	2.05	1.966029	4.10
	b _{main} [m]	4.32	4.8701	12.73
	n _{main} [-]	4	5.41689	35.42
	n _{cross} [-]	7	5.840571	16.56
	n _{rib} [-]	54	35.436185	34.38
	H _{bottom} [mm]	1200	1046.332304	12.81
	W _{bottom} [mm]	300	348.881602	16.29
	t _{w,bottom} [mm]	16	17.278938	7.99
	t _{f,bottom} [mm]	20	32.838012	64.19

BRU0274	Parameter	Real value	Prediction	Inaccuracy [%]
	L ₂ [m]	0.35	1.477429	322.12
	L ₃ [m]	3.191	3.954246	23.92
	L ₄ [m]	3.107	3.734606	20.20
	L ₅ [m]	5.743	5.694976	0.84
	L ₇ [m]	0.277	0.488904	76.50
	L ₈ [m]	2.633	2.308128	12.34
	b _{main} [m]	3.8	7.7258	103.31
	n _{main} [-]	7	7.848619	12.12
	n _{cross} [-]	7	9.93152	41.88
	n _{rib} [-]	85	56.404613	33.64
	H _{bottom} [mm]	1200	1140.295818	4.98
	W _{bottom} [mm]	310	404.45347	30.47
	t _{w,bottom} [mm]	19	24.340584	28.11
	t _{f,bottom} [mm]	39	40.030954	2.64

BRU0314	Parameter	Real value	Prediction	Inaccuracy [%]
	L ₂ [m]	0.917	0.955576	4.21
	L ₃ [m]	3.045	2.989629	1.82
	L ₄ [m]	3.045	2.631158	13.59
	L ₅ [m]	4.93	4.811254	2.41
	L ₇ [m]	0.355	0.141284	60.20
	L ₈ [m]	1.89	1.96385	3.91
	b _{main} [m]	4.125	4.900889	18.81
	n _{main} [-]	5	5.419503	8.39
	n _{cross} [-]	5	5.885333	17.71
	n _{rib} [-]	24	35.608245	48.37
	H _{bottom} [mm]	1130	1045.923022	7.44
	W _{bottom} [mm]	300	349.979346	16.66
	t _{w,bottom} [mm]	19	17.380332	8.52

	$t_{f, \text{bottom}}$ [mm]	36	32.843451	8.77
--	-----------------------------	----	-----------	------

BRU0485	Parameter	Real value	Prediction	Inaccuracy [%]
	L_2 [m]	0.525	1.686028	221.15
	L_3 [m]	4.44	4.332399	2.42
	L_4 [m]	3.75	4.179532	11.45
	L_5 [m]	7.455	5.871833	21.24
	L_7 [m]	0	0.585231	
	L_8 [m]	2.7	2.442956	9.52
	b_{main} [m]	4.08	9.00576	120.73
	n_{main} [-]	7	8.971728	28.17
	n_{cross} [-]	9	11.654657	29.50
	n_{rib} [-]	73	63.883136	12.49
	H_{bottom} [mm]	1400	1177.020678	15.93
	W_{bottom} [mm]	310	422.470969	36.28
	$t_{w, \text{bottom}}$ [mm]	19	27.126783	42.77
	$t_{f, \text{bottom}}$ [mm]	39	42.457592	8.87

BRU0050	Parameter	Real value	Prediction	Inaccuracy [%]
	L_2 [m]	0.471	0.965495	104.99
	L_3 [m]	2.481	3.016108	21.57
	L_4 [m]	2.311	2.660679	15.13
	L_5 [m]	5.515	4.815712	12.68
	L_7 [m]	0	0.146334	
	L_8 [m]	2.41	1.967498	18.36
	b_{main} [m]	4.3	4.965699	15.48
	n_{main} [-]	5	5.455898	9.12
	n_{cross} [-]	6	5.978617	0.36
	n_{rib} [-]	60	36.103582	39.83
	H_{bottom} [mm]	1041	1046.833208	0.56
	W_{bottom} [mm]	288	351.831724	22.16
	$t_{w, \text{bottom}}$ [mm]	19	17.576463	7.49
	$t_{f, \text{bottom}}$ [mm]	33	32.972468	0.08

BRU2038	Parameter	Real value	Prediction	Inaccuracy [%]
	L_2 [m]	1.62	0.522487	67.75
	L_3 [m]	3.532	2.092647	40.75
	L_4 [m]	3.411	1.690794	50.43
	L_5 [m]	2.011	2.755102	37.00
	L_7 [m]	0	0.026168	
	L_8 [m]	1.982	1.471049	25.78
	b_{main} [m]	6.88	3.701708	46.20
	n_{main} [-]	2	3.671044	83.55
	n_{cross} [-]	4	4.2004	5.01
	n_{rib} [-]	21	19.984334	4.84
	H_{bottom} [mm]	1200	829.341158	30.89

	W_{bottom} [mm]	400	267.725101	33.07
	$t_{w,\text{bottom}}$ [mm]	12	11.302222	5.81
	$t_{f,\text{bottom}}$ [mm]	40	22.329671	44.18

BRU0151	Parameter	Real value	Prediction	Inaccuracy [%]
	L_2 [m]	1.05	0.794381	24.34
	L_3 [m]	2.665	2.689177	0.91
	L_4 [m]	1.041	2.30418	121.34
	L_5 [m]	3.981	4.237035	6.43
	L_7 [m]	0.25	0.074233	70.31
	L_8 [m]	1.469	1.828125	24.45
	b_{main} [m]	4.08	4.306321	5.55
	n_{main} [-]	6	4.744567	20.92
	n_{cross} [-]	5	5.044059	0.88
	n_{rib} [-]	27	29.192267	8.12
	H_{bottom} [mm]	1040	1006.53772	3.22
	W_{bottom} [mm]	350	330.308478	5.63
	$t_{w,\text{bottom}}$ [mm]	12	15.32469	27.71
	$t_{f,\text{bottom}}$ [mm]	26	29.930866	15.12

Fold 5

BRU0171	Parameter	Real value	Prediction	Inaccuracy [%]
	L ₂ [m]	0.88	0.566493	35.63
	L ₃ [m]	2.33	2.500674	7.33
	L ₄ [m]	2.33	1.998059	14.25
	L ₅ [m]	4.035	3.63764	9.85
	L ₇ [m]	0.23	0.019199	91.65
	L ₈ [m]	1.61	1.748435	8.60
	b _{main} [m]	4.135	3.777143	8.65
	n _{main} [-]	4	3.74664	6.33
	n _{cross} [-]	5	4.575988	8.48
	n _{rib} [-]	19	21.972772	15.65
	H _{bottom} [mm]	1000	958.564459	4.14
	W _{bottom} [mm]	450	290.238817	35.50
	t _{w,bottom} [mm]	15	13.162012	12.25
	t _{f,bottom} [mm]	25	26.100982	4.40

BRU0173	Parameter	Real value	Prediction	Inaccuracy [%]
	L ₂ [m]	0.48	0.854275	77.97
	L ₃ [m]	2.3	3.126845	35.95
	L ₄ [m]	2.16	2.73903	26.81
	L ₅ [m]	6.04	4.706313	22.08
	L ₇ [m]	0.26	0.074435	71.37
	L ₈ [m]	3.09	2.01966	34.64
	b _{main} [m]	5.435	4.539256	16.48
	n _{main} [-]	4	5.065562	26.64
	n _{cross} [-]	4	5.649951	41.25
	n _{rib} [-]	29	33.668842	16.10
	H _{bottom} [mm]	1420	1084.267187	23.64
	W _{bottom} [mm]	400	336.553556	15.86
	t _{w,bottom} [mm]	15	16.734369	11.56
	t _{f,bottom} [mm]	40	32.422653	18.94

BRU0155	Parameter	Real value	Prediction	Inaccuracy [%]
	L ₂ [m]	1.223	0.920009	24.77
	L ₃ [m]	2.868	3.228732	12.58
	L ₄ [m]	2.788	2.854995	2.40
	L ₅ [m]	3.794	4.822624	27.11
	L ₇ [m]	0.606	0.095473	84.25
	L ₈ [m]	1.548	2.054449	32.72
	b _{main} [m]	3.055	4.78877	56.75
	n _{main} [-]	8	5.249657	34.38
	n _{cross} [-]	5	5.945639	18.91
	n _{rib} [-]	34	36.654882	7.81
	H _{bottom} [mm]	1013	1095.047537	8.10
	W _{bottom} [mm]	350	341.852418	2.33
	t _{w,bottom} [mm]	12	17.049412	42.08

	$t_{f,bottom}$ [mm]	24	33.299126	38.75
--	---------------------	----	-----------	-------

BRU1787	Parameter	Real value	Prediction	Inaccuracy [%]
	L_2 [m]		0.327081	
	L_3 [m]		1.655343	
	L_4 [m]		1.124617	
	L_5 [m]		1.7311	
	L_7 [m]		0.00518	
	L_8 [m]		1.17554	
	b_{main} [m]	5.3	3.438086	35.13
	n_{main} [-]	2	2.529431	26.47
	n_{cross} [-]	12	3.940119	67.17
	n_{rib} [-]	0	13.548583	
	H_{bottom} [mm]		581.415151	
	W_{bottom} [mm]		180.352465	
	$t_{w,bottom}$ [mm]		7.638053	
	$t_{f,bottom}$ [mm]		14.495087	

BRU0350	Parameter	Real value	Prediction	Inaccuracy [%]
	L_2 [m]	0.143	0.800881	460.06
	L_3 [m]	1.786	3.002133	68.09
	L_4 [m]	1.786	2.575778	44.22
	L_5 [m]	2.218	4.509683	103.32
	L_7 [m]	0	0.057285	
	L_8 [m]	1.34	1.971605	47.13
	b_{main} [m]	2.685	4.390247	63.51
	n_{main} [-]	13	4.747982	63.48
	n_{cross} [-]	3	5.423355	80.78
	n_{rib} [-]	82	31.667124	61.38
	H_{bottom} [mm]	1000	1065.418163	6.54
	W_{bottom} [mm]	310	329.060445	6.15
	$t_{w,bottom}$ [mm]	35	15.72364	55.08
	$t_{f,bottom}$ [mm]	50	31.546171	36.91

BRU0238	Parameter	Real value	Prediction	Inaccuracy [%]
	L_2 [m]	1.21	1.049097	13.30
	L_3 [m]	3.72	3.442639	7.46
	L_4 [m]	3.53	3.114275	11.78
	L_5 [m]	3.9	5.082214	30.31
	L_7 [m]	0.45	0.149959	66.68
	L_8 [m]	1.52	2.125603	39.84
	b_{main} [m]	3.675	5.304456	44.34
	n_{main} [-]	8	5.678587	29.02
	n_{cross} [-]	4	6.566101	64.15
	n_{rib} [-]	42	42.225934	0.54
	H_{bottom} [mm]	900	1118.866552	24.32

	W_{bottom} [mm]	300	353.060582	17.69
	$t_{w,\text{bottom}}$ [mm]	16	18.081831	13.01
	$t_{f,\text{bottom}}$ [mm]	31	34.763137	12.14

BRU0487	Parameter	Real value	Prediction	Inaccuracy [%]
	L_2 [m]	1	1.200454	20.05
	L_3 [m]	2.4	3.685665	53.57
	L_4 [m]	2.13	3.41502	60.33
	L_5 [m]	6.07	5.363188	11.64
	L_7 [m]	0.65	0.229054	64.76
	L_8 [m]	2.386	2.200496	7.77
	b_{main} [m]	4.15	5.990998	44.36
	n_{main} [-]	7	6.145235	12.21
	n_{cross} [-]	6	7.365448	22.76
	n_{rib} [-]	72	48.592198	32.51
	H_{bottom} [mm]	1000	1144.118276	14.41
	W_{bottom} [mm]	310	365.267143	17.83
	$t_{w,\text{bottom}}$ [mm]	19	19.336078	1.77
	$t_{f,\text{bottom}}$ [mm]	39	36.094767	7.45

F.4. SCIA Model validation

F.4.1. MatrixFrame models of main beams

Case 1



Figure F.2: 2D model of loaded main beam in validation case one.

Case 2

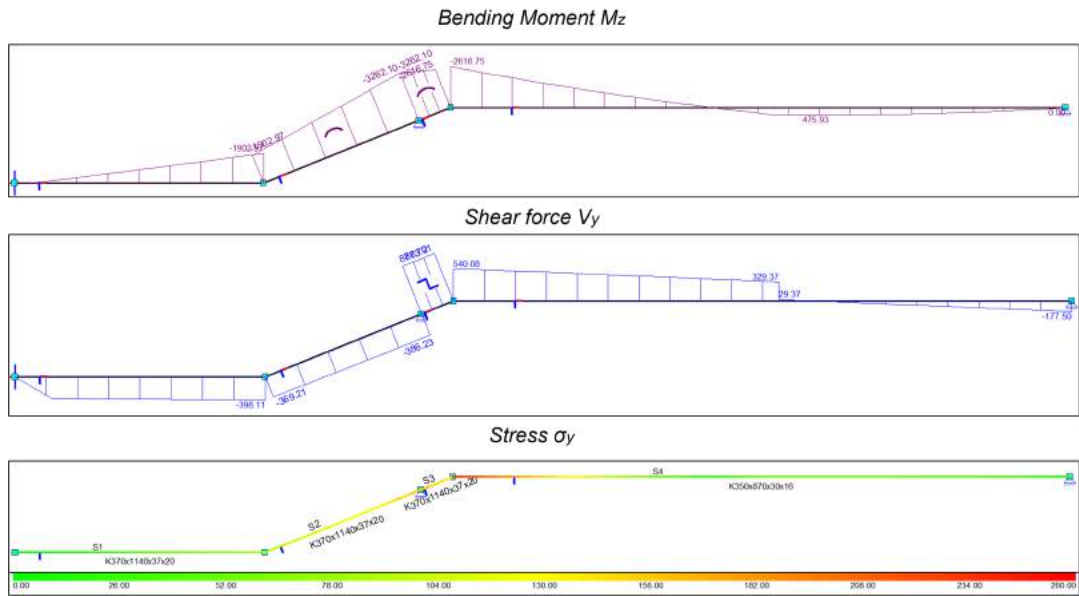


Figure F.3: 2D model of loaded main beam in validation case two.

Case 3

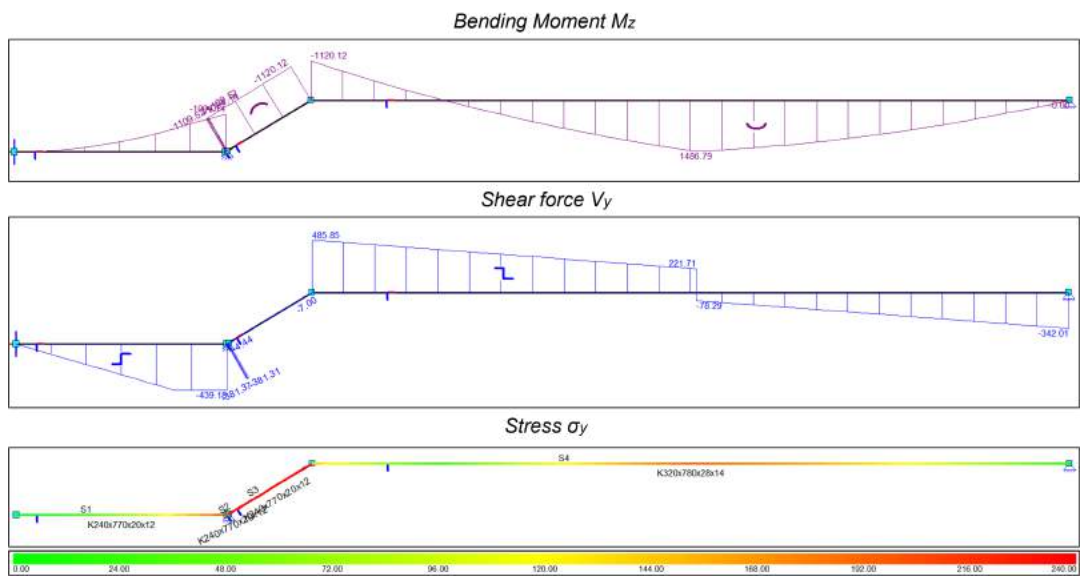


Figure F.4: 2D model of loaded main beam in validation case three.

Case 4

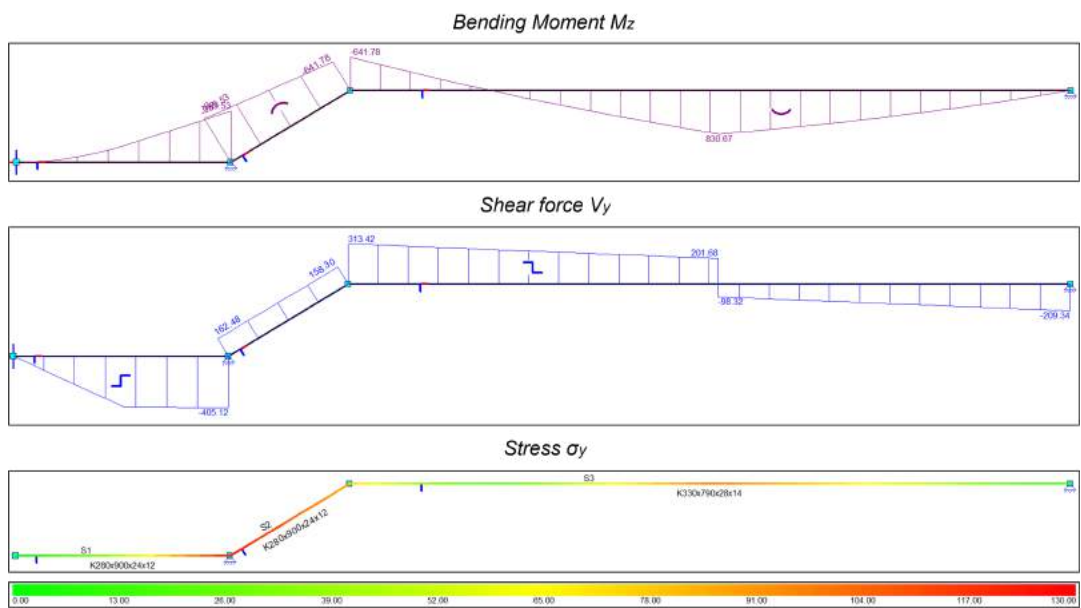


Figure F.5: 2D model of loaded main beam in validation case four.

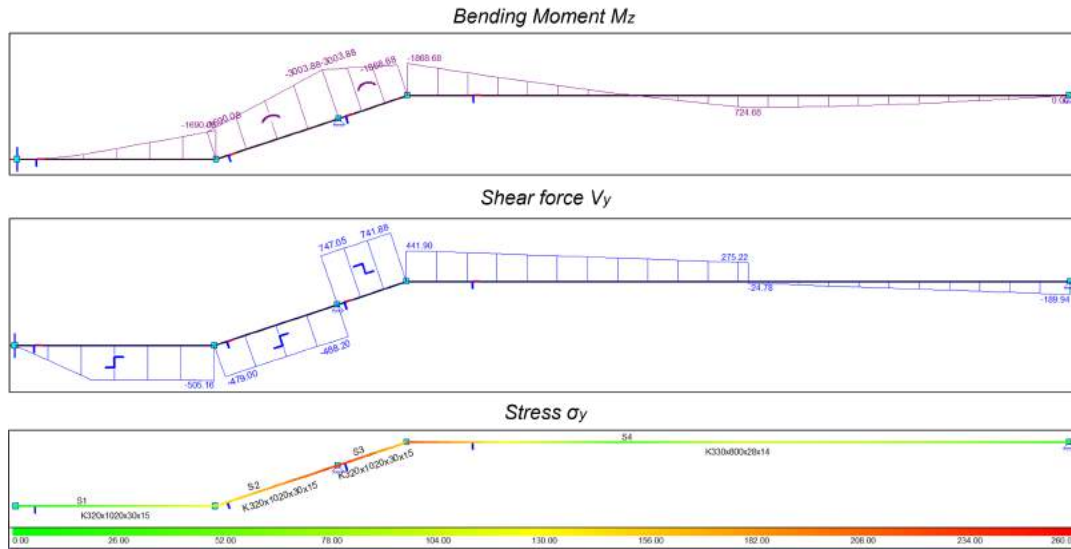
Case 5

Figure F.6: 2D model of loaded main beam in validation case five.

F.4.2. Hand calculation for loading on cross beam

This section explains how the moment, shear force and stress is calculated for cross sections E and F in the cross beam, per load case.

Self-weight

The distributed load of the self-weight of the cross beam is calculated with:

$$q_{selfweight} = \rho_{steel} \cdot A_{cross} [kN/m] \quad (F.1)$$

In which the steel density is equal to 78.5 kN/m^3 and A_{cross} is equal to the cross sectional area of the cross beam. The self-weight of the beam leads to the following moments and shear forces in cross sections E and F.

$$M_E = -\frac{q_{self} \cdot b_{main}^2}{24} [kNm] \quad (F.2)$$

$$M_F = \frac{q_{self} \cdot b_{main}^2}{12} [kNm] \quad (F.3)$$

$$V_E = 0 \quad (F.4)$$

$$V_F = -\frac{b_{main} \cdot q_{self}}{2} [kN] \quad (F.5)$$

Surface load bridge deck

The same surface load of 5 kN/m^2 can be taken up by the cross beams. Transforming the area load to a line load is done by the following equation.

$$q_{deck} = \frac{L_1}{(n_{cross} - 1)} \cdot q_{deck} [kN/m] \quad (F.6)$$

The occurring moments and shear forces are calculated with equation F.31 to F.34, where q_{self} can be replaced with the obtained value for the deck load q_{deck} .

Point load

The point load in the middle of the cross beam, leads to the following moments and shear forces.

$$M_E = -\frac{F_{cross} \cdot b_{main}}{8} [kNm] \quad (F.7)$$

$$M_F = -M_E [kNm] \quad (F.8)$$

$$V_E = \pm \frac{F_{cross}}{2} [kN] \quad (F.9)$$

$$V_F = -\frac{F_{cross}}{2} [kN] \quad (F.10)$$

F.4.3. Excel sheets hand calculations

Case 1

Input		
Parameter	Value	Unit
L1	6.25	m
W1	23.92	m
L2 [m]	0.55	m
L3 [m]	2.393	m
L4 [m]	1.921	m
L5 [m]	3.387	m
L6 [m]	1.94	m
L7 [m]	0.029	m
L8 [m]	1.624	m
bmain [m]	5.6	m
ncross [-]	4	
nrrib [-]	21	
Izz,top [x104 mm4]	615123.73	[x104 mm4]
Izz,cross [x104 mm4]	108626.25	[x104 mm4]
Izz,rib [x104 mm4]	5085.1	[x104 mm4]
Hbottom [mm]	940	mm
Wbottom [mm]	290	mm
tw,bottom [mm]	13	mm
tf,bottom [mm]	26	mm
b _{out}	1.1	m
A _{cross}	0.02128	m ²
H _{top}	900	mm
H _{cross}	540	mm

Properties		
Steel Density	78.5	kN/m ³
W _{mainbeam}	1366.941622	[x10 ⁶ mm ³]
W _{crossbeam}	402.3194444	[x10 ⁶ mm ³]

Cross beam		
Selfweight		Surface load deck
A _{cross}	0.02128 [m ²]	Q _{deck} 5 [kN/m ²]
Q _{selfweight}	1.67048 [kN/m]	Q _{deck} 10.41667 [kN/m]
Fa	[kN]	Me -13.6111 [kNm]
Fb	[kN]	Mf 27.22222 [kNm]
Me	-2.18276 [kNm]	Ve 0 [kN]
Mf	4.365521 [kNm]	Vf -29.1667 [kN]
Ve	0 [kN]	
Vf	-4.67734 [kN]	

Point load	
F	200 [kN]
Fa	100 [kN]
Fb	100 [kN]
Me	-140 [kNm]
Mf	0 [kNm]
Ve	100 [kN]
Vf	-100 [kN]

Result	
Me	-155.794 [kNm]
Mf	31.56774 [kNm]
Ve	100
Vf	-133.844

σ _{max,e}	-38.7239 [Mpa]
σ _{max,f}	7.851409 [Mpa]

Figure F.7: Hand calculation validation case one.

Case 2

Input		
Parameter	Value	Unit
L1	12.5	m
W1	31.6	m
L2 [m]	1.125	m
L3 [m]	3.467	m
L4 [m]	3.207	m
L5 [m]	5.348	m
L6 [m]	1.38	m
L7 [m]	0.266	m
L8 [m]	2.192	m
bmain [m]	5.52	m
nmain [-]	6	
ncross [-]	7	
nrib [-]	51	
Izz,top [x104 mm4]	812621.65	[x104 mm4]
Izz,cross [x104 mm4]	124144.29	[x104 mm4]
Izz,rib [x104 mm4]	7424.94	[x104 mm4]
Hbottom [mm]	1140	mm
Wbottom [mm]	370	mm
tw,bottom [mm]	20	mm
tf,bottom [mm]	37	mm

d_{out}	0.8	m
A_{cross}	0.02265	m ²
H_{top}	870	mm
H_{cross}	590	mm

Properties		
Steel Density	78.5	kN/m ³
$W_{mainbeam}$	1868.095747	[x10 ⁶ mm ³]
$W_{crossbeam}$	420.8281017	[x10 ⁶ mm ³]

Cross beam			
Selfweight		Surface load deck	
A_{cross}	0.02265 [m ²]	q_{deck}	5 [kN/m ²]
$q_{selfweight}$	1.778025 [kN/m]	q_{deck}	10.41667 [kN/m]
Fa	[kN]	Me	-13.225 [kNm]
Fb	[kN]	Mf	26.45 [kNm]
Me	-2.25738 [kNm]	Ve	0 [kN]
Mf	4.514761 [kNm]	Vf	-28.75 [kN]
Ve	0 [kN]		
Vf	-4.90735 [kN]		

Result	
Me	-153.482 [kNm]
Mf	30.96476 [kNm]
Ve	100 [kN]
Vf	-133.657 [kN]

$\sigma_{max,c}$	-36.4715 [Mpa]
$\sigma_{max,t}$	7.358055 [Mpa]

Figure F.8: Hand calculation validation case two.

Case 3

Input		
Parameter	Value	Unit
L1	14.15	m
W1	6.59	m
L2 [m]	0.415	m
L3 [m]	1.97	m
L4 [m]	1.7	m
L5 [m]	4	m
L6 [m]	1.8	m
L7 [m]	0.019	m
L8 [m]	1.37	m
bmain [m]	5	m
nmain [-]	2	
ncross [-]	4	
nrib [-]	12	
Izz,top [x104 mm4]	225956.82	[x104 mm4]
Izz,cross [x104 mm4]	245929.83	[x104 mm4]
Izz,rib [x104 mm4]	2451.68	[x104 mm4]
Hbottom [mm]	770	mm
Wbottom [mm]	240	mm
tw,bottom [mm]	10	mm
tf,bottom [mm]	20	mm

b _{cwt}	3	m
A _{gross}	0.02858	m ²
H _{top}	780	mm
H _{cross}	790	mm

Properties	
Steel Density	78.5 kN/m ³
W _{mainbeam}	579.3764615 [x10 ⁶ mm ³]
W _{crossbeam}	622.6071646 [x10 ⁶ mm ³]

Cross beam			
Selfweight		Surface load deck	
A _{gross}	0.02858 [m ²]	Q _{deck}	5 [kN/m ²]
Q _{selfweight}	2.24353 [kN/m]	Q _{deck}	23.58333 [kN/m]
Fa	[kN]	Me	-24.566 [kNm]
Fb	[kN]	Mf	49.13194 [kNm]
Me	-2.33701 [kNm]	Ve	0 [kN]
Mf	4.674021 [kNm]	Vf	-58.9583 [kN]
Ve	0 [kN]		
Vf	-5.60883 [kN]		

Result	
Me	-151.903 [kNm]
Mf	53.80597 [kNm]
Ve	100 [kN]
Vf	-164.567 [kN]

σ _{max,c}	-24.3979 [Mpa]
σ _{max,f}	8.642041 [Mpa]

Figure F.9: Hand calculation validation case three.

Case 4

Input		
Parameter	Value	Unit
L1	10.8	m
W1	14.28	m
L2 [m]	0.509	m
L3 [m]	2.276	m
L4 [m]	1.81	m
L5 [m]	3.3	m
L6 [m]	2.1	m
L7 [m]	0.024	m
L8 [m]	1.559	m
bmain [m]	3.58	m
nmain [-]	4	
ncross [-]	4	
nrib [-]	19	
Izz,top [x104 mm4]	367222.695	[x104 mm4]
Izz,cross [x104 mm4]	187706.16	[x104 mm4]
Izz,rib [x104 mm4]	3355.318989	[x104 mm4]
Hbottom [mm]	900	mm
Wbottom [mm]	280	mm
tw,bottom [mm]	12	mm
tf,bottom [mm]	24	mm
b _{cwt}	1.7	m
A _{cross}	0.02605	m ²
H _{top}	790	mm
H _{cross}	690	mm
Properties		
Steel Density	78.5	kN/m ³
W _{mainbeam}	929.6777089	[x10 ⁶ mm ³]
W _{crossbeam}	544.0758261	[x10 ⁶ mm ³]

Cross beam					
Selfweight		Surface load deck		Point load	
A _{cross}	0.02605 [m ²]	Q _{deck}	5 [kN/m ²]	F	200 [kN]
Q _{selfweight}	2.044925 [kN/m]	Q _{deck}	18 [kN/m]	Fa	100 [kN]
		Me	-9.6123 [kNm]	Fb	100 [kN]
Fa	[kN]	Mf	19.2246 [kNm]	Me	-89.5 [kNm]
Fb	[kN]	Ve	0 [kN]	Mf	0 [kNm]
Me	-1.09202 [kNm]	Vf	-32.22 [kN]	Ve	100 [kN]
Mf	2.184048 [kNm]			Vf	-100 [kN]
Ve	0 [kN]				
Vf	-3.66042 [kN]				
Result					
Me	-100.204 [kNm]				
Mf	21.40865 [kNm]				
Ve	100				
Vf	-135.88				
σ _{max,c}	-18.4173 [Mpa]				
σ _{max,f}	3.934865 [Mpa]				

Figure F.10: Hand calculation validation case four.

Case 5

Input		
Parameter	Value	Unit
L1	13.5	m
W1	18.5	m
L2 [m]	0.738	m
L3 [m]	2.771	m
L4 [m]	2.381	m
L5 [m]	4.186	m
L6 [m]	1.85	m
L7 [m]	0.07	m
L8 [m]	1.857	m
bmain [m]	4.14	m
nmain [-]	5	
ncross [-]	5	
nrib [-]	30	
Izz,top [x104 mm4]	380594.95	[x104 mm4]
Izz,cross [x104 mm4]	187706.16	[x104 mm4]
Izz,rib [x104 mm4]	2753.022	[x104 mm4]
Hbottom [mm]	1020	mm
Wbottom [mm]	320	mm
tw,bottom [mm]	15	mm
tf,bottom [mm]	30	mm
b _{cwt}	1.6	m
A _{cross}	0.02605	m ²
H _{top}	800	mm
H _{cross}	690	mm
Properties		
Steel Density	78.5	kN/m ³
W _{mainbeam}	951.487375	[x10 ⁶ mm ³]
W _{crossbeam}	544.0758261	[x10 ⁶ mm ³]

Cross beam					
Selfweight		Surface load deck			
A _{cross}	0.02605 [m ²]	Q _{deck}	5 [kN/m ²]		
Q _{selfweight}	2.044925 [kN/m]	Q _{deck}	16.875 [kN/m]		
		Me	-12.0513 [kNm]		
Fa	[kN]	Mf	24.10256 [kNm]		
Fb	[kN]	Ve	0 [kN]		
		Vf	-34.9313 [kN]		
Me	-1.46038 [kNm]				
Mf	2.920766 [kNm]				
Ve	0 [kN]				
Vf	-4.23299 [kN]				
Result					
Me	-117.012 [kNm]				
Mf	27.02333 [kNm]				
Ve	100 [kN]				
Vf	-139.164 [kN]				
σ _{max,c}	-21.5065 [Mpa]				
σ _{max,f}	4.966831 [Mpa]				

Point load	
F	200 [kN]
Fa	100 [kN]
Fb	100 [kN]
Me	-103.5 [kNm]
Mf	0 [kNm]
Ve	100 [kN]
Vf	-100 [kN]

Figure F.11: Hand calculation validation case five.

F.4.4. Forces in the main beam flanges

Case 1

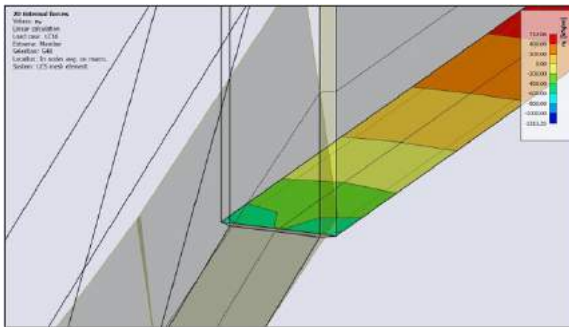


Figure F.12: Zoom on force n_y in the bottom flange of the main beam in case one.

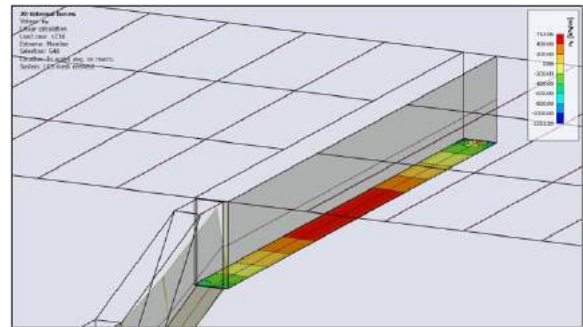


Figure F.13: Force n_y in the bottom flange of the main beam in case one.

Case 2

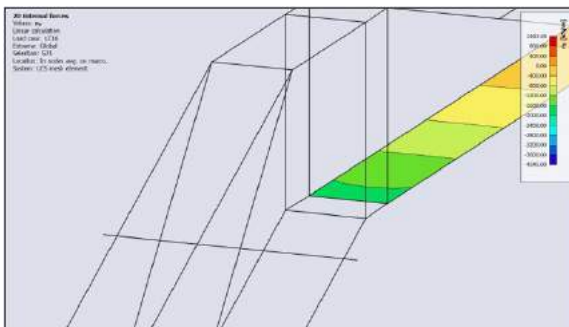


Figure F.14: Zoom on force n_y in the bottom flange of the main beam in case two.

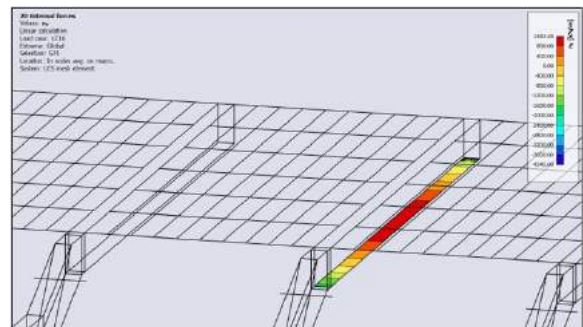


Figure F.15: Force n_y in the bottom flange of the main beam in case two.

Case 3

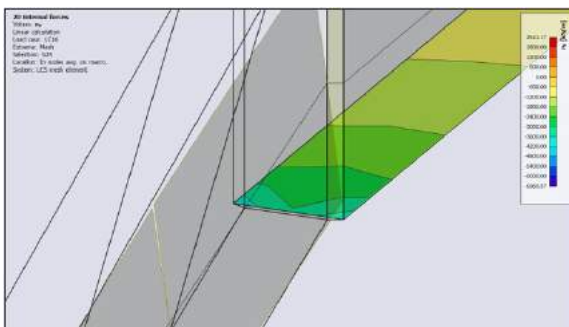


Figure F.16: Zoom on force n_y in the bottom flange of the main beam in case three.

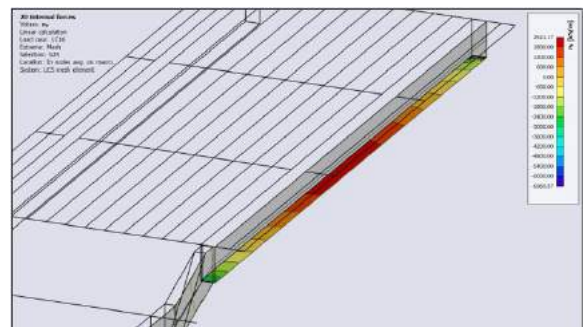


Figure F.17: Force n_y in the bottom flange of the main beam in case three.

Case 4

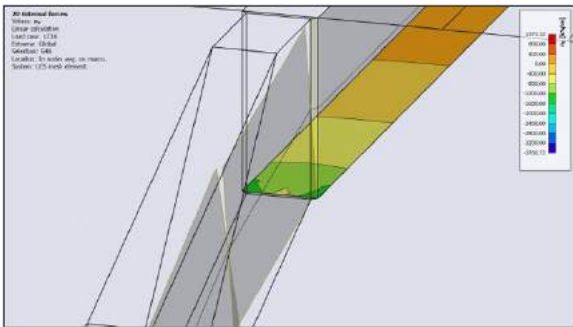


Figure F.18: Zoom on force n_y in the bottom flange of the main beam in case four.

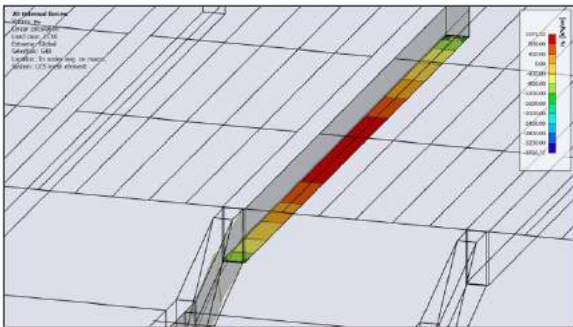


Figure F.19: Force n_y in the bottom flange of the main beam in case four.

Case 5

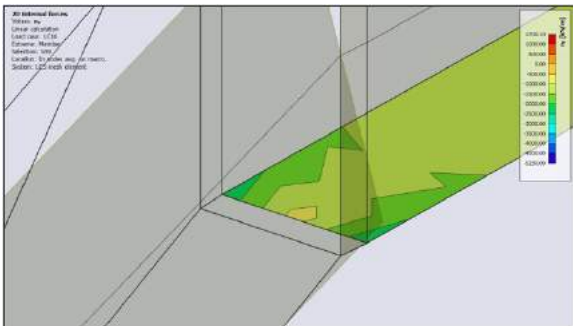


Figure F.20: Zoom on force n_y in the bottom flange of the main beam in case five.

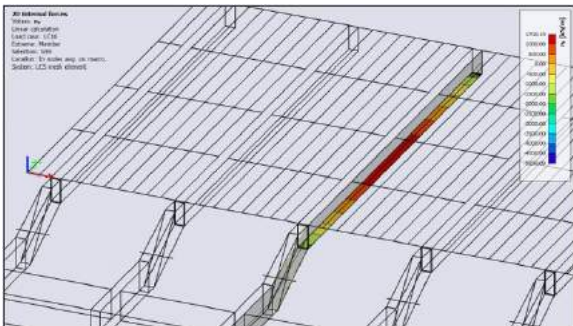


Figure F.21: Force n_y in the bottom flange of the main beam in case five.

F.4.5. Stress distribution bridge leaf

Case 1

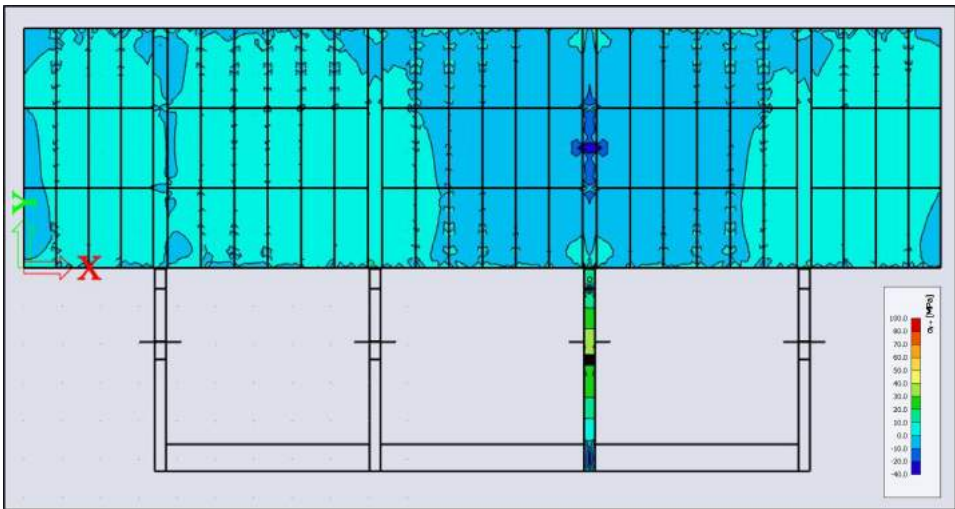


Figure F.22: Stresses σ_y in the top flange of the main beam and deck plate.

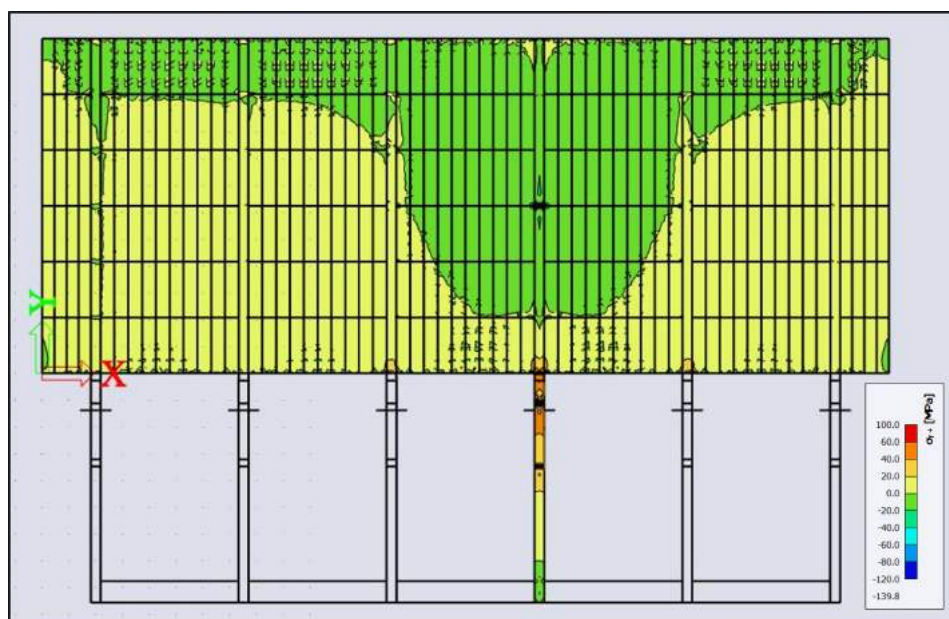
Case 2

Figure F.23: Stresses σ_y+ in the top flange of the main beam and deck plate.

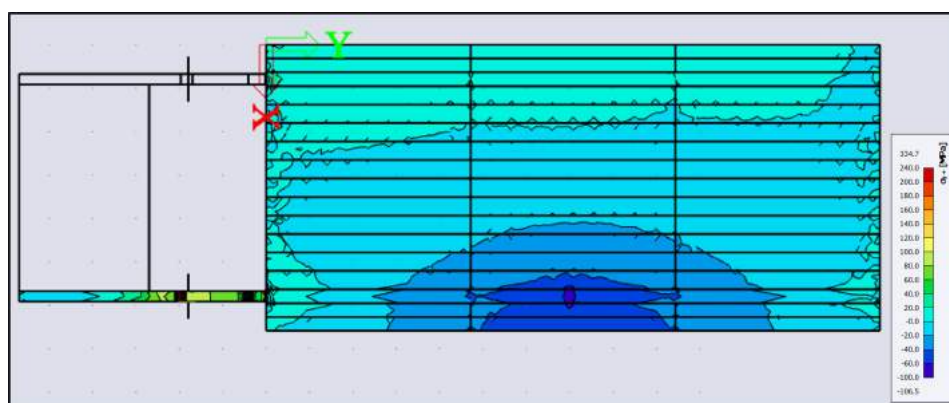
Case 3

Figure F.24: Stresses σ_y+ in the top flange of the main beam and deck plate.

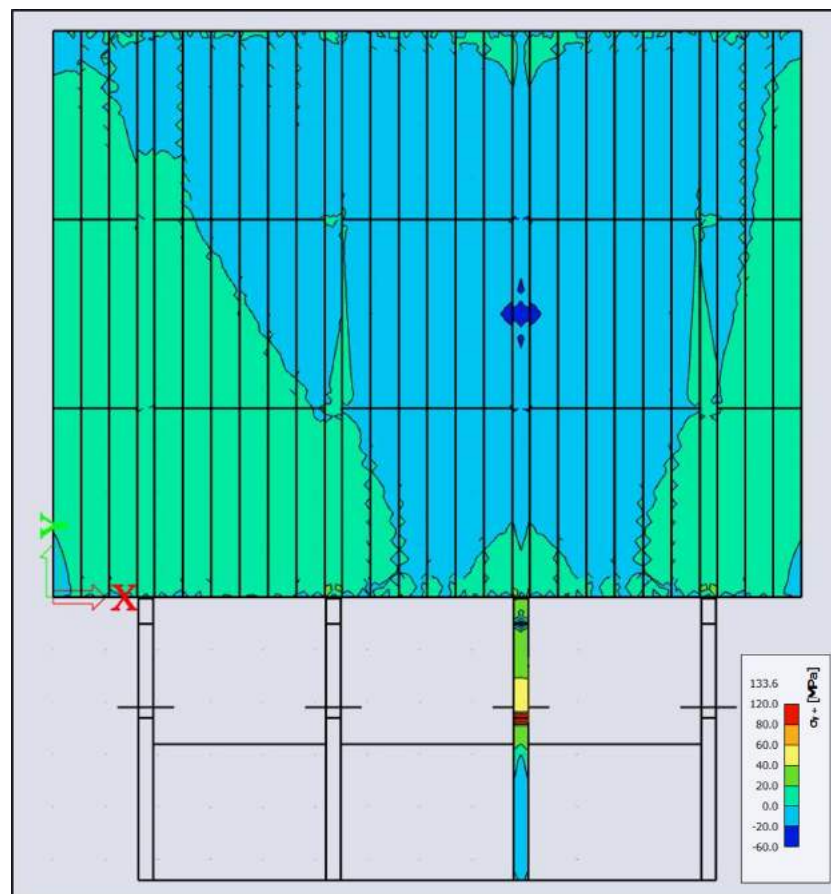
Case 4

Figure F.25: Stresses σ_y in the top flange of the main beam and deck plate.

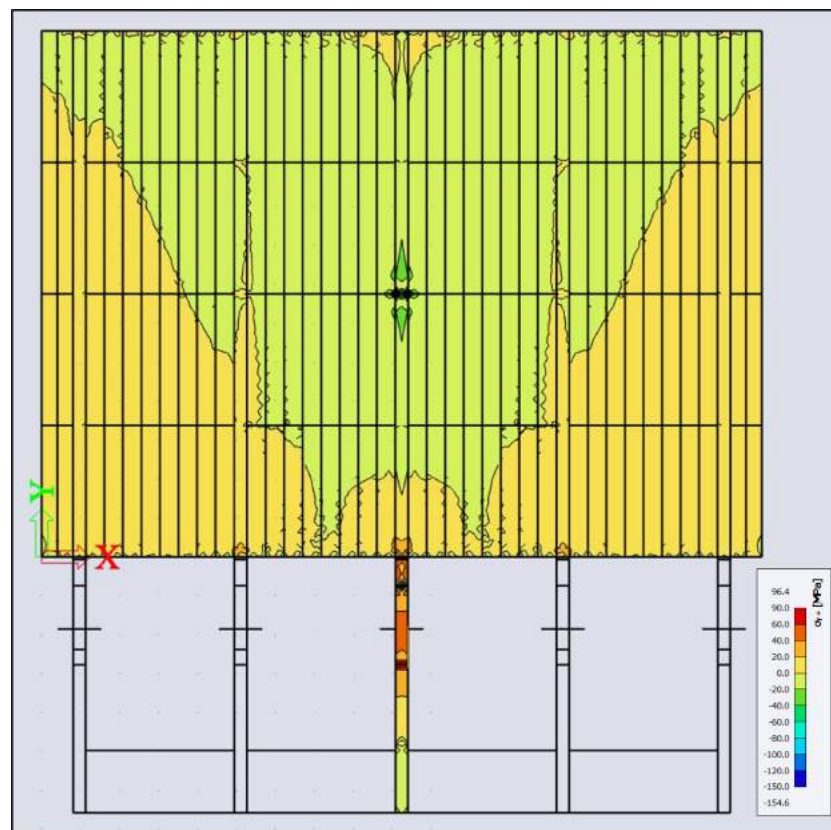
Case 5

Figure F.26: Stresses $\sigma_y +$ in the top flange of the main beam and deck plate.

G

Results

G.1. Case Study 1: Renovation Berlagebrug

General Description

The Berlagebrug is located in the Amstel neighborhood and spans across the river Amstel, connecting the Vrijheidslaan and Mr. Treublaan. Recently, the bridge leaf has been renovated. The Berlagebrug is open for all types of traffic, and has two tram tracks running over it in the middle of the bridge. A view on a new bridge leaf part being hoisted in to place, can be seen in figure G.1. Figure G.2 shows a top view of the new bridge leaf. Because of its monumental value, the old bascule chamber had to be reused. This led to challenges in construction, the new bridge leaf needed to be 1.5 times stronger than the old leaf, while still fitting in the old bascule chamber (Mobilis, 2023). Both the bridge leaf and counterweight were divided into three parts and installed sequentially. The middle part of the bridge leaf houses the two inner traffic lanes and tram tracks. The two outer parts of the bridge leaf are identical but mirrored.



Figure G.1: A bridge leaf part being hoisted into place.

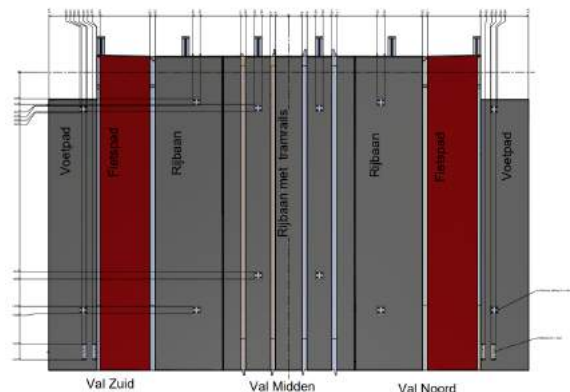


Figure G.2: Overview of new bridge leaf.

The traffic profile on the bridge is symmetrical. On both sides there is a sidewalk and cycle path present, in the middle the bridge provides space for four lanes of traffic. The tram tracks are forged into the middle two lanes. The sidewalks are 2.3 meters wide, the cycle paths 2.4 meters wide. The space in between has a total width of 12.8 meters, which is divided into the four traffic lanes.

Like all new bridges in Amsterdam, the bridge is designed for a design lifetime of 100 years in consequence class two. The steel bridge leaf is fully designed with S355 steel. The bridge is operated using a hydraulic operating system, which is connected to each of the three ballast blocks, each one accompanying one part of the bridge leaf. The parapets reach out 1.1 meters above the bridge surface, and are reused from the old bridge.

Structural properties

The part of the bridge leaf that spans the waterway, has a total length of 13.006 meters, and a total width of 23.18 meters. The distance to the rotational axis is equal to 1.285 meters. In total, the three bridge leaves combine for the use of six main beams, six cross beams and 34 rib elements. These are all directly welded onto the deck plate of twenty millimeters in thickness. On average, the main beams are spaced 3.6 meters apart. The main beams consist of welded I-shaped beams. They taper towards the toe of the leaf, where their profile is smaller than around the rotational axis, as can be seen in figure G.4.

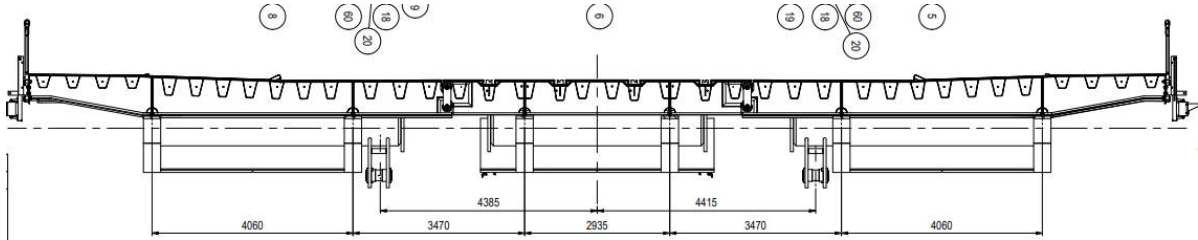


Figure G.3: Cross section of bridge deck.

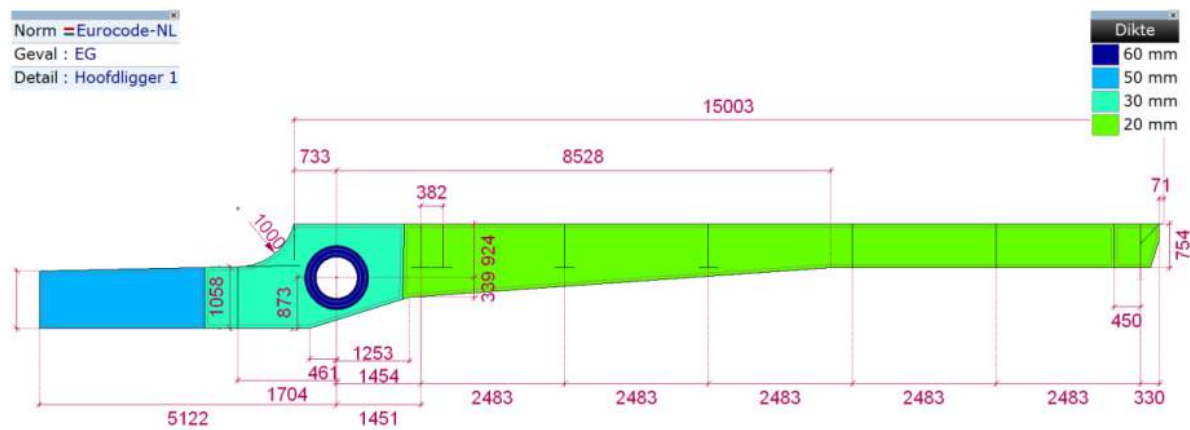


Figure G.4: Side view on the bridge leaf.

The thickness of web and bottom flange of the main beam is equal to twenty millimeters. At the toe of the leaf, the height of the main beam is equal to 574 millimeters, while at the beginning of the span, the height of the main beam is 1263 millimeters. The cross beams consist of a web of 20 millimeters thickness and a flange of 40 millimeters thickness, which are evenly spaced along the length of the span. No further information could be deducted about their height and width. Throughout the structure, different types of rib profiles are used with thicknesses of six and eight millimeters, all of similar dimension. No information could be gathered about their height and width.

In the rear part of the bottom main beam, the counterweights are forged in between the main beams. These bottom main beam parts have a box shape, and have webs and flanges of fifty millimeters thickness. The height of the bottom main beams is equal to 985 millimeters. The structure of the three bridge leaves combined has a total weight of 447020 kg, including bridge deck finishing elements and tram masts for the overhead cable system.

Structural Performance

This section describes the normative load situations for the Berlagebrug, which are compared to the design alternative in paragraph 5.1.1.

For the Berlagebrug, it appeared that load combination one was normative for the main beams.

Figure G.5 shows the normative stress situations for the envelope of load combinations. In this load combination, the normative stresses in the main beam occur in the top flange near the support axis.

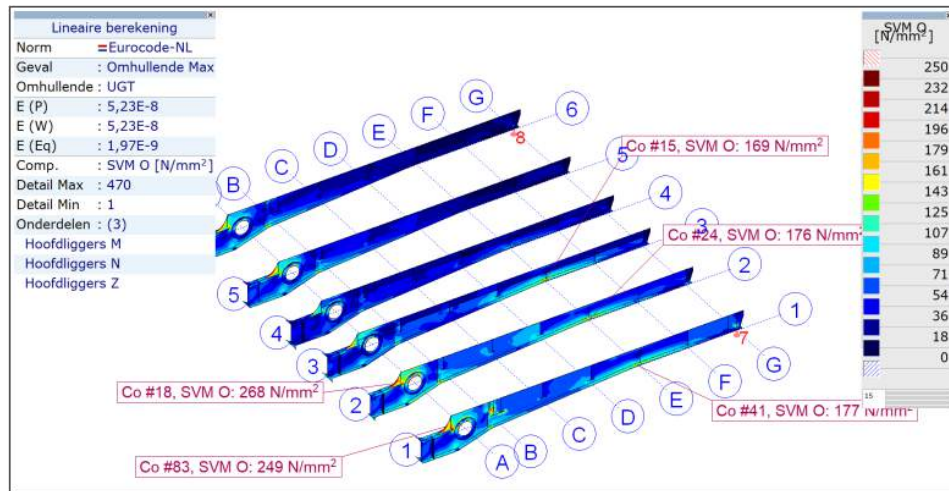


Figure G.5: Governing Von Mises stresses in main beams for ULS envelope.

This normative stress is equal to 268 MPa, which translates into a unity check of 0.75 for the main beams.

The second load combination appeared to be normative for the fore-most cross beam, the "voorhar". This cross beam is shown in the next figure on axis G.

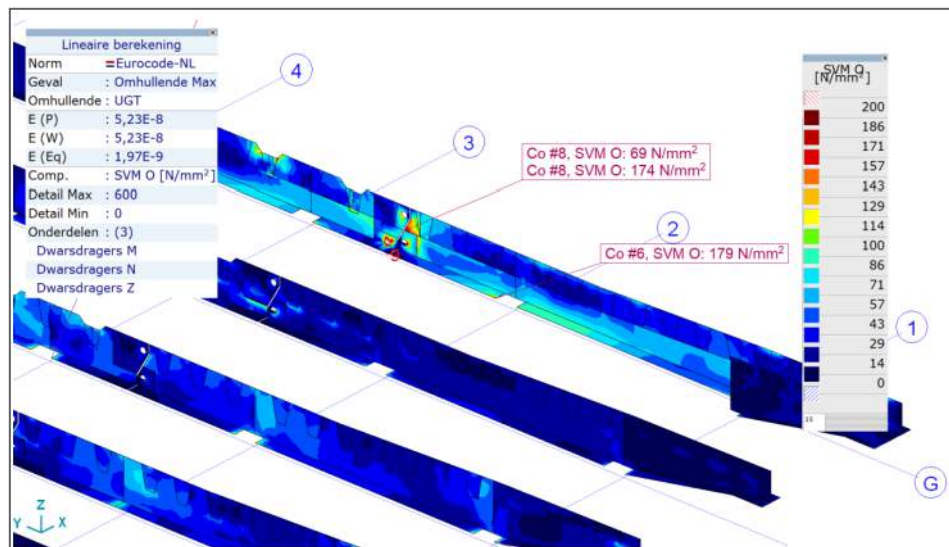


Figure G.6: Governing Von Mises stresses in cross beam G for ULS envelope.

The maximum stress in the cross beam occurs near the connection to the second main beam, and is equal to 179 MPa. This leads to a unity check of 0.5.

Load combination three was normative for the rear-most cross beam, which is shown in the next figure on axis B.

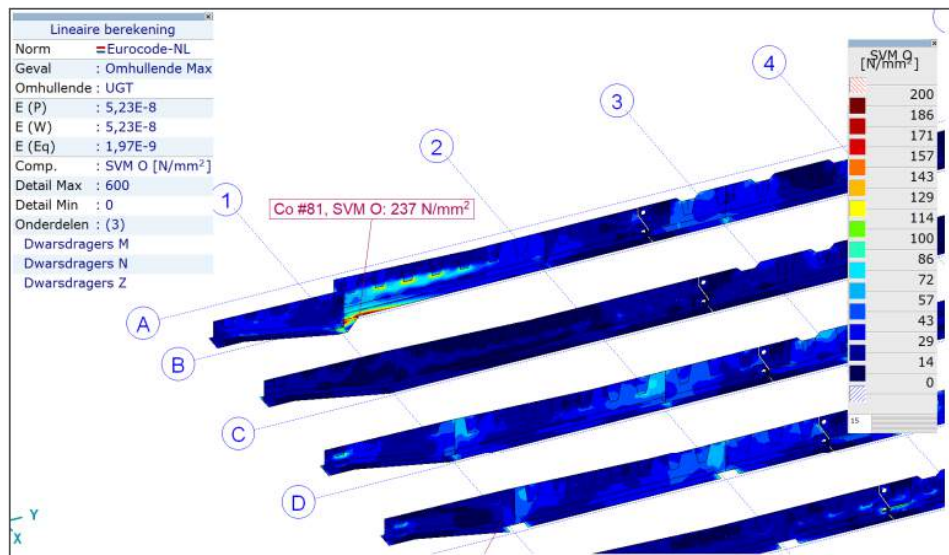


Figure G.7: Governing Von Mises stresses in cross beam B for ULS envelope.

The maximum stress in the cross beam occurs near the connection to the first main beam on axis one, and is equal to 237 MPa. This translates into a unity check of 0.67.

G.2. Case Study 2: Elizabeth Admiraalbrug

General description

This pedestrian and cyclebridge, bridge 0925, will be part of the new neighborhood Elzenhagen-Zuid in Amsterdam-North. It will run over the Noordhollandsch canal and will be placed right next to the existing lift bridge in the IJdoornlaan. Figure G.8 shows a view on the bridge in its environment, and figure G.9 shows a top view of the bridge.



Figure G.8: 3D render of bridge 0925.

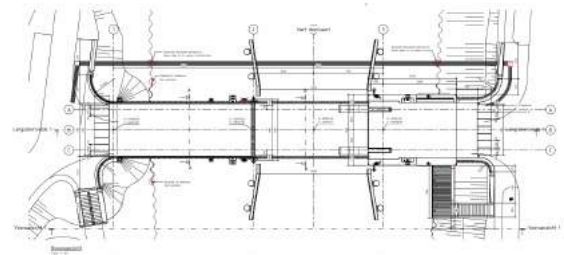


Figure G.9: Top view of bridge 0925.

The bridge will be accessible for pedestrians and cyclists only, but is designed for an accidental vehicle, in the form of an emergency services vehicle. The footpath is 2.5 meters wide and the cycle path 4.9 meters. The bridge is designed with a slim steel structure, onto which a thin epoxy layer of six millimeters will be applied as bridge deck finishing. The bascule chamber will be placed on the eastern embankment, and will house an electro-mechanical operating system. There will be one system of a panama wheel and push-pull rod, which will be directly connected to the counterweight.

The bridge is designed for a design life time of 100 years in consequence class two. Further relevant information is that the design is based on a traffic class TC2 and joggers class JC3 for dynamic traffic calculations. The parapets on the openable part are made out of aluminium and reach a height of 1.3 meters above the deck surface, according to the rules of the Bouwbesluit. The bridge opens to a maximum angle of 82 degrees. The steel bridge leaf is constructed with S355 steel.

Structural properties

The bridge deck of the openable part has a length of 15.88 meters and a width of 7.4 meters. The distance to the rotational axis, called L_6 , is equal to 2.145 meters. The bridge leaf is made out of two main beams, five cross beams and nine rib elements, which are all directly welded onto the bridge deck plate, as can be seen in figure G.10. The bridge deck plate has a thickness of ten millimeters. The main beams have a custom, tubular profile. They have a varying height and width over the length of the bridge deck, and are spaced at 5.7 meters heart to heart distance. The height of the main beams decreases along the span. At the beginning of the span at the bascule chamber, the height is equal to 700 millimeters, while at the toe of the leaf, the height is 525 millimeters. The width of the main beams at the base is equal to 500 millimeters, while the width at the top varies from 660 mm at the beginning of the bridge leaf, to 640 mm at the toe. The thickness of the bottom flange is equal to 25 millimeters and of both webs fifteen millimeters.

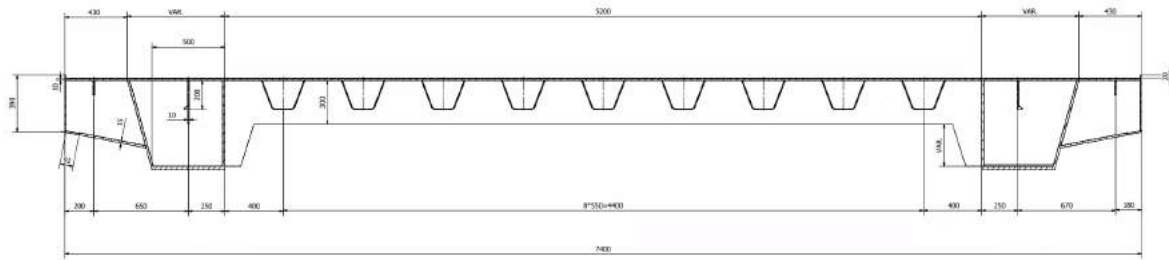


Figure G.10: Cross section of bridge deck.

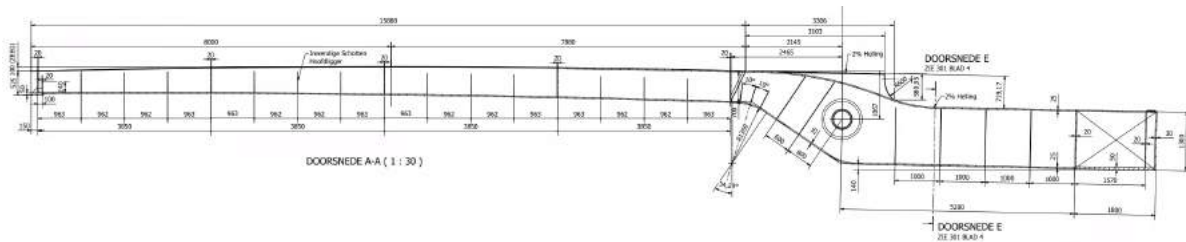


Figure G.11: Side view on the bridge leaf.

The cross beam elements in this bridge design are constructed as very slim steel sheets, because the bridge is susceptible to minimal loading. The sheets have a height of 300 millimeters across most of the cross section, and increase in height around the main beams and sides of the bridge decks. The thickness of these sheets is equal to twenty millimeters. The deck uses nine rib elements which are all placed in between the two main beams. In the exterior parts of the bridge deck outside of the main beams, a custom stiffening element is placed. The rib elements have dimensions as shown in figure G.12.

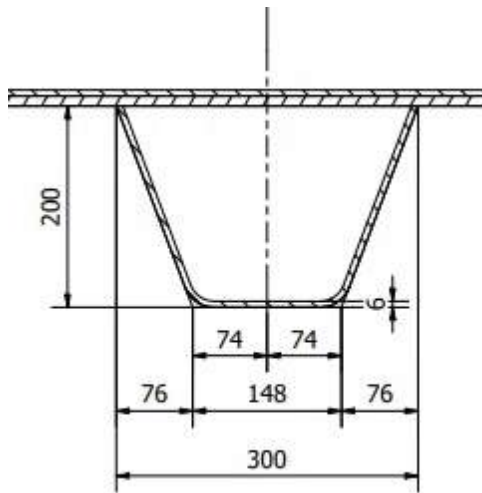


Figure G.12: Rib element in the bridge deck.

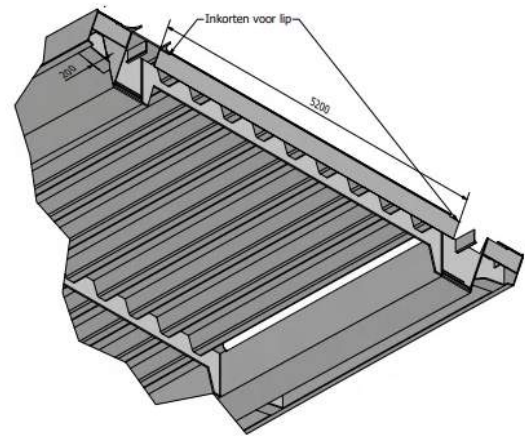


Figure G.13: View on the bridge deck from underneath.

Lastly, the bottom main beams have a rectangular box shape. They have a width of 500 millimeters, a height of 1300 millimeters, flange thickness of 25 millimeters and web thickness of fifteen millimeters. The total depth of the main beams in the bascule chamber, defined by parameter L_8 in this thesis, is equal to approximately two meters. The counterweight has a depth of 1.8 meters inwards, and is fitted into the rear part of the two main beams, which have a total length of seven meters measured from the rotational axis.

The total weight of this steel bridge leaf design is approximately equal to 46324.59 kilograms.

Structural Performance

In the definitive design for bridge 0925, it appeared that load combination four was normative for the main beams. The maximum Von Mises stress occurs right before the bridge deck, in the top flange of the main beam. Under this loading combination, the stress distribution over the main beam, can be seen in figure G.14.

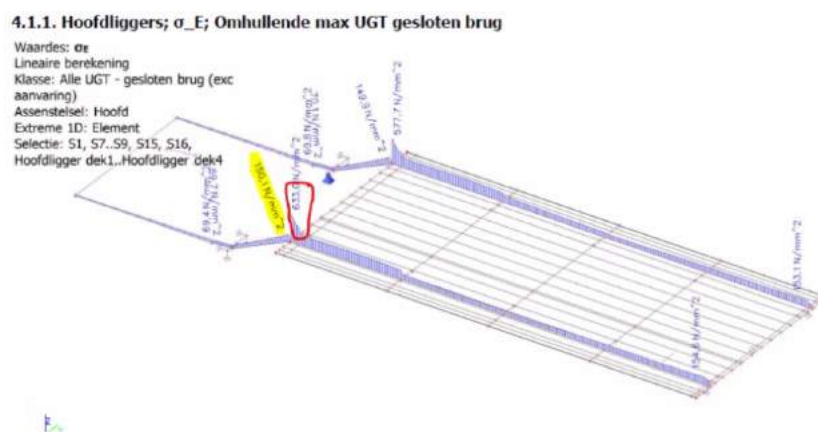


Figure G.14: Governing Von Mises stresses in main beam of Elizabeth Admiraalbrug.

In the definitive design, the maximum stress occurs in the top flange right in front of the bridge deck plate, this stress is equal to $\sigma_E = 150.1$ MPa. Which means a unity check of 0.42.

Load combination five was normative for the cross beams in this design, more specifically the front most cross beam called the "voorhar". In case the emergency vehicle is positioned at the edge of

the bridge deck, the cross beam is subjected to the maximum possible stresses. The stress distribution in the cross beams due to this load combination can be seen in the next figure.

4.2.1. Dwarsdragers; σ_E ; Omhullende Alle UGT gesloten en open brug (excl aanvaring)

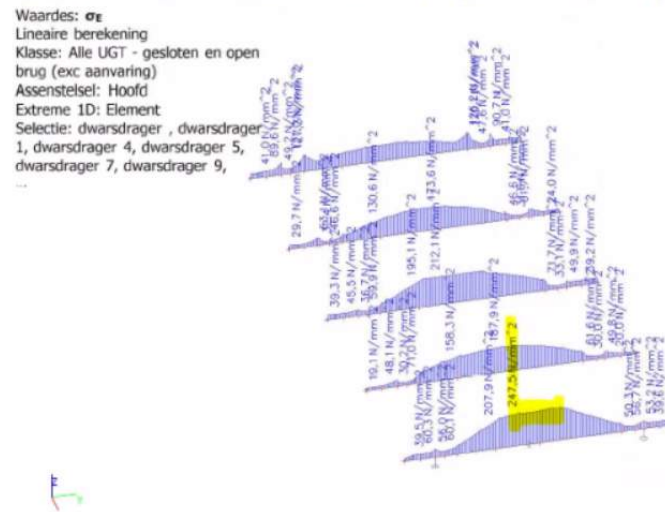


Figure G.15: Governing Von Mises stresses in "voorhar" of Elizabeth Admiraalbrug.

The maximum stress occurring in the crossbeam is equal to 248 MPa. Which translates into a unity check of 0.70.

Load combination six appeared to be normative for the rib profiles in the definitive design. As explained in chapter 3, this load combination involves the partial departure of the accidental vehicle, where only the rear axle is placed on the bridge deck. This leads to the following stress distribution of σ_E over the governing rib element.

4.3.1. Trogverstijvers; σ_E ; Omhullende Alle UGT gesloten en open brug (excl aanvaring)

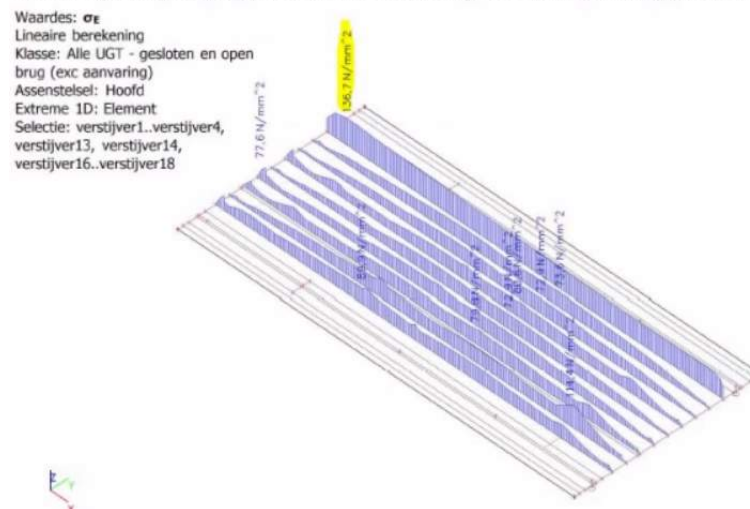


Figure G.16: Governing Von Mises stresses in rib of Elizabeth Admiraalbrug.

The maximum stress in the rib profiles occurs in the outermost rib, at the beginning of the bridge deck. The maximum stress is equal to 137 MPa. Which translates into a unity check of 0.39.

G.3. Results for design alternative Berlagebrug

The generated structure as alternative for the Berlagebrug was verified against load combinations one to three.

Load combination one

The following figure shows the occurring Von Mises stresses in the structure as result of load combination one.

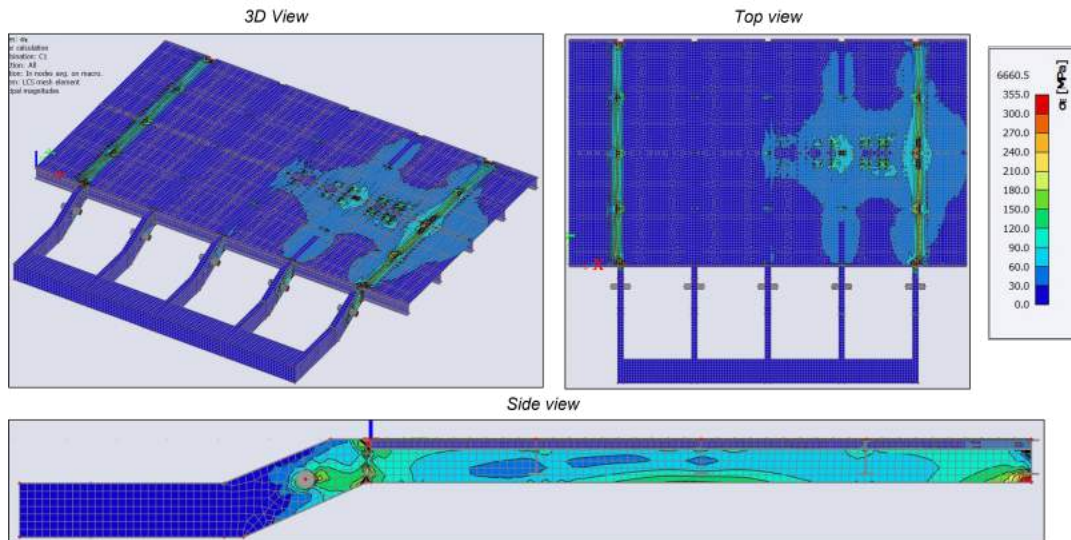


Figure G.17: Von Mises stresses under load combination one.

Load combination two

The following figure shows the occurring Von Mises stresses in the structure as result of load combination two.

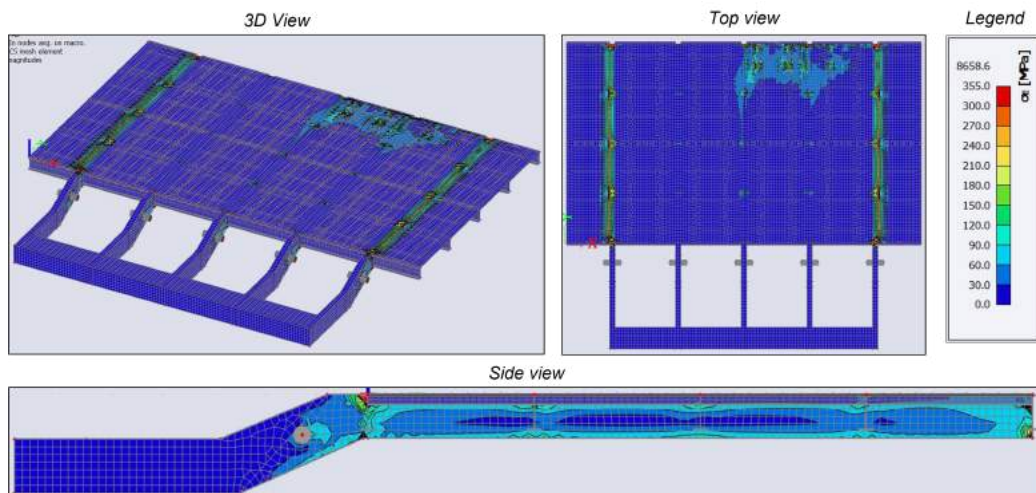


Figure G.18: Von Mises stresses under load combination two.

The maximum stress in the cross beams occurs in the front most cross beam, B199, which is located approximately in the middle of the bridge deck.

	Name	dx [m]	Fibre	Case	σ_1 [MPa]	σ_2 [MPa]	τ_{tot} [MPa]	σ_E [MPa]
197	B197	0.494	1	C2/8	89.5	0.0	1.1	89.5
198	B198	0.000	1	C2/9	90.4	0.0	1.5	90.5
199	B199	0.494	3	C2/6	123.3	-0.1	3.2	123.3
200	B200	0.000	3	C2/5	116.4	0.0	0.4	116.4
201	B201	0.000	3	C2/5	96.1	-0.1	3.4	96.2
202	B202	0.494	20	C2/5	61.8	-58.5	60.1	104.1
203	B203	0.329	8	C2/5	33.8	-26.0	29.7	52.0

Figure G.19: Von Mises stress in governing element B199.

Load combination three

The following figure shows the occurring Von Mises stresses in the structure as result of load combination three.

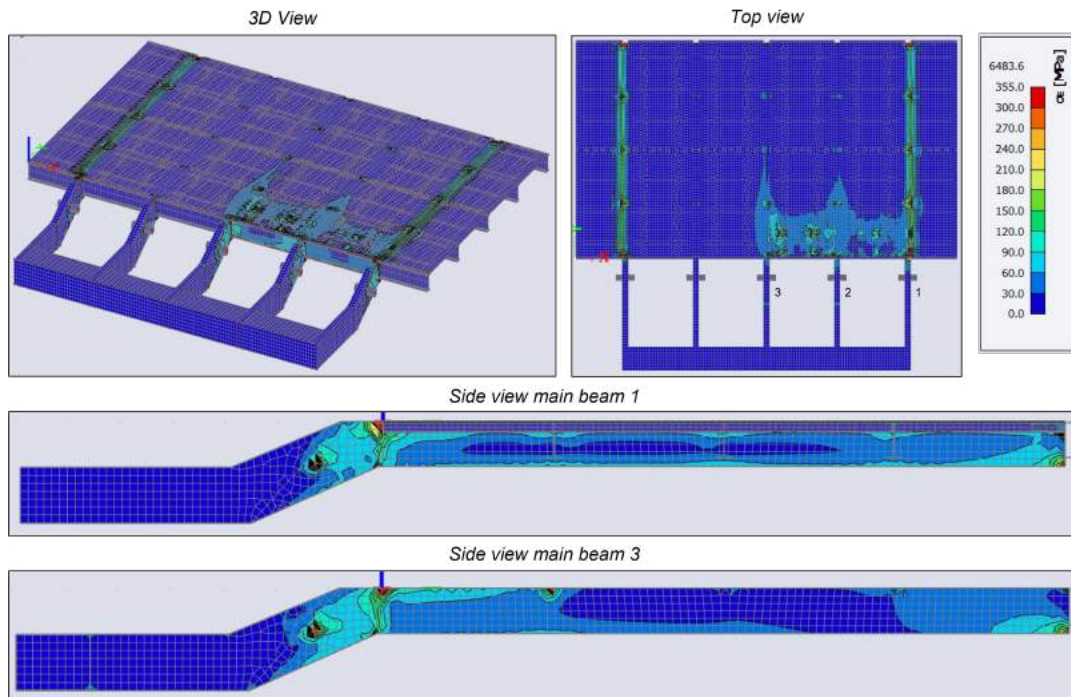


Figure G.20: Von Mises stresses under load combination three.

In this load combination, the stresses in the rear most cross beam are governing. The following table shows the results of this calculation in SCIA.

	Name	dx [m]	Fibre	Case	σ_1 [MPa]	σ_2 [MPa]	τ_{tot} [MPa]	σ_E [MPa]
67	B67	0.329	20	C3/2	61.5	-53.2	57.4	99.8
68	B68	0.000	1	C3/2	73.3	0.0	0.1	73.3
69	B69	0.494	3	C3/2	83.3	0.0	0.8	83.3
70	B70	0.000	3	C3/2	83.5	0.0	1.8	83.5
71	B71	0.494	1	C3/2	122.6	0.0	2.3	122.6
72	B72	0.000	1	C3/2	117.6	0.0	0.3	117.6
73	B73	0.000	1	C3/2	94.2	-0.2	4.2	94.3
74	B74	0.329	20	C3/2	52.6	-47.5	50.0	86.7

Figure G.21: Von Mises stresses under load combination three.

G.4. Results for design alternative Elizabeth Admiraalbrug

The generated structure as alternative for the Elizabeth Admiraalbrug was verified against load combinations four to six.

Load combination four

The following figure shows the occurring Von Mises stresses in the structure as result of load combination four.

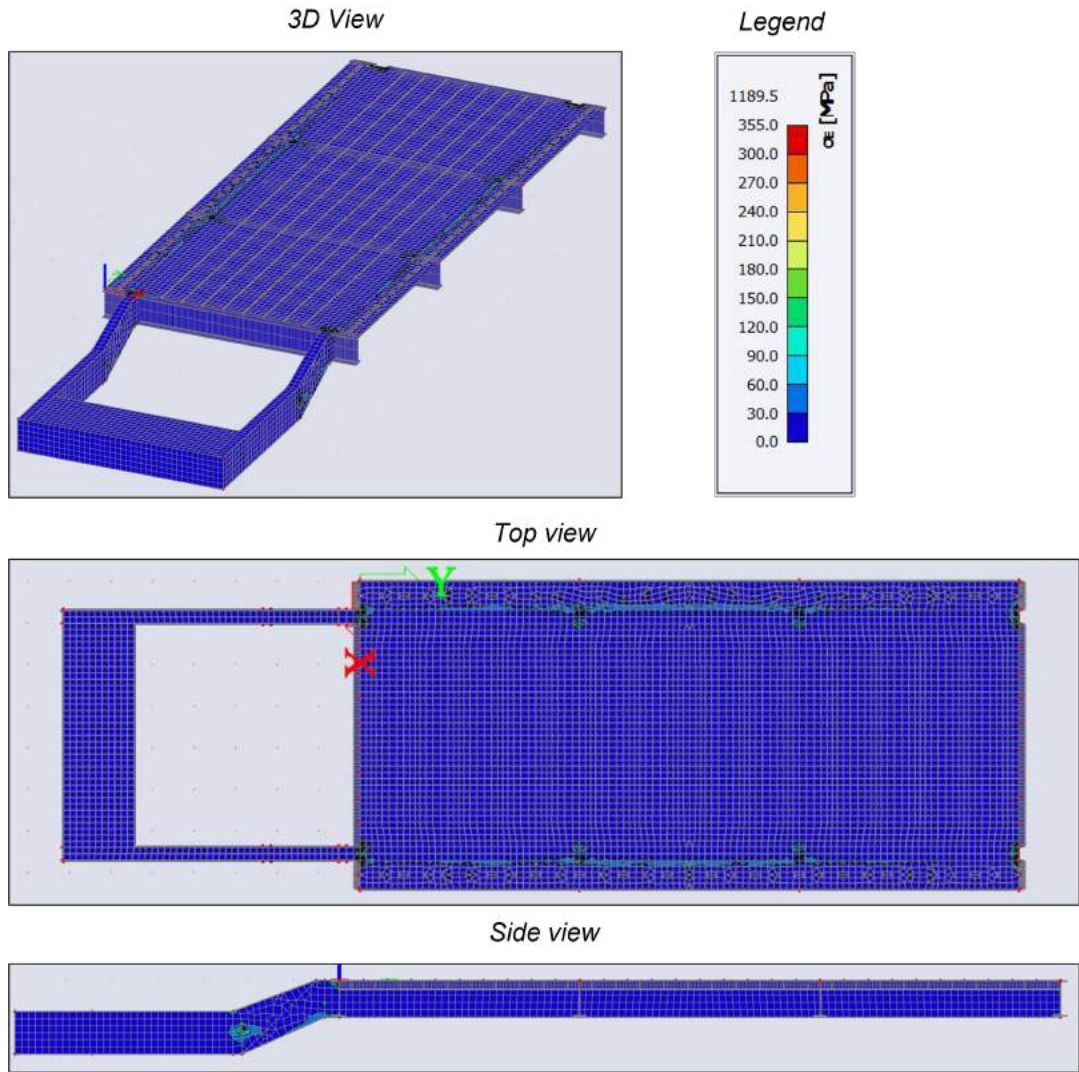


Figure G.22: Von Mises stresses under load combination four.

The maximum Von Mises stress occurs in the top flange of the main beam, which is plate element S26. The following table shows the results of the structural analysis.

Figure G.23: Von Mises stresses in governing plate element S26.

	Name	Mesh	x [m]	y [m]	z [m]	Case	σE^+ [MPa]	σE^- [MPa]
183	S25	Element: 3673...	6.550	7.940	-0.860	C4/1	16.4	16.7
184	S26	Element: 3781...	6.550	-0.320	0.000	C4/1	17.1	14.2
185	S26	Element: 3782...	6.393	-0.160	0.000	C4/1	26.9	37.1
186	S26	Element: 3784...	6.385	0.000	0.000	C4/1	145.4	130.6
187	S26	Element: 3783...	6.715	0.000	0.000	C4/1	214.7	245.4
188	S26	Element: 3781...	6.550	-0.160	0.000	C4/1	9.0	17.0
189	S27	Element: 3785...	0.700	-6.995	-1.614	C4/1	0.3	0.3
190	S27	Element: 3846...	1.000	-2.493	-1.614	C4/1	17.8	15.3

Load combination five

The following figure shows the occurring Von Mises stresses in the structure as result of load combination five.

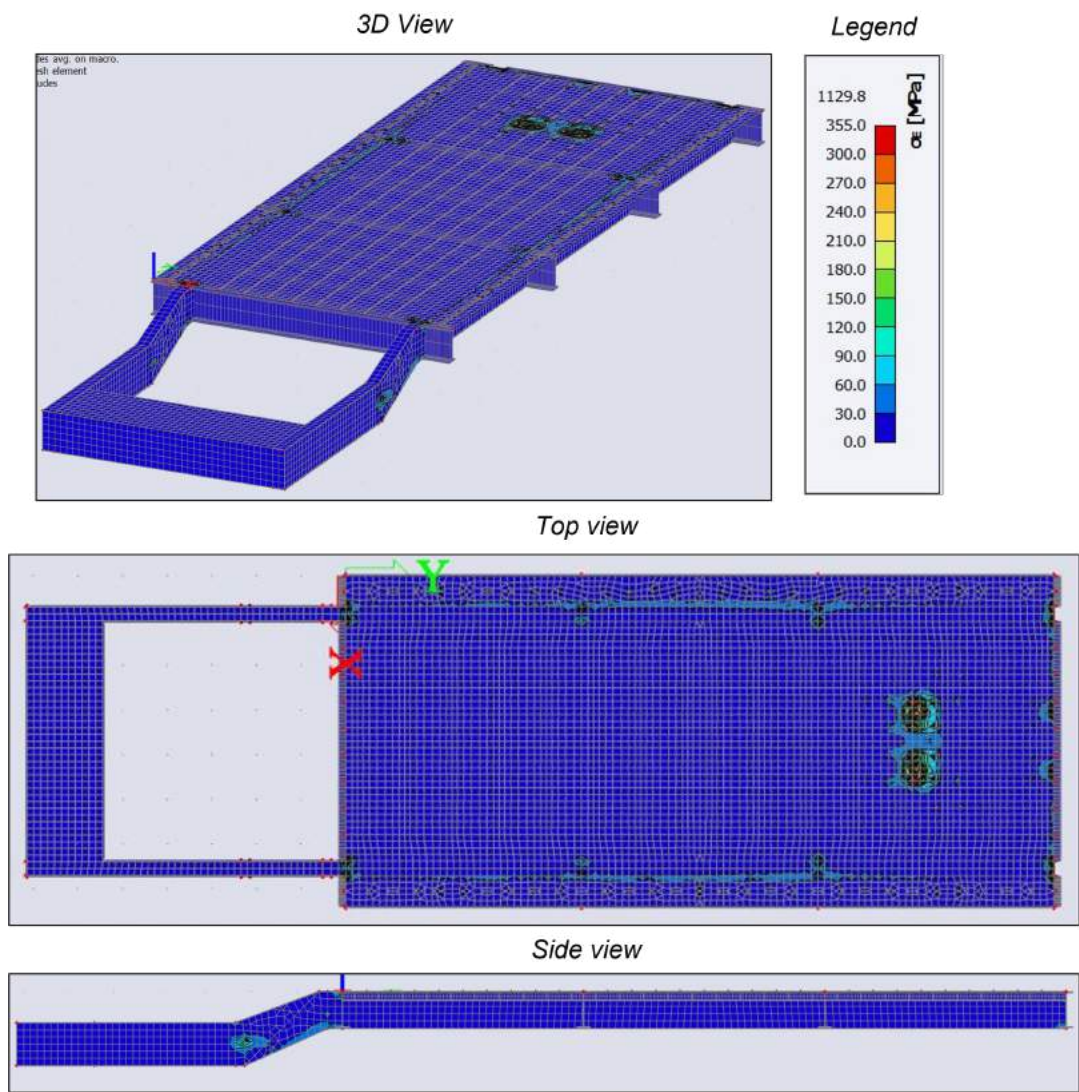


Figure G.24: Von Mises stresses under load combination five.

The maximum Von Mises stress occurs in the foremost crossbeam. The following table shows the result of the governing line elements.

Figure G.25: Von Mises stresses in governing cross beam elements.

Name	dx [m]	Fibre	Case	σ_1 [MPa]	σ_2 [MPa]	σ_{tot} [MPa]	σ_E [MPa]
45 B45	0.597	7	C5/1	10.2	-3.0	5.5	11.9
46 B46	0.597	3	C5/2	24.7	-0.1	1.7	24.8
47 B47	0.597	3	C5/2	23.1	0.0	0.9	23.1
48 B48	0.597	3	C5/2	22.3	0.0	0.1	22.3
49 B49	0.000	3	C5/2	23.1	0.0	0.9	23.1
50 B50	0.000	3	C5/2	24.8	-0.1	1.6	24.8
51 B51	0.000	7	C5/1	10.1	-3.0	5.5	11.9
52 B52	0.000	3	C5/2	24.8	-0.1	1.6	24.8

Load combination six

The following figure shows the occurring Von Mises stresses in the structure as result of load combination six.

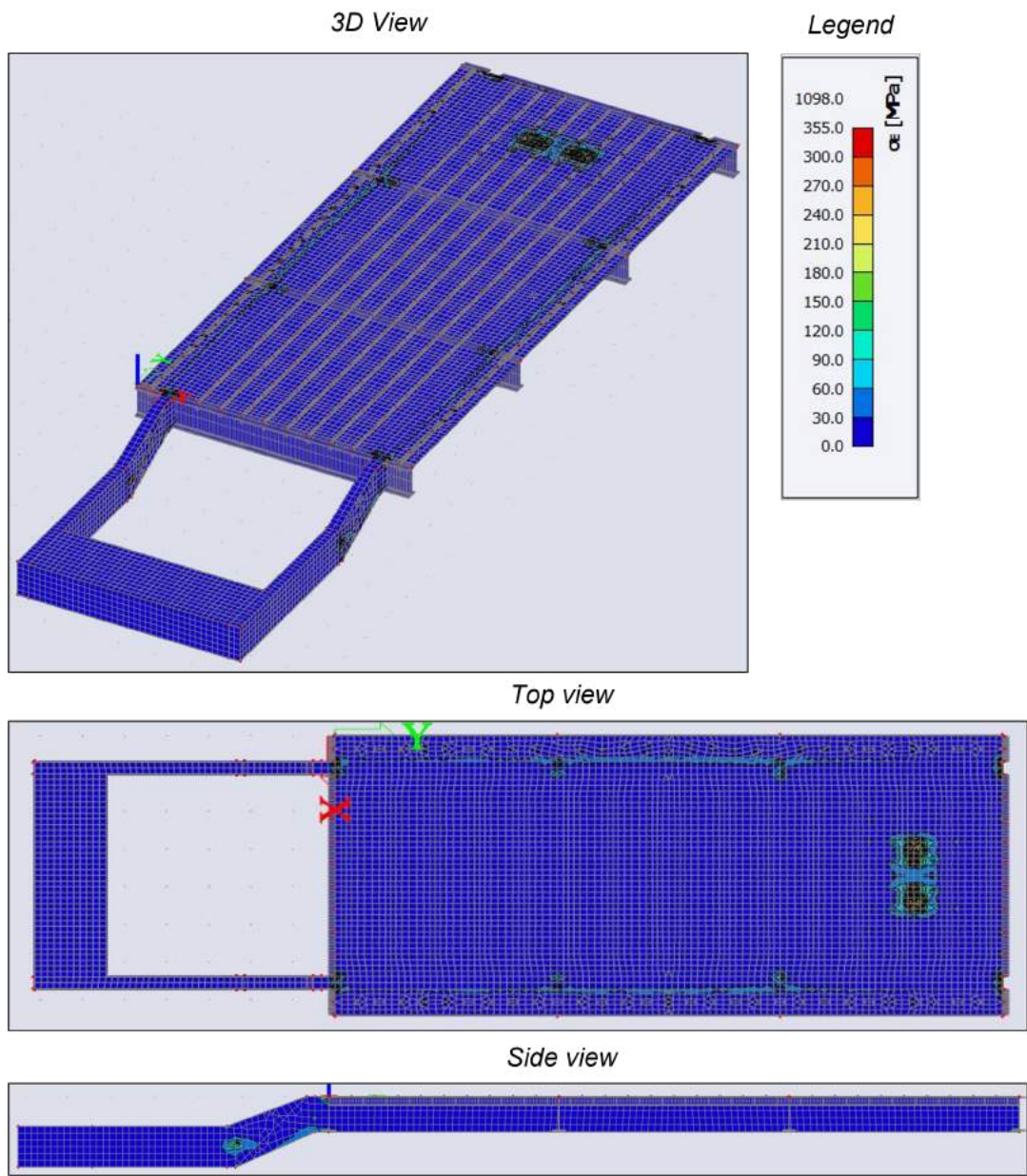


Figure G.26: Von Mises stresses under load combination six.

In this load combination, the maximum Von Mises stress occurs in a rib element. The table output of SCIA model is shown in figure G.27.

	Name	dx [m]	Fibre	Case	$\sigma 1$ [MPa]	$\sigma 2$ [MPa]	τ_{tot} [MPa]	σE [MPa]	
1	B289	0.000	1	C6/1	67.6	-0.3	4.8	67.8	
2	B199	0.000	3	C6/1	67.6	-0.4	5.0	67.8	
3	B198	0.529	3	C6/1	66.3	-0.1	2.8	66.4	
4	B288	0.529	1	C6/1	66.3	-0.1	3.0	66.4	
5	B258	0.529	3	C6/1	54.1	-0.1	2.1	54.2	
6	B228	0.529	1	C6/1	54.1	-0.1	2.2	54.2	
7	B259	0.000	3	C6/1	54.1	-0.2	3.0	54.2	
8	B230	0.000	1	C6/1	54.1	0.2	3.0	54.2	

Figure G.27: Maximum stresses in governing rib elements.